

5-2017

CHARACTERIZATION OF THE ROLE OF THE pKM101-ENCODED T4SS OUTER MEMBRANE CORE COMPLEX IN SUBSTRATE TRANSFER, PILUS BIOGENESIS, AND RECIPIENT CELL CONTACT

Jay E. Gordon

Follow this and additional works at: https://digitalcommons.library.tmc.edu/utgsbs_dissertations



Part of the [Bacteriology Commons](#), and the [Medicine and Health Sciences Commons](#)

Recommended Citation

Gordon, Jay E., "CHARACTERIZATION OF THE ROLE OF THE pKM101-ENCODED T4SS OUTER MEMBRANE CORE COMPLEX IN SUBSTRATE TRANSFER, PILUS BIOGENESIS, AND RECIPIENT CELL CONTACT" (2017). *The University of Texas MD Anderson Cancer Center UTHealth Graduate School of Biomedical Sciences Dissertations and Theses (Open Access)*. 779.
https://digitalcommons.library.tmc.edu/utgsbs_dissertations/779

This Dissertation (PhD) is brought to you for free and open access by the The University of Texas MD Anderson Cancer Center UTHealth Graduate School of Biomedical Sciences at DigitalCommons@TMC. It has been accepted for inclusion in The University of Texas MD Anderson Cancer Center UTHealth Graduate School of Biomedical Sciences Dissertations and Theses (Open Access) by an authorized administrator of DigitalCommons@TMC. For more information, please contact digitalcommons@library.tmc.edu.

CHARACTERIZATION OF THE ROLE OF THE pKM101-ENCODED T4SS OUTER
MEMBRANE CORE COMPLEX IN SUBSTRATE TRANSFER, PILUS BIOGENESIS,
AND RECIPIENT CELL CONTACT

by

Jay E. Gordon, B.S.

APPROVED:

Peter J. Christie, Ph.D., Advisory Professor

Mikhail Bogdanov, Ph.D.

Heidi B. Kaplan, Ph.D.

Michael Lorenz, Ph.D.

William Margolin, Ph.D.

APPROVED:

Dean, The University of Texas
MD Anderson Cancer Center UTHHealth Graduate School of Biomedical Sciences

CHARACTERIZATION OF THE ROLE OF THE pKM101-ENCODED T4SS OUTER
MEMBRANE CORE COMPLEX IN SUBSTRATE TRANSFER, PILUS BIOGENESIS,
AND RECIPIENT CELL CONTACT

A
THESIS

Presented to the Faculty of
The University of Texas
MD Anderson Cancer Center UTHealth
Graduate School of Biomedical Sciences

In Partial Fulfillment
of the Requirements
for the Degree of

Doctor of Philosophy

by
Jay E. Gordon, B.S.
Houston, Texas
August 2017

Acknowledgements

I would like to acknowledge my mentor, Dr. Peter Christie for his guidance and support throughout my time as a graduate student. He has always been a key source of insight and enthusiasm during this process, for which I am thankful.

I would like to acknowledge the faculty members of my advisory committee including Dr. William Margolin, Dr. Heidi Kaplan, Dr. Michael Lorenz, and Dr. Mikhail Bogdanov. Throughout this process, I have been able to easily approach each of you with questions and concerns, for which I have always received helpful advice. Additionally, being able to obtain second opinions from each of you with regard to experimental design, manuscript writing, and presentation setup has been tremendously helpful. I would also like to thank our department program director, Dr. Ambro van Hoof, for his additional guidance during my time here. Your door has always been open and I have always felt welcome to speak with you about my progress. Finally, I would like to thank Dr. Steve Norris for his guidance and support during my time as a trainee in the Molecular Basis of Infectious Disease (MBID) training program. I also appreciate the financial support and the opportunity to mentor undergraduate students as Summer trainees.

I would like to thank past and current members of the Christie lab for their friendship and support. Dr. Jennifer Kerr and Dr. Simon Jakubowski were extremely helpful during my first months in the Christie lab. I would like to give special mention to members with whom I have developed lasting friendships with including Trista Berry, Dr. Christian Gonzalez-Rivera, Dr. Minny Bhatti, Dominik Awad, Roosheel Patel, Maxim Bogisch, Dr. Yang “Grace” Li, and Dr. Martha Camacho-Hernandez. Your friendship has meant the world to me and I have enjoyed discussing science as well as life in general. I have enjoyed it all from working, to going out to eat, to much-needed coffee breaks. I would also like to thank Dr. Camacho-Hernandez for

introducing me to yoga as a means of stress relief. It has been incredibly helpful during this past year.

I would also like to thank my friends from my undergraduate years at The University of Kansas, with special mention of Josh Breger, Garrett Pinzur, Matt Rissien, Miriam Ofstein, and Ben “Squints” Geller. I love catching up with all of you and seeing you whenever I am able to visit Chicago. I also want to thank my long-time friends from Beren Academy in Houston including Paul Brokhin, Scott Hamilton, Nick Lerman, and Moshe Ephron for providing much-needed stress relief and being willing to hang out whenever possible.

I next want to thank my family. My parents, Gerilyn and John, have been my biggest fans and supporters since day one. They have provided me with the love and support I have needed to get through this process and I know they will continue to do so. I would like to thank my grandmother, Lillie Farb, for always being my daily motivational speaker. She has always been a key person in my life and I enjoy being with her and doing things such as going out to eat, discussing America’s crazy political situation, and watching Kansas Jayhawk men’s basketball games. I want to thank my Uncle Joel Farb, for his love and guidance during this whole process. You are always willing to talk with me during all hours of the night and that has been tremendously helpful. Finally, there is my brother and sister-in-law, Jeffrey and Doni. You are always great to talk to and I always enjoyed coming up to Kansas to visit you along with the non-human family of Clea, Delilah, Sampson, and Brody.

I want to thank my wife, Ilyse Kornblau. You have always been there for me and have always motivated me to do better than I thought I could. I am so happy you are in my life and I couldn’t ask for a better person to have by my side during my studies. I would also like to thank

Ilyse's family, Drs. Steven Kornblau and Abbey Berenson, for their love and support during this process. It is wonderful to know that I have you all for support and guidance.

Finally, I want to thank my canine companions who have helped me through this process. Lucky and Charlie, I know you won't be able to read this or know what is going on, but you both have always put a smile on my face. Thanks for always playing with me when I needed a break and for always providing much needed emotional support. Both of you have provided relief and happiness in a way no one else can.

Characterization of the role of the pKM101-encoded T4SS outer membrane core complex in substrate transfer, pilus biogenesis, and recipient cell contact

Jay Gordon, B.S.

Advisory Professor: Peter Christie, Ph.D.

The bacterial type IV secretion systems (T4SS) encoded on the *Escherichia coli* pKM101 and R388 conjugative plasmids and the *Agrobacterium tumefaciens* *virB* operon are composed of 12 subunits arranged in an architecturally similar fashion. Structural studies of the T4SS from R388 (Trw_{R388}) highlighted the presence of a distinct outer membrane core complex (OMCC) and inner membrane complex (IMC) joined together by a central stalk. This thesis is focused on the development of the pKM101 model system and the role of an OMCC cap region formed by alpha helical antenna projections (AP) found in VirB10 and TraF_{pKM101}. I introduced various internal deletions, truncations, and substitutions between TraF_{pKM101} and VirB10 to study the role of the AP cap in (i) substrate transfer to recipient plant or bacterial cells, (ii) pilus biogenesis and donor-specific bacteriophage sensitivity, and (iii) recipient cell contact. My results demonstrate that the C-terminal tails of VirB10 and TraF_{pKM101} are essential for DNA transfer and pilus biogenesis, whereas the AP domains are only important for pilus biogenesis. Neither of these domains is critical for recipient cell contact as monitored by sensitivity to *Pseudomonas aeruginosa* containing a functional type VI secretion system. Finally, I demonstrated that the IMC of pKM101 is able to functionally pair with the OMCCs from either VirB/VirD4, Trw_{R388}, or the Ptl T4SS of *Bordetella pertussis* restoring recipient cell contact and plasmid transfer. These results highlight the common ancestry between these functionally distinct machines and support a model where functionally independent IMCs and OMCCs have co-evolved to form the T4SS in Gram-negative bacteria.

Table of Contents

Approval Sheet.....	i
Title Page.....	ii
Acknowledgements.....	iii
Abstract.....	vi
Table of Contents.....	vii
List of Illustrations.....	xii
List of Tables.....	xiv
Abbreviations.....	xv
Chapter 1. Introduction	1
Introduction to Gram-negative bacterial type IV secretion systems	2
Type IV secretion systems are one of many dedicated macromolecular translocation systems in bacteria.....	2
Classification of T4SSs.....	10
Conjugative T4SSs.....	10
Protein translocation T4SSs.....	13
Substrate uptake and release T4SSs.....	14
Conjugation systems.....	15
Substrate processing.....	16
Substrate recognition.....	16
Translocation through the mating channel.....	19
T4SSs in <i>Agrobacterium tumefaciens</i>	20
T4SS subunit composition and function.....	24
The pKM101 plasmid.....	32

Contributions of T4SS subunits to channel assembly and functionality.....	35
VirD4.....	35
VirB4.....	37
VirB11.....	38
VirB3.....	39
VirB6.....	39
VirB8.....	40
VirB7.....	40
VirB9.....	41
VirB10.....	41
The conjugative pilus.....	44
T4SSs: Substrate channel vs. pilus assembly machines.....	47
The goals of my research.....	48
Chapter 2. Materials and Methods.....	53
Bacterial strains and growth and induction conditions.....	54
Plasmid modifications.....	69
Construction of pKM101 <i>tra</i> gene deletions.....	69
Construction of mini-pKM101 plasmids.....	70
Construction of pRP100 and pCGR108 variants and a mobilization plasmid.....	71
Construction of pKM101 complementing plasmids	73
Construction of <i>traF</i> alleles.....	75
Construction of chimeric operons.....	82
Construction of <i>traF</i> amber mutants for photocrosslinking.....	83
Construction of <i>A. tumefaciens</i> plasmids.....	87
Conjugation assays.....	93
Phage infection assays.....	94

Steady state level detection.....	94
<i>Pseudomonas aeruginosa</i> type VI killing assay.....	95
pBpa incorporation and UV crosslinking.....	95
Membrane solubilization and TraF purification.....	96
T-DNA transfer assays.....	96
Colony immunoblot (<i>Agrobacterium tumefaciens</i>).....	97
Colony immunoblot (<i>Escherichia coli</i>).....	97
Chapter 3: The role of the VirB10 GxxGxxG motif and antenna projection in T-DNA	
transfer and pilus biogenesis.....	98
Introduction.....	99
Results.....	106
Mutations in G269 and G272 attenuate T-DNA transfer into plant cells.....	106
The VirB10 AP is essential for pilus production, but not for	
substrate transfer.....	111
The structure of the <i>A. tumefaciens</i> VirB core complex resembles those	
of pKM101 and R388.....	114
Discussion.....	118
Model for the role of GxxGxxG and the AP domain.....	121
Chapter 4: Defining the Genetic Requirements for Plasmid Transfer and Phage	
Sensitivity through the pKM101-encoded type IV secretion system	125
Introduction.....	126
Results.....	130
Complementation of <i>tra</i> mutants in filter matings.....	130
Susceptibility of <i>tra</i> mutants to PRD1 and IKe bacteriophages.....	130
Complementation of <i>tra</i> mutants in broth matings.....	135
Complementation of <i>tra</i> mutants in mini-pKM101.....	136

Discussion.....	141
Contributions of TraC and KikA to pKM101 plasmid transfer.....	141
Contributions of TraL to pKM101 plasmid transfer and pilus biogenesis.....	142
Complementation of <i>tra</i> mutants for PRD1 and IKE infection.....	143
Transfer of pKM101 in broth matings.....	144
Chapter 5: Defining the role of a novel outer membrane alpha helical domain in pKM101-encoded TraF for plasmid transfer, donor-specific bacteriophage sensitivity, and recipient cell contact.....	145
Introduction.....	146
Results.....	155
The TraF AP is critical for phage sensitivity, but dispensable for plasmid transfer.....	155
The C-terminal domain of TraF is critical for both plasmid transfer and phage sensitivity.....	158
The N-terminal region of TraF does not tolerate substitutions of corresponding VirB10 domains.....	161
Neither the AP nor the C-terminal tail are surface displayed.....	165
Heterologous OMCCs paired with the pKM101 IMC support plasmid transfer.....	165
Neither the TraF AP nor C-terminal tail are required for recipient cell contact.....	171
Discussion.....	177
Contributions of the TraF AP to plasmid transfer and pilus biogenesis.....	177
Contributions of the TraF C-terminal tail to plasmid transfer and pilus biogenesis.....	178

The role of the TraF N-terminal half.....	180
Flexibility throughout Gram-negative bacterial T4SSs.....	180
Separation of the IMC from the OMC.....	181
Conclusions.....	182
Chapter 6: Summary and future directions.....	184
Summary.....	185
Remaining questions and future experiments.....	188
Do the TraF AP and C-terminal tail directly interact with pilin subunits TraM and TraC?.....	188
What is the role of the conserved GxxGxxG sequence?.....	202
How can phage sensitivity be restored to pKM101 deletion mutants?.....	203
What is the composition of the OM pore?.....	203
Are the IMC and OMC subassemblies functionally independent?.....	204
Which pKM101-encoded proteins are responsible for recipient cell contact?.....	205
Conclusion.....	210
References.....	211
Vita.....	225

List of Illustrations

Figure 1.1 Depiction of the type I through type VI secretion systems.....	5
Figure 1.2 Secretion of substrates through various bacterial secretion systems.....	7
Figure 1.3 The role of bacterial type IV secretion systems.....	12
Figure 1.4 Conjugative transfer of DNA to recipient cells.....	18
Figure 1.5 Plant cell infection by <i>Agrobacterium tumefaciens</i>	23
Figure 1.6 Positions of the T4SS subunits relative to the Gram-negative bacterial cell envelope...26	
Figure 1.7 Pathway of T-DNA through the <i>A. tumefaciens</i> VirB/VirD4 T4SS.....	29
Figure 1.8 Structure of the Trw _{R388} type IV secretion system along with localization of subunits...31	
Figure 1.9 The pKM101 plasmid.....	34
Figure 1.10 Structure of the pKM101 core complex.....	43
Figure 1.11 Pilus biogenesis in <i>Agrobacterium</i> and F-like pED208.....	46
Figure 1.12 Substrate versus pilus channel.....	50
Figure 3.1 Alignment of VirB10 and homologs.....	102
Figure 3.2 Location of the conserved GxxGxxG motif.....	104
Figure 3.3 Substitution of the conserved glycines.....	108
Figure 3.4 Effects of glycine belt mutations on T-DNA transfer and pilus biogenesis.....	110
Figure 3.5 Effects of AP FLAG tag insertion on T-DNA transfer and pilus biogenesis.....	113
Figure 3.6 Structure of the <i>A. tumefaciens</i> VirB core complex.....	117
Figure 3.7 Summary of phenotypes associated with GxxGxxG motif.....	120
Figure 3.8 Models for pilus biogenesis in <i>A. tumefaciens</i>	123
Figure 4.1 Layouts of the gene clusters encoding the VirB, Tra, and Trw T4SSs.....	128
Figure 4.2 Genetic requirements for plasmid transfer through the pKM101 T4SS.....	132
Figure 4.3 Restoration of PRD1 and IKe sensitivity.....	134
Figure 4.4 Plasmid transfer through the mini-pKM101.....	137

Figure 4.5 Enhancement of plasmid transfer through overexpression of <i>traL</i>	140
Figure 5.1 The OMC and its potential role in plasmid transfer.....	148
Figure 5.2 Plasmid transfer through the conjugative pilus.....	150
Figure 5.3 Similarities between the TraF and VirB10 AP and C-terminal domains.....	153
Figure 5.4 Functionality of TraF truncation mutants.....	157
Figure 5.5 Functionality of the TraF/VirB10 chimeras.....	160
Figure 5.6 Functionality of the TraF/VirB10 N-terminal chimeras.....	164
Figure 5.7 Surface display of TraF.....	167
Figure 5.8 Functionality of chimeric T4SSs.....	170
Figure 5.9 Measuring the ability of the chimeric T4SSs to form contacts with recipient cells	174
Figure 5.10 Determining the role of the TraF AP-CT in recipient cell contact.....	176
Figure 6.1 BS ³ crosslinking of TraF and TraC.....	191
Figure 6.2 pBpa incorporation into TraF.....	193
Figure 6.3 Mechanism of p-benzoyl-L-phenylalanine crosslinking.....	195
Figure 6.4 Locations of TraF pBpa incorporation.....	197
Figure 6.5 pBpa-mediated crosslinking of TraF.....	199
Figure 6.6 Sample preparation for mass spectrometry analysis.....	201
Figure 6.7 Schematic of TraJ/VirD4 _{Xac} periplasmic translocation assay.....	207
Figure 6.8 Xac2609 kills donor cells in a manner dependent on the presence of a functional T4SS.....	209

List of Tables

Table 2.1 Bacterial Strains.....	55
Table 2.2 <i>E. coli</i> vectors.....	56
Table 2.3 <i>E. coli</i> expression plasmids.....	56
Table 2.4 <i>A. tumefaciens</i> expression plasmids.....	60
Table 2.5 Native pKM101 deletion primers.....	61
Table 2.6 Inverse PCR deletion primers.....	62
Table 2.7 pKM101 gene cloning primers.....	62
Table 2.8 <i>traF</i> cloning primers.....	63
Table 2.9 <i>traF</i> amber mutant primers.....	65
Table 2.10 Mini-pKM101 primers.....	66
Table 2.11 <i>A. tumefaciens virB10</i> primers.....	67

List of Abbreviations

AAD: all alpha domain

ABC: ATP binding cassette

AHL: acylhomoserine lactone

AP: antenna projection

At: *Agrobacterium tumefaciens*

ATP: adenosine 5' triphosphate

BAM: β -barrel assembly machinery

BB: β -barrel

Bp: *Bordetella pertussis*

Cam: chloramphenicol

CFU: colony forming units

Crb: carbenicillin

CT: C terminus

DNA: deoxyribonucleic acid

Dtr: DNA transfer and replication

GFP: green fluorescent protein

GSP: general secretory pathway

HRP: horseradish peroxidase

ICE: integrative conjugative element

IM: inner membrane

IMC: inner membrane complex

Kan: kanamycin

LB: lysogeny broth

MFP: membrane fusion protein

MPF: mating pair formation

NBD: nucleotide binding domain

NT: N terminus

O-layer: outer layer

OD: optical density

OM: outer membrane

OMCC: outer membrane core complex

OMF: outer membrane factor

ORF: open reading frame

PAGE: polyacrylamide gel electrophoresis

pBpa: p-benzoyl-L-phenylalanine

PCR: polymerase chain reaction

PFU: plaque forming units

PRR: proline rich region

RNAP: RNA Polymerase

SCAM: substituted cysteine accessibility method

SD: soluble domain

SDS: sodium dodecyl sulfate

Spc: spectinomycin

T1SS: type I secretion system

T2SS: type II secretion system

T3SS: type III secretion system

T4SS: type IV secretion system

T4CP: type IV coupling protein

T5SS: type V secretion system

T6SS: type VI secretion system

TAT: twin arginine translocation

Tc: transconjugant

T-DNA: transfer DNA

Tet: tetracycline

Ti: tumor inducing

TM: transmembrane

Tn: transposon

TrIP: transfer DNA immunoprecipitation

UV: ultraviolet

WT: wild type

Chapter 1: Introduction

Introduction to the Gram-negative bacterial type IV secretion system

Bacteria constantly adapt to their changing environment. Although they are able to sense changes in their surroundings and adapt accordingly, many species acclimate to environmental shifts by delivering DNA and protein substrates through a type IV secretion system (T4SS). These substrates provide a selective advantage to the bacterium when environmental shifts are not favorable for survival. For example, DNA substrates often contain genes conferring resistance to antibiotics and heavy metals. Acquisition of these traits in clinically-relevant pathogens has led to an increase in resistance to most commercially-available antibiotics. Additionally, many pathogens contain altered T4SSs for delivery of important protein effectors during the course of infection. Organisms that utilize T4SSs for delivery of protein substrates, such as *Helicobacter pylori*, *Legionella pneumophila*, and *Bordetella pertussis* will be discussed later in this chapter (1–4).

These T4SSs can be divided into three classes: (1) Conjugation channels involved in the dissemination of DNA substrates to recipient prokaryotic cells (2) Protein translocation machines that deliver protein effectors to target eukaryotic cells (3) Substrate uptake and release T4SSs responsible for either taking up or releasing protein and DNA substrates into the extracellular milieu (5). Each of these three classes of T4SSs will be described in greater detail in this chapter.

Type IV secretion systems are one of many dedicated macromolecular translocation systems in bacteria

The T4SSs are one of six characterized secretion systems in Gram-negative bacteria. These secretion systems vary in terms of their overall architecture, subunit makeup, substrate repertoire, and target cell range. Below, I will briefly discuss each of the secretion systems.

The type I secretion systems (T1SSs) are found in pathogens, such as uropathogenic *Escherichia coli*, which utilize them to secrete monomeric protein effectors, such as the pore-forming toxin hemolysin A (6,7). T1SSs are architecturally the simplest of the dedicated secretion pathways, consisting of three components: (i) An inner membrane complex (IMC) formed by an ATP-binding cassette (ABC) transporter responsible for energizing the T1SS and substrate recognition, (ii) a Membrane Fusion Protein (MFP) that forms the inner membrane (IM) platform, and (iii) the TolC outer membrane factor (OMF) (6) (Figure 1.1). Substrates are recognized by the T1SS via a C-terminal signal sequence. Upon docking of a substrate with the ABC transporter/MFP complex, the entire inner membrane platform undergoes a conformational change that results in recruitment of TolC to the complex (7). In turn, ATP-mediated conformational changes open a channel enabling passage of the substrate across the cell envelope (Figure 1.2).

The type II secretion system (T2SS) is ancestrally related to the type IV pilus system used by other Gram-negative bacteria for surface adhesion and movement. As with the T1SSs, the T2SSs characteristically secrete toxins or other enzymes to the milieu (7). For example, *Vibrio cholerae* uses a T2SS to secrete the multisubunit cholera toxin during infection (6). There are four major components to the T2SS: (i) a cytoplasmic ATPase responsible for energizing the machine, (ii) an IM platform, (iii) an outer membrane pore-forming secretin, and (iv) a periplasmic pseudopilus (7,8). For secretion via this pathway, substrates are delivered to the periplasm via the general secretory pathway (GSP) or the twin arginine translocation (TAT) pathway. Substrates then fold and, in some cases, oligomerize. The folded substrates are then recruited to the T2SS, where they are thought to localize at the tip of a pseudopilus. Through a

Figure 1.1 Depiction of the type I through type VI secretion systems: Schematic illustrating the compositional and structural differences in Gram-negative bacterial secretion systems. Depicted are examples of RND multiefflux pumps dedicated to pumping out antimicrobial compounds, T1SS (uropathogenic *Escherichia coli*), T2SS (*Vibrio cholerae*), T3SS (*Salmonella* species), T4SS (*Agrobacterium tumefaciens*), and T6SS (*Pseudomonas aeruginosa*). This is Figure 1 in Costa TRD et al. *Secretion systems in Gram-negative bacteria: structural and mechanistic insights*. Nat Rev Microbiol. 2015;13:343–59. This figure was re-published with permission from Nature Publishing Groups. License number 4072830049272.

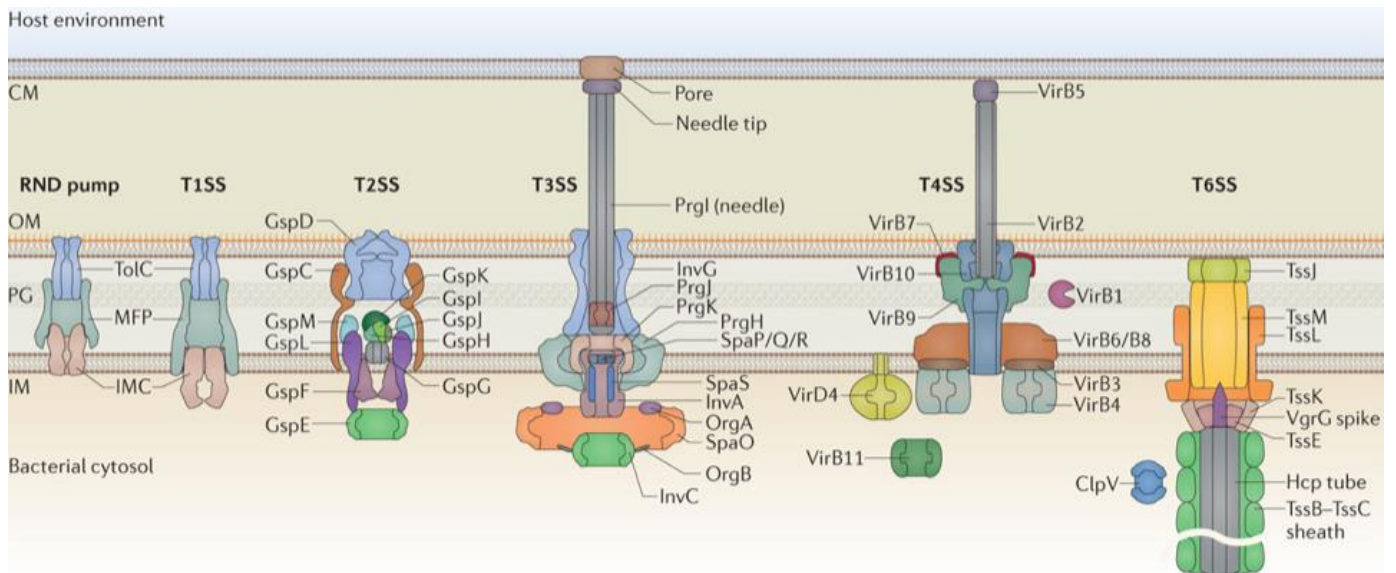
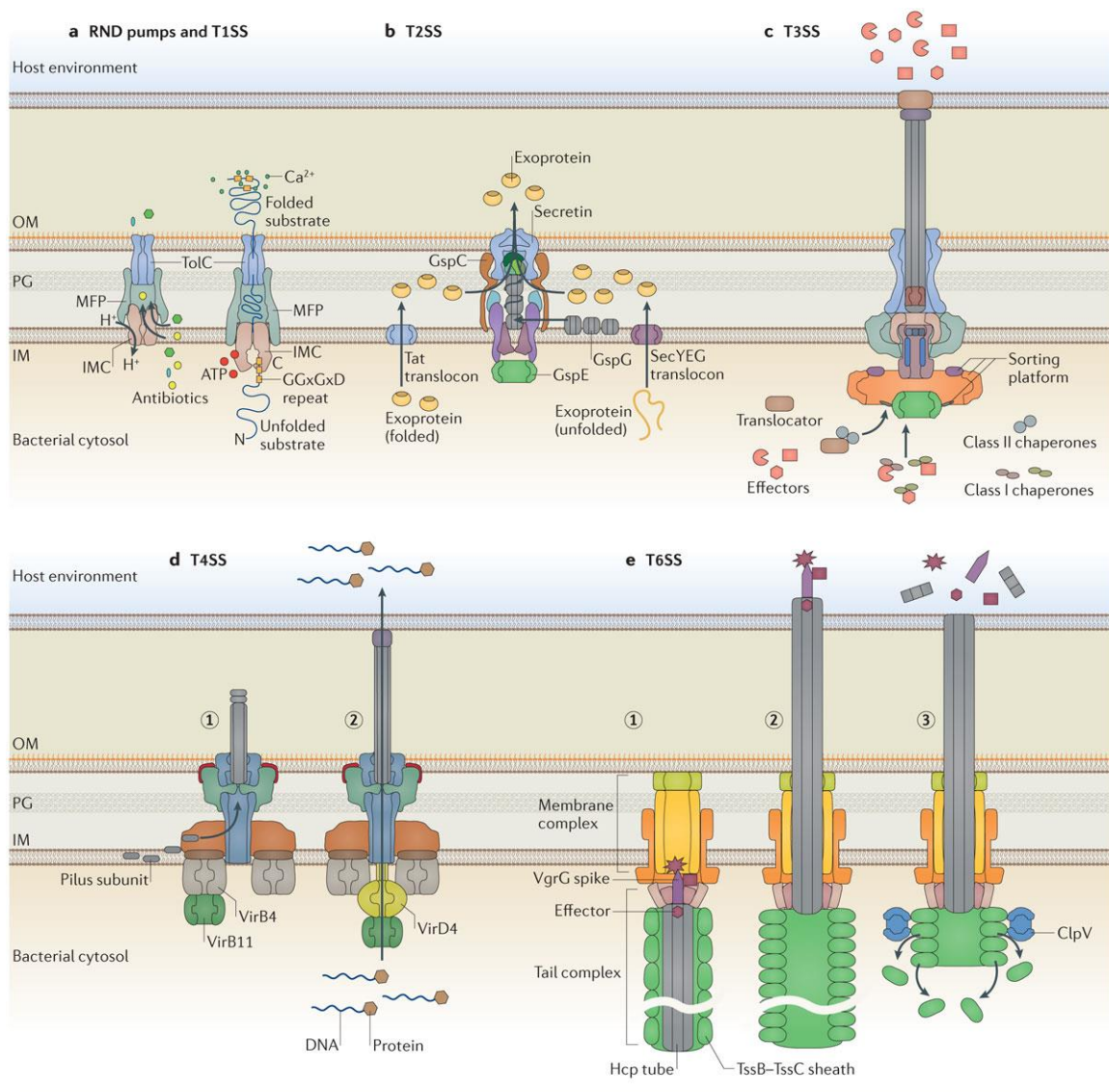


Figure 1.2 Secretion of substrates through various bacterial secretion systems.

Illustration of the substrate pathways outside of the cell. a) In RND pumps and the T1SS, substrates are recognized by the ABC transporter at the IM and shunted into the periplasm where they are then translocated outside of the cell by the TolC OM protein. b) Substrates of the T2SS are first moved into the periplasm either through the GSP or TAT pathways. They are then recognized by the OM secretin which mobilizes them into the extracellular milieu using force from the pseudopilus piston. c) T3SSs utilize a needle and translocon protein to form a pore in the target cell membrane. Substrates are then recognized by an N-terminal signal sequence followed by passage outside of the cell. d) T4SS substrates are recognized by the VirD4 substrate receptor and are then mobilized into the target cell in a contact-dependent manner (Discussed in more detail in this introduction). e) T6SS effectors are loaded into the hollow Hcp tube located in the cytoplasm. Upon activation, the TssB-TssC tail sheath will contract and move the tail and substrates outside of the cell. The VgrG spike protein will then puncture the target cell allowing for the effector and Hcp tube to enter. These illustrations are from Figure 3 in Costa TRD et al. *Secretion systems in Gram-negative bacteria: structural and mechanistic insights*. Nat Rev Microbiol. 2015;13:343–59.. This figure was re-published with permission from Nature Publishing Groups. License number 4072830049272.



piston-like extension and retraction mechanism, the pseudopilus is thought to push the substrate through the secretin pore to the cell exterior (Figure 1.2).

Type III secretion systems (T3SSs) are used by pathogens such as *Salmonella*, *Shigella*, and *Yersinia* species to inject effector proteins into eukaryotic cells. T3SSs can be divided into three functional components: (i) a basal body forming the cell envelope-spanning region of the complex, (ii) the hollow needle complex that allows for target cell contact and substrate passage, and (iii) translocon proteins at the tip of the needle (7,9). Interestingly, most of the proteins forming the basal structure are related to the proteins forming the base of the flagella system involved in motility. During secretion, needle tip and translocon proteins make contact with target cells and form a pore for substrate passage. Upon pore formation in the target cell, effector proteins are recognized by a non-cleavable N-terminal signal sequence and shunted through the T3SS into the target cell (Figure 1.2).

Type V secretion systems (T5SSs) are unique in that there is no membrane spanning channel. These systems are also known as autotransporters, since the protein being secreted mediates its own release (10). Autotransporters generally consist of a single polypeptide with two domains: (i) a C-terminal pore-forming β -barrel domain that inserts into the OM and (ii) an N-terminal passenger domain. Autotransporters are delivered into the periplasm via the GSP. Once in the periplasm, the autotransporter interacts with chaperones Skp or SurA, and the resulting complex is delivered to the β -barrel assembly machinery (BAM) at the OM. The BAM complex catalyzes the folding and insertion of the C-terminal β -barrel domain and also coordinates the surface exposure of the passenger domain. Passenger domains are either retained at the cell surface or released by proteolytic cleavage so that it is free to interact with target cells. One example of a clinically-relevant autotransporter is the *H. pylori* vacuolating toxin A (VacA),

which is involved in target cell pore formation (11,12).

Type VI secretion systems (T6SSs) are employed by Gram-negative bacteria to deliver toxic effector proteins to prokaryotic and eukaryotic target cells (13). One such example of a T6SS is the *Pseudomonas aeruginosa* H1-T6SS. This T6SS is activated upon membrane perturbation and delivers toxic effector proteins to neighboring prokaryotic cells. Utilization of this T6SS for determining requirements within the T4SS for recipient cell contact will be discussed later in this thesis. The T6SS is composed of two primary components: (i) a membrane spanning complex with components similar to the T4SS and (ii) a tubular structure that delivers the effectors to the recipient cell (14). The tubular structure is ancestrally related to contractile tails from bacteriophages. This tube can be further divided into three subcomponents: (a) a hollow tube comprised of the Hcp proteins, (b) a sheath made of TssB-TssC heterodimers, and (c) a VgrG spike protein (7). Once activated, the TssB-TssC sheath contracts in a similar manner to a phage tail. This contraction forces the Hcp tail protein and toxic effectors through the sheath to the cell surface and into target cells (Figure 1.2).

Of all the Gram-negative bacterial secretion systems, the T4SS is the most versatile. The secretion systems described above have evolved to secrete only protein monomers or heteromultimeric complexes. T4SSs are able to deliver both protein monomers (*H. pylori* CagA) and heteromultimers (*B. pertussis* Ptx AB toxin) (4,15). Many are also able to deliver DNA substrates to target cells. *Agrobacterium tumefaciens* and *L. pneumophila* utilize the VirB and Dot/Icm T4SSs, respectively, to deliver DNA or protein effectors to eukaryotic cells as a natural part of their infection processes. However, these systems also mobilize the transfer of the promiscuous IncQ plasmid RSF1010 to recipient prokaryotic cells, highlighting the plasticity of these systems with respect to substrate recognition (16,17). Because these effector translocation

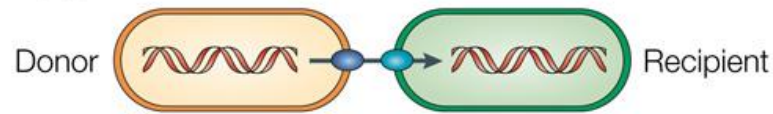
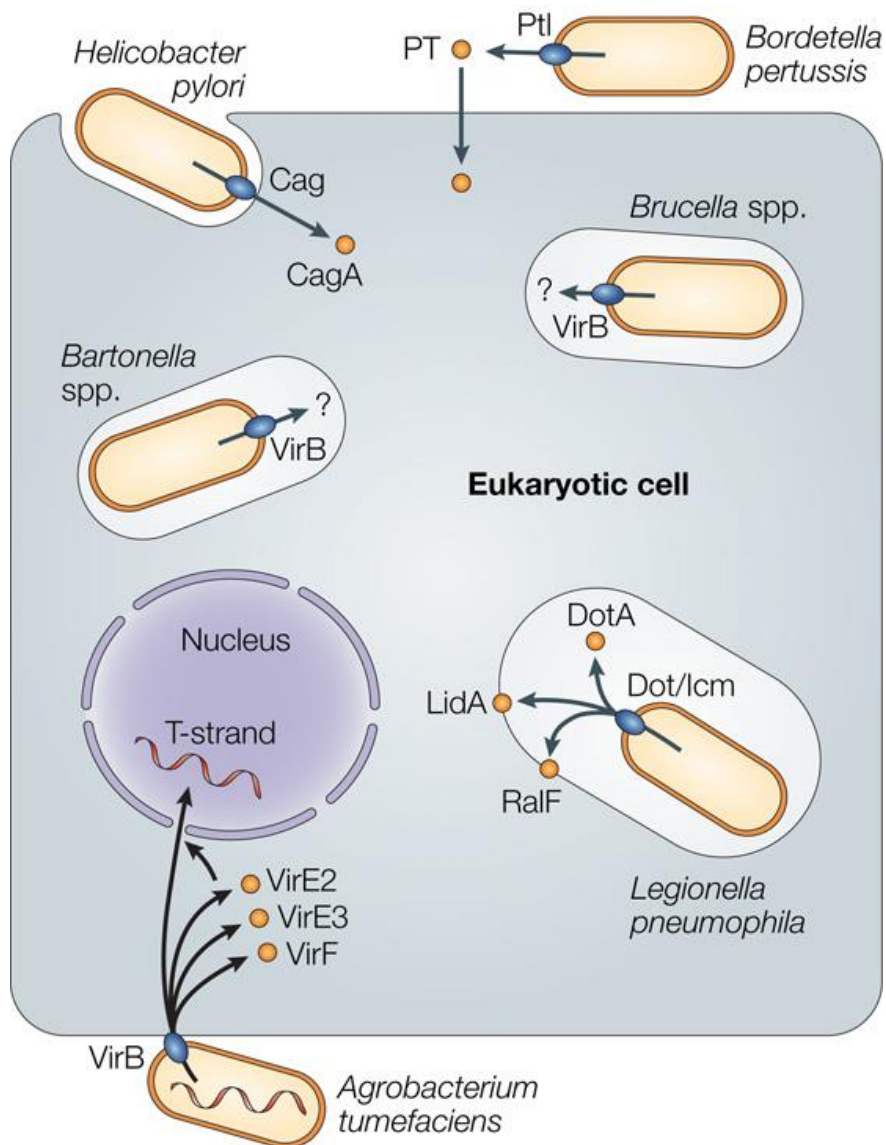
T4SSs are similar to their conjugative counterparts in subunit composition and operon structure, and several of these machines translocate both DNA and protein substrates, conjugative T4SSs likely evolved first as a means to exchange DNA among bacteria. Then, with the appearance of eukaryotic cells, these machines were adapted for specialized functions such as establishing commensal, symbiotic, or pathogenic relationships. Interestingly, all of the other dedicated secretion systems target either prokaryotic or eukaryotic cells. By contrast, T4SSs can utilize the same channel for substrate delivery into both types of cells. For example, *A. tumefaciens* utilizes its VirB/VirD4 T4SS to deliver oncogenic T-DNA and effector proteins to plant cells and also to mobilize the transfer of promiscuous IncQ plasmids to recipient bacterial cells (18–21). The details of the *A. tumefaciens* VirB/VirD4 T4SS will be described in more detail below.

Classification of T4SSs

There are three classes of Gram-negative bacterial T4SSs. These are a) conjugation systems b) effector translocation systems and c) substrate release and uptake systems (Figure 1.3). In this section, I will discuss each of the three classes in more detail.

Conjugative T4SSs: These are some of the better-studied T4SSs. They include proteins responsible for the dissemination of virulence traits and antibiotic resistance genes in clinical settings. Indeed, rapid horizontal transfer of mobile elements encoding multiple antibiotic resistance genes is threatening to jeopardize our ability to effectively treat many bacterial infections. These T4SSs are encoded on conjugative plasmids or integrative conjugative elements (ICEs; formerly known as conjugative transposons).

Figure 1.3 The role of bacterial type IV secretion systems. Schematic depicting the three different types of type IV secretion systems: a) Conjugations systems used to deliver plasmids from a donor cell to a recipient cell. b) DNA uptake and release systems used to exchange genetic information outside of the cell. c) Effector translocators used to deliver protein substrates into target eukaryotic cells. This is Figure 1 from “*The versatile bacterial type IV secretion systems.*” *Nature Reviews Microbiology* 1, 137-14; November 2003. This figure was re-published with permission from Nature Publishing Group. License # 4081060827678

a Conjugation**b DNA uptake and release****c Effector translocators**

Conjugative T4SSs can be divided into two functional sets of proteins. First, there are the mating pair formation (MPF) proteins, which assemble together to form the translocation channel (22). The MPF can be further divided into two subassemblies: (1) The membrane spanning complex and (2) the conjugative pilus at the cell surface. The second set of proteins is called DNA transfer and replication (Dtr) factors. These proteins process the DNA and localize it at the entrance of the MPF channel (23). The Dtr system consists of: (1) the conjugative relaxase that catalyzes a DNA nicking reaction required for transfer, (2) accessory factors that aid the relaxase in substrate processing and MPF localization, and (3) the substrate receptor, termed the type IV coupling protein (T4CP), which recognizes signals within the relaxase and accessory factors and delivers the substrate to the MPF channel.

Protein Translocation T4SSs: Many pathogens utilize the T4SS in order to translocate toxic effector proteins to target eukaryotic cells. There has been much effort spent trying to understand the role that these effectors play in the infection process. Developing new drugs to inhibit effector translocation and activity and vaccines against surface-localized T4SS proteins are important strategies in fighting these infections.

While conjugative T4SSs deliver both DNA and proteins related to DNA metabolism, protein translocation T4SSs only deliver protein substrates to their target cell (24). However, these machines are capable of translocating a wide variety of protein substrates. Although some translocation channels only have one recognized substrate, others can recognize and deliver hundreds of protein substrates. *H. pylori* utilizes the Cag T4SS to infect gastric epithelial cells. This system only recognizes and delivers one substrate, CagA, which is critical for *H. pylori* infection (15,25). However, the Dot/Icm T4SS from *L. pneumophila* delivers hundreds of protein effectors during the course of infection. Some of these important effectors include DotA

(prevents formation of phagolysosome) and RalF (promotes formation of a *Legionella*-containing vacuole using membranes from the endoplasmic reticulum) (26–28). The effect that these effectors have in target cells is an area of intense research to develop new strategies aimed at prevention and treatment of Legionnaire's Disease.

In addition to extracellular pathogens, many obligate intracellular organisms use a T4SS to deliver effectors to their hosts. These include *Anaplasma phagocytophilum* (human granulocytic anaplasmosis) and *Rickettsia rickettsii* (Rocky Mountain spotted fever) (29–31). Due to their inability to grow outside of a host cell, these pathogens have been difficult to study and genetically manipulate. Our lab has recently developed an assay system utilizing chimeric T4CPs to identify effector proteins (29). This assay will be discussed later in this chapter.

Substrate uptake and release T4SS: Although conjugative and protein translocation T4SSs require recipient-cell contact prior to substrate delivery, there are examples that secrete substrates outside of the cell in the absence of target cell interaction. One well-studied pathogen that utilizes this class of T4SS is *B. pertussis*. *B. pertussis* assembles the Ptl T4SS that is responsible for secretion of multimeric pertussis toxin. This channel does not contain a T4CP. Instead, individual toxin subunits are delivered into the periplasm through the GSP. Once in the periplasm, all the toxin subunits fold and assemble and then interact with the T4SS prior to extracellular release (32–36). Because there is no need for recipient contact, these cells lack detectable pili on the cell surface.

This class is also able to mediate the extracellular release of DNA. *Neisseria gonorrhoeae* contains a T4SS encoded on a large 57-kb gonococcal genetic island located on the chromosome. This machine is responsible for DNA release outside of the cell, which can serve

as a source of DNA for uptake by other *N. gonorrhoeae* cells through a process of natural transformation (37,38).

The *H. pylori* ComB T4SS is a unique example of a T4SS involved in DNA uptake. This system contains all of the homologs of the *Agrobacterium tumefaciens* VirB T4SS except VirB1 and VirB5 (15). This T4SS, however, is not essential for virulence as demonstrated during gerbil infection experiments.

The initial T4SS classification rubric assigned machines as F-like, P-like, or I-like based on their subunit similarity to T4SSs encoded by the F, RP4, or R64 plasmids, respectively. However, these systems can alternatively be broadly classified as type IVA or type IVB systems (T4SSA and T4SSB). T4SSA machines are similar to the *A. tumefaciens* VirB/VirD4 system and those encoded by the pKM101, R388, RP4 and F plasmids (P- and F-like systems). Studies of *L. phenumophila* identified genes on its chromosome that had similarities to those of the T4SS encoded on the IncI R64 plasmid (2,3). Although these loci encode a few proteins distantly related to subunits of the T4SSA systems, differences in genetic composition, gene order, and relatedness of homologs suggest a distinct phylogenetic origin. Consequently, these T4SSs were classified as T4SSB.

I will utilize the functional classification system for the remainder of this thesis, as the diversity in the T4SSs mentioned in my results section are best highlighted by their functional differences.

Conjugation systems

As mentioned above, the conjugation systems represent a major T4SS subfamily. Conjugative plasmids encode the necessary processing factors and T4SS channel for delivery of

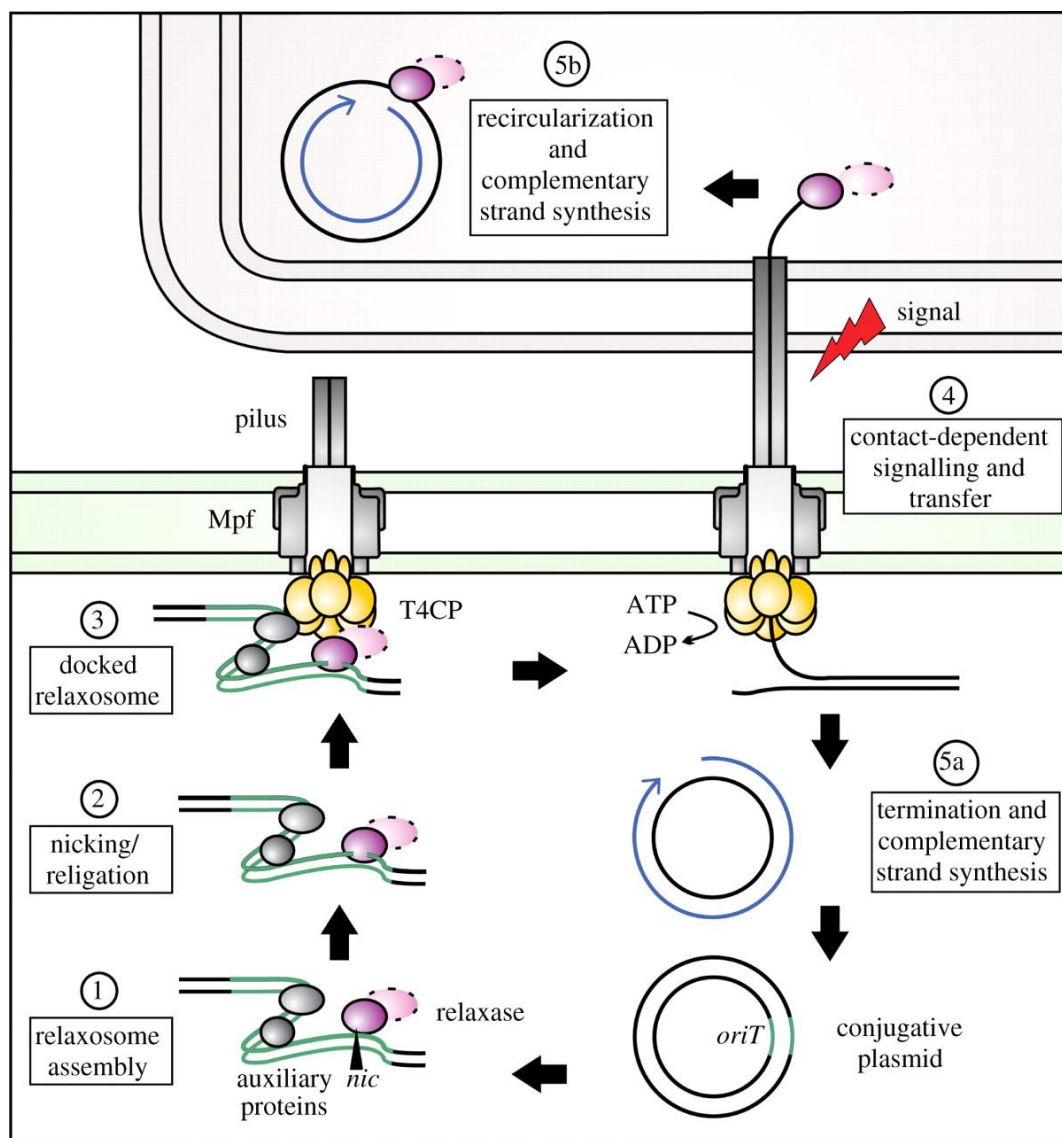
DNA substrates to target cells. Conjugative transfer can be divided into three steps: (i) substrate processing, (ii) substrate docking with the substrate receptor, also known as the type IV coupling protein (T4CP), and (iii) substrate transfer through the mating channel (Figure 1.4). Below, I will discuss each of these steps.

Substrate Processing: For this section, I will describe the events prior to DNA translocation through the *A. tumefaciens* VirB system. Preparation of the T-DNA substrates begins with the formation of the nucleoprotein complex termed the relaxosome. This complex consists of VirC1, VirC2, and VirD1. VirC1 is a member of the ParA family of proteins containing a canonical Walker A and B box (39). Members of the ParA family are localized to the cell pole and are responsible for plasmid segregation after DNA replication (40). VirC1 is a critical factor during the initiation steps of T-DNA transfer. VirC1, with the help of the VirC2 accessory protein, binds to a sequence adjacent to the right T-DNA border termed *overdrive* (41,42). Binding to this site results in the melting of the double-stranded DNA and recruitment of the VirD2 relaxase (Figure 1.4). VirD2 relaxase cleaves the T-DNA borders to initiate transfer of the T-DNA substrate through the T4SS. VirC1 recruits the relaxosome to the cell pole where the T4SS is located to begin transfer of T-DNA into the target plant cell.

Substrate recognition: The relaxosome possesses the signals for recognition by the substrate receptor or T4CP. In the *A. tumefaciens* VirB/VirD4 system, the VirD2 relaxase contains a cluster of positively charged residues at its C-terminus that mediate docking with the VirD4 receptor (43). Other internal signals and accessory factors, such as VirD1, VirC1, and VirC2, also contribute to docking of the relaxosome with VirD4 (39) (Figure 1.4).

Most Dtr proteins carry signals for docking only with a cognate T4CP/T4SS. Some Dtr proteins, however, appear to carry distinct types of signals enabling relaxosome docking and

Figure 1.4 Conjugative Transfer of DNA to recipient cells. Key events during conjugation. (1) The relaxase and other accessory factors gather at the *oriT* on the plasmid. (2) The relaxase catalytically nicks the plasmid at the *nic* site. The conserved active site Tyr residue covalently binds to the free 5' end of the nicked DNA. (3) Utilizing the relaxase translocation signal, the relaxosome docks at MPF with the T4CP. (4) Upon an unidentified signal, the relaxosome is shunted through the channel into the MPF. (5a) The free 3' end of the nicked strand of the conjugative plasmid primes second strand synthesis in order to re-create the double-stranded plasmid. (5b) The relaxosome inside the recipient cell will prime synthesis of a new DNA strand, leading to a new copy of the plasmid in the recipient cell. This is Figure 1 in Zechner EL et al. *Assembly and mechanisms of bacterial type IV secretion machines*. Philos Trans R Soc Lond B Biol Sci. 2012 367:1073–87. This article is an open-access article under the terms of The Creative Commons Attribution License.



subsequent transfer through many different T4SS channels. One prominent example of a promiscuous Dtr protein is the MobA relaxase encoded on plasmid RSF1010 (44). MobA, along with accessory proteins MobB and MobC, is able to mediate the transfer of RSF1010 through numerous T4SSs, including VirB_{At}, Tra_{pKM101}, Trw_{R388}, and Trb_{RP4} (16,21,45–48). MobA contains a cluster of positively-charged residues at its C-terminus similar to VirD2, which are important for mobilization through the VirB_{At} T4SS. However, MobA also contains additional signals within its N- and C-terminal regions, distinct from the positively-charged cluster that are important for mobilization through the RP4 plasmid-encoded T4SS (44). This combination of various signal domains throughout MobA likely contributes to its ability to recognize a multitude of T4CPs. MobB is a membrane protein that is predicted to act as a chaperone by coupling MobA to the T4CP (44). It is still unclear which regions of the T4CP are responsible for recognition of MobA.

Translocation through the mating channel: Upon engagement of the DNA substrate with the T4CP receptor, the substrate is delivered to other subunits of the T4SS for further processing and ultimately for transfer through the T4SS. As the transferred strand of DNA (T-strand) is unwound from its template and delivered through the T4SS, second-strand synthesis reconstitutes the mobile element in the donor cell. Similarly, when the T-strand is delivered to the recipient cell, it first re-circularizes and then undergoes second-strand synthesis for generation of a double-stranded, circular element which either replicates autonomously or inserts into the chromosome (Figure 1.4) (22). The transferred mobile element can reiteratively assemble a T4SS for further propagation to plasmid-free recipient cells.

T4SSs in *Agrobacterium tumefaciens*

The paradigm T4SS from *Agrobacterium tumefaciens* consists of 11 VirB proteins and a VirD4 T4CP, which is utilized to deliver oncogenic T-DNA into plant cells (5). This pathogen causes devastation of many agriculturally important crop species. Virulent strains of *A. tumefaciens* contain a large 194-kb plasmid termed the tumor-inducing plasmid (Ti plasmid) (49). Infection by the VirB/VirD4 system also requires protein effectors (VirE2, VirE3, and VirF), Dtr factors (VirC1, VirC2, VirD1, and VirD2), and a two-component regulatory system (VirA and VirG; See below) (39,43,50–57). Another Ti-encoded T4SS is the Trb machine, which is responsible for conjugative transfer of the Ti plasmid to *A. tumefaciens* recipient cells. This operon is similar in gene composition to the *trb* locus carried on the *E. coli* conjugative plasmid RP4, indicative of a common ancestry (58).

The VirB and Trb T4SSs are composed of similar sets of T4SS subunits and they are both able to transfer the promiscuous plasmid RSF1010 to *A. tumefaciens* recipient cells (49). However, there are notable differences between these two systems. The Trb T4SS does not contain a VirB8 homolog, which is important in the VirB system for T4SS localization, T-DNA transfer, and pilus biogenesis (59–67). Additionally, the VirB6 homolog in the Trb system, TrbL, has an extended soluble region at its C-terminus. TrbL is, therefore, part of the “extended VirB6” family (5). Similar proteins, such as TraG from F-plasmid, are important for mating pair stabilization and entry exclusion (discussed later) (68).

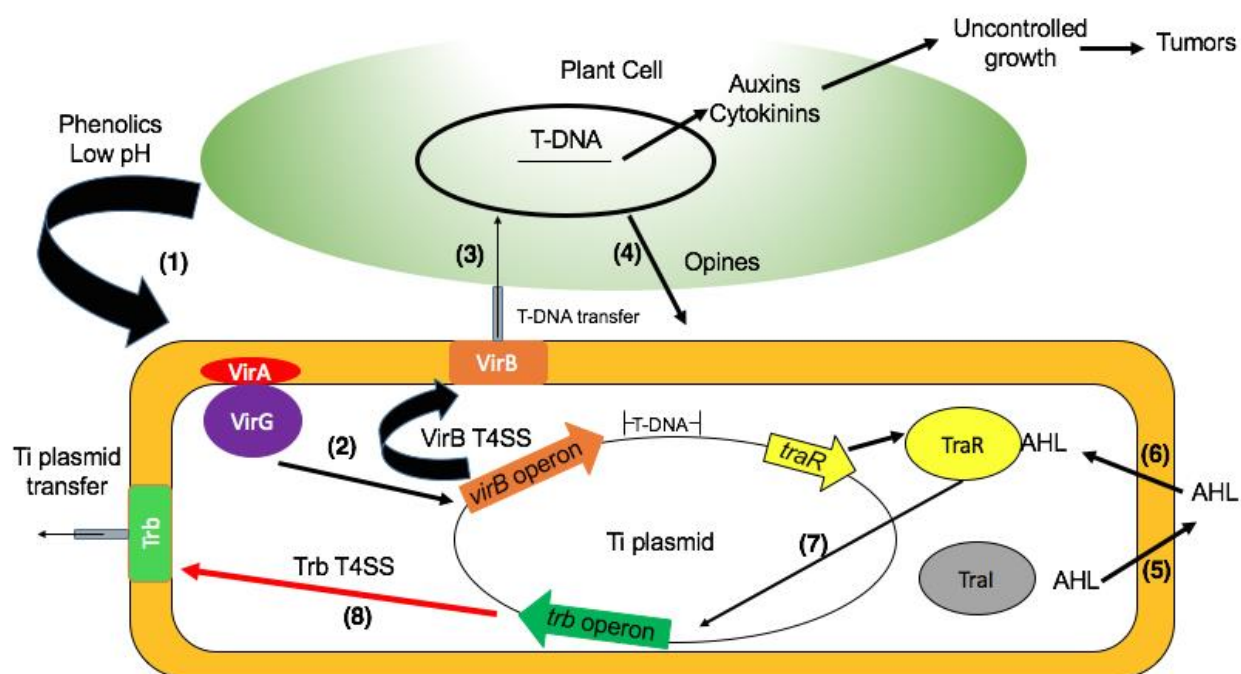
Once integrated into the plant cell genome, T-DNA gene products synthesize opines, which are small molecules that serve as important nitrogen and energy sources for the *A. tumefaciens* cells (49). Ti plasmids are often categorized based on the opine biosynthetic genes encoded on the T-DNA. Two of the primary Ti plasmids studied are the octopine pTiA6 and

nopaline pTiC58 plasmids. Although these plasmids contain similar VirB T4SSs, there is sequence variation between the different subunits. The Christie lab has utilized the pTiA6 plasmid for its studies.

Both VirB and Trb proteins are absent under non-inducing conditions. Upon wounding, plant cells release phenolic compounds, which are sensed by the membrane-bound VirA sensor kinase (69–71). VirA will autophosphorylate at a critical histidine residue followed by transferring of the phosphate group to an important aspartate residue on the cytoplasmic response regulator, VirG. Phosphorylated VirG will, in turn, activate transcription of genes in the *vir* regulon (Figure 1.5) (69). This initiates T-DNA processing and assembly of the VirB/VirD4 T4SS culminating in transfer of the oncogenic DNA substrate into plant cells. The VirB/T4SS system also translocates effector proteins, such as the VirE2 single-stranded DNA binding protein, to plant cells. Upon transfer, VirE2 binds the single-stranded T-DNA to protect it from host cell nucleases and transfers it to the plant cell nucleus (51). In the nucleus, the T-DNA integrates into the genome and T-DNA-associated genes are expressed. Once synthesized in the plant cell, opines are released from the cell where they can then be imported by *A. tumefaciens* (Figure 1.5).

Opines are not only useful as a nutrient source, but they can also serve as signaling molecules. The presence of high levels of opines induces the expression of Ti plasmid-encoded *traR* (Figure 1.5) (49,72). The product, TraR, is a transcriptional regulator that is activated in the presence of high concentrations of acylhomoserine-lactones (AHL). AHL is produced by Ti-encoded TraI and is secreted outside of the cell (Figure 1.5). When cell density is high, the concentration of AHL outside of the cell will increase as well. After reaching a threshold concentration, AHL will re-enter the cell and interact with TraR. This AHL-TraR interaction

Figure 1.5 Plant cell infection by *Agrobacterium tumefaciens*. An overview of the *A. tumefaciens* plant infection process is shown. Once a wounded plant secretes phenolic compounds, these are sensed by the VirA/VirG two-component signaling system (1). The VirG response regulator then activates expression of the *virB* operon (2). These proteins form the VirB T4SS, which will transmit T-DNA into target plant cells (3). Once T-DNA is in the plant nucleus, it leads to synthesis of opines, which are then secreted and taken up by the *A. tumefaciens* cells (4). Sensing of opines leads to opine metabolism and expression of *traR*. TraR is a transcriptional regulator that senses the presence of AHL. TraI is responsible for production of AHL, which is secreted outside of the cell (5). Once cell density rises and the extracellular concentration of AHL reaches a threshold, it re-enters the cell where it is detected by TraR (6). TraR then activates Ti plasmid replication and expression of the *trb* operon (7). The Trb T4SS then allows for the Ti plasmid to be mobilized into other *A. tumefaciens* cells.



will lead to activation of the *tra/trb* operon resulting in increased conjugative transfer frequencies of the Ti plasmid (Figure 1.5). Therefore, while the VirB/VirD4 and Trb T4SSs may serve different functions, their activation is tied to an abundant food source released by plant cells and high cell density.

T4SS subunit composition and function.

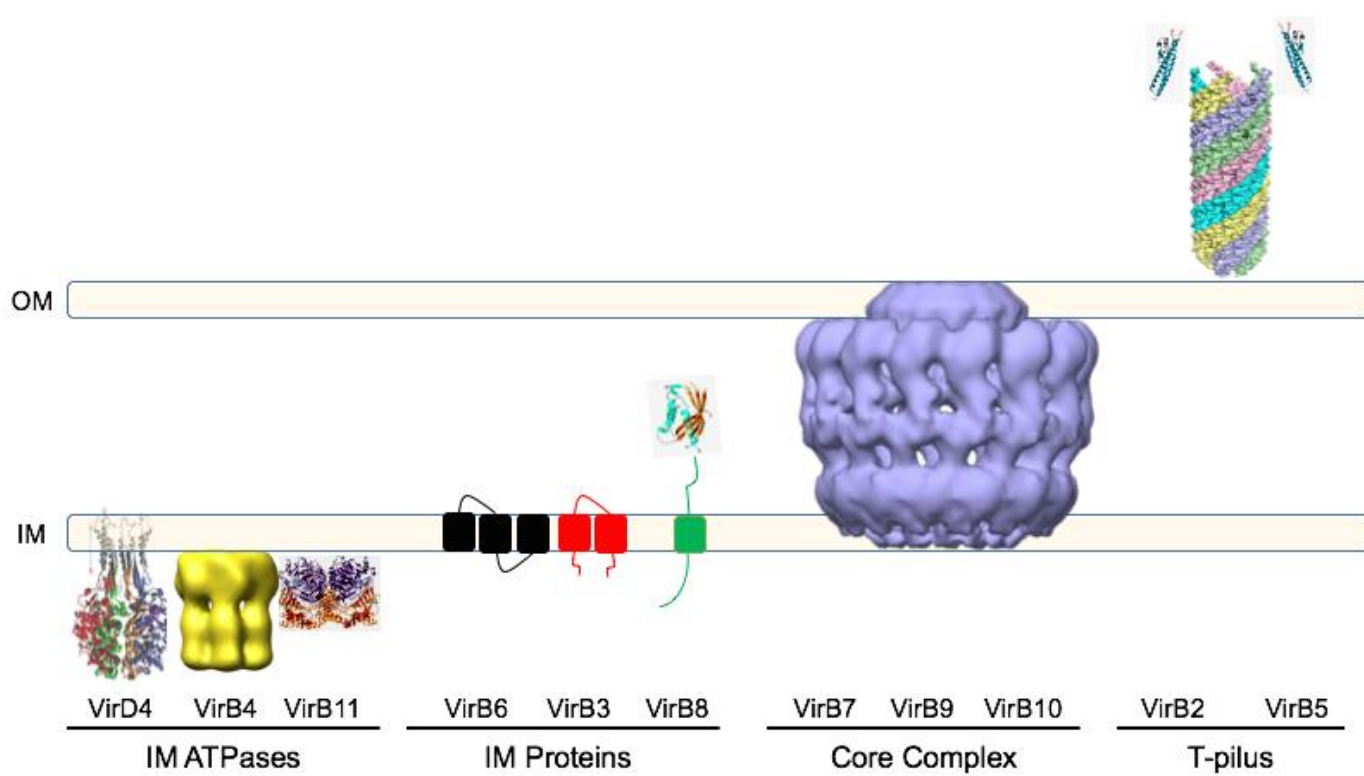
The *A. tumefaciens* VirB/VirD4_{Ti} system can be considered an archetypal T4SS. It contains homologs found in most other T4SSs. For the rest of this chapter, the VirB/VirD4 nomenclature will be used to describe the various subunits. The VirB/VirD4 system can be divided into different subsets of proteins: (i) The IM ATPases (VirD4 T4CP, VirB11, VirB4), (ii) the inner membrane complex (VirB3, VirB6, and VirB8), (iii) the outer membrane “core complex” (OMCC) (VirB7, VirB9, and VirB10), (iv) and a conjugative pilus (VirB2 and VirB5) (Figure 1.6) (73). Additionally, most Gram-negative bacterial T4SSs encode a cell wall hydrolase responsible for making localized degradations in the cell wall. Each of these subunits will be discussed in greater detail later in this chapter.

An important goal in the Christie lab has been to localize the T4SS within live cells and determine the genetic and biochemical requirements for its spatial positioning. Previous work involving fluorescent tagging of Vir subunits in *A. tumefaciens* has identified the cell pole as the primary point for machine assembly. GFP-tagged VirC1 was observed bringing the relaxosome to the cell pole (39). Additionally, our lab has observed polar localization during split-GFP fluorescence assays (50). Briefly, VirE2 was tagged with the N-terminal half of GFP (residues 1-157) while VirD4 was tagged with its C-terminal half (residues 158-238). Although neither of these two proteins is individually fluorescent, they form bright foci when produced in the same

Figure 1.6 Localization of the T4SS subunits relative to the Gram-negative bacterial cell envelope.

Arrangement of the different T4SS components including the IM ATPases (VirD4, VirB4, and VirB11), the IM proteins (VirB3, VirB6, and VirB8), the core complex (VirB7, VirB9, and VirB10), and a conjugative pilus (VirB2 and VirB5).

The structure of TrwB is Figure 2C from Gomis-Rüth FX et al. *The bacterial conjugation protein TrwB resembles ring helicases and F1-ATPase*. Nature 2001 409:637–41. This image was re-published with permission from Nature Publishing Group. License Number 4078401439237. The image of VirB4-like TrwK was derived from Figure 2C in Peña A et al. *The hexameric structure of a conjugative VirB4 protein ATPase provides new insights for a functional and phylogenetic relationship with DNA translocases*. J Biol Chem. 2012 287:39925–32. The American Society for Biochemistry and Molecular Biology does not require prior permission for re-publication of figures. The structure of the VirB11-like HP0525 was published as Figure 3C in Yeo HJ et al. *Crystal structure of the hexameric traffic ATPase of the Helicobacter pylori type IV secretion system* Mol Cell. 2000 6:1461–72. This image was re-published with permission from Elsevier. License Number 4078430588294. The structure of *Brucella suis* VirB8 was published in Terradot L, et al. *Structures of two core subunits of the bacterial type IV secretion system, VirB8 from Brucella suis and ComB10 from Helicobacter pylori*. Proc Natl Acad Sci U S A. 2005 102:4596–601. pKM101-encoded TraC was published in Yeo HJ, et al. *Structural and functional characterization of the VirB5 protein from the type IV secretion system encoded by the conjugative plasmid pKM101*. Proc Natl Acad Sci U S A. 2003 100:15947–52. No prior permission is required for reproduction of VirB8 or TraC. The structure of the F-pilus generated by electron microscopy was published as Figure 2A in Costa TRD, et al. *Structure of the bacterial sex F pilus reveals an assembly of a stoichiometric protein-phospholipid complex*. Cell 2016 166:1436–1444.e10. No prior permission from Elsevier is required for reproduction of this figure. The pKM101 core complex is figure 2A in Fronzes R, et al. *Structure of a Type IV Secretion System Core Complex* Science 2009 323:266–8. This figure was re-published with permission from The American Association for the Advancement of Science. License # 4113830881899.



cell, indicating that VirE2 interacts with VirD4 as full length GFP is reconstituted. As the green foci were localized to the cell pole, these data further validate previous observations with regards to machine assembly. Once the T4SS is localized within the cell, the requirements for localization can be uncovered using various deletion mutants and the structure of the channel in intact cells can be resolved using high-resolution electron microscopy.

Another major breakthrough in our lab's studies of the VirB/VirD4 T4SS was the definition of T-DNA translocation pathway. Eric Cascales, a former postdoctoral researcher in the Christie lab, developed the Transfer DNA Immunoprecipitation (TrIP) Assay to specify the route of T-DNA (74). In this assay, *A. tumefaciens* cells were incubated in the presence of inducing phenolic compounds followed by treatment with formaldehyde to crosslink T-DNA to the channel components. After membrane isolation and solubilization, VirB proteins were immunoprecipitated and tested for associated T-DNA.

As predicted based on previous findings, T-DNA first makes contact with the VirD4 substrate receptor. The T-DNA is then shunted to the VirB11 ATPase followed by the VirB6 and VirB8 IM proteins. Finally, T-DNA is translocated to the OM with assistance from the OM-associated VirB9 subunit and the VirB2 pilus protein (Figure 1.7). One striking observation was the ability to uncouple proteins in the IM from those in the OM. Deletion of genes such as *virB2*, *virB9*, and *virB10* still allowed for stable DNA contacts with the IM ATPases and the VirB6 and VirB8 IM proteins, but abolished any contacts with OM proteins. These data supported a "Two-Subassembly" model for the T4SS, in which IM proteins function to deliver substrates across the IM independently of the OMCC. This model was further supported by the structure of the Trw_{R388} VirB3-VirB10 structure, which shows a clear demarcation between IM and OM proteins (Figure 1.8).

Figure 1.7 Pathway of T-DNA through the *A. tumefaciens* VirB/VirD4 T4SS. The pathway of T-DNA through the T4SS is shown with a red arrow. T-DNA has been demonstrated to interact with VirD4 and VirB11 in the cytoplasm, VirB6 and VirB8 at the inner membrane, and VirB2 and VirB9 at the outer membrane.

The structure of TrwB is Figure 2C from Gomis-Rüth FX et al. *The bacterial conjugation protein TrwB resembles ring helicases and F1-ATPase*. Nature 2001 409:637–41. This image was re-published with permission from Nature Publishing Group. License Number 4078401439237. The structure of the VirB11-like HP0525 was published as Figure 3C in Yeo HJ et al. *Crystal structure of the hexameric traffic ATPase of the Helicobacter pylori type IV secretion system* Mol Cell. 2000 6:1461–72. This image was re-published with permission from Elsevier. License Number 4078430588294. This image was re-published with permission from Elsevier. License Number 4078430588294. The structure of *Brucella suis* VirB8 was published in Terradot L, et al. *Structures of two core subunits of the bacterial type IV secretion system, VirB8 from Brucella suis and ComB10 from Helicobacter pylori*. Proc Natl Acad Sci U S A. 2005 102:4596–601. No prior permission is required for reproduction of VirB8. The pKM101 core complex structure is Figure 4 from Fronzes R, et al. *The structural biology of type IV secretion systems*. Nat Rev Microbiol. 2009 7:703–14. This image was re-published with permission from Nature Publishing Group. License # 4092681298982.

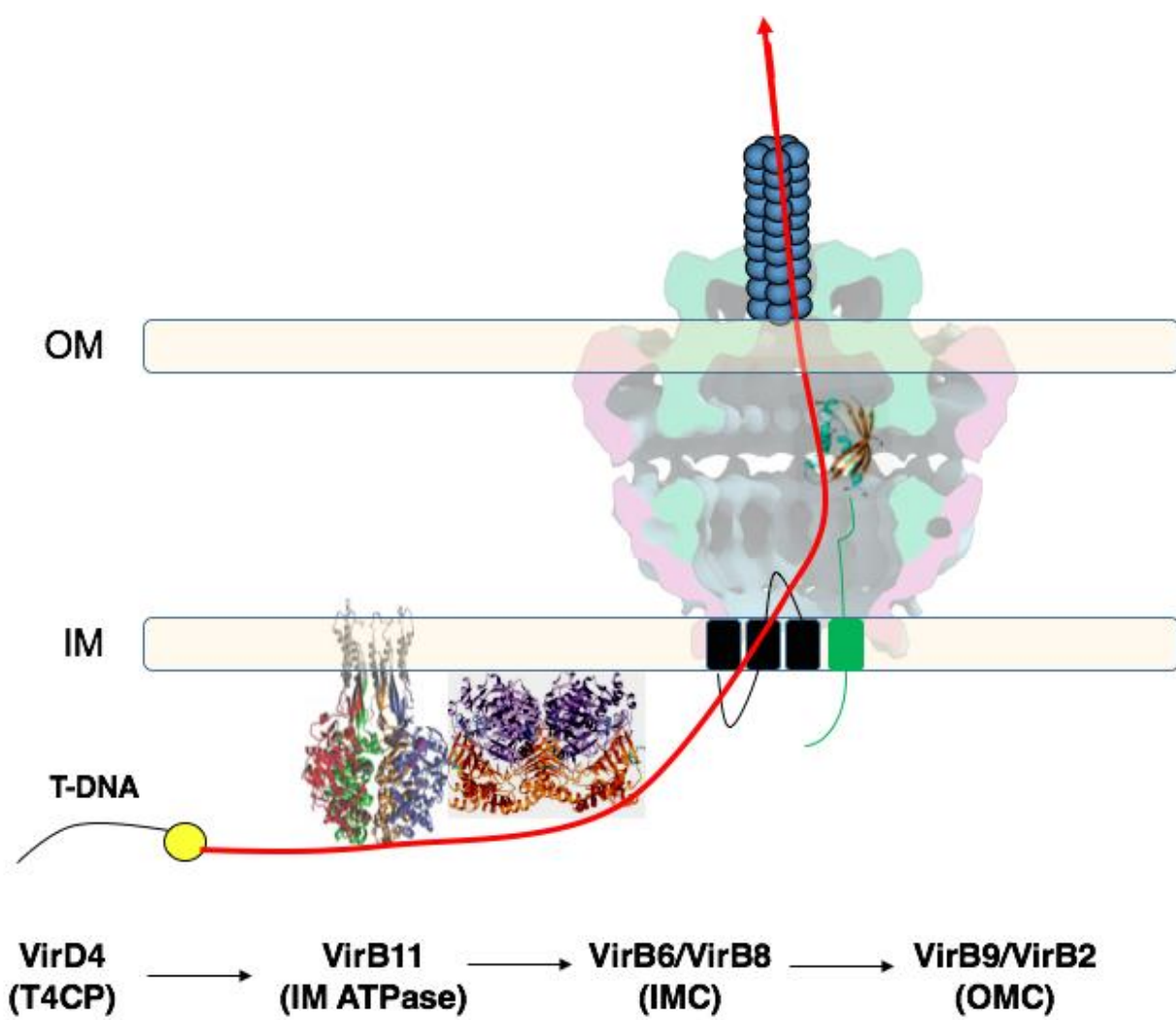
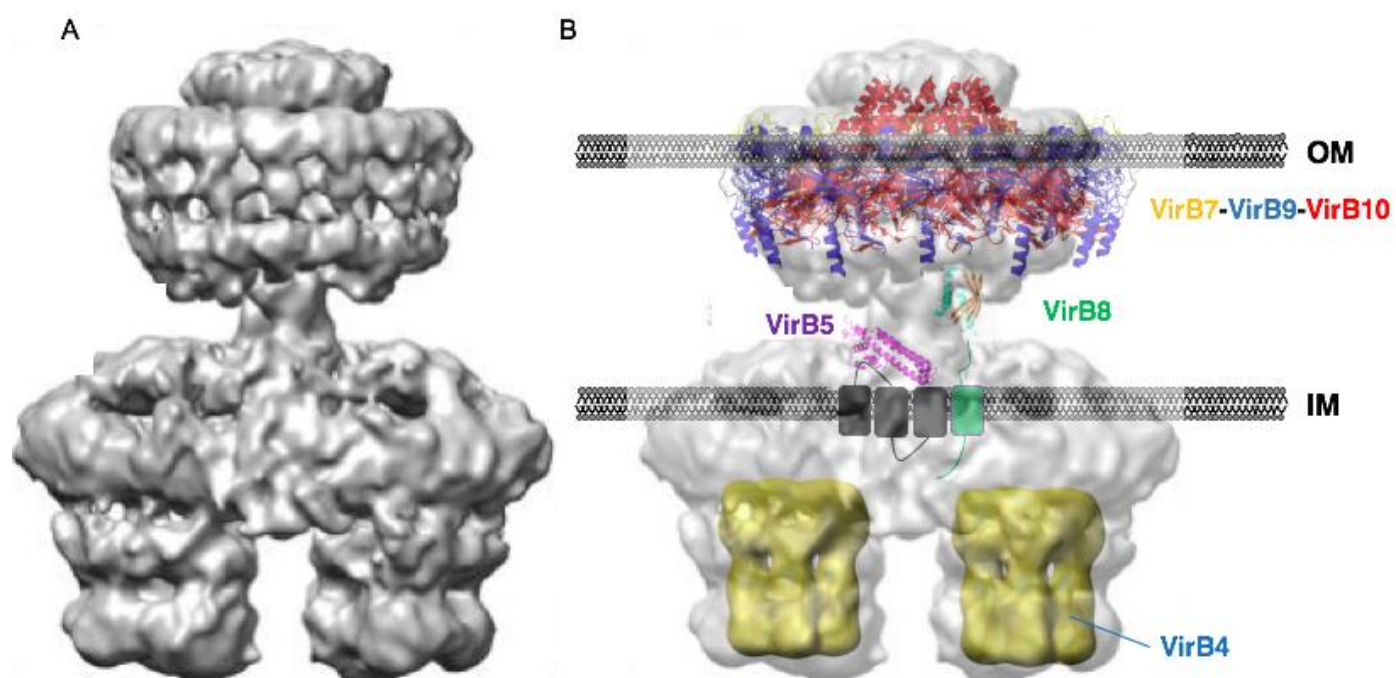


Figure 1.8 Structure of the Trw_{R388} type IV secretion system along with localization of subunits. (A) Structure of the Trw_{R388} TrwM/VirB3-TrwE/VirB10 structure generated by the Waksman laboratory. (B) Localization of a subset of subunits including VirB4 (blue; structure of VirB4 from plasmid R388), VirB8 (structure of VirB8 periplasmic domain from *Brucella suis*), and the VirB7-VirB9-VirB10 outer membrane complex (yellow, blue, and red; structure of the TraN-TraO-TraF outer membrane complex from pKM101).

The image of VirB4-like TrwK was derived from Figure 2C in Peña A et al. *The hexameric structure of a conjugative VirB4 protein ATPase provides new insights for a functional and phylogenetic relationship with DNA translocases*. J Biol Chem. 2012 287:39925–32. The American Society for Biochemistry and Molecular Biology does not require prior permission for re-publication of figures. The structure of *Brucella suis* VirB8 was published in Terradot L, et al. *Structures of two core subunits of the bacterial type IV secretion system, VirB8 from Brucella suis and ComB10 from Helicobacter pylori*. Proc Natl Acad Sci U S A. 2005 102:4596–601. pKM101-encoded TraC was published in Yeo HJ, et al. *Structural and functional characterization of the VirB5 protein from the type IV secretion system encoded by the conjugative plasmid pKM101*. Proc Natl Acad Sci U S A. 2003 100:15947–52. No prior permission is required for reproduction of VirB8 or TraC. The structure of the TraN-TraO-TraF heteromultimer was generated using pymol (<http://pymol.org>) based on the 3ZBI file deposited into the NCBI protein database. The structure of the R388 core complex is Figure 2A from Low H, et al. *Structure of a type IV secretion system* Nature 2014 508:550–3. This figure was re-published with permission from Nature Publishing Group. License #4113871389804.

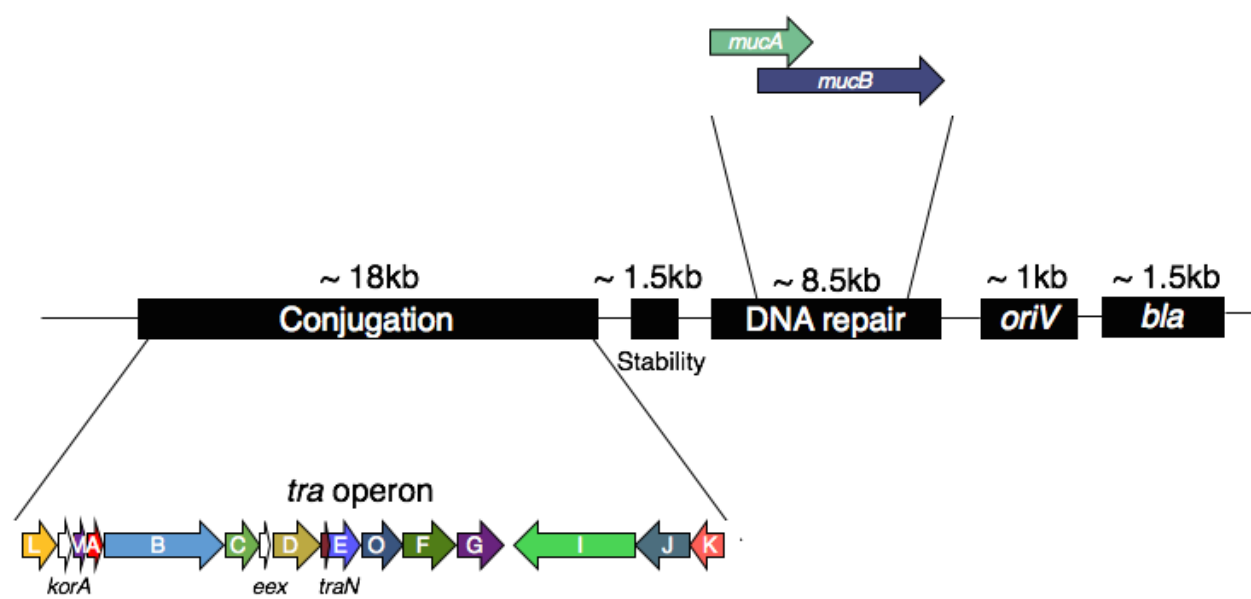


The pKM101 plasmid

pKM101 has historical significance for its use in the Ames test (75) for detection of mutagens. One of the hallmark features of the pKM101 plasmid is the presence of two genes, *mucA* and *mucB*, which are under the control of a LexA repressor (Figure 1.9) (76). The proteins encoded by these genes, MucA and MucB, form an error-prone DNA polymerase which, similar to the DNA polymerase involved in the SOS response, incorporates many mutations into the bacterial chromosome and can even synthesize DNA across double-stranded breaks (77–81). Besides antibiotic resistance, this plasmid provides the cell with a greater ability to survive exposure to UV light and other mutagenic compounds. For this reason, *Salmonella* containing pKM101 was chosen as the strain for use in the Ames test (75).

Recently, structural studies described an overall architecture for the distal portion of pKM101-encoded T4SS (82,83). Importantly, this T4SS is highly related to other systems, such as the VirB/VirD4_{Ti} and Trw_{R388} T4SSs (82–85). The respective *tra/virB/trw* gene clusters are similar in size and are composed of genes encoding functional homologs. Although the sequence identities among homologs of these systems range from 20% to 40%, there have been demonstrated instances of cross-complementation between them. For example, pKM101 deleted of its region encoding the Dtr proteins (TraK, TraJ, and TraI) is complemented by the corresponding proteins from R388 (TrwA, TrwB, and TrwC) (86). The TrwB substrate receptor, therefore interacts productively not only with the R388 relaxosome, but also with the pKM101-encoded channel. Furthermore, the TraC_{pKM101} pilin subunit partially restores pilus biogenesis when produced in an *A. tumefaciens* $\Delta virB5$ mutant (87). Additionally, complementation of a $\Delta virB6$ mutant with *traD* leads to release of VirB2 and VirB5 to the extracellular environment (88). Finally, expression of *TraL*_{pKM101} partially complements a $\Delta virB1$ mutation in

Figure 1.9 The pKM101 plasmid. A linear layout of the pKM101 plasmid depicting the regions of interest on the plasmid. The *tra* operon is shown associated with the conjugation-encoding region of the plasmid. Additionally, the genes encoding MucA and MucB are depicted in the region associated with DNA damage repair. Other regions of interest include the origin of replication (*oriV*) and beta-lactamase (*bla*).



A. tumefaciens (89). These results highlight a common ancestry between these three systems, which will be explored in further detail throughout this thesis.

The Waksman lab has solved structures of both the Tra_{pKM101} and Trw_{R388} OMCCs (82,85,90). Both subassemblies are composed of 14 copies of homologs of the *A. tumefaciens* VirB7, VirB9, and VirB10 subunits arranged as a 1 MDa tetradecameric structure. Both OMCCs are similar in their overall size of 180Å in width and height. The Waksman lab also solved a larger Trw_{R388} substructure composed of the OMCC joined to the IMC. The IMC is a 2.5 MDa structure that contains leg-like structures consisting of two hexamers of VirB4 homologs. These hexamers are attached to an IM platform composed of 12 copies each of homologs of VirB3, VirB5, and VirB8 and 24 copies of a VirB6 homolog. This IMC is connected to the OMCC by a thin central stalk. The IMC and OMCC are two distinct complexes (Figure 1.8). Along with the data from the TrIP assay in *A. tumefaciens*, these findings suggest the possibility that the T4SS is composed of two functionally independent subassemblies.

Contributions of T4SS subunits to channel assembly and functionality

Although subunit composition across Gram-negative bacterial T4SSs can vary, many resemble that of the type IVA system from *A. tumefaciens*. Below, I will discuss each of the subunits in detail. I will use the VirB/VirD4 nomenclature for each of the subunits unless otherwise specified.

VirD4: VirD4 serves two important roles during secretion: (i) Substrate recognition and delivery to the MPF and (ii) IM ATPase activity. This family of proteins can be divided into three domains: an N-terminal transmembrane domain, a nucleotide binding domain (NBD), and

an all-alpha domain (AAD). The crystal structure of the TrwB_{R388} soluble domain (SD; NBD and AAD) depicts a ball-structure 110Å in diameter and 90Å in height with a 20Å central channel (91). Together with the TM domain, the structure of VirD4 contains a “ball and stem” structure similar to the F₁F₀ ATPases. These proteins are also structurally related to the FtsK and SpoIIIE double-stranded DNA pumps found in *E. coli* and *Bacillus* species respectively, leading to a proposed model of VirD4 pumping DNA through its central channel (92–94).

The VirD4 N-terminal domain is located in the first 87 residues and is important for anchoring the SD into the membrane. The Llosa laboratory demonstrated that the TM domain of TrwB_{R388} was necessary for associations with the rest of the channel, particularly with the VirB10 homolog, TrwE (95). While deletion of the TM domain would abolish transfer in most T4SSs, there are unique T4CPs that contain separate TM domains. One notable example is Orf10 from the *Streptococcus agalactiae* pIP501 conjugative plasmid (5,96). A small open reading frame (ORF) upstream of *orf10* encodes a protein with transmembrane helices. Introduction of a frameshift mutation near the end of this small ORF restored an architecture similar to VirD4, indicating that these peculiar T4CPs arose from previous frameshift mutations. Interestingly, some SDs can still retain attenuated functionality when the TM is deleted. The TcpA T4CP from the *Clostridium perfringens* pCW3 plasmid is still able to transfer DNA in the absence of a TM domain (5). These results suggest that the SD is able to associate with the T4SS, likely using contacts with IMC subunits.

The NBD contains a canonical Walker A box (GxxxxGK(T/S)). It is the region most similar to the FtsK and SpoIIIE DNA pumps. The AAD consists of seven alpha helices and bears structural resemblance to the XerD recombinase (5). The Christie lab has demonstrated that SD is primarily involved in substrate recruitment and recognition. When the SD of VirD4

was fused to the DivIVA polar localization protein, VirE2 was then localized at the cell poles (50). Recent work in our lab, however, has focused on substrate recognition. Neal Whitaker and Trista Berry, both former members of the Christie lab, made chimeric T4CPs containing the N-terminal TM domain of TraJ_{pKM101} and the SD from other VirD4s, including those from *A. tumefaciens*, *A. phagocytophilum*, and *Wolbachia pipientis*. These chimeric T4CPs lost their ability to transfer pKM101, but were able to transfer heterologous protein substrates from their respective T4SSs (29). These results highlighted a common ancestry between T4CPs from both conjugative and effector T4SSs as well as the conservation of functionality for all of the different SDs. However, the exact mechanism of substrate recognition by the T4CP remains unclear. Previous work from our lab using the VirB/VirD4_{Ti} and Prg/Pcf_{pCF10} systems suggests that the AAD at the base of the SD is responsible for substrate recognition (97). Dr. Yang “Grace” Li, a current member of the Christie lab, is currently using unnatural amino acid photocrosslinking, a technology that will be discussed later in this thesis, to identify amino acids in TraJ_{pKM101} which are responsible for recognition of the TraI_{pKM101} relaxase.

VirB4: VirB4 is a universally important IM ATPase among T4SSs in both Gram-negative and Gram-positive bacteria. It is a large protein >80kDa in size and contains both a Walker A and Walker B box for ATPase activity. The Walker A domain has been demonstrated to be important for substrate transfer in the VirB/VirD4_{Ti} and Trw₃₈₈ T4SSs (98–101). Despite being important for transfer, the TriP assay did not detect an interaction between T-DNA and VirB4. However, some evidence suggests that there may be an interaction despite these previous results. The structure of VirB4 C-terminal domain from *Thermoanaerobacter pseudethanolicus* was solved by X-ray crystallography and appeared structurally similar to Trw_{BR388} (91,102). Additionally, the VirB4 homolog in the *Enterococcus faecalis* Prg/Pcf T4SS, PrgJ, was bound to

substrates as this system does not contain a VirB11 protein (103). This is likely the case in other Gram-negative bacterial T4SSs, such as the F-plasmid, that also do not contain a VirB11 homolog.

The VirB4 subunit has also been implicated as an important player in pilus biogenesis. Studies by the Christie lab highlighted conformational changes in VirB2 pilin subunits induced by VirB4 using the substituted cysteine accessibility method (SCAM) (104). SCAM was also used to demonstrate that VirB4 mediates pilin subunit dislodging from the IM as Cys residues located in the cytoplasm were labeled in the presence of VirB4 indicating movement of the pilin subunit into the periplasm. It is not known at this time if pilin subunits come into direct contact with VirB4. Using unnatural amino acid photocrosslinking, future studies will address a potential VirB4-VirB2 interaction as well as the genetic requirements for this interaction.

VirB11: The VirB11 family of ATPases form a double-ringed hexamer with the N-terminal ring associated with the inside leaflet of the IM and the C-terminal ring forming a tight constriction in the cytoplasm (105). VirB11 contains Walker A and B boxes in its N-terminal ring which is used to power the channel. The TrIP assay demonstrated close contacts between T-DNA and VirB11 during substrate transfer with deletions of *virB11* blocking movement to the IMC (74). Because substrates going through the T4SS are unfolded prior to translocation, VirB11 is predicted to be the “unfoldase” preparing protein substrates for movement into the channel. This prediction is also supported by work from the Galan laboratory in which they demonstrated that InvC, a VirB11-like protein, unfolded substrates prior to translocation through a *Salmonella* T3SS (106). In addition to directly interacting with substrates, VirB11 is also an important ATPase for powering translocation across the OM. VirB11 ATPase activity, along

with that of VirD4, is important for switching VirB10 into an active conformation (107). It is likely that VirB10 acts as an energy transducer and activates proteins in the OM. (see below)

Additional work in our lab highlighted the importance of VirB11-mediated conformational changes in VirB2 using SCAM (104). These results have led to a model suggesting VirB11 acts as a “Traffic ATPase”. VirB11 will associate with VirB4 in order to aid in pilin subunit release from the IM during pilus biogenesis and will then associate with VirD4 and VirB10 during substrate transfer (106).

VirB3: VirB3 is a small peptide containing two TM domains placing the N and C termini in the cytoplasm. VirB3 is not very well characterized, but its importance in T-DNA transfer and pilus biogenesis has been well demonstrated. Interestingly, the placement of the *virB3* gene directly upstream of the *virB4* is seen in other operons encoding T4SSs (5). VirB4 has been shown to be critical for VirB3 stability in *A. tumefaciens* and this might be the case in other systems. In addition to VirB4, VirB3 also requires VirB2, VirB7, and VirB8 for stability (109). However, how these proteins maintain proper levels of VirB3 is still unknown.

VirB6: VirB6 is a polytopic IM protein which comprises an integral part of the IMC (5,110). VirB6 is part of the translocation route for T-DNA across the IM as it makes close contact with the substrate (110). The VirB6 protein family can be divided into two categories: (i) Non-extended VirB6 and (ii) extended VirB6. VirB6_{Ti} and TraD_{pKM101} are examples of non-extended VirB6 proteins as they only contain TM helices along with short cytoplasmic and periplasmic tails. VirB6 proteins classified as ‘extended-VirB6’s’, by contrast, contain large, soluble domains at their C-terminal ends. This domain in TraG_F was shown to interact with entry exclusion (Eex) proteins in the IM of the target cell (68). Thus, the soluble C-terminal extension could either stretch into the target cell or a C-terminal fragment derived by protease

cleavage could be delivered into the target cell to exert its inhibitory function in donor-donor cell contacts.

VirB8: VirB8 is a bitopic protein found in most Gram-negative T4SSs. It contains a short cytoplasmic N-terminal tail, a TM domain, and a large periplasmic domain consisting of extended beta sheets and five alpha helices. This arrangement has been observed with the structures of VirB8 homologs including VirB8_{*B. suis*}, TcpC_{pCW3}, VirB8_{*B. henselae*}, and TraE_{pKM101} (111–114). VirB8 is important for T-DNA transfer as it makes contacts with T-DNA going across the IM and it has been demonstrated to make contact with VirB5 during pilus biogenesis in *A. tumefaciens*. Additionally, VirB8 has been postulated to act as a nucleation factor. The Das laboratory demonstrated tight clustering of VirB9 and VirB10 only in the presence of VirB8 (61). However, the extent of this role is not resolved as VirB6 and VirD4 also display similar localization patterns as VirB8 in the absence of a T4SS (115,116).

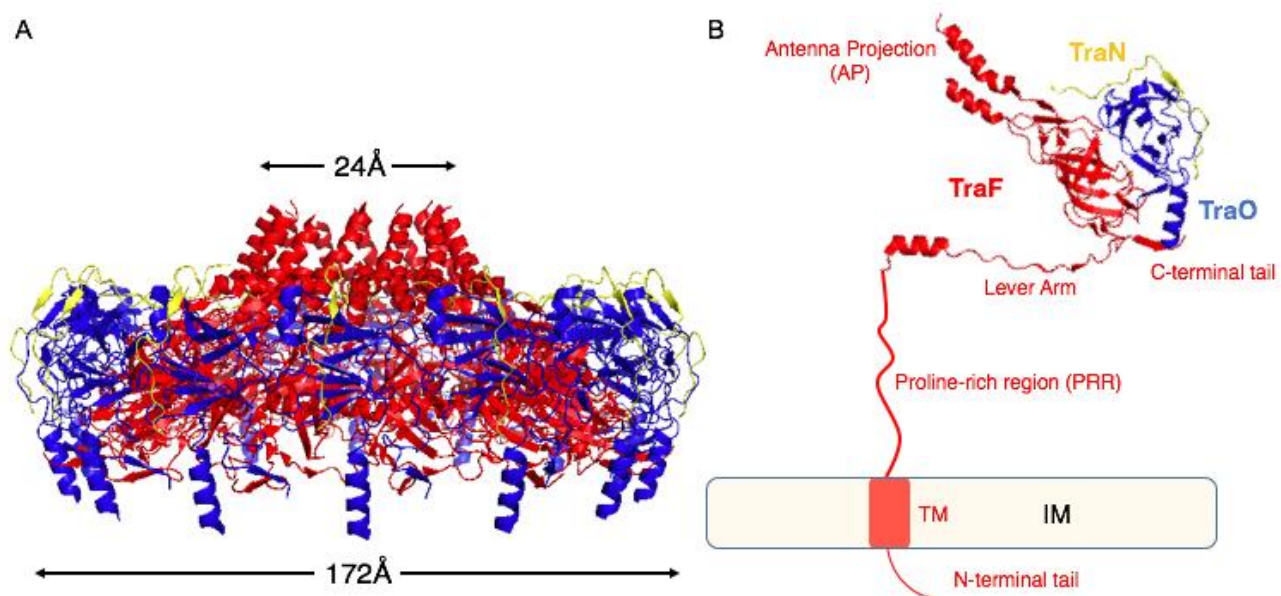
VirB7: VirB7 was shown to be an OM lipoprotein which is responsible for anchoring the core complex into the OM (117,118). VirB7 is anchored on the periplasmic side of the OM where it makes contact with and stabilizes the VirB9 subunit. The VirB7-VirB9 heterodimer also stabilizes VirB10 and other components of the IMC (119). VirB7 forms a disulfide crosslink with VirB9 and fits along groove-like structures at the outer face of VirB9 (118,120–122). VirB7 was also shown to be critical for movement of T-DNA substrates between VirD4 and VirB11 during T-DNA translocation (74). While VirB7 is critical for building a functional channel, TrwH_{R388} is not essential for plasmid transfer of R388 (123). Therefore, the Trw_{R388} T4SS must have another mechanism for anchoring into the OM not seen in other T4SSs. While VirB7 is a small protein in most conjugative T4SSs, some larger versions have been previously described. For example, HP0532 from *H. pylori* contains a large, surface-displayed C-terminal

end which was associated with the pilus structure (124). The biological significance of this observation is not well understood.

VirB9: VirB9 is a largely hydrophilic protein localized in the periplasm which is critical for structural integrity of the core complex. As mentioned above, VirB9 makes contacts with VirB7 that are necessary for its stability as well as proper positioning in the OM (122). VirB9 also makes critical contacts with VirB10 which are necessary for the stability of VirB10 (119). The crystal structure of the pKM101 core complex reveals that VirB9 is on the outer face of the complex while VirB10 is on the inside forming the hollow chamber which likely allows for substrates to pass through (82,125). These essential VirB9-VirB10 contacts occur at the outer face of the VirB10 β -barrel. In addition to structural integrity of the T4SS, VirB9 also plays a role in substrate discrimination as various insertion mutations alternatively block T-DNA transfer or RSF1010 mobilization (126).

VirB10: VirB10 is a critical component of the OMC, but unlike the VirB7 and VirB9, it is also part of the IMC as it makes contacts with the IM ATPases as well as IM proteins, such as VirB8 (59). VirB10 consists of a small cytoplasmic N-terminal tail, a single α -helical domain that spans the IM, a large proline-rich region (PRR) in the periplasm, a large periplasmic β -barrel structure, a small alpha helical projection spanning the OM termed the antenna projection (AP), and a small C-terminal tail, which folds back into the hollow channel chamber (Figure 1.10) (82,127). Because it spans both membranes, VirB10 is predicted to have two critical roles. One is that of a scaffolding protein in which VirB10 bridges the two separate IM and OM complexes. Secondly, VirB10 likely acts as an energy transducer between the IM ATPases and the OM proteins such as VirB9 (107).

Figure 1.10 Structure of the pKM101 core complex. (A) The structure of the pKM101 core complex depicting the arrangement of TraN (yellow), TraO (blue), and TraF (red). Dimensions of the core complex are listed above and below. (B) Crystal structure of the C-terminal half of TraF. The domains of interest of TraF are listed including the cytoplasmic N-terminal tail, the TM domain, the proline-rich region, the lever arm, the antenna projection (AP), and the C-terminal tail. The structure of the TraN-TraO-TraF heteromultimer was generated using pymol (<http://pymol.org>) based on the 3ZBI file deposited into the NCBI protein database.



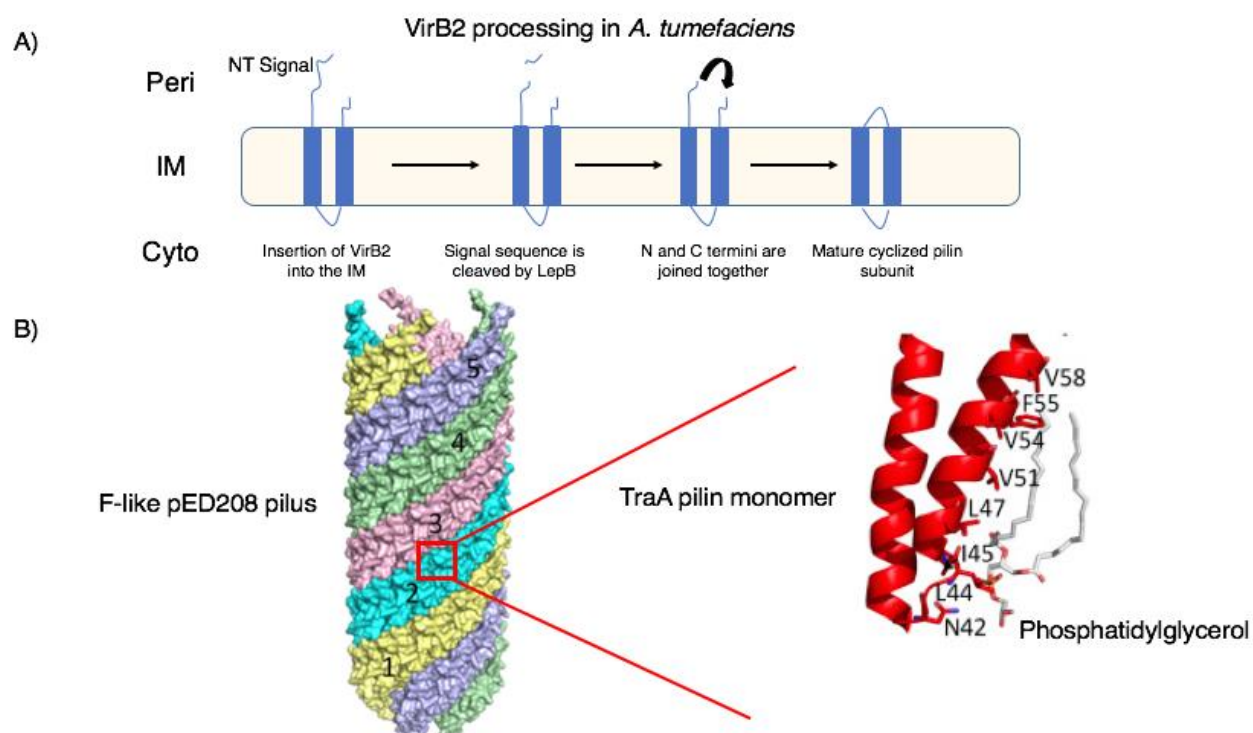
VirB10 also plays a critical role in pilus biogenesis. Previous studies on VirB10 have highlighted the importance of the N-terminal half and β -barrel of VirB10 for pilus biogenesis (128). But recently, the C-terminal domain of VirB10 has also been examined for its role. The middle of three invariant glycines at the N-terminal end of the AP (G₂₆₉xxG₂₇₂xxG₂₇₅) has been shown to be critical for pilus biogenesis and a G272R mutation resulted in a gating defect for VirE2 release and loss of detectable pilus (125). Additionally, deletions and partial deletions within the AP resulted in a loss of pilus biogenesis while only moderately affecting substrate transfer (127). Therefore, one intriguing model is that VirB10 also functions as a pilus-building platform that interacts with pilin subunits and mediates their assembly into the pilus polymer at the outer membrane. Data presented in the Results section below will address this model.

The conjugative pilus: One of the key features of most Gram-negative bacterial T4SSs is the presence of a conjugative pilus. Conjugative pili are utilized by the T4SS in order to establish mating junctions between donor and recipient cells. While the VirB2 major pilin subunit was previously shown to make contact with DNA substrates in *A. tumefaciens*, passage of substrates through a pilus structure has not yet been demonstrated. While previous studies using the F-plasmid T4SS have demonstrated transfer of substrates across long distances, these studies were inconclusive as to whether DNA was passing through a pilus structure (129–132).

Pilus biogenesis has also been extensively studied in the *A. tumefaciens* VirB T4SS (Figure 1.11). During pilin subunit maturation, VirB2 subunits are inserted into the IM. VirB2 contains a long signal sequence which is cleaved by the LepB signal peptidase (133). Following cleavage of the signal sequence, the N and C termini are joined together by an unidentified protein to form a cyclic peptide (133,134). These subunits are then subsequently used to form a mature pilus.

Figure 1.11 Pilus biogenesis in *Agrobacterium* and F-like pED208. (A) Depiction of the pilin subunit processing pathway previously described in *A. tumefaciens*. VirB2 is composed of two large hydrophobic regions and two hydrophilic regions in the cytoplasm and periplasm. After insertion into the membrane, the 47-residue signal sequence is cleaved by the LepB signal peptidase. The N- and C-terminal tails are covalently joined to create a cyclic peptide. (B) Structure of the pilus from the F-like pED208 plasmid. The pilus is composed of five layers wrapped together. Each layer is composed of the TraA pilin subunit which is joined to a phosphatidylglycerol molecule which orients the head group into the pilus channel lumen.

The structures of the F-pilus generated by electron microscopy and TraA subunit were published as Figures 2A and 5SB in Costa TRD, et al. *Structure of the bacterial sex F pilus reveals an assembly of a stoichiometric protein-phospholipid complex*. Cell 2016 166:1436–1444.e10. No prior permission from Elsevier is required for reproduction of these figures.



The pilin subunit of F plasmid, TraA_F, is structurally similar to VirB₂, but processed differently. TraA_F uses proton motive force to drive itself into the IM (135). TraA_F insertion also requires the presence of the pilin subunit chaperone, TraQ (136). Once inside the IM, TraA_F is subjected to cleavage of its N-terminal signal sequence by LepB followed by acetylation of the new N-terminal amino acid by TraX (137,138). Unlike VirB₂, TraA_F is not cyclized during pilus maturation. These processed TraA_F pilin subunits are then incorporated into a mature pilus. Recently, the structure of the pilus from the F-like plasmid pED208 was solved using cryo-electron microscopy at 3.6Å resolution (139). The pED208 pilus is comprised of five helical arrangements that are all composed of the TraA pilin subunit. TraA subunits are oriented in such a way that the N- and C-termini are oriented outward while the small cytoplasmic loop connecting the two alpha helices are located inside of the pilus lumen. In addition to TraA_F, these studies confirmed the presence of phosphatidylglycerol in the pilus contributing to its structure (Figure 1.11). The lipid heads were shown to be localized inside of the pilus lumen giving it a slight electronegative charge. The Waksman laboratory predicts that this allows for efficient transfer of DNA through the pilus lumen. Future studies are needed to confirm the presence of DNA or protein substrates inside of the pilus.

T4SSs: Substrate channel vs. Pilus Assembly Machines

The Christie lab has identified numerous mutations in the VirB_{Ti} and Tra_{pKM101} (discussed below) that block substrate transfer or pilus biogenesis, but not both (125,127). These types of mutations have been referred to as “uncoupling mutations” as they uncouple these two important processes. Various mutational analyses have uncovered these in different T4SSs highlighting some similarities as well as informative differences. For example, TrwH_{R388} is not

important for R388 plasmid transfer, although its homolog in the VirB_{Ti} system, VirB7, is essential (67,123). Additionally, deletion of *virB1* in the VirB_{Ti} system abolishes detectable pilus production while still allowing for attenuated T-DNA transfer (67). During my analysis of TraF and the OMCC from pKM101, I uncovered more of these mutations, which I will discuss in more detail later in this thesis.

Although most uncoupling mutations yield a Tra⁺Pil⁻ phenotype, mutations and deletions of components in the Dtr proteins have revealed a Tra⁻Pil⁺ phenotype, including deletions of the relaxase and T4CP. When transposon insertions were constructed in the RP4 Dtr region, *E. coli* cells containing these mutant plasmids were more sensitive to killing by *P. aeruginosa* containing a functional T6SS than cells containing wild-type RP4 (140). These mutants might make more pili to provide better contact with recipient cells.

Taken together, these suggest that the T4SS functions either as “pilus assembly” or a “substrate translocation” machine. In its default mode, the T4SS mediates assembly of the pilus, which extends and retracts stochastically in ‘search’ of bacterial recipient cells. Once the pilus establishes contact with a potential recipient, the pilus retracts to bring the two cells together to form the mating junction. The T4SS then switches to the substrate transfer mode, where it engages substrates and pumps them into recipient cells. (Figure 1.12).

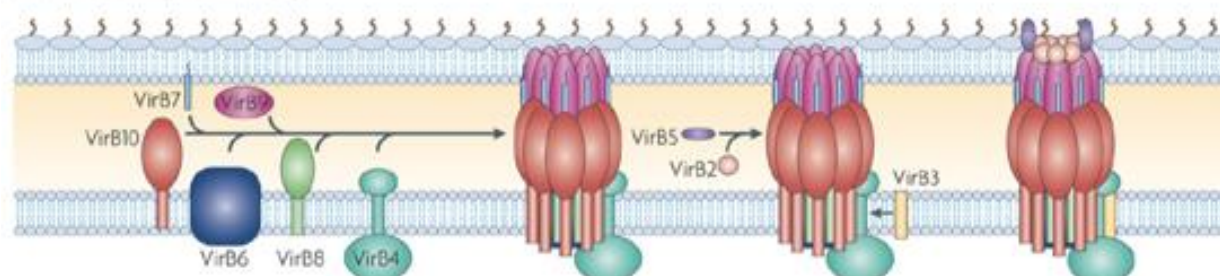
The goals of my research

Shortly before I joined the Christie lab, the Waksman laboratory published the crystal structure of the pKM101 OMCC O-layer (90). Similar to the ComB10 crystal structure, VirB10-like TraF displayed a unique alpha-helical projection at its C-terminal end (90,111). When

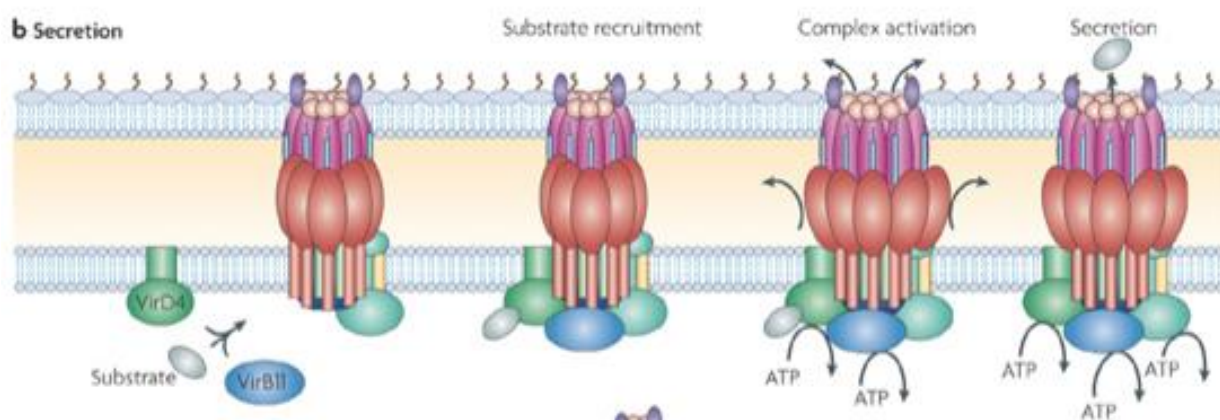
Figure 1.12 Substrate versus pilus channel. (a) Cartoon illustration of the T4SS assembly pathway with VirB3, VirB6, VirB8, and VirB4 forming the IMC, VirB7, VirB9, and VirB10 forming the OMC, and VirB2 and VirB5 arranging themselves into a conjugative pilus. (b) During substrate translocation, VirD4 and VirB11 will associate with the MPF channel. Upon substrate docking and ATPase activity, these IM ATPases will trigger VirB10 into an active conformation. This will allow the substrate to pass through the channel. (c) During pilus biogenesis, VirB4 will associate with VirB11. These ATPases will trigger the release of VirB2 from the membrane in order to form an extracellular pilus.

This is Figure 6 from Fronzes R, et al. *The structural biology of type IV secretion systems*. Nat Rev Microbiol. 2009 7:703–14. This figure was re-published with permission from Nature Publishing Groups. License number 4073250457937.

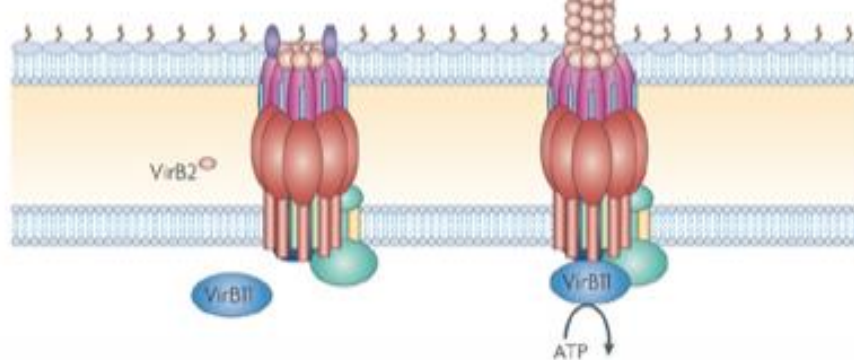
a Translocation pore assembly



b Secretion



c Pilus biogenesis



placed in the context of the core complex, these helices appeared to form the OM substrate pore, though previous experiments in the Christie lab identified this region as an important factor in pilus biogenesis. My goal was to further define the role of the AP in building a functional T4SS. Some of the questions I sought to address included: (i) Which regions of the AP and C-terminal tail are critical for substrate transfer, pilus biogenesis, and recipient-cell contact? (ii) Are the AP and C-terminal domains of VirB10 and TraF functionally similar? (iii) Are the IMC and OMCC subassemblies separate functional complexes? Important observations made during my time in the Christie lab include: (i) both the AP and C-terminal tail are critical for building of a cognate conjugative pilus, although only the C-terminal tail is essential for plasmid transfer, (ii) the C-terminal half of VirB10 and TraF are functionally similar as demonstrated by mutual substitutions between the two proteins, (iii) the IMC and OMCC are functionally-distinct subassemblies as demonstrated by the ability to pair heterologous OMCCs and IMCs along with the different TraF/VirB10 N-terminal sequence requirements in the IMC.

During my investigation into the role of the OMCC in building a functional T4SS, I, along with other members of the Christie lab began developing and utilizing the pKM101 T4SS. Our initial motivation for choosing a new model system was related to the structural information available. Because a crystal structure of TraF was available, we could use it to make testable predictions about the roles of various domains of interest. Additionally, much less time is required to perform genetic analysis using *E. coli* pKM101 for our model system. Finally, *E. coli* provided tools that were not available with *A. tumefaciens*, such as donor-specific bacteriophages PRD1 and IKe (141,142). These phages are not only useful tools for monitoring pilus production, but they can also act as morphologically distinct markers when identifying the location of the T4SS in the cell membrane.

I contributed to this effort by assisting in developing the *E. coli* pKM101 T4SS as the new model system in the Christie lab. I, along with other members of the Christie lab, developed markerless deletions of each pKM101 *tra* gene on the native plasmid, allowing us to minimize polar effects on downstream genes, and complementing plasmids under the arabinose-inducible P_{BAD} promoter. Additionally, I developed the use of new tools and assays not available in the *A. tumefaciens* system, including the use of donor-specific bacteriophages and the *Pseudomonas aeruginosa* T6SS killing assay to monitor T4SS machine function. These tools allowed for new insight into the stages at which mutations block conjugation. In Chapters 3-6, I will describe my efforts to develop the pKM101 T4SS and define the contributions of the VirB10/TraF AP and C-terminal tail in building a functional translocation channel.

Chapter 2: Materials and Methods

Bacterial strains and growth conditions

Escherichia coli strain DH5 α was used for plasmid construction and the *Pseudomonas aeruginosa* type VI killing assay. *P. aeruginosa* strain PW9164, a strain of PAO1 with as IS*phoA* insertion in the *retS* locus was used for the type VI killing assays. *E. coli* strain MG1655 was used during conjugation assays and phage sensitivity assays (143). Strain WM1650 was used as recipient cell during conjugation assays (144). Strain MC4100 was used for surface display assays and TOP10 was used for p-benzoyl-L-phenylalanine (pBpa) crosslinking experiments (145). All *E. coli* and *P. aeruginosa* strains were grown in Lysogeny Broth (LB) at 37°C with shaking. When necessary, *E. coli* cells were grown in the presence of the following antibiotics: carbenicillin (50 μ g/ml), kanamycin (50 μ g/ml), spectinomycin (100 μ g/ml), chloramphenicol (20 μ g/ml), tetracycline (20 μ g/ml), and rifampicin (50 μ g/ml). *P. aeruginosa* was grown in LB without antibiotic selection.

Agrobacterium tumefaciens strains A348 and PC1010 variants were used for studies exploring T4SS function with T-DNA transfer and VirB2 surface assays (67,146). *A. tumefaciens* cells were grown in MG/L at room temperature with shaking (110). During induction of virulence genes, cells were incubated in acidic ABIM along with 100 μ M acetosyringone for 24 hours (125). When necessary, *A. tumefaciens* was grown in MG/L in the presence of carbenicillin (100 μ g/ml), kanamycin (100 μ g/ml), and gentamycin sulfate (100 μ g/ml). During *vir* gene induction, cells were grown in the absence of antibiotics.

Table 2.1 Bacterial strains

Strains	Relevant characteristics	Source
<i>E. coli</i>		
DH5 α	Genotype: F ⁻ Φ 80 <i>lacZ</i> Δ M15 Δ (<i>lacZYA-argF</i>) U169 <i>recA1 endA1 hsdR17</i> (rK ⁻ , mK ⁺) <i>phoA supE44</i> λ ⁻ <i>thi-1 gyrA96 relA1</i>	Gibco-BRL/ Invitrogen
MG1655	Genotype: K-12 F ⁻ λ ⁻ <i>ilvG</i> ⁻ <i>rfb-50 rph-1</i>	(143)
HME45	W3110 <i>gal490 pgl</i> \square 8 λ CI857 \square (<i>cro-bioA</i>)	(154)
MC4100	Genotype: F ⁻ [<i>araD139</i>] _{B/r} Δ (<i>argF-lac</i>)169* & λ e14- <i>flhD5301</i> Δ (<i>fruK-yeiR</i>)725 (<i>fruA25</i>) \ddagger <i>relA1 rpsL150</i> (str ^R) <i>rbsR22</i> Δ (<i>fimB-fimE</i>)632(::IS1) <i>deoC1</i>	(145)
TOP10	Genotype: F- <i>mcrA</i> Δ (<i>mrr-hsdRMS-mcrBC</i>) ϕ 80 <i>lacZ</i> Δ M15 Δ <i>lacX74 nupG recA1 araD139</i> Δ (<i>ara-leu</i>)7697 <i>galE15 galK16 rpsL</i> (Str ^R) <i>endA1</i> λ ⁻	Invitrogen
WM1650	CAG18477; Tet linked to <i>priA</i> (+)	(144)
<i>A. tumefaciens</i>		
A348	A136 containing the pTiA6NC plasmid	(146)
PC1010	A348 deleted of the <i>virB10</i> gene from pTiA6NC	(67)
<i>P. aeruginosa</i>		
PW9164	PAO1 containing an IS <i>phoA</i> in the <i>retS</i> locus	<i>Pseudomonas aeruginosa</i> Stock Center, University of Washington

Table 2.2 *E. coli* vectors

Name	Relevant characteristics	Source
pBAD24	Crb ^r ; ColE1 expression vector with arabinose-inducible P _{BAD} promoter.	(147)
pBAD33	Cam ^r ; pACYC184/p15 plasmid with arabinose-inducible P _{BAD} promoter	(147)
pBAD24Spc	Spc ^r ; pBAD24 with spectinomycin resistance gene from pHP45Ω inserted into <i>bla</i> gene.	This study
pBAD24Kan	Kan ^r ; pBAD24 with kanamycin resistance gene from pUC4K inserted into the <i>bla</i> gene	(29)
pHP45Ω	Spc ^r ; source of <i>spc</i> ^r cassette	(148)
pBB50	Kan ^r ; source of <i>sacB-kan</i> cassette	(67)
pGB2	Spc ^r ; plasmid with pSC101 origin of replication	(149)
pUC4K	Kan ^r ; source of <i>kan</i> cassette	Amersham
pKVD10	Crb ^r ; source of <i>virB10</i> cassette	(127)
pSU1443	Kan ^r ; R388 containing a deletion of the <i>trwB</i> locus	(150)
pZZ11	Crb ^r ; pPC914KS expressing P _{virB} ::GST	(110)
pEVOL	Cam ^r ; pACYC184/p15 plasmid encoding tRNA synthetase/tRNA for incorporation of p-benzoyl-l-phenylalanine into proteins of interest	(168)
pSJ503	Crb ^r ; pZZ11 with a 3xFLAG tag sequence cloned between <i>NcoI</i> and <i>BamHI</i>	This study

Table 2.3 *E. coli* expression plasmids

Name	Relevant characteristics	Source
pKM101	Crb ^r ; Deletion derivative of IncN conjugative plasmid R46	(152)
pJG57	Kan ^r ; pBAD24Kan with P _{BAD} :: <i>traF</i> /AP-CT _{virB10}	This study
pJG58	Kan ^r ; pBAD24Kan with P _{BAD} :: <i>traF</i> /BB-CT _{virB10}	This study
pJG59	Spc ^r ; pBAD24Spc with P _{BAD} :: <i>traF</i>	This study
pJG60	Spc ^r ; pBAD24Spc with P _{BAD} :: <i>traF</i> /AP _{virB10}	This study
pJG61	Spc ^r ; pBAD24Spc with P _{BAD} :: <i>traF</i> /5xGly loop substitution	This study
pJG62	Spc ^r ; pBAD24Spc with P _{BAD} :: <i>traF</i> with NT His tag	This study
pJG65	Spc ^r ; pBAD24Spc with P _{BAD} :: <i>traF</i> /AP flexible loop _{virB10}	This study
pJG66	Spc ^r ; pBAD24Spc with P _{BAD} :: <i>traF</i> /CT _{virB10}	This study
pJG68	Spc ^r ; pBAD24Spc with P _{BAD} :: <i>traF</i> /NT _{virB10}	This study
pJG69	Spc ^r ; pBAD24Spc with P _{BAD} :: <i>traF</i> /TM _{virB10}	This study

pJG70	Spc ^r ; pBAD24Spc with P _{BAD} :: <i>traF</i> /PRR _{virB10}	This study
pJG2005	Spc ^r ; pBAD24Spc with P _{BAD} :: <i>traF</i> /TM-CT _{virB10}	This study
pJG76	Spc ^r ; pBAD24Spc with P _{BAD} :: <i>traF</i> Δ307-354 (Deletion of the TraF AP domain)	This study
pJG95	Spc ^r ; pBAD24Spc with P _{BAD} :: <i>traF</i> Δ302-386 (Deletion of the TraF AP and C-terminal tail)	This study
pJG96	Spc ^r ; pBAD24Spc with P _{BAD} :: <i>traF</i> Δ354-386 (Deletion of the TraF C-terminal tail)	This study
pJG97	Spc ^r ; pBAD24Spc with P _{BAD} :: <i>traF</i> ΔCT9	This study
pJG98	Spc ^r ; pBAD24Spc with P _{BAD} :: <i>traF</i> ΔCT1	This study
pJG99	Spc ^r ; pBAD24Spc with P _{BAD} :: <i>traFR</i> 373E	This study
pJG101	Spc ^r ; pBAD24Spc with P _{BAD} :: <i>traF</i> Δ373-377 (Deletion of the conserved RDLDF domain)	This study
pJG134	Spc ^r ; pBAD24Spc with P _{BAD} :: <i>traF</i> /BB-AP _{virB10}	This study
pJG150	Spc ^r ; pBAD24Spc with P _{BAD} :: <i>traF</i> /BB _{virB10}	This study
pMS22	Kan ^r ; pBAD24Kan with P _{BAD} :: <i>traL</i>	This study
pMS24	Kan ^r ; pBAD24Kan with P _{BAD} :: <i>traM</i>	This study
pMS26	Kan ^r ; pBAD24Kan with P _{BAD} :: <i>traA</i>	This study
pMS28	Kan ^r ; pBAD24Kan with P _{BAD} :: <i>traB</i>	This study
pMS30	Kan ^r ; pBAD24Kan with P _{BAD} :: <i>traC</i>	This study
pMS32	Kan ^r ; pBAD24Kan with P _{BAD} :: <i>traD</i>	This study
pMS35	Crb ^r ; pBAD24 with P _{BAD} :: <i>traN</i>	This study
pMS36	Kan ^r ; pBAD24Kan with P _{BAD} :: <i>traE</i>	This study
pMS38	Kan ^r ; pBAD24Kan with P _{BAD} :: <i>traO</i>	This study
pMS40	Kan ^r ; pBAD24Kan with P _{BAD} :: <i>traG</i>	This study
pJG125	Crb ^r ; pCGR108 containing a deletion of <i>traF</i> flanked by <i>SacI</i> and <i>XhoI</i> restriction sites	This study
pJG142	Spc ^r ; <i>oriT-traI</i> fragment was cloned into the pGB2 cloning vector	This study
pJG143	Crb ^r ; pCGR108 containing a deletion of <i>traN</i> through <i>traF</i> flanked by <i>SacI</i> and <i>XhoI</i> restriction sites	This study
pJG144	Crb ^r ; pCGR108 encoding the chimeric <i>tra:virB</i> operon (<i>virB7-traE-virB9-traF/virB10</i> fragment cloned into pJG143 using <i>SacI</i> and <i>XhoI</i> restriction sites.)	This study
pJG145	Crb ^r ; pCGR108 encoding chimeric <i>tra:trw</i> operon (<i>trwH-traE-trwF-traF/trwE</i> fragment cloned into pJG143 using <i>SacI</i> and <i>XhoI</i> restriction sites.)	This study
pJG151	Crb ^r ; pCGR108 encoding chimeric <i>tra:ptl</i> operon (<i>ptlI-traE-ptlF-traF/ptlG</i> fragment cloned into pJG143 using <i>SacI</i> and <i>XhoI</i> restriction sites.)	This study
pJG152	Crb ^r ; pJG125 with the allele encoding for NT FLAG	This study

	TraF cloned between the <i>SacI</i> and <i>XhoI</i> restriction sites	
pJG160	Crb ^r ; pCGR108 containing a deletion of <i>traC</i> flanked by <i>SacI</i> and <i>XhoI</i> restriction sites	This study
pJG161	Crb ^r ; pCGR108 containing a deletion of <i>traE</i> flanked by <i>SacI</i> and <i>XhoI</i> restriction sites	This study
pJG162	Crb ^r ; pJG125 with the allele encoding for AP FLAG TraF cloned between the <i>SacI</i> and <i>XhoI</i> restriction sites	This study
pJG163	Crb ^r ; pJG125 with the allele encoding for CT FLAG TraF cloned between the <i>SacI</i> and <i>XhoI</i> restriction sites	This study
pJG164	Crb ^r ; pJG125 with the allele encoding for Lever FLAG TraF cloned between the <i>SacI</i> and <i>XhoI</i> restriction sites	This study
pJG165	Crb ^r ; pJG160 with the allele encoding for CT FLAG TraC cloned between the <i>SacI</i> and <i>XhoI</i> restriction sites	This study
pJG166	Crb ^r ; pJG161 with the allele encoding for CT FLAG TraE cloned between the <i>SacI</i> and <i>XhoI</i> restriction sites	This study
pJG158	Crb ^r ; pJG125 with the allele encoding for NT FLAG TraF Δ 307-354 cloned between the <i>SacI</i> and <i>XhoI</i> restriction sites	This study
pJG153	Crb ^r ; pJG125 with the allele encoding for NT FLAG TraF Δ CT9 cloned between the <i>SacI</i> and <i>XhoI</i> restriction sites	This study
pJG154	Crb ^r ; pJG125 with the allele encoding for NT FLAG TraF Δ 373-377 cloned between the <i>SacI</i> and <i>XhoI</i> restriction sites	This study
pJG155	Crb ^r ; pJG125 with the allele encoding for NT FLAG TraF / AP-CT _{virB10} cloned between the <i>SacI</i> and <i>XhoI</i> restriction sites	This study
pJG156	Crb ^r ; pJG125 with the allele encoding for NT FLAG TraF / AP-CT _{ptlG} cloned between the <i>SacI</i> and <i>XhoI</i> restriction sites	This study
pJG157	Crb ^r ; pJG125 with the allele encoding for NT FLAG TraF / AP-CT _{trwE} cloned between the <i>SacI</i> and <i>XhoI</i> restriction sites	This study
pJG202	Crb ^r ; pUC57 plasmid containing the <i>tra:virB</i> operon	This study
pJG203	Crb ^r ; pUC57 plasmid containing the <i>tra:ptl</i> operon	This study
pJG1002	Spc ^r ; pKM101 containing a deletion of the <i>traM</i> locus	This study
pJG1003	Crb ^r ; pKM101 containing a deletion of the <i>traA</i> locus	This study
pJG1004	Spc ^r ; pKM101 containing a deletion of the <i>traB</i> locus	This study

pJG1005	Spc ^r ; pKM101 containing a deletion of the <i>traC</i> locus	This study
pJG1006	Spc ^r ; pKM101 containing a deletion of the <i>traD</i> locus	This study
pJG1008	Spc ^r ; pKM101 containing a deletion of the <i>traE</i> locus	This study
pJG1010	Crb ^r ; pKM101 containing a deletion of the <i>traF</i> locus	This study
pJG1011	Spc ^r Kan ^r ; pKM101 containing a <i>sacB-kan</i> insertion into the <i>traG</i> locus	This study
pCGR100	Cam ^r ; mini-pKM101 in pBAD33 (<i>korB-traG</i> cloned between the <i>SacI</i> and <i>XbaI</i> sites. (This plasmid is missing the <i>kikA</i> locus.)	This study
pJG122	Cam ^r ; pCGR100 containing a deletion of <i>traL</i>	This study
pJG123	Cam ^r ; pCGR100 containing a deletion of <i>traO</i>	This study
pJG124	Cam ^r ; pCGR100 containing a deletion of <i>traN</i>	This study
pCGR108	Crb ^r ; mini-pKM101 in pBAD24 (<i>korB-traG</i> cloned between the <i>NcoI</i> and <i>XbaI</i> sites. This plasmid is missing the <i>kikA</i> locus.)	This study
pCGR113	Cam ^r ; <i>kikA</i> cloned in pBAD33 between <i>SacI</i> and <i>XbaI</i> restriction sites	This study
pJG111	Spc ^r ; pBAD24Spc with P _{BAD} :: <i>traF</i> /NT 6xHis:CT FLAG P185Amber mutation	This study
pJG112	Spc ^r ; pBAD24Spc with P _{BAD} :: <i>traF</i> /NT 6xHis:CT FLAG W304Amber mutation	This study
pJG113	Spc ^r ; pBAD24Spc with P _{BAD} :: <i>traF</i> /NT 6xHis:CT FLAG F316Amber mutation	This study
pJG114	Spc ^r ; pBAD24Spc with P _{BAD} :: <i>traF</i> /NT 6xHis:CT FLAG N325Amber mutation	This study
pJG115	Spc ^r ; pBAD24Spc with P _{BAD} :: <i>traF</i> /NT 6xHis:CT FLAG Y334Amber mutation	This study
pJG116	Spc ^r ; pBAD24Spc with P _{BAD} :: <i>traF</i> /NT 6xHis:CT FLAG Q343Amber mutation	This study
pJG117	Spc ^r ; pBAD24Spc with P _{BAD} :: <i>traF</i> /NT 6xHis:CT FLAG Y352Amber mutation	This study
pJG118	Spc ^r ; pBAD24Spc with P _{BAD} :: <i>traF</i> /NT 6xHis:CT FLAG F377Amber mutation	This study
pJG119	Spc ^r ; pBAD24Spc with P _{BAD} :: <i>traF</i> /NT 6xHis:CT FLAG N386Amber mutation	This study
pJG204	Crb ^r ; pBAD24 with P _{BAD} :: <i>traF</i> / CT FLAG A2Amber mutation	This study
pJG205	Crb ^r ; pBAD24 with P _{BAD} :: <i>traF</i> / CT FLAG V6Amber mutation	This study
pJG206	Crb ^r ; pBAD24 with P _{BAD} :: <i>traF</i> / CT FLAG E11Amber mutation	This study
pJG207	Crb ^r ; pBAD24 with P _{BAD} :: <i>traF</i> / CT FLAG T16Amber mutation	This study
pJG208	Crb ^r ; pBAD24 with P _{BAD} :: <i>traF</i> / CT FLAG	This study

	S23Amber mutation	
pJG209	Crb ^r ; pBAD24 with P _{BAD} :: <i>traF</i> / CT FLAG G27Amber mutation	This study
pJG210	Crb ^r ; pBAD24 with P _{BAD} :: <i>traF</i> / CT FLAG N32Amber mutation	This study
pJG211	Crb ^r ; pBAD24 with P _{BAD} :: <i>traF</i> / CT FLAG V43Amber mutation	This study
pJG212	Crb ^r ; pBAD24 with P _{BAD} :: <i>traF</i> / CT FLAG L45Amber mutation	This study
pJG213	Crb ^r ; pBAD24 with P _{BAD} :: <i>traF</i> / CT FLAG L49Amber mutation	This study
pJG214	Crb ^r ; pBAD24 with P _{BAD} :: <i>traF</i> / CT FLAG	This study
pRP100	Kan ^r ; mini-pKM101 containing an IncN origin of replication	This study
pRP101	Kan ^r ; pRP100 containing a deletion of the <i>traL</i> locus	This study
pRP107	Kan ^r ; pRP100 containing a deletion of the <i>traN</i> locus	This study
pRP109	Kan ^r ; pRP100 containing a deletion of the <i>traO</i> locus	This study
pRP110	Kan ^r ; pRP100 containing a deletion of the <i>traF</i> locus	This study
pYGL24	Spc ^r ; pJG142 containing an HA tag on the C-terminal end of TraK, a strep tag on the C-terminal end of TraJ, and a 6xHis tag on the C-terminal end of TraI	This study

Table 2.4 *Agrobacterium tumefaciens* expression plasmids

Name	Relevant characteristics	Source
pJG1	Crb ^r Kan ^r ; pKVD10 with a G269R mutation in VirB10	This Study
pJG2	Crb ^r Kan ^r ; pKVD10 with a G269K mutation in VirB10	This Study
pJG3	Crb ^r Kan ^r ; pKVD10 with a G269W mutation in VirB10	This Study
pJG4	Crb ^r Kan ^r ; pKVD10 with a G269C mutation in VirB10	This Study
pJG5	Crb ^r Kan ^r ; pKVD10 with a G269D mutation in VirB10	This Study
pJG6	Crb ^r Kan ^r ; pKVD10 with a G272R mutation in VirB10	This Study
pJG7	Crb ^r Kan ^r ; pKVD10 with a G272K mutation in VirB10	This Study
pJG8	Crb ^r Kan ^r ; pKVD10 with a G272W mutation in VirB10	This Study
pJG9	Crb ^r Kan ^r ; pKVD10 with a G272C mutation in VirB10	This Study
pJG10	Crb ^r Kan ^r ; pKVD10 with a G272D mutation in VirB10	This Study
pJG11	Crb ^r Kan ^r ; pKVD10 with a G275R mutation in VirB10	This Study
pJG12	Crb ^r Kan ^r ; pKVD10 with a G275K mutation in VirB10	This Study
pJG13	Crb ^r Kan ^r ; pKVD10 with a G275W mutation in VirB10	This Study
pJG14	Crb ^r Kan ^r ; pKVD10 with a G275C mutation in VirB10	This Study
pJG15	Crb ^r Kan ^r ; pKVD10 with a G275D mutation in VirB10	This Study
pJG40	Crb ^r Kan ^r ; pKVD10 with a 3xFLAG tag cloned into an SphI site at <i>virB10</i> codon 298.	This study
pJG42	Crb ^r Kan ^r ; pKVD10 with a 3xFLAG tag cloned into an	This study

	SphI site at <i>virB10</i> codon 329.	
pJG44	Crb ^r Kan ^r ; pKVD10 with a 3xFLAG tag cloned into an SphI site at <i>virB10</i> codon 332.	This study
pJG52	Crb ^r Kan ^r ; pKVD10 with a 2xFLAG tag inserted between <i>virB10</i> codons 310 and 311.	This study
pSJ501	Crb ^r ; pKVD10 with codons 284-337 of <i>virB10</i> replaced with codons 302-353 of <i>traF</i>	This study
pSJ502	Crb ^r ; pKVD10 with codons 284-377 of <i>virB10</i> replaced with codons 302-386 of <i>traF</i>	This study
pSJ510	Crb ^r ; pBSIISK ⁺ NdeI expressing P _{lac} :: <i>virB10.298 SphI</i>	This study
pSJ511	Crb ^r ; pBSIISK ⁺ NdeI expressing P _{lac} :: <i>virB10.329 SphI</i>	This study
pSJ512	Crb ^r ; pBSIISK ⁺ NdeI expressing P _{lac} :: <i>virB10.331 SphI</i>	This study

Table 2.5 Native pKM101 deletion primers

Name	Sequence
TraM_FWD_SacB/Kan	5' TCTGCAATCAACAGAAGATAGTGAGTAAGGAGAAA CCATGGTCGACCTGCAGGTCGACTC 3'
TraM_RVS_SacB/Kan	5' CGCACCTTTGAAAAGCGGTCTTTTCCCGTCAACGA CCATGGGAAAGCCACGTTGTGTCT 3'
TraA_FWD_SacB/Kan	5' GGGGACTTTTGTCCCCCAAAGTGAGGACTACAAAG CCATGGTCGACCTGCAGGTCGACTC 3'
TraA_RVS_SacB/Kan	5' ATCAATTTTTTTTGGCTTCGTAGCGGTGGCAGCTCCCTGG CCATGGGAAAGCCACGTTGTGTCT 3'
TraB_FWD_SacB/Kan	5' TCCTCTGTTGACTACTAACGTAAGGGTTTAAATA CCATGGTCGACCTGCAGGTCGACTC 3'
TraB_RVS_SacB/Kan	5' GCCGGTGGTCAGCAGCACTGCCGTAAGTGATTTTT CCATGGGAAAGCCACGTTGTGTCT 3'
TraC_FWD_SacB/Kan	5' CTGGCGCCTGACGGCTTAACAACGAGGCAAACT CCATGGTCGACCTGCAGGTCGACTC 3'
TraC_RVS_SacB/Kan	5' CACCAGGAAGAAAGGGATAAGCAGCfAGTAGTTTTT CCATGGATCCTGATGTTACATTGCAC 3'
TraD_FWD_SacB/Kan	5' AATTAACCTACCGAAAATTTAAGAGTAAGGAGGCA CCATGGTCGACCTGCAGGTCGACTC 3'
TraD_RVS_SacB/Kan	5' GCTAATCAGAAGAACTCCCATAAGCAATAAGCTG CCCATGGGAAAGCCACGTTGTGTCT 3'
TraE_FWD_SacB/Kan	5' CGGTTGATACGCAAGGTGGTCGAAATGAAAGCTAA CCATGGTCGACCTGCAGGTCGACTC 3'
TraE_RVS_SacB/Kan	5' GACTGACAAAACGACTGCTGAAAGAAGTAGTTTTT CCATGGATCCTGATGTTACATTGCAC 3'
TraF_FWD_SacB/Kan	5' ATGTGCGCAGGGTTCAAATTGGGGAGGATAACTGA CCATGGTGGTATGAAAGCCTTTGTCA 3'
TraF_RVS_SacB/Kan	5' GCGCAGTGGGCCAAGTTGATAGAAAGCTGCATCAG CCATGGGGGAAAGCCACGTTGTGTCTCA 3'

TraG_FWD_SacB/Kan	5' AAAGTCGCTTAGCGCCCGCTTTTCTTCAGGAGTAA CCATGGTCGACCTGCAGGTCGACTC 3'
TraG_RVS_SacB/Kan	5' AAATGCTGCGGCCAGAAGCCAGGTTGCTAATTTTT CCATGGATCCTGATGTTACATTGCAC 3'

Table 2.6 Inverse PCR deletion primers

Name	Sequence
TraL_Del_Inv._FWD	5' GGTTATGAATGGAACGTTTGTATC 3'
TraL_Del_Inv._RVS	5' TTATGTTTCACCGCGTAATTG 3'
TraO_Del_Inv._FWD	5' ATGGCCCGTAAAAGTGTCG 3'
TraO_Del_Inv._RVS	5' GGGGCAGCCCTCAGTTAAC 3'
TraN_Del_Inv._FWD	5' ATGAAAGCTAATAAAAAAACAGGGC 3'
TraN_Del_Inv._RVS	5' TACGGCATCCATTATCGG 3'
TraN Del. RVS SacI	5' GATATGAGCTCTACGGCATCCATTATCGG 3'
TraF_Del_Inv._FWD	5'CTTCAGGAGTAATCATGACTGATGCAGC 3'
TraF_Del_Inv._RVS	5' CAGTTATCCTCCCAATTTGAACCC 3'
TraC_Del._RVS_SacI	5' ATATATGAGCTCGAGTTTTGCCTCGTTGTTAAGCCGTCAG 3'
TraC_Del._FWD_XhoI	5'ATATATACTCGAGTATGAAAAAACTACTGCTGCTTATCCCTTTC TTCCTGG 3'
TraE_Del._RVS_SacI	5' TATATATGAGCTCATTAGCTTTCATTTCGACCACCTTGCGTATC 3'
TraE_Del._FWD_XhoI	5'ATATATACTCGAGCCCCATGAAAAAACTACTTCTTTCAGCAGT C 3'
TraF Del. RVS SacI	5' TATATGAGCTCTCAGTTATCCTCCCAATTTG 3'
TraF Del. FWD XhoI	5' ATATACTCGAGAAAAGTCGCTTAGCGCCC 3'

Table 2.7 pKM101 gene cloning primers

Name	Sequence
traL_FWD_NcoI	5'CATGCCATGGATGAGTAAACATCCAAAACCTCCTGGTTCTC 3'
traL_RVS_XhoI_KpnI	5'GATGGTACCATGCTCGAGTCATTCCCCCTTCGCTGTTTC 3'
traM_FWD_NcoI	5' CATGCCATGGATGACCACGTTGTTTAAGAAGTATGGCC3'
traM_RVS_XhoI_KpnI	5' CGGGGTACCCCGCTCGAGTCAGCTTCCTACGCCCCGTCA 3'
traA_FWD_NcoI	5' CATGCCATGGATGTTTCGTTGACGGGAAAAGACCG 3'
traA_RVS_XhoI_KpnI	5' CGGGGTACCCCGCTCGAGTTAAACCCTTACGTTAGT AGTCAACAGAGGAATAAGAC 3'
traB_FWD_NcoI	5' CATGCCATGGATGAGAGCTGCCACCGCTACG 3'
traB_RVS_XhoI	5' CCGCTCGAGTTAAGCCGTCAGGCGCCAG 3'
traC_FWD_NcoI	5' CATGCCATGGATGAAAAAATCACTTACGGCAGTGCTG 3'
traC_RVS_XhoI_KpnI	5' CGGGGTACCCCGCTCGAGTCAGTTAATTGAAGGTGACGC

	GGTAAC 3'
TraC_FWD_SacI	5' GATATGAGCTCATGAAAAAATCACTTACGGCAGTGCTGCTG 3'
TraC_FLAG_RVS_XhoI	5'CTATATACTCGAGTCATTTGTCATCGTCATCTTTATAATCGTT AATT GAAGGTGACGCGGTAACGTCC 3'
traD_FWD_NcoI	5' CATGCCATGGCATTACCCCTGGTACAAGACAT 3'
traD_RVS_XhoI_KpnI	5' CGGGGTACCCCGCTCGAGTTATGCAGCCTTCTTCCCGCG 3'
traN_FWD_NcoI	5' CATGCCATGGATGCGCAGCTTATTGCTTATGGGA 3'
traN_RVS_XhoI_KpnI	5'CGGGGTACCCCGCTCGAGTTAGCTTTCATTTTCGACCACCTTGC 3'
traE_FWD_NcoI	5'CATGCCATGGATGAAAGCTAATAAAAAAACAGGGCTTACAC GT 3'
traE_RVS_XhoI_KpnI	5' CGGGGTACCCCGCTCGAGTCAGTTAACTTCCGGGTTGACGC 3'
TraE FWD SacI	5' GATATGAGCTCAAAAAAACAGGGCTTACACGTGAAGCC 3'
TraE FLAG RVS XhoI	5'CATATATCTCGAGTCATTTGTCATCGTCATCTTTATAATCGTT AACTTCCGGGTTGACGCGATAACTC 3'
traO_FWD_NcoI	5'CATGCCATGGATGAAAAAACTACTTCTTTCAGCAGTCGTTTT GT 3'
traO RVS XhoI KpnI	5'CGGGGTACCCCGCTCGAGTCAGTTATCCTCCCAATTTGAAC CC 3'
traG_FWD_NcoI	5' CATGCCATGGATGACTGATGCAGCTTTCTATCAACTTGG 3'
traG_RVS_XhoI_KpnI	5' CGGGGTACCCCGCTCGAGTTACAGGCTCCCGTTCACACACTG 3'
kikA_sacI_F	5' AAAGAGCTCAGGAGGAATTCACCATGAAGAACTCTTAATA CCTCTGAT 3'
kikA_xbaI_R	5' CCTGTCTAGACTATAAGCGAACTTTCCC 3'

Table 2.8 traF cloning primers

Name	Sequence
TraF_FWD_NcoI	5' CATGCCATGGCCCGTAAAAGTGTCGATGTAGA 3'
TraF_RVS_XhoI	5' GCTCTCGAGTTAGTTGTCTGCGAGCGTATAAACGCC 3'
TraF_RVS_L307_B10	5' GCATGGCTCCGCTCAGACGCTCCCACATATGGGC 3'
B10_FWD_S286_TraF	5' GTGGGAGCGTCTGAGCGGAGCCATGCTCTTGAGTG 3'
B10_RVS_XhoI	5' CAACTCGAGTTAAGAGCGGCGGTTCTTCCC 3'
TraF_RVS_A193_B10	5' GCGGCAAGAGCGTAGCGCGGCTAGCCTTCAGC 3'
B10_FWD_T173_TraF	5' GGCTAGCCGCGCTACGGCTCTTGCCGCACCC 3'
B10_AP_RVS_TraF	5' GAGGGTAGGGGGTATGTTGATGGTCGCCTTAAGGGCTG 3'
TraF_CT_FWD_B10	5' ACCATCAACATACCCCCTACCCTCTACGATCAGCAGG 3'
TraF_AP2_RVS_B10	5' GGTGCTAGCTGCCGTTAAGGTGTCAGAGAACACGAA ATCATG 3'
B10_Loop_FWD_TraF	5' GCAGCTAGCACCTACGCTGGCAG 3'
B10_Loop_RVS_TraF	5' AGTTGTTTGTTCACCGTTATTTTGAAAGCTG 3'

TraF_AP3_FWD_B10	5' GAACAAACAACCTTCTGAAGCACTCCGCTCTTACATGTCTATC 3'
TraF_NT_His_FWD_NcoI	5' GATACCATGGGACATCATCATCACCACCACAATAACGATAGTCAGCAAGCGGCACATG 3'
TraF_5xGly_FWD	5' GGAGGTGGAGGTGGATCTGAAGCACTCCGCTCTTACATGTCTATCC 3'
TraF_5xGly_RVS	5' TCCACCTCCACCTCCCGTTAAGGTGTCAGAGAACAACGAAATCATG 3'
TraF_R373E_RVS	5'GTATCTCGAGTTAGTTGTCTGCGAGCGTATAAACGCCGCTGAAATCGAGGTCCCTCGGCAAC 3'
TraF_N386_Amber_RVS	5'GTATCTCGAGTTACTAGTCTGCGAGCGTATAAACGCCGCTG 3'
TraF_S354_RVS_B10	5' GGTTGGCGGTATAGACATGTAAGAGCGGAGTGCTTAGAC 3'
B10_I355_FWD_TraF	5' TCTTACATGTCTATACCGCCAACCCTGAAGAAGAATCAG 3'
TraF ΔAP_FWD	5' ATGTGGGAGCGTATCCCCCTACCCTCTACGATCAGC 3'
TraF ΔAP_RVS	5' GGTAGGGGGGATACGCTCCACATATGGGCATCC 3'
TraF_FLAG_331_FWD	5' GATTACAAGGACGATGACGATAAAAACATTCAGTACAACAGCACAGAAAACAGCG 3'
TraF_FLAG_330_RVS	5' TTTATCGTCATCGTCCTTGTAATCATTACTCTGCGTCTGGTTAACCAGCGC 3'
TraF ΔAPCT_RVS	5' GTATCTCGAGCTAGGCATCCACCTGGCCCGG 3'
TraF ΔCT_RVS	5' GTATCTCGAGCTAAGACATGTAAGAGCGGAGTGTTCAGACG 3'
TraF_F377_Amber_RVS	5' GTATCTCGAGTTAGTTGTCTGCGAGCGTATAAACGCGCTCTAATCGAGGTCGCGGGCAAC 3'
TraF ΔRDLDLDF_RVS	5' CTATATCTCGAGTTAGTTGTCTGCGAGCGTATAAACGCGCTGGCAACAAAATGCTCACCGCATCAC 3'
F:TrwE_O.L._APCT_FWD	5' CCGGGCCAGGTGGATGATCGGCATTTTGGGAGCGTTTCG 3'
F:TrwE_O.L._APCT_RVS	5' CCAAAAATGCCGATCATCCACCTGGCCCGGAATCCC 3'
F:PtlG_O.L._FWD	5' ATGTGGGAGCGTCTGGGCGGTGCACTGTTACTGAGTGTTCTGG 3'
F:PtlG_O.L._RVS	5'TAACAGTGCACCGCCCAGACGCTCCCACATATGGGCATCC 3'
PtlG_RVS_XhoI	5' CATATATCTCGAGTCATTCATTTGTGCCGCGCAGG 3'
VirB10_FWD_NcoI	5'GATACCATGGGACATCATCATCACCACCACAATAACGATAGTCAGCAAGCGGCACATG 3'
VirB10_NT_RVS_TraF	5' CATCAGTATGACAAATTTCTGAGACCCCGAAAGACGCC 3'
TraF_TM_FWD_VirB10	5' CGGCGTCTTTCGGGGGCCTTTGTCATACTGATGGCGCTGC 3'
TraF_NT_RVS_B10_TM	5' TAACGATAACGCGAGAACGACACCTCCGACGATCAATTTCTGAGATTTCATACGAGGAGCCGAACGG 3'
B10_TM_FWD	5' CAGAAATTGATCGTCGGAGGTGTCGTTTC 3'

TraF_PRR_FWD_B10_TM	5' GTCGGAGGTGTCGTTCTCGCGTTATCGTTAAGCCTCA TTTGGCTAGGTAATAATTCGCGCCCCGGCTAAAGC 3'
TraF_TM_RVS_B10	5'CTTCTTTTGACGCCACCCATGACCGTAATCCCGATGAAT AC 3'
B10_PRR_FWD_TraF	5'ATTACGGTCATGGGTGGGCGTCAAAGAAGGTGAATGAC AAC 3'
B10_PRR_RVS_TraF	5' ATTAGCCATGACTCCGGCCCTGCTGGGCTGCAG 3'
TraF_FWD_B10_PRR	5'CAGCCCAGCAGGGCCGGAGTCATGGCTAATCCCAGCCTG ACTG 3'
VirB10_RVS_R284_TraF	5' GATCGCACCCAGCCAGACGCTGCCAGAAGTGGCTGTCTG 3'
TraF_FWD_L307_VirB10	5' CACTTCTGGCAGCGTCTGGCTGGTGCATCATGATTTC 3'
VirB10_RVS_I335_TraF	5' GTAGAGGGTAGGGGGTATGTTGATGGTCGCCTTAAGG GCTGTCTC 3'
TraF_FWD_P356_VirB10	5'GCGACCATCAACATACCCCCTACCCTCTACGATCAGCAGG 3'
TraF_FWD_SacI	5'GATAGAGCTCATGGCCCGTAAAAGTGTCGATGTAGATCAG GAAC 3'
TraF_NT_FLAG_SacI_FWD	5' GATAGAGCTCATGGATTATAAAGATGACGATGACAAAGC CCGTAAAAGTGTCGATGTAGATCAGGAAC 3'
TraF_FLAG_CT_RVS_XhoI	5' CTATCTCGAGTTATTTGTCATCGTCATCTTTATAATCGTTG TCTGCGAGCGTATAAACGCCG 3'
Lever_FLAG_FWD	5'GATTATAAAGATGACGATGACAAAACCTCCTGCAAGGCTG AAGGCTAGC 3'
Lever_FLAG_RVS	5'TTTGTCATCGTCATCTTTATAATCCAGGTTTTTAGCGAGTG CTGAACCTTCGC 3'

Table 2.9 *traF* amber mutant primers

Name	Sequence
2_amber_Inv_FWD	5' TAGCGTAAAAGTGTCGATGTAGATCAGG 3'
2_amber_Inv_RVS	5' CATGGTGAATTCCTCCTGCTAG 3'
6_amber_Inv_FWD	5' TAGGATGTAGATCAGGAACCTCGATGAAAAC 3'
6_amber_Inv_RVS	5' ACTTTTACGGGCCATGGTG 3'
11_amber_Inv_FWD	5' TAGCTCGATGAAAACACCGGAG 3'
11_amber_Inv_RVS	5' CTGATCTACATCGACACTTTTACGG 3'
16_amber_Inv_FWD	5' TAGGGAGACGGTGAATTTGAAAG 3'
16_amber_Inv_RVS	5' TTCACCGTCTCCGGTGTTTTTC 3'
23_amber_Inv_FWD	5' TAGAACCGCCGTTTCGGCTCCTCG 3'
23_amber_Inv_RVS	5' GCCATTAAATCCGCCACGC 3'
27_amber_Inv_FWD	5' TAGGCTCCTCGTATGAAAGCCTTTG 3'
27_amber_Inv_RVS	5' ACGGCGGTTACTGCCATTAAATC 3'
32_amber_Inv_FWD	5' TAGGCCTTTGTCATACTGATGGCGC 3'
32_amber_Inv_RVS	5' CATACGAGGAGCCGAACGGC 3'

43_amber_Inv_FWD	5' TAGGTATTCATCGGGATTACGGTCATG 3'
43_amber_Inv_RVS	5' AGCAAGCAGCGCCATCAG 3'
45_amber_Inv_FWD	5' TAGATCGGGATTACGGTCATGGG 3'
45_amber_Inv_RVS	5' TACCAAAGCAAGCAGCGCC 3'
49_amber_In_FWD	5' TAGGTCATGGGTAAAATTCGCGCC 3'
49_amber_Inv_RVS	5' AATCCCGATGAATACCAAAGCAAG 3'
P185_FWD_Overlap	5' GCTAAAAACCTGACTTAGGCAAGGCTGAAGGCTAGCCGC 3'
P185_RVS_Overlap	5' AGCCTTCAGCCTTGCCTAAGTCAGGTTTTTAGCGAGTGCTGAACTACCTTC 3'
W304_FWD_Overlap	5' GTGGATGCCCATATGTAGGAGCGTCTGGCTGGTGCGATC 3'
W304_RVS_Overlap	5' ACCAGCCAGACGCTCCTACATATGGGCATCCACCTGGCC 3'
F316_FWD_Overlap	5' ATCATGATTTTCGTTGTAGTCTGACACCTTAACGGCGCTGG 3'
F316_RVS_Overlap	5' CGTTAAGGTGTCAGACTACAACGAAATCATGATCGCACCAGC 3'
N325_FWD_Overlap	5' TTAACGGCGCTGGTTTAGCAGACGCAGAGTAATAACATTCAGTACAACAGCAC 3'
N325_RVS_Overlap	5' ATTACTCTGCGTCTGCTAAACCAGCGCCGTTAAGGTGTCAGAG 3'
Y334_FWD_Overlap	5' AGTAATAACATTCAGTAGAACAGCACAGAAAACAGCGGTGGG 3'
Y334_RVS_Overlap	5' GTTTTCTGTGCTGTTCTACTGAATGTTATTACTCTGCGTCTGGT TAACCAGC 3'
Q343_FWD_Overlap	5' GAAAACAGCGGTGGGTAGCTGGCGTCTGAAGCACTCCGC 3'
Q343_RVS_Overlap	5' TGCTTCAGACGCCAGCTACCCACCGCTGTTTTCTGTGCTG 3'
Y352_FWD_Overlap	5' GAAGCACTCCGCTCTTAGATGTCTATCCCCCTACCCTCTACGATCAG 3'
Y352_RVS_Overlap	5' AGGGGGGATAGACATCTAAGAGCGGAGTGCTTCAGACGCC 3'
F377_FWD_Overlap	5' GCCCGCGACCTCGATTAGAGCGGCGTTTATACGCTCGCAG 3'
F377_RVS_Overlap	5' CGTATAAACGCCGCTCTAATCGAGGTCGCGGGCAACAAAATG 3'
N386_RVS_FLAG_XhoI	5' CTATCTCGAGTTATTTGTCATCGTCATCTTTATAATCCTAGTCTGCGAGCGTATAAACGCCGC 3'

Table 2.10 Mini-pKM101 primers

pKM101_2700SacI_F	5' GCGAGCTCTCCGCAAAATCAATAAGTTTCG 3'
pKM101_2700NcoI_F	5' TTTCCATGGTCCGCAAAATCAATAAGTTTCGC 3'
pKM101_13500Xba_R	5' AATTCTAGAGCCAGAAGCCAGGTTGCTAAT 3'
oriT_NcoI_F	5' GCTCCATGGTACCCTCATTTAGAATGAT 3'
TraI_HindIII_R	5' CGATAAGCTTCATCAGATTTTCATGGCC 3'
TraJ_CT_Strep_F	CAATTCGAAAAGTGAAGGAGGAATTCACCATGCTTGATATAACCACGATTACC
TraJ_CT_Strep_R	5' AGGATGAGACCAGATCTCCCTCAGTTCAATGCC 3'
TraI_CT_6HIS_F	5' CATCATCATTGATGAAGCTTGGCTGTTTTGGCGGATG 3'

TraI_CT_6HIS_R	5' ATGATGATGGATTTTCATGGCCCCCTTCTTCATGCTC 3'
TraK_CT_HA_F	5' CCAGATTATGCTTGAAGGAGGAATTCACCATGGACGATAGAGA AAGAGGCTTAGCATT TTTTATTTGC 3'
TraK_CT_HA_R	5' AACATCATATGGATAGCGCTCCTTTTTTGGTTCCAGACTTTG 3'
RSP005	5' ACACACCCATGGCTTCAACTCAGCAAAAGTT 3'
RSP006	5' AAATCGTACTTGTATTGACCGATGTTACATTGCACAAGAT 3'
RSP007	5' ATCTTGTGCAATGTAAACATCGGTCAATACAAGTACGATTT 3'
RSP008	5' ACACACTCTAGAAATCTATCATGAACAGATCTCAC 3'
TrwH_FWD_KpnI_SacI	5' GATATGGTACCAGGAGGAAGAGCTCATGAAAA CCATCATTTTTTGCAATTTTGATGACG 3'
TrwH_RVS_TraE	5' TTTTTTTATTAGCTTTCATAGTGCCCCCTCGCTGAATTTCC 3'
TraE_FWD_TrwH	5' TCAGCGAGGGGCACTATGAAAGCTAATAAAAAA CAGGGCTTACACGTGAAGC 3'
TraE_RVS_TrwF	5' AGCTAGTTTCTTCATGGGGCAGCCCTCAGTTAACTTCCG 3'
TrwF_FWD_TraE	5' ACTGAGGGCTGCCCCATGAAGAACTAGCTATCGTT GCATTGCTGGC 3'
TrwF_RVS_TraF	5' CACTTTTACGGGCCATTAGTTGCCTCCTTTGTTGACGCGAC 3'
TraF_FWD_TrwF	5' CAAAGGAGGCAACTAATGGCCCGTAAAAGTGTCGATG TAGATCAG 3'
TraF_RVS_TrwE	5' GTTGCCAAGGCGGCCAGCGCGGCTAGCCTTCAGCC 3'
TrwE_FWD_TraF	5' AAGGCTAGCCGCGCTGGCCGCCTTGGCAACCGTGAC 3'
TrwE_RVS_XhoI	5' CATATCTCGAGCTACTTAGTGGGGATGCTTTCGAGA CTGTAGACATC 3'

Table 2.11 *Agrobacterium tumefaciens virB10* primers

B10_298_SphI_FWD	5' TGCCAGGCAGCTAGCACCTACGCTGGC 3'
B10_298_SphI_RVS	5' TGCGAAGGCGCCTTGAACAGCACTCAAGAG 3'
B10_329_SphI_FWD	5' TGCAAGGCGACCATCAACATACCGCCAAC 3'
B10_329_SphI_RVS	5' TGCAAGGGCTGTCTCAGTTGTTTGTTCACCG 3'
B10_332_SphI_FWD	5' TGCATCAACATACCGCCAACCCTGAAGAAGA 3'
B10_332_SphI_RVS	5' TGCGGTCGCCTTAAGGGCTGTCTCAGTTGTTTGTTC 3'
B10_288_RVS_TraF	5' CTTCTGGCAGCGTTTTAGCGGAGCCCTGGCTGGTGCGATC 3'
TraF_307_FWD_B10	5' CGTTTTAGCGGAGCCCTGGCTGGTGCGATCATGATTTTCG 3'
TraF_335_RVS_B10	5' ACCCTGATTCTTCTTGATAGACATGTAAGAGCGGAGTGCTTCAGA C 3'
B10_339_FWD_TraF	5' TCTTACATGTCTATCAAGAAGAATCAGGGTGACACGGTTTCC 3'
3xFLAG_FWD_SphI	5' GATATATAGCATGCGATTACAAGGACGATGACGATAAGGACTA TAAAGATGACG 3'
3xFLAG_RVS_SphI	5' CATATATGCATGCCTTATCATCATCATCCTTATAATCCTTGTCAT CG 3'
3xFLAG_Sense_NcoI_NdeI_XhoI_BamHI	5' GATATATACCATGGGATTACAAGGACGATGACGATAAGGACTA TAAAGATGACGATGACAAGGATTATAAGGATGATGATGATAAGC

	ATATGCTCGAGGGATCCATATATC 3'
3xFLAG_Antisense_NcoI_NdeI_XhoI_BamHI	5'GATATATGGATCCCTCGAGCATATGCTTATCATCATCATCCTTA TAATCCTTGTTCATCGTCATCTTTATAGTCCTTATCGTCATCGTCCTT GTAATCCCATGGTATATATC 3'
VirB10_FWD_NdeI	5'GATATATATACATATGGGAAATAACGATAGTCAGCAAGC GGCACATG 3'
virB10_310_2xFLAG_FWD	5'GATGACGATAAGGACTATAAAGATGACGATGACAAGGGG ATGAGCTTCAACAGCTTTCAAAATAACGGTG 3'
virB10_310_2xFLAG_RVS	5'ATCTTTATAGTCCTTATCGTCATCGTCCTTGTAATCGCCAC CCGAGCTGCCAGCGTAGG 3'
B10_AP_Del_RVS	5' TCCGCTAAAACGCTGCCAG 3'
B10_AP_Del_FWD	5' ACCCTGAAGAAGAATCAGGGTG 3'
B10_288_RVS_TraF	5'CTTCTGGCAGCGTTTTAGCGGAGCCCTGGCTGGTGCGATC 3'
TraF_307_FWD_B10	5'CGTTTTAGCGGAGCCCTGGCTGGTGCGATCATGATTTTCG 3'
TraF_335_RVS_B10	5'ACCCTGATTCTTCTTGATAGACATGTAAGAGCGGAGTGCT TCAGAC 3'
B10_339_FWD_TraF	5'TCTTACATGTCTATCAAGAAGAATCAGGGTGACACGGTTT CC 3'
G269R_FWD	5' GGACGAACTCCGTCGCCCAGGATTGCCGG 3'
G269R_RVS	5' ATCCTGGGCGACGGAGTTCGTCCGCGCTTGGCG 3'
G269K_FWD	5' GGACGAACTCAAGCGCCAGGATTGCCGG 3'
G269K_RVS	5' ATCCTGGGCGCTTGAGTTCGTCCGCGCTTGGCG 3'
G269W_FWD	5' GGACGAACTCTGGCGCCAGGATTGCCGG 3'
G269W_RVS	5' ATCCTGGGCGCCAGAGTTCGTCCGCGCTTGGCG 3'
G269C_FWD	5' GGACGAACTCTGCCGCCAGGATTGCCGG 3'
G269C_RVS	5' ATCCTGGGCGGCAGAGTTCGTCCGCGCTTGGCG 3'
G269D_FWD	5' GGACGAACTCGACCGCCAGGATTGCCGG 3'
G269D_RVS	5' ATCCTGGGCGGTTCGAGTTCGTCCGCGCTTGGCG 3'
G272R_FWD	5' CTCGGTGCCACGTTTGCCGGGCTCGGTCGAC 3'
G272R_RVS	5' CGAGCCCGGCAAACGTGGGCGACCGAGTTCGTCC 3'
G272K_FWD	5' CTCGGTGCCCAAAGTTGCCGGGCTCGGTCGAC 3'
G272K_RVS	5' CGAGCCCGGCAACTTTGGGCGACCGAGTTCGTCC 3'
G272W_FWD	5' CTCGGTGCCCATGGTTGCCGGGCTCGGTCGAC 3'
G272W_RVS	5' CGAGCCCGGCAACCATGGGCGACCGAGTTCGTCC 3'
G272C_FWD	5' CTCGGTGCCCATGCTTGCCGGGCTCGGTCGAC 3'
G272C_RVS	5' CGAGCCCGGCAAGCATGGGCGACCGAGTTCGTCC 3'
G272D_FWD	5' CTCGGTGCCAGACTTGCCGGGCTCGGTCGAC 3'
G272D_RVS	5' CGAGCCCGGCAAGTCTGGGCGACCGAGTTCGTCC 3'
G275R_FWD	5' CCAGGATTGCCGCGTTCGGTTCGACAGCCACTTCTGG 3'
G275R_RVS	5' GCTGTCGACCGAACGCGGCAATCCTGGGCGACC 3'
G275K_FWD	5' CCAGGATTGCCGAAGTCGGTTCGACAGCCACTTCTGG 3'
G275K_RVS	5' GCTGTCGACCGACTTCGGCAATCCTGGGCGACC 3'
G275W_FWD	5' CCAGGATTGCCGTGGTTCGGTTCGACAGCCACTTCTGG 3'

G275W_RVS	5' GCTGTCGACCGACCTCGGCAATCCTGGGCGACC 3'
G275C_FWD	5' CCAGGATTGCCGTGCTCGGTTCGACAGCCACTTCTGG 3'
G275C_RVS	5' GCTGTCGACCGAGCACGGCAATCCTGGGCGACC 3'
G275D_FWD	5' CCAGGATTGCCGGACTCGGTTCGACAGCCACTTCTGG 3'
G275D_RVS	5' GCTGTCGACCGAGTCCGGCAATCCTGGGCGACC 3'

Plasmid modifications

Plasmid pBAD24Spc was created by isolation of the *spc^r* gene as a *Sma*I fragment from pHP45Ω and inserting it into the *Sca*I site within the *crb^r* gene on pBAD24 (147,148). pKM101Spc^r was constructed by introduction of the same *spc^r* gene as an *Eco*RI fragment into the unique *Eco*RI site within the *crb^r* gene of pKM101.

Construction of pKM101 *tra* gene deletions

Eight of the 11 *tra* genes were deleted from pKM101 by recombineering. Briefly, pKM101 or pKM101Spc^r were transferred by conjugation into *E. coli* strain HME45, which contains the bacteriophage λ *red* system under the control of the cI857 repressor. For construction of each *tra* gene deletion, the *sacB*-kan^r cassette from plasmid pBB50 was PCR amplified, so that it carried flanking *Nco*I sites and 35 basepairs (bps) of 5' and 3' sequences that were complementary to regions immediately upstream and downstream of a *tra* gene of interest. HME45(pKM101Crb^r) or HME45(pKM101Spc^r) cells were temperature-induced for expression of the *red-gam* genes, and the kan^r amplicons were introduced by electroporation with Kan^r selection for transformants. Because pKM101 is a multicopy plasmid, we eliminated plasmids lacking the integrated *sacB*-kan cassette by subculturing the Kan^r transformants for 4 days in LB broth containing kanamycin (200 µg ml⁻¹). Isolated plasmids were digested with *Nco*I and religated to delete the *sacB*-kan^r cassette, and ligation mixes were introduced into DH5α with

selection for Crb^r or Spc^r . Transformants were screened for kanamycin sensitivity, and *tra* deletion mutations were confirmed by sequencing across the deletion junction.

Construction of mini-pKM101 plasmids

The Christie lab constructed 3 mini-pKM101 plasmids with a goal of simplifying genetic manipulations of the *tra* gene cluster. We constructed pCGR108 by introduction of the *tra* region from pKM101 into pBAD24. For this region, we amplified a ~10-kilobase region of pKM101 encompassing the upstream regulatory region and *tra* promoter through *traG*. This fragment was amplified with primers pKM101_2700NcoI_F and pKM101_13500XbaI_R and the resulting PCR product was introduced into pBAD24 using *NcoI* and *XbaI* restriction sites. The second mini-pKM101 plasmid, pCGR100, was constructed by amplifying the same ~10-kilobase region from pCGR108 using primers pKM101_2700SacI_F and pKM101_13500XbaI_R with pKM101 as a template. The resulting PCR product was digested with *SacI* and *XbaI* and ligated into a *SacI/XbaI* digested pBAD33 plasmid. The third mini-pKM101 plasmid, pRP100, was constructed by joining three PCR amplification products: i) the *tra* gene cluster extending from the 3' end of *kikA* through the end of *traG*, ii) the pKM101 oriV replication origin, and iii) an *nptII* gene encoding Kan^r . The ~10-kb *tra* gene cluster was cut from plasmid pCGR125, a variant of pCGR108 containing the upstream *kikA* locus, using *SacI* and *XbaI* restriction enzymes, a ~3-kb region encompassing the replication origin was amplified with primers RSP007 and RSP008, and the *nptII* gene was amplified with primers RSP005 and RSP006 using plasmid pUC4K as a template. The replication origin and *nptII* gene were joined together using overlapping PCR, digested with *SacI* and *XbaI*, and ligated to the *tra* operon. The resulting product was transformed into *E. coli* DH5 α with Kan^r as a selection for self-replicating pRP100.

Transformants were screened for plasmids bearing the three PCR fragments followed by sequence analysis of the PCR fragment junctions. We also confirmed that each of the mini-pKM101 plasmids encodes a fully functional Tra T4SS.

Construction of pRP100 and pCGR108 variants and a mobilization plasmid

Plasmid pJG125 contains a deletion of the *traF* locus flanked by 5' *SacI* and 3' *XhoI* restriction sites. It was constructed using inverse PCR using primers TraF_Del._RVS_SacI and TraF_Del._FWD_XhoI with pCGR108 as a template.

Plasmid pJG143 contains a deletion of *traN* through *traF* flanked by 5' *SacI* and 3' *XhoI* restriction sites. It was constructed using inverse PCR using primers TraN_Del._RVS_SacI and TraF_Del._FWD_XhoI with pCGR108 as a template.

Plasmid pRP101 contains a deletion of the *traL* locus. It was constructed using inverse PCR using primers TraL_Del._Inv._FWD and TraL_Del._Inv._RVS with pRP100 as a template.

Plasmid pRP107 contains a deletion of the *traN* locus. It was constructed using inverse PCR using primers TraN_Del._Inv._FWD and TraN_Del._Inv._RVS with pRP100 as a template.

Plasmid pRP109 contains a deletion of the *traO* locus. It was constructed using inverse PCR using primers TraO_Del._Inv._FWD and TraO_Del._Inv._RVS with pRP100 as a template.

Plasmid pRP110 contains a deletion of the *traF* locus. It was constructed using inverse PCR using primers TraF_Del._Inv._FWD and TraF_Del._Inv._RVS with pRP100 as a template.

Plasmid pJG142 contains the pKM101 origin of transfer (*oriT*) as well as the genes encoding the TraK accessory protein, TraJ T4CP, and TraI relaxase. This region was PCR amplified using primers oriT_NcoI_F and TraI_HindIII_R with pKM101 as a template. This PCR product was

cloned into a pGB2 plasmid which had been digested with *Hind*III followed by blunt-ending with Klenow polymerase (149).

Plasmid pJG160 contains a deletion of the *traC* locus flanked by 5' *Sac*I and 3' *Xho*I restriction sites. It was constructed using inverse PCR using primers TraC_Del._RVS_SacI and TraC_Del._FWD_XhoI with pCGR108 as a template.

Plasmid pJG161 contains a deletion of the *traE* locus flanked by 5' *Sac*I and 3' *Xho*I restriction sites. It was constructed using inverse PCR using primers TraE_Del._RVS_SacI and TraE_Del._FWD_XhoI with pCGR108 as a template.

Plasmid pJG165 contains mini-pKM101 with a C-terminally FLAG tagged TraC. It was constructed by amplifying *traC* using primers TraC_FWD_SacI and TraC_FLAG_RVS_XhoI with pKM101 as a template. The resulting PCR product was digested with *Sac*I and *Xho*I and ligated into a *Sac*I/*Xho*I digested pJG60 plasmid.

Plasmid pJG166 contains mini-pKM101 with a C-terminally FLAG tagged TraE. It was constructed by amplifying *traC* using primers TraE_FWD_SacI and TraE_FLAG_RVS_XhoI with pKM101 as a template. The resulting PCR product was digested with *Sac*I and *Xho*I and ligated into a *Sac*I/*Xho*I digested pJG61 plasmid.

Plasmid pYGL24 contains the *oriT* through *traI* region of pKM101 with TraK, TraJ, and TraI tagged with HA, Strep, and 6xHis tags, respectively. It was made through sequential additions of tags using inverse PCR. A Strep tag was added to TraJ by amplifying pJG142 with primers TraJ_CT_Strep_F and TraJ_CT_Strep_R. Once *traJ* contained a Strep tag sequence at its 3' end, *traI* had a 6xHis tag sequence added to its 3' end with primers TraI_CT_6HIS_F and TraI_CT_6HIS_R. A sequence encoding an HA tag at the 3' end of *traK* was added using primers TraK_CT_HA_F and TraK_CT_HA_R

Construction of pKM101 complementing plasmids

Plasmid pMS22 expresses $P_{BAD}::traL$, producing TraL. It was constructed by PCR amplification of *traL* using primers *traL_FWD_NcoI* and *traL_RVS_XhoI_KpnI* and pKM101 as a template. The resulting PCR fragment was digested with *NcoI* and *KpnI* for introduction into *NcoI/KpnI*-digested pBAD24Kan.

Plasmid pMS24 expresses $P_{BAD}::traM$, producing TraM. It was constructed by PCR amplification of *traM* using primers *traM_FWD_NcoI* and *traM_RVS_XhoI_KpnI* and pKM101 as a template. The resulting PCR fragment was digested with *NcoI* and *KpnI* for introduction into *NcoI/KpnI*-digested pBAD24Kan.

Plasmid pMS26 expresses $P_{BAD}::traA$, producing TraA. It was constructed by PCR amplification of *traA* using primers *traA_FWD_NcoI* and *traA_RVS_XhoI_KpnI* and pKM101 as a template. The resulting PCR fragment was digested with *NcoI* and *KpnI* for introduction into *NcoI/KpnI*-digested pBAD24Kan.

Plasmid pMS28 expresses $P_{BAD}::traB$, producing TraB. It was constructed by PCR amplification of *traB* using primers *traB_FWD_NcoI* and *traB_RVS_XhoI_KpnI* and pKM101 as a template. The resulting PCR fragment was digested with *NcoI* and *KpnI* for introduction into *NcoI/KpnI*-digested pBAD24Kan.

Plasmid pMS30 expresses $P_{BAD}::traC$, producing TraC. It was constructed by PCR amplification of *traC* using primers *traC_FWD_NcoI* and *traC_RVS_XhoI_KpnI* and pKM101 as a template. The resulting PCR fragment was digested with *NcoI* and *KpnI* for introduction into *NcoI/KpnI*-digested pBAD24Kan.

Plasmid pMS32 expresses $P_{BAD}::traD$, producing TraD. It was constructed by PCR amplification of *traD* using primers *traD_FWD_NcoI* and *traD_RVS_XhoI_KpnI* and pKM101

as a template. The resulting PCR fragment was digested with *Nco*I and *Kpn*I for introduction into *Nco*I/*Kpn*I-digested pBAD24Kan.

Plasmid pMS35 expresses $P_{BAD}::traN$, producing TraN. It was constructed by PCR amplification of *traN* using primers traN_FWD_*Nco*I and traN_RVS_*Xho*I_*Kpn*I and pKM101 as a template. The resulting PCR fragment was digested with *Nco*I and *Kpn*I for introduction into *Nco*I/*Kpn*I-digested pBAD24.

Plasmid pMS36 expresses $P_{BAD}::traE$, producing TraE. It was constructed by PCR amplification of *traE* using primers traE_FWD_*Nco*I and traE_RVS_*Xho*I_*Kpn*I and pKM101 as a template. The resulting PCR fragment was digested with *Nco*I and *Kpn*I for introduction into *Nco*I/*Kpn*I-digested pBAD24Kan.

Plasmid pMS38 expresses $P_{BAD}::traO$, producing TraO. It was constructed by PCR amplification of *traO* using primers traO_FWD_*Nco*I and traO_RVS_*Xho*I_*Kpn*I and pKM101 as a template. The resulting PCR fragment was digested with *Nco*I and *Kpn*I for introduction into *Nco*I/*Kpn*I-digested pBAD24Kan.

Plasmid pMS40 expresses $P_{BAD}::traG$, producing TraG. It was constructed by PCR amplification of *traG* using primers traG_FWD_*Nco*I and traG_RVS_*Xho*I_*Kpn*I and pKM101 as a template. The resulting PCR fragment was digested with *Nco*I and *Kpn*I for introduction into *Nco*I/*Kpn*I-digested pBAD24Kan.

Plasmid pCGR113 expresses native *kikA* from the pBAD promoter. It was constructed by PCR amplification of *kikA* using primers kikA_sac1_F and kikA_xba1_R and pKM101 as a template. The resulting PCR fragment was digested with *Sac*I and *Xba*I for introduction into *Sac*I/*Xba*I-digested pBAD33.

Construction of *traF* alleles

Plasmid pJG59 expresses $P_{BAD}::traF$, producing TraF. It was constructed by PCR amplification of *traF* using primers TraF_FWD_NcoI and TraF_RVS_XhoI and pKM101 as a template. The resulting PCR fragment was digested with *NcoI* and *XhoI* for introduction into *NcoI/SalI*-digested pBAD24Spc.

Plasmid pJG62 expresses $P_{BAD}::his_6-traF$, producing N-terminally 6xHis-tagged TraF. It was constructed by PCR amplification of *traF* using primers TraF_NT_His_FWD_NcoI and TraF_RVS_XhoI and pKM101 as a template. The resulting PCR product was digested with *NcoI* and *XhoI* for introduction into *NcoI/SalI*-digested pBAD24Spc.

Plasmid pJG95 expresses $P_{BAD}::traF1-301$, producing TraF deleted of its antennae projection (AP) and C-terminal tail (CT). It was constructed by amplifying basepairs (bps) 1-903 of *traF* using primers TraF_NT_His_FWD_NcoI and TraF_ΔAPCT_RVS, and pKM101 as a template. The resulting PCR product was digested with *NcoI* and *XhoI* for introduction into *NcoI/SalI*-digested pBAD24Spc.

Plasmid pJG96 expresses $P_{BAD}::traF1-353$, producing TraF deleted of its CT. It was constructed by amplifying bps 1-1059 of *traF* using primers TraF_NT_His_FWD_NcoI and TraF_ΔCT_RVS and pKM101 as a template. The resulting PCR product was digested with *NcoI* and *XhoI* for introduction into *NcoI/SalI*-digested pBAD24Spc.

Plasmid pJG76 expresses $P_{BAD}::traF \Delta 307-354$, producing TraF deleted of its AP domain. It was constructed by PCR amplifying *traF* codons 1-307 using TraF_NT_His_FWD_NcoI and TraF_ΔAP_RVS and codons 355-386 using TraF_ΔAP_FWD and TraF_RVS_XhoI_off of pKM101. These PCR products were joined together by overlapping PCR, and the resulting

fragment was digested with *NcoI* and *XhoI* for introduction into *NcoI/SalI*-digested pBAD24Spc.

Plasmid pJG61 expresses $P_{BAD}::traF\text{-}5xGly$, producing TraF with a pentaglycine substitution of the AP loop. It was created by using primers TraF_NT_His_FWD_NcoI and TraF_5xGly_RVS to PCR amplify codons 1-322, and primers TraF_5xGly_FWD and TraF_RVS_XhoI to amplify codons 346-386. The two PCR products were joined together by overlapping PCR, and the resulting product was digested with *NcoI* and *XhoI* for introduction into *NcoI/SalI*-digested pBAD24Spc.

Plasmid JG101 expresses $P_{BAD}::traF\Delta 373\text{-}377$, producing TraF deleted of the conserved RDLDF (residues 369-373) motif in the CT. It was created by using primers TraF_NT_His_FWD_NcoI and TraF_ARDLDF_RVS and pKM101 as a template for PCR amplification. The PCR product was digested with *NcoI* and *XhoI* for introduction into *NcoI/SalI*-digested pBAD24Spc.

Plasmids pJG97 expresses $P_{BAD}::traF\Delta CT9$, producing TraF deleted of its last 9 residues. *traF* $\Delta CT9$ was PCR amplified using primers TraF_NT_His_FWD_NcoI and TraF_F377_Amber_RVS and pKM101 as a template. The PCR product was digested with *NcoI* and *XhoI* for introduction into *NcoI/SalI*-digested pBAD24Spc.

Plasmids pJG98 expresses $P_{BAD}::traF\Delta CT1$, producing TraF deleted of its last residues. *traF* $\Delta CT1$ was PCR amplified using primers TraF_NT_His_FWD_NcoI and TraF_N386_Amber_RVS and pKM101 as a template. The PCR product was digested with *NcoI* and *XhoI* for introduction into *NcoI/SalI*-digested pBAD24Spc.

Plasmids pJG99 expresses $P_{BAD}::traFR373E$, producing TraF with an R373E mutation. *traF* was PCR amplified using primers TraF_NT_His_FWD_NcoI and TraF_R373E_RVS and

pKM101 as a template. The PCR product was digested with *Nco*I and *Xho*I for introduction into *Nco*I/*Sal*I-digested pBAD24Spc.

Plasmid pJG68 expresses $P_{BAD}::traF/NT_{virB10}$, producing the TraF/NT_{VirB10} chimera. It was constructed by amplifying *virB10* codons 1-29 using primers VirB10_FWD_*Nco*I and VirB10_NT_RVS_TraF with pKVD10 as a template and *traF* codons 40-386 were amplified using primers TraF_TM_FWD_VirB10 and TraF_RVS_*Xho*I with pKM101 as a template. The two fragments were combined using overlapping PCR and the resulting product was digested with *Nco*I and *Xho*I for introduction into *Nco*I/*Sal*I-digested pBAD24Spc.

Plasmid pJG69 expresses $P_{BAD}::traF/TM_{virB10}$, producing the TraF/TMD_{VirB10} chimera. It was constructed by amplifying *traF* codons 1-40 using primers TraF_NT_His_FWD_*Nco*I and TraF_NT_RVS_B10_TM and codons 60-386 with TraF_PRR_FWD_B10_TM and TraF_RVS_*Xho*I with pKM101 as a template. The two fragments were combined using overlapping PCR and the resulting product was digested with *Nco*I and *Xho*I for introduction into *Nco*I/*Sal*I-digested pBAD24Spc.

Plasmid pJG2005 expresses $P_{BAD}::traF/TM-CT_{virB10}$, producing the TraF/TMD-CT_{VirB10} chimera. It was constructed by amplifying *traF* codons 1-40 using primers TraF_NT_His_FWD_*Nco*I and TraF_NT_RVS_B10_TM with pKM101 as a template and amplifying *virB10* codons 29-377 using primers B10_TM_FWD and B10_RVS_*Xho*I with pKVD10 as a template. The two fragments were combined using overlapping PCR and the resulting product was digested with *Nco*I and *Xho*I for introduction into *Nco*I/*Sal*I-digested pBAD24Spc.

Plasmid pJG70 expresses $P_{BAD}::traF/PRR_{virB10}$, producing the TraF/PRR_{VirB10} chimera. It was constructed by amplifying *traF* codons 1-60 using primers TraF_NT_His_FWD_*Nco*I and

TraF_TM_RVS_B10 and codons 194-386 using primers TraF_FWD_B10_PRR and TraF_RVS_XhoI with pKM101 as a template. Codons 51-172 of *virB10* were amplified using primers B10_PRR_FWD_TraF and B10_PRR_RVS_TraF with pKVD10 as a template. The three fragments were combined using overlapping PCR and the resulting product was digested with *NcoI* and *XhoI* for introduction into *NcoI/SalI*-digested pBAD24Spc.

Plasmid pJG150 expresses $P_{BAD}::traF/BB_{virB10}$, producing the TraF/BB_{VirB10} chimera. It was constructed by amplifying *traF* codons 1-193 and *virB10* codons 173-286 using TraF_NT_His_FWD_NcoI and VirB10_RVS_R284_TraF with pJG58 as a template. Codons 307-386 of *traF* were amplified using TraF_FWD_L307_VirB10 and TraF_RVS_XhoI with pKM101 as a template. The two fragments were combined using overlapping PCR and the resulting product was digested with *NcoI* and *XhoI* for introduction into *NcoI/SalI*-digested pBAD24Spc.

Plasmid pJG134 expresses $P_{BAD}::traF/BB-AP_{virB10}$, producing the TraF/BB-AP_{VirB10} chimera. It was constructed by amplifying *traF* codons 1-193 and *virB10* codons 173-335 using primers TraF_NT_His_FWD_NcoI and VirB10_RVS_I335_TraF with pJG58 as a template. Codons 356-386 of *traF* were amplified using primers TraF_FWD_P356_VirB10 and TraF_RVS_XhoI and pKM101 as a template. The two fragments were combined using overlapping PCR and the resulting product was digested with *NcoI* and *XhoI* for introduction into *NcoI/SalI*-digested pBAD24Spc.

Plasmid pJG57 expresses $P_{BAD}::traF/AP-CT_{virB10}$, producing the TraF/AP-CT_{VirB10} chimera. It was constructed by amplifying codons 1-307 of *traF* using TraF_NT_His_FWD_NcoI and TraF_RVS_L307_B10 with pKM101 as a template, and the region of *virB10* encoding residues 286-377 was amplified using B10_FWD_S286_TraF and B10_RVS_XhoI with pKVD10 as a

template. The two PCR products were joined by overlapping PCR, and the resulting product was digested with *Nco*I and *Xho*I for introduction into *Nco*I/*Sal*I-digested pBAD24Kan.

Plasmid pJG58 expresses $P_{BAD}::traF/BB-CT_{virB10}$, producing the TraF/BB-AP-CT_{VirB10} chimera. It was constructed by amplifying codons 1-193 of *traF* using TraF_NT_His_FWD_*Nco*I and TraF_RVS_A193_B10 with pKM101 as a template, and the region of *virB10* encoding residues 173-377 was amplified using B10_FWD T173_TraF and B10_RVS_*Xho*I with pKVD10 as a template. The two PCR products were joined by overlapping PCR, and the resulting product was digested with *Nco*I and *Xho*I for introduction into *Nco*I/*Sal*I-digested pBAD24Kan.

Plasmid pJG60 expresses $P_{BAD}::traF/AP_{virB10}$, producing the TraF/AP_{VirB10} chimera. It was constructed by amplifying codons 1-307 of *traF* and codons 286-335 of *virB10* using TraF_NT_His_FWD_*Nco*I and B10_AP_RVS TraF with pJG57 as a template. Codons 356-386 of *traF* were amplified using TraF_CT_FWD_B10 and TraF_RVS_*Xho*I with pKM101 as a template. These fragments were joined by overlapping PCR, and the resulting product was digested with *Nco*I and *Xho*I for introduction into *Nco*I/*Sal*I-digested pBAD24Spc.

Plasmid pJG65 expresses $P_{BAD}::traF/APL_{virB10}$, producing the TraF/APL_{VirB10} chimera. It was constructed by amplifying codons 1-322 of *traF* using TraF_NT_His_FWD_*Nco*I and TraF_AP2_RVS_B10, and codons 364-386 using TraF_AP3_FWD_B10 and TraF_RVS_*Xho*I with pKM101 as a template. Codons 301-325 of *virB10* were PCR amplified using B10_Loop_FWD_TraF and B10_Loop_RVS_TraF with pKVD10 as a template. The three PCR fragments were joined by overlapping PCR, and the resulting fragment was digested with *Nco*I and *Xho*I for introduction into *Nco*I/*Sal*I-digested pBAD24Spc.

Plasmid pJG66 expresses $P_{BAD}::traF/CT_{virB10}$, producing the TraF/CT_{VirB10} chimera. It was constructed by amplifying codons 1-354 of *traF* using primers TraF_NT_His_FWD_NcoI and TraF_S354_RVS_B10 with pKM101 as a template, and codons 335-377 of *virB10* using primers B10_I355_FWD_TraF and B10_RVS_XhoI with pKVD10 as a template. These PCR products were joined by overlapping PCR, and the resulting fragment was digested with *NcoI* and *XhoI* for introduction into *NcoI/SalI*-digested pBAD24Spc.

Plasmid pJG152 contains mini-pKM101 which produces NT FLAG TraF. It was constructed by amplifying *traF* using TraF_NT_FLAG_SacI_FWD and TraF_RVS_XhoI and pKM101 as a template. The resulting fragment was digested with *SacI* and *XhoI* and introduced into a *SacI/XhoI* digested pJG125 plasmid.

Plasmid pJG158 contains mini-pKM101 which produces NT FLAG TraF deleted of its AP domain ($\Delta 307-354$). It was constructed by amplifying *traF* using TraF_NT_FLAG_SacI_FWD and TraF_RVS_XhoI and pJG76 as a template. The resulting fragment was digested with *SacI* and *XhoI* and introduced into a *SacI/XhoI* digested pJG125 plasmid.

Plasmid pJG154 contains mini-pKM101 which produces NT FLAG TraF deleted of the conserved RDLDF motif ($\Delta 373-377$). It was constructed by amplifying *traF* using TraF_NT_FLAG_SacI_FWD and TraF_ Δ RDLDF_RVS and pJG101 as a template. The resulting fragment was digested with *SacI* and *XhoI* and introduced into a *SacI/XhoI* digested pJG125 plasmid.

Plasmid pJG153 contains mini-pKM101 which produces NT FLAG TraF deleted of the the C-terminal nine residues (Δ CT9). It was constructed by amplifying *traF* using TraF_NT_FLAG_SacI_FWD and TraF_F377_Amber_RVS and pJG97 as a template. The

resulting fragment was digested with *SacI* and *XhoI* and introduced into a *SacI/XhoI* digested pJG125 plasmid.

Plasmid pJG155 contains mini-pKM101 which produces NT FLAG TraF/AP-CT_{VirB10}. It was constructed by amplifying *traF*/AP-CT_{virB10} using TraF_NT_FLAG_SacI_FWD and B10_RVS_XhoI and pJG57 as a template. The resulting fragment was digested with *SacI* and *XhoI* and introduced into a *SacI/XhoI* digested pJG125 plasmid.

Plasmid pJG157 contains mini-pKM101 which produces NT FLAG TraF/AP-CT_{TrwE}. It was constructed by amplifying *traF* codons 1-300 using primers TraF_NT_FLAG_SacI_FWD and F:TrwE_O.L._APCT_RVS with pKM101 as a template and *trwE* codons 303-395 using F:TrwE_O.L._APCT_FWD and TrwE_RVS_XhoI with pJG145 as a template. The resulting 2 PCR fragments were joined together by overlapping PCR and the resulting fragment was digested with *SacI* and *XhoI* and introduced into a *SacI/XhoI* digested pJG125 plasmid.

Plasmid pJG156 contains mini-pKM101 which produces NT FLAG TraF/AP-CT_{PtlG}. It was constructed by amplifying *traF* codons 1-307 using primers TraF_NT_FLAG_SacI_FWD and F:PtlG O.L. RVS with pKM101 as a template and *ptlG* codons 294-374 using F:PtlG_O.L._FWD and PtlG_RVS_XhoI using pJG203 as a template. The resulting 2 PCR fragments were joined together by overlapping PCR and the resulting fragment was digested with *SacI* and *XhoI* and introduced into a *SacI/XhoI* digested pJG125 plasmid.

Plasmid pJG162 contains mini-pKM101 which produces AP FLAG TraF. It was constructed by amplifying *traF* codons 1-330 using primers TraF_FWD_SacI and TraF_FLAG_330_RVS and codons 331-386 with primers TraF_FLAG_331_FWD and TraF_RVS_XhoI with pKM101 as a template. The resulting fragments were joined via overlapping PCR and the resulting PCR

fragment was digested with *SacI* and *XhoI* and introduced into a *SacI/XhoI* digested pJG125 plasmid.

Plasmid pJG163 contains mini-pKM101 which produces CT FLAG TraF. It was constructed by amplifying *traF* using primers TraF_FWD_SacI and TraF_FLAG_CT_RVS_XhoI with pKM101 as a template. The resulting fragment was digested with *SacI* and *XhoI* and introduced into a *SacI/XhoI* digested pJG125 plasmid.

Plasmid pJG164 contains mini-pKM101 which produces Lever FLAG TraF. It was constructed by amplifying *traF* codons 1-183 using primers TraF_FWD_SacI and Lever_FLAG_RVS and codons 184-386 with primers Lever_FLAG_FWD and TraF_RVS_XhoI with pKM101 as a template. The resulting fragments were joined via overlapping PCR and the resulting PCR fragment was digested with *SacI* and *XhoI* and introduced into a *SacI/XhoI* digested pJG125 plasmid.

Construction of chimeric operons

Plasmid pJG202 contains the chimeric *tra:virB* operon. A DNA fragment encoding *virB7-traE-virB9-traF/BB-CT_{virB10}* was designed with each gene codon optimized for expression in *E. coli*. The DNA fragment contained flanking *SacI* and *XhoI* restriction sites and was cloned as a blunt-ended fragment into an *EcoRV*-digested pUC57-Amp plasmid. DNA fragment synthesis and cloning was performed by Genewiz Inc.

Plasmid pJG203 contains the chimeric *tra:ptl* operon. A DNA fragment encoding *ptlI-traE-ptlF-traF/BB-CT_{ptlG}* was designed with each gene codon optimized for expression in *E. coli*. The chimeric *traF:ptlG* gene contains codons 1-172 of *traF* followed by codons 160-374 of *ptlG*. The DNA fragment contained flanking *SacI* and *XhoI* restriction sites and was cloned as a blunt-

ended fragment into an *EcoRV*-digested pUC57-Amp plasmid. DNA fragment synthesis and cloning was performed by Genewiz Inc.

Plasmid pJG144 contains mini-pKM101 producing the chimeric Tra:VirB T4SS. The *tra:virB* fragment from pJG202 was digested from the plasmid using *SacI* and *XhoI* and introduced into a *SacI/XhoI* digested pJG143 plasmid.

Plasmid pJG151 contains mini-pKM101 producing the chimeric Tra:Ptl T4SS. The *tra:ptl* fragment from pJG203 was digested from the plasmid using *SacI* and *XhoI* and introduced into a *SacI/XhoI* digested pJG143 plasmid.

Plasmid pJG145 contains mini-pKM101 producing the chimeric Tra:Trw T4SS. It was constructed by amplifying *trwH* using primers TrwH_FWD_KpnI_SacI and TrwH_RVS_TraE, *trwF* using primers TrwF_FWD_TraE and TrwF_RVS_TraF, and *trwE* codons 197-395 using primers TrwE_FWD_TraF and TrwE_RVS_XhoI using pSU1443 as a template (150). *traE* was amplified using primers TraE_FWD_TrwH and TraE_RVS_TrwF and *traF* codons 1-193 were amplified using primers TraF_FWD_TrwF and TraF_RVS_TrwE using pKM101 as a template. The five PCR products were joined together by overlapping PCR and the resulting product was digested with using *SacI* and *XhoI* and introduced into a *SacI/XhoI* digested pJG143 plasmid.

Construction of *traF* amber mutants for photocrosslinking

Plasmid pJG111 expresses *P_{BAD}::traF*-P185amber producing TraF with pBpa incorporated at position 185. It was constructed by amplifying codons 1-184 using primers TraF_NT_His_FWD_NcoI and P185_RVS_Overlap and codons 186-386 using primers P185_FWD_Overlap and TraF_FLAG_CT_RVS_XhoI with pKM101 as a template. These

fragments were joined through overlapping PCR and the resulting PCR fragment was digested with *NcoI* and *XhoI* and ligated into an *NcoI/SalI* digested pBAD24Spc.

Plasmid pJG112 expresses *P_{BAD}::traF-W304*amber producing TraF with pBpa incorporated at position 304. It was constructed by amplifying codons 1-303 using primers TraF_NT_His_FWD_NcoI and W304_RVS_Overlap and codons 305-386 using primers W304_FWD_Overlap and TraF_FLAG_CT_RVS_XhoI with pKM101 as a template. These fragments were joined through overlapping PCR and the resulting PCR fragment was digested with *NcoI* and *XhoI* and ligated into an *NcoI/SalI* digested pBAD24Spc.

Plasmid pJG113 expresses *P_{BAD}::traF-F316*amber producing TraF with pBpa incorporated at position 316. It was constructed by amplifying codons 1-315 using primers TraF_NT_His_FWD_NcoI and F316_RVS_Overlap and codons 317-386 using primers F316_FWD_Overlap and TraF_FLAG_CT_RVS_XhoI with pKM101 as a template. These fragments were joined through overlapping PCR and the resulting PCR fragment was digested with *NcoI* and *XhoI* and ligated into an *NcoI/SalI* digested pBAD24Spc.

Plasmid pJG114 expresses *P_{BAD}::traF-N325*amber producing TraF with pBpa incorporated at position 325. It was constructed by amplifying codons 1-324 using primers TraF_NT_His_FWD_NcoI and N325_RVS_Overlap and codons 326-386 using primers N325_FWD_Overlap and TraF_FLAG_CT_RVS_XhoI with pKM101 as a template. These fragments were joined through overlapping PCR and the resulting PCR fragment was digested with *NcoI* and *XhoI* and ligated into an *NcoI/SalI* digested pBAD24Spc.

Plasmid pJG115 expresses *P_{BAD}::traF-Y334*amber producing TraF with pBpa incorporated at position 334. It was constructed by amplifying codons 1-333 using primers TraF_NT_His_FWD_NcoI and Y334_RVS_Overlap and codons 335-386 using primers

Y334_FWD_Overlap and TraF_FLAG_CT_RVS_XhoI with pKM101 as a template. These fragments were joined through overlapping PCR and the resulting PCR fragment was digested with *NcoI* and *XhoI* and ligated into an *NcoI/SalI* digested pBAD24Spc.

Plasmid pJG116 expresses *P_{BAD}::traF-Q343*amber producing TraF with pBpa incorporated at position 343. It was constructed by amplifying codons 1-342 using primers TraF_NT_His_FWD_NcoI and Q343_RVS_Overlap and codons 344-386 using primers Q343_FWD_Overlap and TraF_FLAG_CT_RVS_XhoI with pKM101 as a template. These fragments were joined through overlapping PCR and the resulting PCR fragment was digested *NcoI* and *XhoI* and ligated into an *NcoI/SalI* digested pBAD24Spc.

Plasmid pJG117 expresses *P_{BAD}::traF-Y352*amber producing TraF with pBpa incorporated at position 352. It was constructed by amplifying codons 1-351 using primers TraF_NT_His_FWD_NcoI and Y352_RVS_Overlap and codons 353-386 using primers Y352_FWD_Overlap and TraF_FLAG_CT_RVS_XhoI with pKM101 as a template. These fragments were joined through overlapping PCR and the resulting PCR fragment was digested with *NcoI* and *XhoI* and ligated into an *NcoI/SalI* digested pBAD24Spc.

Plasmid pJG118 expresses *P_{BAD}::traF-F377*amber producing TraF with pBpa incorporated at position 377. It was constructed by amplifying codons 1-376 using primers TraF_NT_His_FWD_NcoI and F377_RVS_Overlap and codons 378-386 using primers F377_FWD_Overlap and TraF_FLAG_CT_RVS_XhoI with pKM101 as a template. These fragments were joined through overlapping PCR and the resulting PCR fragment was digested *NcoI* and *XhoI* and ligated into an *NcoI/SalI* digested pBAD24Spc.

Plasmid pJG119 expresses *P_{BAD}::traF-N386*amber producing TraF with pBpa incorporated at position 386. It was constructed by amplifying traF using primers TraF_NT_His_FWD_NcoI

and N386_RVS_FLAG_XhoI with pKM101 as a template. This PCR product was digested with *NcoI* and *XhoI* and ligated into an *NcoI/SalI* digested pBAD24Spc.

Plasmid pJG214 expresses $P_{BAD}::traF-CT_FLAG$, producing TraF with a C-terminal FLAG tag. It was constructed by PCR amplification of *traF* using primers TraF_FWD_*NcoI* and TraF_CT_FLAG_RVS_*XhoI* and pKM101 as a template. The resulting PCR fragment was digested with *NcoI* and *XhoI* and ligated into an *NcoI/SalI* digested pBAD24Spc.

Plasmid pJG204 expresses $P_{BAD}::traF-A2amber$ producing TraF with pBpa incorporated at position 2. It was constructed using inverse PCR using primers 2_amber_Inv_FWD and 2_amber_Inv_RVS with pJG214 as a template.

Plasmid pJG205 expresses $P_{BAD}::traF-V6amber$ producing TraF with pBpa incorporated at position 6. It was constructed using inverse PCR using primers 6_amber_Inv_FWD and 6_amber_Inv_RVS with pJG214 as a template.

Plasmid pJG206 expresses $P_{BAD}::traF-E11amber$ producing TraF with pBpa incorporated at position 11. It was constructed using inverse PCR using primers 11_amber_Inv_FWD and 11_amber_Inv_RVS with pJG214 as a template.

Plasmid pJG207 expresses $P_{BAD}::traF-T16amber$ producing TraF with pBpa incorporated at position 16. It was constructed using inverse PCR using primers 16_amber_Inv_FWD and 16_amber_Inv_RVS with pJG214 as a template.

Plasmid pJG208 expresses $P_{BAD}::traF-S23amber$ producing TraF with pBpa incorporated at position 23. It was constructed using inverse PCR using primers 23_amber_Inv_FWD and 23_amber_Inv_RVS with pJG214 as a template.

Plasmid pJG209 expresses $P_{BAD}::traF$ -G27amber producing TraF with pBpa incorporated at position 27. It was constructed using inverse PCR using primers 27_amber_Inv_FWD and 27_amber_Inv_RVS with pJG214 as a template.

Plasmid pJG210 expresses $P_{BAD}::traF$ -N32amber producing TraF with pBpa incorporated at position 32. It was constructed using inverse PCR using primers 32_amber_Inv_FWD and 32_amber_Inv_RVS with pJG214 as a template.

Plasmid pJG211 expresses $P_{BAD}::traF$ -V43amber producing TraF with pBpa incorporated at position 43. It was constructed using inverse PCR using primers 43_amber_Inv_FWD and 43_amber_Inv_RVS with pJG214 as a template.

Plasmid pJG212 expresses $P_{BAD}::traF$ -L45amber producing TraF with pBpa incorporated at position 45. It was constructed using inverse PCR using primers 45_amber_Inv_FWD and 45_amber_Inv_RVS with pJG214 as a template.

Plasmid pJG213 expresses $P_{BAD}::traF$ -L49amber producing TraF with pBpa incorporated at position 49. It was constructed using inverse PCR using primers 49_amber_Inv_FWD and 49_amber_Inv_RVS with pJG214 as a template.

Construction of *A. tumefaciens* plasmids

Plasmid pJG1 expresses $P_{lac}::virB10$ -G269R encoding VirB10 with a G269R mutation. It was constructed by amplifying codons 1-268 using primers VirB10_FWD_NdeI and G269R_RVS and codons 270-377 using primers G269R_FWD and B10_RVS_XhoI with pKVD10 as a template. These two fragments were joined together via overlapping PCR and the resulting PCR product was cloned into a *NdeI/XhoI* digested pKVD10 vector.

Plasmid pJG2 expresses *P_{lac}::virB10-G269K* encoding VirB10 with a G269K mutation. It was constructed by amplifying codons 1-268 using primers VirB10_FWD_NdeI and G269K_RVS and codons 270-377 using primers G269K_FWD and B10_RVS_XhoI with pKVD10 as a template. These two fragments were joined together via overlapping PCR and the resulting PCR product was cloned into a *NdeI/XhoI* digested pKVD10 vector.

Plasmid pJG3 expresses *P_{lac}::virB10-G269W* encoding VirB10 with a G269W mutation. It was constructed by amplifying codons 1-268 using primers VirB10_FWD_NdeI and G269W_RVS and codons 270-377 using primers G269W_FWD and B10_RVS_XhoI with pKVD10 as a template. These two fragments were joined together via overlapping PCR and the resulting PCR product was cloned into *NdeI/XhoI* digested pKVD10 vector.

Plasmid pJG4 expresses *P_{lac}::virB10-G269C* encoding VirB10 with a G269C mutation. It was constructed by amplifying codons 1-268 using primers VirB10_FWD_NdeI and G269C_RVS and codons 270-377 using primers G269C_FWD and B10_RVS_XhoI with pKVD10 as a template. These two fragments were joined together via overlapping PCR and the resulting PCR product was cloned into a *NdeI/XhoI* digested pKVD10 vector.

Plasmid pJG5 expresses *P_{lac}::virB10-G269D* encoding VirB10 with a G269D mutation. It was constructed by amplifying codons 1-268 using primers VirB10_FWD_NdeI and G269D_RVS and codons 270-377 using primers G269D_FWD and B10_RVS_XhoI with pKVD10 as a template. These two fragments were joined together via overlapping PCR and the resulting PCR product was cloned into a *NdeI/XhoI* digested pKVD10 vector.

Plasmid pJG6 expresses *P_{lac}::virB10-G272R* encoding VirB10 with a G272R mutation. It was constructed by amplifying codons 1-271 using primers VirB10_FWD_NdeI and G272R_RVS and codons 273-377 using primers G272R_FWD and B10_RVS_XhoI with pKVD10 as a

template. These two fragments were joined together via overlapping PCR and the resulting PCR product was cloned into a *NdeI/XhoI* digested pKVD10 vector.

Plasmid pJG7 expresses *P_{lac}::virB10-G272K* encoding VirB10 with a G272K mutation. It was constructed by amplifying codons 1-271 using primers VirB10_FWD_NdeI and G272K_RVS and codons 273-377 using primers G272K_FWD and B10_RVS_XhoI with pKVD10 as a template. These two fragments were joined together via overlapping PCR and the resulting PCR product was cloned into a *NdeI/XhoI* digested pKVD10 vector.

Plasmid pJG8 expresses *P_{lac}::virB10-G272W* encoding VirB10 with a G272W mutation. It was constructed by amplifying codons 1-271 using primers VirB10_FWD_NdeI and G272W_RVS and codons 273-377 using primers G272W_FWD and B10_RVS_XhoI with pKVD10 as a template. These two fragments were joined together via overlapping PCR and the resulting PCR product was cloned into a *NdeI/XhoI* digested pKVD10 vector.

Plasmid pJG9 expresses *P_{lac}::virB10-G272C* encoding VirB10 with a G272C mutation. It was constructed by amplifying codons 1-271 using primers VirB10_FWD_NdeI and G272C_RVS and codons 273-377 using primers G272C_FWD and B10_RVS_XhoI with pKVD10 as a template. These two fragments were joined together via overlapping PCR and the resulting PCR product was cloned into a *NdeI/XhoI* digested pKVD10 vector.

Plasmid pJG10 expresses *P_{lac}::virB10-G272D* encoding VirB10 with a G272D mutation. It was constructed by amplifying codons 1-271 using primers VirB10_FWD_NdeI and G272D_RVS and codons 273-377 using primers G272D_FWD and B10_RVS_XhoI with pKVD10 as a template. These two fragments were joined together via overlapping PCR and the resulting PCR product was cloned into a *NdeI/XhoI* digested pKVD10 vector.

Plasmid pJG11 expresses *P_{lac}::virB10-G275R* encoding VirB10 with a G275R mutation. It was constructed by amplifying codons 1-274 using primers VirB10_FWD_NdeI and G275R_RVS and codons 276-377 using primers G275R_FWD and B10_RVS_XhoI with pKVD10 as a template. These two fragments were joined together via overlapping PCR and the resulting PCR product was cloned into a *NdeI/XhoI* digested pKVD10 vector.

Plasmid pJG12 expresses *P_{lac}::virB10-G275K* encoding VirB10 with a G275K mutation. It was constructed by amplifying codons 1-274 using primers VirB10_FWD_NdeI and G275K_RVS and codons 276-377 using primers G275K_FWD and B10_RVS_XhoI with pKVD10 as a template. These two fragments were joined together via overlapping PCR and the resulting PCR product was cloned into a *NdeI/XhoI* digested pKVD10 vector.

Plasmid pJG13 expresses *P_{lac}::virB10-G275R* encoding VirB10 with a G275W mutation. It was constructed by amplifying codons 1-274 using primers VirB10_FWD_NdeI and G275W_RVS and codons 276-377 using primers G275W_FWD and B10_RVS_XhoI with pKVD10 as a template. These two fragments were joined together via overlapping PCR and the resulting PCR product was cloned into a *NdeI/XhoI* digested pKVD10 vector.

Plasmid pJG14 expresses *P_{lac}::virB10-G275C* encoding VirB10 with a G275C mutation. It was constructed by amplifying codons 1-274 using primers VirB10_FWD_NdeI and G275C_RVS and codons 276-377 using primers G275C_FWD and B10_RVS_XhoI with pKVD10 as a template. These two fragments were joined together via overlapping PCR and the resulting PCR product was cloned into a *NdeI/XhoI* digested pKVD10 vector.

Plasmid pJG15 expresses *P_{lac}::virB10-G275D* encoding VirB10 with a G275D mutation. It was constructed by amplifying codons 1-274 using primers VirB10_FWD_NdeI and G275D_RVS and codons 276-377 using primers G275D_FWD and B10_RVS_XhoI with

pKVD10 as a template. These two fragments were joined together via overlapping PCR and the resulting PCR product was cloned into a *NdeI/XhoI* digested pKVD10 vector.

Plasmid pSJ501 expresses *P_{lac}::virB10-TraF_AP* encoding VirB10 containing the AP of TraF. It was constructed through PCR amplification of *virB10* codons 1-287 with primers *VirB10_FWD_NdeI* and *B10_288_RVS_TraF* and codons 339-377 with primers *B10_339_FWD_TraF* and *B10_RVS_XhoI* with pKVD10 as a template. Codons 307-335 of *traF* were amplified using primers *TraF_307_FWD_B10* and *TraF_335_RVS_B10* with pKM101 as a template. These three fragments were joined together using overlapping PCR and the resulting PCR fragment was digested with *NdeI* and *XhoI* and ligated into an *NdeI/XhoI* digested pKVD10 vector.

Plasmid pSJ502 expresses *P_{lac}::virB10-TraF_AP-CT* encoding VirB10 containing the AP and C-terminal tail of TraF. It was constructed through PCR amplification of *virB10* codons 1-287 with primers *VirB10_FWD_NdeI* and *B10_288_RVS_TraF* with pKVD10 as a template and *traF* codons 307-386 with primers *TraF_307_FWD_B10* and *TraF_RVS_XhoI*. These fragments were joined together with overlapping PCR and the resulting PCR fragment was digested with *NdeI* and *XhoI* and ligated into an *NdeI/XhoI* digested pKVD10 vector.

Plasmid pSJ503 contains a 3x FLAG sequence cloned into a pZZ11 plasmid. It was constructed by annealing primers *3xFLAG_Sense_NcoI_NdeI_XhoI_BamHI* and *3xFLAG_Antisense_NcoI_NdeI_XhoI_BamHI* followed by digestion with *NcoI* and *XhoI* and ligating into an *NcoI/XhoI* digested pZZ11 plasmid.

Plasmid pSJ504 expresses *P_{lac}::virB10-ΔAP* encoding VirB10 with an AP deletion (residues 288-337). It was constructed through inverse PCR with primers *B10_AP_Del_FWD* and *B10_AP_Del_RVS* with pKVD10 as a template.

Plasmid pSJ510 expresses $P_{lac}::virB10-298.SphI$ encoding VirB10 with an Ala-Cys insertion at position 298. It was constructed through inverse PCR with primers B10_298_SphI_FWD and B10_298_SphI_RVS with pKVD10 as a template.

Plasmid pSJ511 expresses $P_{lac}::virB10-329.SphI$ encoding VirB10 with an Ala-Cys insertion at position 329. It was constructed through inverse PCR with primers B10_329_SphI_FWD and B10_329_SphI_RVS with pKVD10 as a template.

Plasmid pSJ512 expresses $P_{lac}::virB10-332.SphI$ encoding VirB10 with an Ala-Cys insertion at position 332. It was constructed through inverse PCR with primers B10_332_SphI_FWD and B10_329_SphI_RVS with pKVD10 as a template.

Plasmid pJG40 expresses $P_{lac}::virB10-298.3xFLAG$ encoding VirB10 with a 3x FLAG insertion at position 298. It was constructed by amplifying the 3x FLAG sequence using primers 3xFLAG_FWD_SphI and 3xFLAG_RVS_SphI with pSJ503 as a template. The resulting PCR product was digested with *SphI* and ligated into an *SphI* digested pSJ510 plasmid.

Plasmid pJG42 expresses $P_{lac}::virB10-329.3xFLAG$ encoding VirB10 with a 3x FLAG insertion at position 329. It was constructed by amplifying the 3x FLAG sequence using primers 3xFLAG_FWD_SphI and 3xFLAG_RVS_SphI with pSJ503 as a template. The resulting PCR product was digested with *SphI* and ligated into an *SphI* digested pSJ511 plasmid.

Plasmid pJG44 expresses $P_{lac}::virB10-332.3xFLAG$ encoding VirB10 with a 3x FLAG insertion at position 332. It was constructed by amplifying the 3x FLAG sequence using primers 3xFLAG_FWD_SphI and 3xFLAG_RVS_SphI with pSJ503 as a template. The

resulting PCR product was digested with *SphI* and ligated into an *SphI* digested pSJ512 plasmid.

Plasmid pJG52 expresses *P_{lac}::virB10-310.2xFLAG* encoding VirB10 with a 2x FLAG insertion at position 310. It was constructed by amplifying codons 1-309 using primers VirB10_FWD_NdeI and virB10_310_2xFLAG_RVS and codons 311-377 using primers virB10_310_2xFLAG_FWD and B10_RVS_XhoI with pKVD10 as a template. These two fragments were joined together via overlapping PCR and the resulting PCR product was digested with *NdeI* and *XhoI* and ligated into an *NdeI/XhoI* digested pKVD10 vector.

Conjugation assays

Donor and recipient cells were inoculated from glycerol stocks into 2 ml of LB containing antibiotics and grown overnight at 37°C with shaking. Cells were diluted 1:100 in antibiotic-free media and incubated for 1 h with shaking at 37°C. For induction from the P_{BAD} promoter, arabinose was added (0.2 % final concentration) followed by incubation for 1 h with shaking at 37°C. Donors and recipients (2.5 µl) were mixed on a nitrocellulose filter on LB media containing 0.2% arabinose and the mating mix was incubated for 2 h at 37°C. For broth matings, induced donors were mixed with recipients at a 1:1 volumetric ratio and incubated at 37°C for 2 h. Filter and broth mating mixtures were serially diluted and plated on media selective for transconjugants and donors. Frequency of transfer was calculated as the number of transconjugants per donor (Tcs/D). Experiments were performed at least three times in duplicate or triplicate, and results are reported as the mean frequency of transfer.

Phage infection assays

Strains carrying plasmids of interest were grown and, when necessary, induced with arabinose as described above for the conjugation assays. Fifty microliters of cells at a concentration of $\sim 10^8 \text{ ml}^{-1}$ were spread on an LB plate containing appropriate antibiotics and arabinose, and allowed to dry. Five microliters of the bacteriophages PRD1 (10^6 pfu, final concentration) or IKe (10^8 pfu, final concentration) were spotted onto the lawns of cells, and plates were incubated overnight at 37°C . Sensitivity to PRD1 and IKe was quantified in a plaque assay, as described previously (45). Briefly, cells were grown and induced with 0.2% arabinose. Approximately 10^7 cells were incubated with a series of 10-fold dilutions of PRD1 or IKe for 20 min at room temperature. The mix was added to 5 ml of 0.4% melted LB agar, which was then overlaid on a 1.5% LB agar plate containing antibiotics and arabinose. Plates were incubated at 37°C overnight, and phage sensitivity was reported as the concentration of phage in plaque forming units (pfu)/ml.

Steady state level detection

E. coli strains were grown and induced for production of TraF variants of interest in LB media, harvested, and normalized to equivalent optical densities (OD_{600}). Total protein extracts were subjected to SDS-PAGE, proteins were transferred to nitrocellulose membranes, and blots were developed with primary antibodies and HRP-conjugated secondary antibodies for detection of the TraF proteins by chemiluminescence.

Pseudomonas aeruginosa type VI killing assay

T4SS-mediated killing of *E. coli* by the *Pseudomonas aeruginosa* type VI secretion system (T6SS) was carried out as previously described (140). Briefly, 2 ml of *E. coli* DH5 α donors and a *P. aeruginosa* PAO1 *retS* mutant were incubated overnight with shaking at 37°C, then resuspended in 2 ml of antibiotic-free LB followed by a 1:100 dilution in 5 ml of antibiotic-free LB. Cells were then incubated with shaking at 37°C for 2 h, pelleted and resuspended in 100 μ l LB. *P. aeruginosa* (17 μ l) were mixed with *E. coli* (3 μ l) on filters placed on LB plates and incubated for 3 h at 37°C. Cells were resuspended in 1 ml of LB and serial dilutions were spotted onto plates containing spectinomycin 300 μ g/ml and rifampicin 100 μ g/ml to select for growth of *E. coli*. T6SS killing of *E. coli* is presented as *E. coli* cell viability in colony forming units (CFU) per ml.

pBpa incorporation and UV crosslinking

Site-directed photocrosslinking of pBpa-incorporated TraF variants was carried as described previously (151). Briefly, *E. coli* TOP10 cells containing the amber mutant of interest and the pEVOL plasmid were grown overnight at 37°C with shaking in the presence of antibiotics. The next day, cells were diluted 1:20 into fresh LB containing antibiotics and grown at 37°C to an OD₆₀₀ between 0.6 and 0.9. The cells were then concentrated 20-fold in antibiotic-free LB containing 0.2% arabinose and 1mM pBpa. The cells were incubated at 37°C with shaking for 1 hour. When testing for interactions between TraF and other proteins, cells were resuspended in PBS and exposed to UV light at 365nm for 10 minutes, while incubated on ice in the dark. Cells were spun down and stored at -80°C until further processing.

Membrane solubilization and TraF purification

Cells frozen at -80°C were thawed and resuspended in TE buffer (Tris-HCl pH8.0, 1mM EDTA pH 8.0). Cells were next lysed with a bead beater homogenizer. Beads and unbroken cells were spun out at 13,000 RPM for 30 minutes at 4°C. The whole cell lysate was spun down at ~200,000 x g for 1 hour. The membrane pellet was resuspended in solubilization buffer (100 mM Tris-HCl pH 8.0, 300 mM NaCl, 1mM EDTA, 2% Triton-X 100) and incubated at 4°C for 2 hours with gentle shaking. Samples were spun again at 200,000 x g for 1 hour to remove insoluble material. The supernatant was incubated with 20 µl of pre-equilibrated α-FLAG magnetic beads (Sigma) overnight at 4°C with gentle shaking. Magnetic beads were washed 3 times with 1ml of solubilization buffer per wash. α-FLAG magnetic beads were incubated with 3xFLAG peptide (Sigma) at a concentration of 200 µg/ml at 4°C for 1 hour to elute TraF off of the beads. The beads were removed from the supernatant, mixed with 2x Laemmli's buffer, and run on an SDS-PAGE gel followed by Western blotting.

T-DNA transfer assays

A. tumefaciens cells were streaked onto MG/L plates containing the appropriate antibiotics and grown from 2-3 days at 28°C. Leaves from *Kalanchoe daigremontiana* were wounded with a sterile toothpick followed by an inoculation of *A. tumefaciens* cells from the MG/L plate into the wound. Following inoculation, wounded *Kalanchoe daigremontiana* were incubated at room temperature in the dark for 5-7 days followed by incubation in light for 1-2 months. Plant tumors were scored based on their size relative to tumors formed by the wild-type A348 strain.

Colony immunoblot (*Agrobacterium tumefaciens*)

Colony immunoblots were used to detect the presence of VirB2 on the cell surface. *A. tumefaciens* were streaked onto MG/L plates and incubated at 28°C for 2-3 days. Following growth on agar plates, colonies were inoculated into 2 ml of MG/L broth containing appropriate antibiotics and grown overnight at room temperature (~25°C). The next day, cells were spun down and resuspended in 2.5 ml ABIM broth containing 100 µM acetosyringone followed by incubation at room temperature for 24 hours. Cells were spotted on ABIM agar and incubated at 18°C for four days. Cells were then blotted onto nitrocellulose membranes for 30 minutes. Membranes were then incubated in 5% non-fat dry milk for 20 minutes in order to block the membrane as well as wash off excess cells. Cells were then incubated with primary α -VirB2 antibodies followed by secondary antibodies and development with chemiluminescence reagents.

Colony immunoblot (*Escherichia coli*)

E. coli cells were inoculated from glycerol stocks into 2 ml LB broth containing antibiotics and incubated overnight at 37°C with agitation. The next day, cells were subcultured 1:100 into fresh LB without antibiotics. These cells were incubated at 37°C with agitation for 2.5 hours. Nitrocellulose was placed on a fresh LB plate without antibiotics and 5 µl of each subculture was added to the nitrocellulose and incubated at 37°C for 2 hours. Afterwards, nitrocellulose membranes were blocked in 5% non-fat dry milk for 20 minutes. Membranes were then incubated with α -FLAG primary antibodies followed by secondary antibodies and development with chemiluminescence reagents.

Chapter 3: Contributions of the VirB10 GxxGxxG Motif and Antenna Projection in T-DNA Transfer and Pilus Biogenesis

Introduction

The *Agrobacterium tumefaciens* VirB/VirD4 type IV secretion system (T4SS) is assembled from 11 VirB proteins and the VirD4 substrate receptor, also termed the type IV coupling protein (T4CP) (5). *A. tumefaciens* uses this T4SS to deliver oncogenic T-DNA and effector proteins to plant cells. Previous analyses established that all of the VirB proteins except VirB1 are essential for delivery of T-DNA and effector proteins to plants and for mobilization of an RSF1010 plasmid substrate to *A. tumefaciens* recipient cells (67). The VirB/VirD4 T4SS is similar to the *Escherichia coli* pKM101-encoded Tra conjugation system in terms of its transfer loci and subunit composition (152). A structure of the pKM101 outer membrane “core complex” was solved by the Waksman laboratory by cryo-electron microscopy, and a portion of this complex (the O-layer) also was solved by X-ray crystallography (82,90). The core complex is predicted to extend from the periplasmic face of the inner membrane across the periplasm to the cell exterior. It consists of 14 copies each of the VirB7-like TraN, VirB9-like TraO and VirB10-like TraF subunits arranged in a ~1 MDa barrel-shaped structure. In the X-ray structure, TraF lines the inner chamber of the translocation channel, TraO comprises the outer wall, and TraN anchors the subassembly to the outer membrane (Figure 1.10).

In collaboration with Dr. Lois Banta, the Christie lab identified and characterized a mutation in VirB10 at position 272 (G272R) that conferred non-specific release of the secretion substrate VirE2 to the cell exterior (125). This mutation had no effect on intercellular transmission of T-DNA or effector proteins, but completely blocked biogenesis of the T-pilus (125). In the crystal structure of the Tra_{pKM101} O-layer, the corresponding Gly residues in TraF line the interior chamber of core complex near the OM-spanning cap domain. G272 is one of three highly conserved Gly residues arrayed as a GxxGxxG motif among VirB10 homologs

(Figures 3.1 and 3.2) (125). Results of the G272R mutational analyses led to a prediction that these conserved Gly residues might mark the site of a gate within the core complex chamber that controls substrate release as well as extension of the T pilus across the OM. In agreement with this proposal, the Christie lab provided evidence that the G272R mutation locks VirB10 in an activated conformation required for substrate transfer that is achieved in wild-type cells only when DNA substrates are docked with the VirD4 receptor and when both VirD4 and VirB11 are competent for hydrolysis of ATP (107,125). When I joined the Christie laboratory, I decided to further define the importance of the GxxGxxG motif in regulating substrate transfer and pilus biogenesis.

The crystal structure of the pKM101 core complex also shows that the conserved GxxGxxG motif is located near the antennae projection (AP) of TraF, which as mentioned in Chapter 1, assembles as a putative OM-spanning cap domain. As part of a mutational analysis of VirB10_{At}, the Christie lab had shown that a “deletion” of the AP attenuated DNA transfer, but blocked detectable pilus biogenesis (127). However, the assignment of this AP domain was based on a previous X-ray structure of the ComB10 subunit associated with the ComB DNA-uptake T4SS in *Helicobacter pylori* (111). With the availability of an X-ray structure of the O-layer of the Tra_{pKM101} T4SS, we reassigned VirB10’s AP domain boundaries and I also evaluated the contributions of the AP to T-DNA transfer and pilus assembly in *A. tumefaciens*.

The goals of my studies in *A. tumefaciens*, therefore, were to further define the contributions of VirB10’s conserved GxxGxxG motif and the AP domain to elaboration of the translocation channel and the T pilus. In the course of my studies, through a collaboration with Dr. Gabriel Waksman’s laboratory, we also succeeded in purifying the core complex from the *A. tumefaciens* VirB/VirD4 T4SS and solving its structure by negative-staining transmission

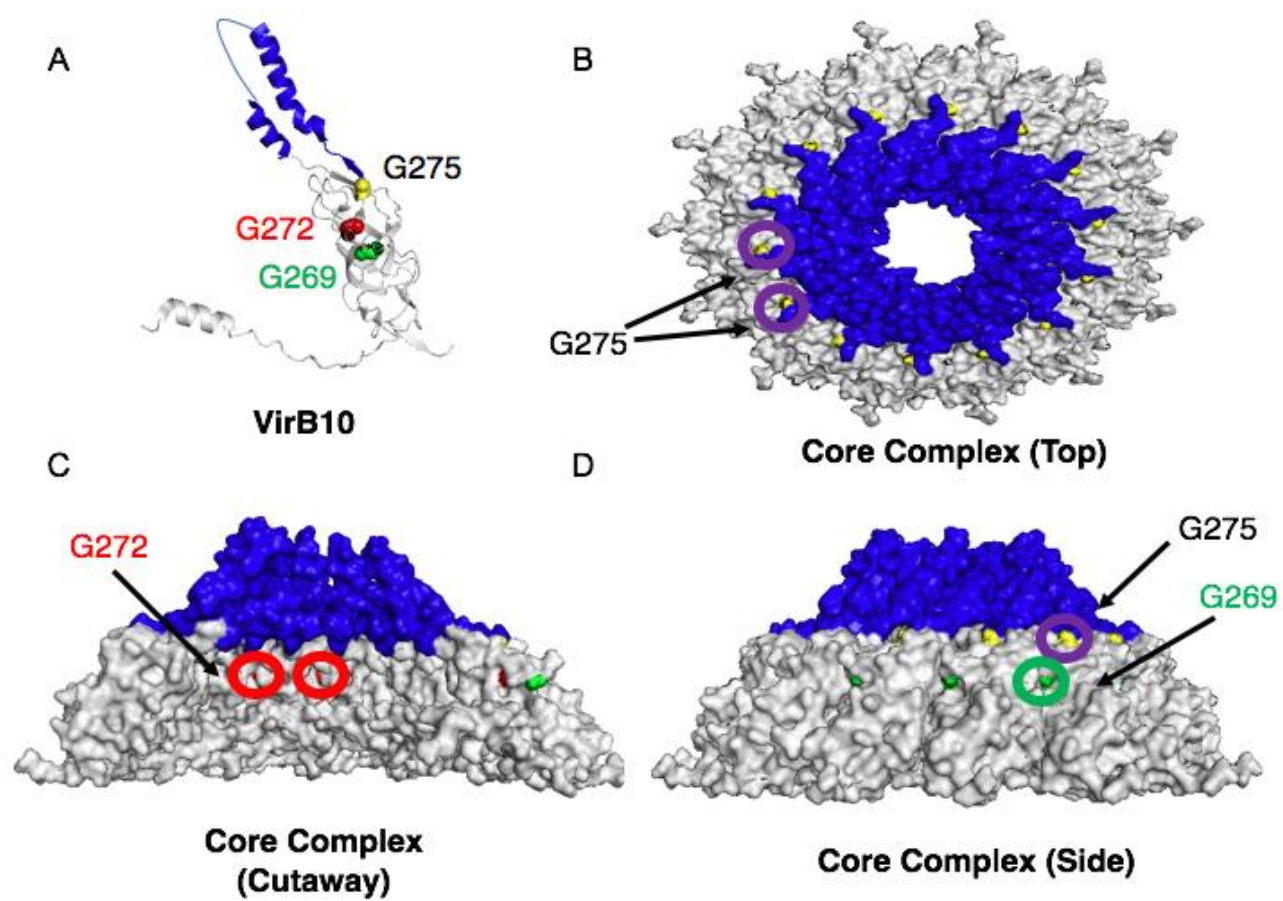
Figure 3.1 Alignment of VirB10 and homologs. VirB10 along with its homologs from plasmid pKM101 (TraF), plasmid R388 (TrwE) and the *Bordetella pertussis* Ptl T4SS (PtlG). Sequences were aligned with Multalin (<http://multalin.toulouse.inra.fr/multalin>); "*Multiple sequence alignment with hierarchical clustering*" F. Corpet, 1988, Nucl. Acids Res., 16 (22), 10881-10890) and recreated for the AP and C-terminal regions. Regions of interest, including the GxxGxxG motif and AP $\alpha 2$ and $\alpha 3$ helices, are highlighted above the sequence and were annotated based on the structure and sequence of TraF.

	<u>GxxGxxG</u>	<u>α2 helix</u>
VirB10	SADELGRPGLP GSV DSHFWQRFS GAMLL SAVQGAFQAASTYAGSSGGG-M	
TraF	GTNSLGSAGIP GQV DAHMERLAGAIMISLFSDT---LTALVNQTQSNNI	
TrwE	GTGPLGEAGLG GWID RHFWERFG AIMIS LIGDLGDWASRQGSRQGNNSI	
PtlG	AVDGTGAAGLP GVV DDKFAQRFG GALLL SVLGDATSYMLARATDARHGVN	

	<u>α3 helix</u>
VirB10	SFNSFQNNGEQTTET ALKATIN IPPTLKKNQ GDTVSI VARDLDFFGVYQ
TraF	QYNSTENSGGQLASE ALRSYMS IPPTLYDQQ GDAVSI VARDLDFSGVYT
TrwE	QFSNTANGVESAAAE ALRNSIN IPPTLYKNQ GERVNI LWARDLDFSDVYS
PtlG	VNLTAAGTMNSLAAS ALNNTIN IPPTLYKNH GDQIGI LVARPLDFSILRG

VirB10	LRLTGGAARGNRRS	377
TraF	LADN-----	386
TrwE	LESIPTK-----	395
PtlG	TNE-----	374

Figure 3.2 Location of the conserved GxxGxxG motif. (A) Structural model of the C-terminal half of VirB10, derived from the TraF structure within the pKM101 O-layer X-ray structure using the Pymol algorithm (<http://pymol.org>). The location of the G269 (Green), G272 (Red), and G275 (Yellow) residues at the base of the helix-loop-helix AP domain (Blue) are shown. (B) Top-down view of the core complex with the position of G275 circled in yellow. (C) Cut-away view of the core complex O-layer highlighting the position of G727 circled in red. (D) Side view depicting the positions of G269 and G275 circled in green and yellow, respectively. The structure of the core complex O-layer was generated using Pymol (<http://pymol.org>) based on the 3ZBI file deposited into the NCBI protein database.



electron microscopy at a resolution of 21Å. Results of these studies, coupled with additional experiments focusing on the Tra_{pKM101} system (see next chapters), underscored the structural and functional conservation of core complexes associated with the type IVa secretion systems.

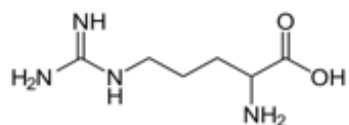
Results

Mutations in G269 and G272 attenuate T-DNA transfer into plant cells

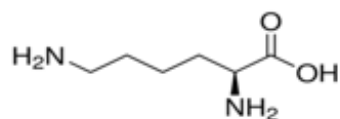
To evaluate the functional importance of the conserved GxxGxxG motif located between residues 269 and 275 of VirB10, I substituted each of the Gly residues with amino acids varying in sized or charge: Arg or Lys (positively-charged), Asp (negatively-charged), Trp (bulky aromatic), Cys (neutral, potentially useful for crosslinking studies) (Figure 3.3). Plasmids expressing the *virB10* mutant alleles were introduced into the Δ *virB10* mutant strain PC1010. I next tested for the capacities of the mutant strains to deliver oncogenic T-DNA to plant cells. Interestingly, all strains delivered T-DNA to plants, as monitored by formation of tumors on infected plants (Figure 3.4). Strains expressing *virB10* alleles bearing Gly275 substitutions generally incited robust tumor development, with the exception of *virB10G275C*, which supported only very attenuated tumor formation. Strains expressing alleles with Gly269 or G272 substitutions were avirulent (G269R), strongly attenuated in virulence (G269K/D, G272R//K/W/D), or moderately attenuated in virulence (G269W/C, G272C). These Gly residues, which are more highly conserved than G275 among the VirB10 homologs, thus do not tolerate distinct types of substitutions.

I next evaluated the effects of Gly substitutions on assembly of the T pilus, whose production can be monitored using a colony immunoblot assay to detect extracellular VirB2 pilin (125,128). Interestingly, Gly275 tolerated all substitutions without detectable effects on accumulation of surface-exposed VirB2 pilin. By contrast, Arg substitutions of both Gly269 and Gly272 abolished detectable surface pilin, as did a Trp substitution of G272 (Figure 3.4). These findings confirm and extend findings from the Christie lab by showing substitutions not only of positively-charged Arg, but also a bulky Trp residue at position 272 completely blocked pilus

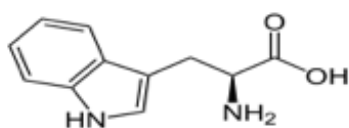
Figure 3.3 Substitution of the conserved glycines. Locations of the G269 G272, and G275 residues on a structural model of the C-terminal half of VirB10 (residues 151 – 377) derived from TraF's structure in the Tra_{pKM101} O-layer X-ray structure (EMDB – 5031) At left, amino acids substituted for each of the conserved Gly residues. The structure of TraF was generated using Pymol (<http://pymol.org>) based on the 3ZBI file deposited into the NCBI protein database.



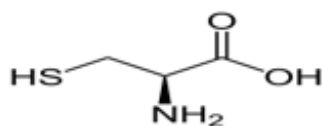
Arginine (Positive Charge)



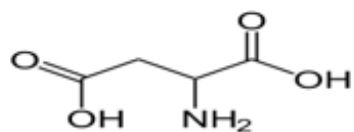
Lysine (Positive Charge)



Tryptophan (Big and Bulky)



Cysteine (Crosslinking)



Aspartate (Negative Charge)

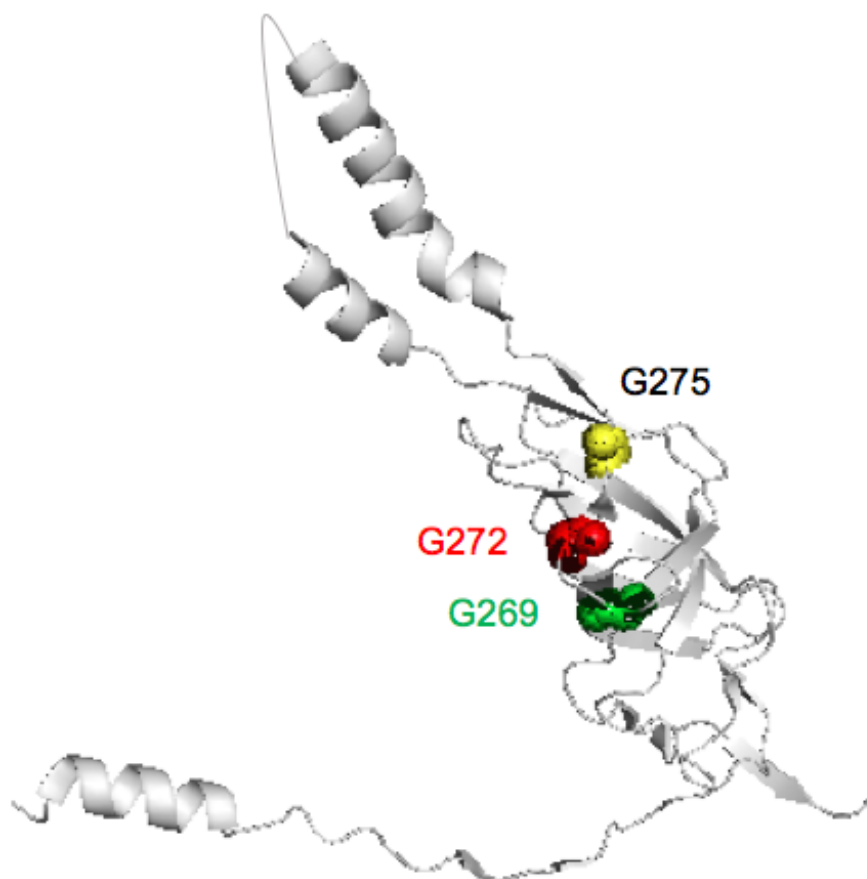
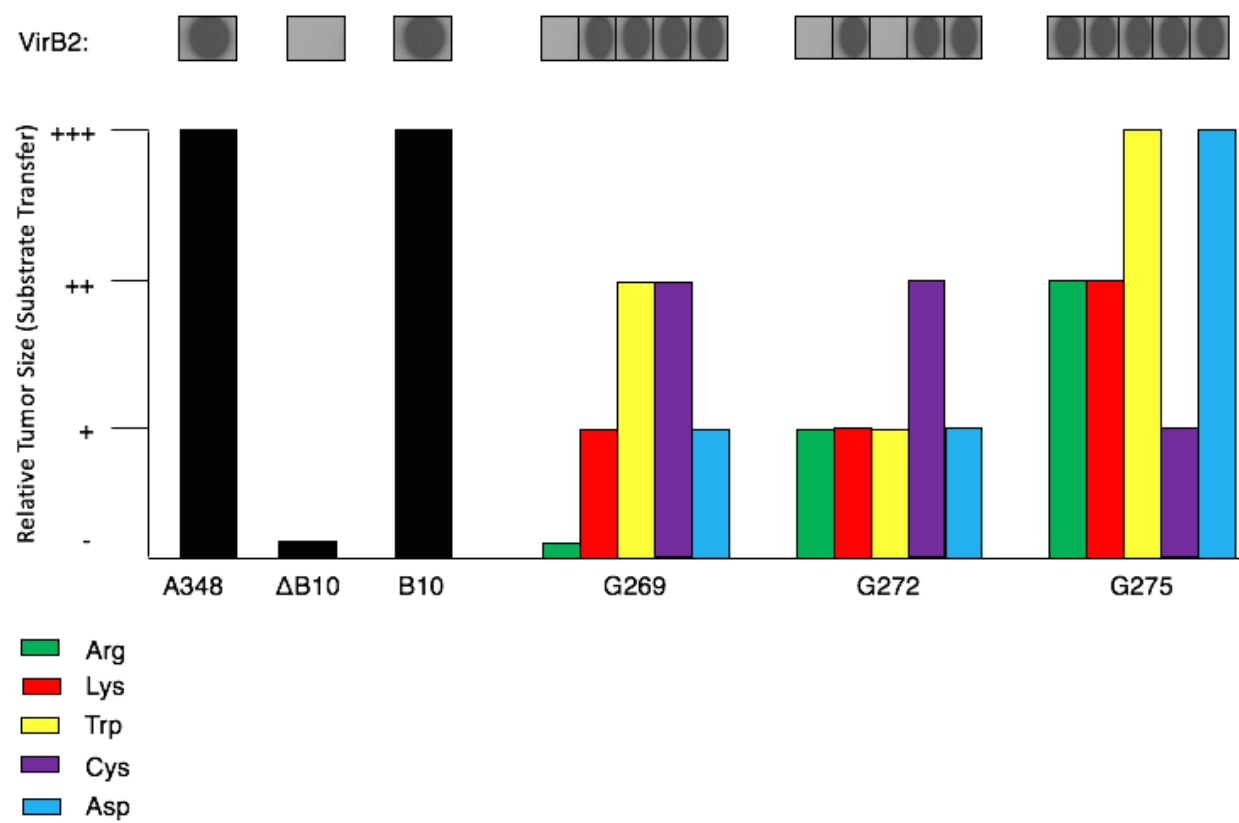


Figure 3.4 Effects of glycine belt mutations on T-DNA transfer and pilus biogenesis.

Histograms depicting the level of T-DNA transfer as relative tumor size on *Kalanchoe daigremontiana* leaves and surface-displayed VirB2 for each GxxGxxG mutant. Each strain was placed on six separate leaves and tumors were scored compared to tumors formed by the wild-type A348 strain. Each strain was inoculated on six leaves and tumors were scored after 1 month incubation. Tumor size on *K. daigremontiana* leaves were scaled from no detectable tumors (-) to tumors similar both in size and kinetics of appearance to tumors incited by wild-type A348 (+++). Tumors that were barely detectable were scored as one plus and tumors that were appreciably smaller than those incited by A348 as two pluses. Surface-localized VirB2 was detected by colony immunostaining using α -VirB2 antibodies as previously described.



production while permitting at least a low level of substrate transfer to plant cells. Other mutations in G272, as well as mutations in G269, conferred attenuated virulence, suggestive of perturbing effects on assembly of the translocation channel. By contrast, the less-highly conserved G275 residue was more tolerant of the engineered substitutions.

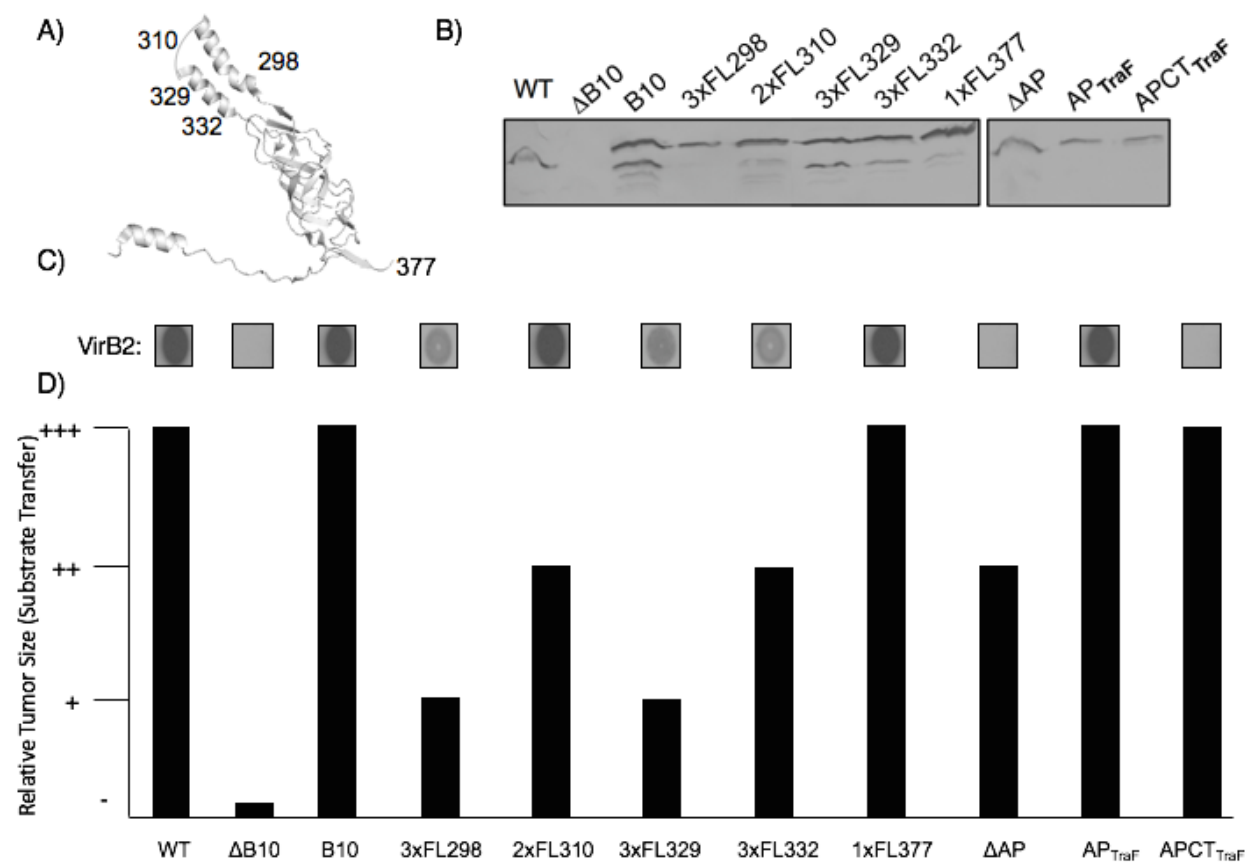
The VirB10 AP is essential for pilus production, but not for substrate transfer.

The VirB10 AP helices are predicted to form the OM pore. As mentioned in the introduction for this chapter, a previously-constructed VirB10 AP deletion mutation did not completely abolish the AP (127). I deleted the VirB10 AP using boundaries based on the alignment with TraF within the Tra_{pKM101} O-layer (90). This new mutant protein, VirB10_{ΔAP}, supported T-DNA transfer but not pilus biogenesis. The VirB10 AP, which is predicted to span the OM, is therefore critical for pilus polymerization but not for intercellular substrate transfer.

I next wanted to determine which regions of the AP contributed to pilus production. I inserted 3x FLAG tags into the $\alpha 2$ or $\alpha 3$ helices, which are predicted to span the OM, and a 2x FLAG tag into the flexible loop presumptively extending from the cell surface. None of these epitope insertions blocked substrate transfer or pilus biogenesis despite the presence of many negatively-charged residues in the FLAG sequence (Figure 3.5). The presence of an AP domain is critical for pilus biogenesis, but this motif is able to withstand sizable mutations without disruption of function.

The AP domains of TraF and VirB10 share approximately 31% identity with no concentrated regions of homology. We next tested whether the AP domains of TraF and VirB10 were functionally exchangeable. S. Jakubowski constructed two chimeras of TraF and VirB10:

Figure 3.5 Effects of AP FLAG tag insertion on T-DNA transfer and pilus biogenesis. (A) Depiction of the VirB10 C-terminal half along with 2x and 3x FLAG insertions. (B) Western blot depicting the steady state levels of the VirB10 AP mutants. Cells numbers were normalized based on OD₆₀₀ readings and cell lysates were run on an SDS-PAGE gel followed by Western blotting with α -VirB10 antibodies. (C) Surface detection of VirB2 pilin subunits using colony immunoblotting. Colonies were grown on acidic ABIM inducing agar for four days at 18°C followed by detection of pilin subunits on the cell surface with α -VirB2 antibodies. (D) Histogram depicting the levels of T-DNA transfer for each of the AP mutants into *K. daigremontiana* leaves. Tumor size on *K. daigremontiana* leaves were scaled from no detectable tumors (-) to tumors similar both in size and kinetics of appearance to tumors incited by wild-type A348 (+++). Tumors that were barely detectable were scored as one plus and tumors that were appreciably smaller than those incited by A348 as two pluses



(i) one containing an AP substitution (VirB10/AP_{TraF}) and (ii) the other including the C-terminal tail as well (VirB10/AP-CT_{TraF}). Similar to the other AP mutant proteins, VirB10/AP_{TraF} and VirB10/AP-CT_{TraF} supported T-DNA transfer, establishing that the APs of these homologs were exchangeable. However, only VirB10/AP_{TraF} supported pilus production, indicating that the C-terminal tail is important for production of an extracellular pilus (Figure 3.5).

The structure of the *A. tumefaciens* VirB core complex resembles those of pKM101 and R388.

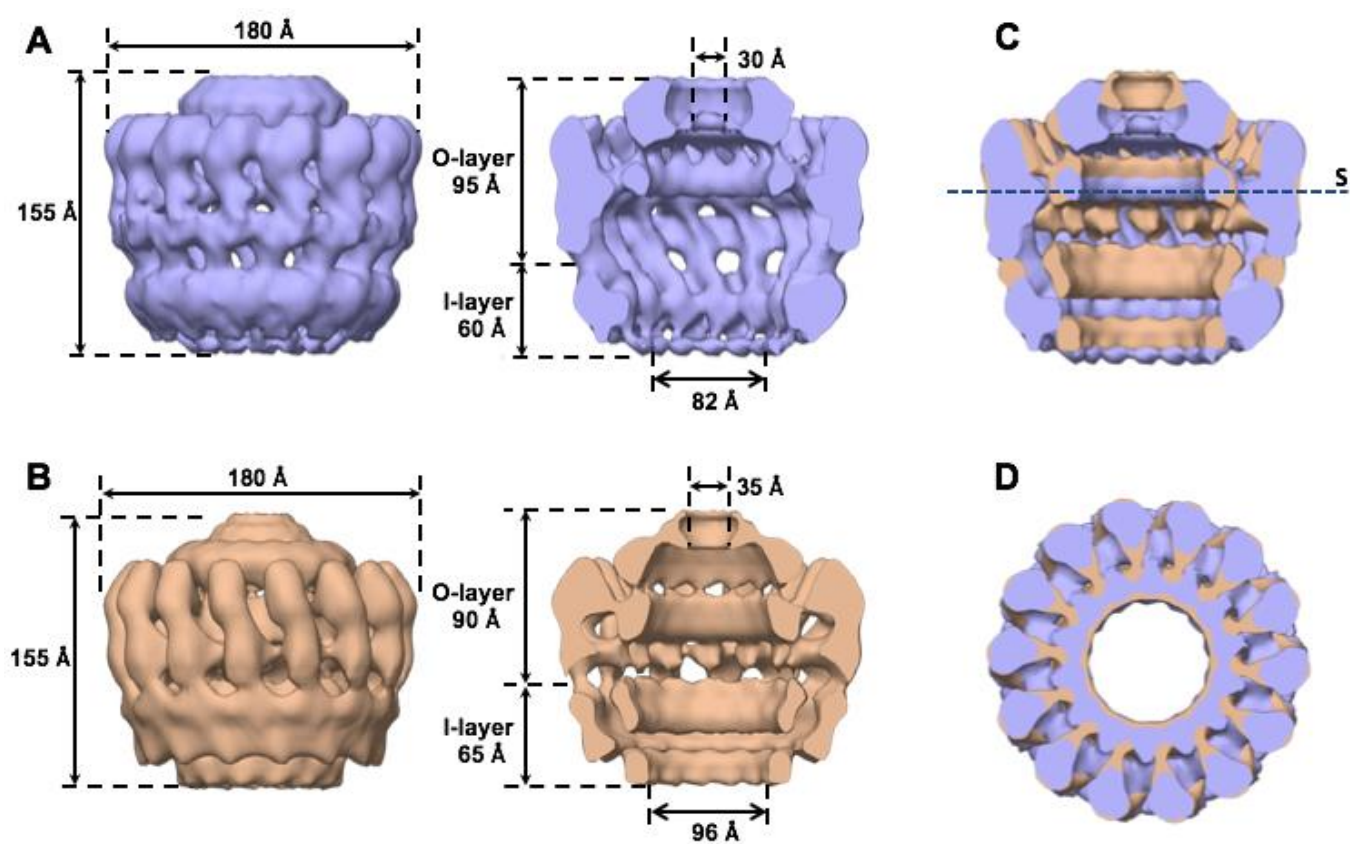
The VirB/VirD4_{At}, Tra_{pKM101}, and Trw_{R388} T4SSs are similar in gene arrangements and subunit compositions. Structures of the OMCC subassemblies from the Tra_{pKM101} and Trw_{R388} have been solved by cryo-electron microscopy or negative-staining electron microscopy (82,84,90). Both of these structures are highly similar, suggesting the possibility that OMCCs associated with the type IVa T4SSs are highly conserved in overall architecture and function. To evaluate this idea further, we collaborated with the Waksman laboratory to obtain a structure of the OMCC from the *A. tumefaciens* VirB/VirD4 T4SS. We inserted a Strep-tag sequence at the end of *virB10* carried on the pTi plasmid, and were able to confirm that subassemblies enriched from the corresponding *A. tumefaciens* strain (A348.B10ST) by detergent solubilization and Strep-tag affinity pull-down assays yielded ring-shaped complexes that were similar in appearance to the pKM101 and R388 OMCCs, as determined by negative-staining EM. We sent this strain to the Waksman laboratory where the VirB/VirD4 OMCC was further purified and structurally resolved at 21Å resolution using negative staining electron microscopy. Similar to the pKM101 OMCC, the VirB complex can be divided into an inner layer (I-layer) and an outer layer (O-layer). The dimensions of the VirB complex are similar to the Tra_{pKM101}, and Trw_{R388}

OMCCs (Figure 3.6). However, the VirB_{At} structure is more cylindrical than its Tra_{pKM101} and Trw_{R388} OMCC counterparts and contains a broad pore-forming cup domain at the cell surface. The significance of these differences is not understood at this time. Future studies on the VirB_{At} core complex producing higher resolution images are required to better define the functional significance of any structural differences observed among the core complexes solved to date.

At this time, however, the findings strongly support a proposal that the OMCCs of the type IVa T4SSs employed by Gram-negative bacterial species share a common structural arrangement, function, and ancestry.

Figure 3.6 Structure of the *A. tumefaciens* VirB core complex. Negative-stain EM structure of the *A. tumefaciens* outer-membrane core complex (OMCC) and comparison with the NS-EM structure of the OMCC (EMDB-5032) encoded by *E.coli* pKM101. A) *A. tumefaciens* OMCC side view (left) and cut-away side view (right). B) *E.coli* pKM101 OMCC side view (left) and cut-away side view (right). C) Representation of the cut-away side view of the overlay of *A. tumefaciens* and *E.coli* pKM101 OMCC's. D) Cross-section of overlaid *A. tumefaciens* and *E.coli* pKM101 OMCC complexes. Dashed line S in panel C indicates the level of the cross section shown in panel D.

This figure was modified from Figure 6 in Gordon et al. *Use of chimeric type IV secretion systems to define contributions of outer membrane subassemblies for contact-dependent translocation* Molecular Microbiology 2017 doi: 10.1111/mmi.13700. It was re-published with permission from John Wiley and Sons Publishing Group. License # 4113880880825



Discussion

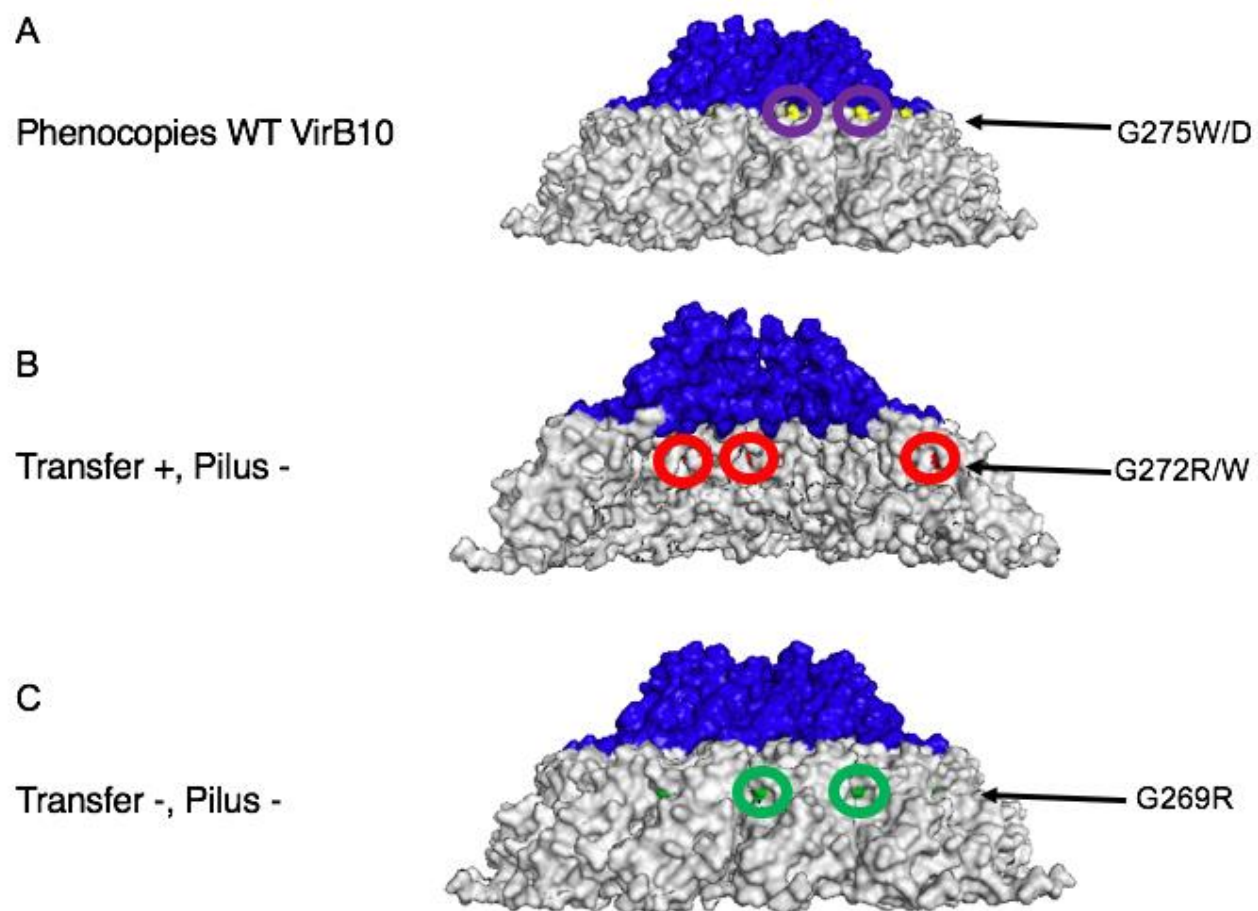
Previous studies in the Christie lab identified unique phenotypes associated with mutations in the VirB10 GxxGxxG motif and AP domain (125,127). Both a G272R and AP partial deletion blocked pilus biogenesis, but still allowed for detectable T-DNA transfer into plant cells. When I joined the Christie lab, I decided to further define the role of G272 and the surrounding G269 and G275 residues through a series of mutations substituting at each position amino acids of different sizes and charges. Additionally, I intended to further define the role of the AP helices through re-construction of another AP deletion as well as FLAG tag insertions. Below, I will discuss my findings in greater detail and propose a model for their role in pilus biogenesis and T-DNA transfer.

Mutations at G269 and G272 had the most detrimental effect on T-DNA transfer. In contrast, most mutations at G275 were generally phenotypically silent. G269 and G272 are located on the side and inner wall of the chamber, respectively where as G275 is predicted to be situated on the outside of the β -barrel possibly in juxtaposition with VirB9 (Figure 3.7). Based on these structural findings, I predicted that G269 and G272 might mark a critical interface of the OMCC and the translocation channel housed within this structural scaffold.

With respect to the AP, we had previously attempted to define the role of the VirB10 AP through construction of an AP deletion (127). The deletion was based on an alignment of VirB10 with *H. pylori* ComB10. However, in view of the new X-ray structure of the pKM101 O-layer, we reassigned the boundaries of APs of TraF and VirB10, the latter through sequence alignments and Phyre 2 modeling. I made a new deletion of the AP and re-tested it for its ability to restore T-DNA transfer and pilus biogenesis to the a $\Delta virB10$ strain. This mutant phenocopied

Figure 3.7 Summary of phenotypes associate with GxxGxxG motif. Depiction of three phenotypes observed during characterization of the GxxGxxG motif. (A) G275W and G275D mutations, located on the outer face of the O-layer, were silent in terms of T-DNA transfer and pilus biogenesis. (B) Uncoupling mutations at positions at G272, located in the channel lumen, allowed for attenuated T-DNA transfer, but blocked detectable pilus biogenesis. (C) A mutation of G269, positioned on the outside of the core complex, to an Arg residue block both T-DNA transfer and pilus biogenesis.

The structure of the core complex O-layer was generated using Pymol (<http://pymol.org>) based on the 3ZBI file deposited into the NCBI protein database.



the previous Δ AP mutant with respect to substrate transfer but completely abolished our ability to detect VirB2 pilin on the cell surface.

Models depicting the contributions of the GxxGxxG and the AP domain for pilus biogenesis.

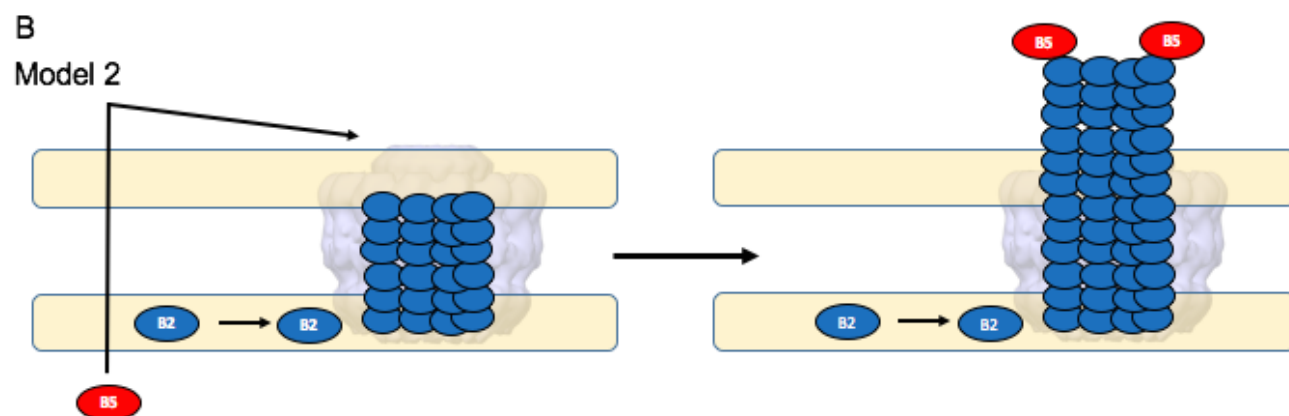
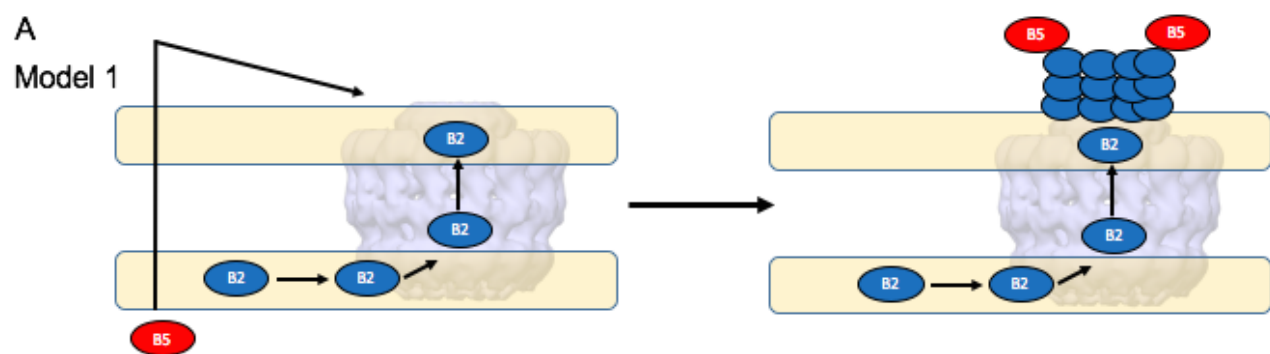
My data are consistent with two models for pilus biogenesis. In both models, upon synthesis, VirB2 pilin subunits are delivered into the inner membrane where they are cleaved of their signal sequences and covalently cyclized by a head-to-tail reaction. Upon receipt of signals that presently are not specified, the pilins are extracted from the inner membrane pool via the ATPase activities of VirB4, together with contributions by VirB11.

Model 1: Outer membrane nucleation. The membrane-extracted VirB2 pilin subunits are delivered into the core complex channel where they transit to the distal region of the OMCC. At the OMCC they interact with the AP either directly or via interaction with another subunit such as the pilus tip protein VirB5 (Figure 3.8). The AP contacts then drive polymerization of the pilin monomers into the extended pilus. According to this model, the AP plays a critical role in pilus biogenesis by dynamically interacting with pilin monomers to direct their self-assembly into the pilus. The G269 and G272 substitutions, which are positioned within the interior of the OMCC chamber, might block pilus biogenesis through steric effects impeding delivery of the pilins to the AP or, by interfering with formation of AP–pilin subunit contacts. Mutations at G275, which interestingly map on the outer face of the β -barrel, do not affect pilus biogenesis.

Model 2: Inner membrane platform model. Pilin subunits nucleate as the growing pilus from an inner membrane platform possibly consisting of VirB6 and VirB8. The pilus extends to the distal end of the OMCC where it is blocked from further extension by the AP domain of

Figure 3.8 Models for pilus biogenesis in *A. tumefaciens*. Depiction of two models for pilus biogenesis. (A) In Model 1, the VirB2 pilin subunit enters the OMCC chamber after being dislodged from the IM. VirB5 will then exit the cell and make contact with the AP helices, triggering the release of VirB2 from the channel. The AP will then serve as an OM platform during pilus polymerization. (B) Model 2 states that VirB2 pilin subunits enter the channel in the IM. Once extracellular VirB5 comes into contact with the AP, the AP will allow for the passage of pilin subunits through the channel and outside of the cell.

The core complex was modified from Figure 6 in Gordon et al. *Use of chimeric type IV secretion systems to define contributions of outer membrane subassemblies for contact-dependent translocation* Molecular Microbiology 2017 doi: 10.1111/mmi.13700. It was re-published with permission from John Wiley and Sons Publishing Group. License # 4113880880825



VirB10 (Figure 3.8). Dr. Christian Gonzalez-Rivera has shown that the VirB5 homolog, TraC_{pKM101}, is secreted outside of the cell in the absence of a T4SS. We postulate that these pilus tip proteins form contacts with the AP on the cell surface and with the tip of the pilus, and that these contacts cause a conformational change in the AP to allow for pilus extraction.

At this time, it is not possible to discriminate between these models. However, my further studies of the pKM101 Tra T4SS further establish the compositional and structural flexibility of the OMCC for substrate transfer, as well as the importance of the OMCC cap for pilus biogenesis.

Chapter 4: Genetic Requirements for Plasmid Transfer and Phage Sensitivity Through the pKM101-encoded Type IV Secretion System

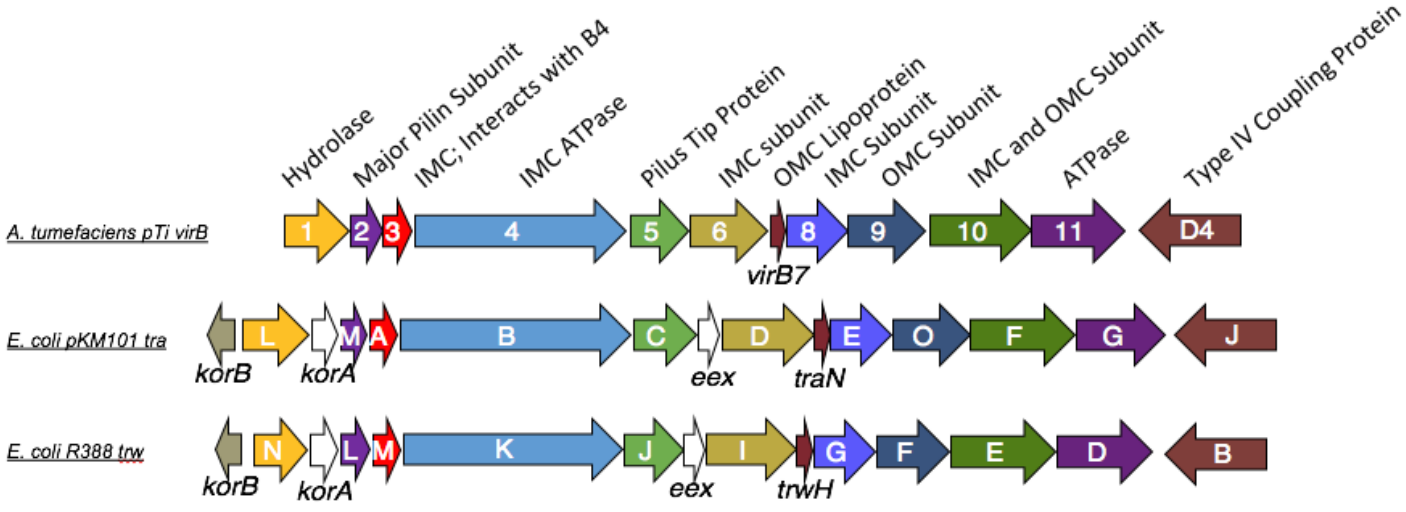
Introduction

Gram-negative bacterial T4SSs are comprised of a core set of subunits that are required for substrate translocation and pilus biogenesis. The Christie laboratory has been characterizing structure and function relationships of the VirB/VirD4 T4SS from *A. tumefaciens* for over 25 years. As mentioned in the Introduction, this T4SS is assembled from the 11 VirB subunits and the VirD4 type IV coupling protein (T4CP) (Figure 4.1). By construction of individual *virB* gene deletions, combined with appropriate complementation analyses, the Christie laboratory established that 10 of the 11 VirB subunits are required to build a functional translocation channel, whereas all 11 subunits are required to build the T-pilus (67). The 11th gene, *virB1*, encodes a lytic transglycosylase whose deletion strongly diminishes T-DNA transfer to plants, but completely abolishes assembly of detectable pili. Corresponding genetic analyses of the R388-encoded Trw T4SS and the RP4-encoded Tra/Trb T4SS similarly established the importance of the associated lytic transglycosylases for pilus biogenesis, as monitored by sensitivity to male-specific phage, but not for elaboration of functional translocation channels (45,123). Surprisingly, in the Trw_{R388} system, the VirB7-like lipoprotein TrwH is not required for assembly of the translocation channel (123). In *A. tumefaciens*, by contrast, VirB7 plays an essential role in stabilizing the outer membrane-associated subunit VirB9 through formation of an intermolecular disulfide bridge (118,120–122).

The early construction of a complete set of *virB* gene deletions and complementing plasmids greatly facilitated studies of the *A. tumefaciens* VirB/VirD4 system in the Christie laboratory as well as many other laboratories devoted to studies of this system. When I entered the laboratory, we were interested in incorporating studies of the *E. coli* pKM101-encoded Tra T4SS (Tra_{pKM101}) in order to capitalize on the ease of genetic manipulation and growth of *E. coli*,

Figure 4.1 Structure of the operons encoding the VirB, Tra, and Trw T4SSs

Operon arrangement of the *A. tumefaciens* VirB T4SS along with the operons encoding the pKM101 Tra and R388 Trw T4SSs. Each of the homologs is depicted in identically colored arrows and the function of each of the proteins is indicated above the corresponding gene.



the availability of large numbers of *E. coli* mutant strains, and *in vivo* assays developed using this model organism for refined studies of this T4SS. I first sought to define the genetic requirements for Tra_{pKM101} T4SS function by construction of a complete set of *tra* gene deletion mutations and a corresponding set of *tra* expression plasmids for complementation studies. In fact, early studies by Winans and Walker (1985) had identified the *tra* gene cluster and provided evidence for the requirements of most of the *tra* genes through a Tn5 transposon mutational analysis (153). However, these Tn insertions potentially have polar effects on downstream gene expression, preventing any firm conclusions regarding the essentiality of each *tra* gene. Construction of precise gene deletions, together with genetic complementation, would not only confirm the importance of each *tra* gene, but also provide a ‘molecular toolkit’ of strains and plasmids for our future studies.

In this chapter, I developed a combination of genetic approaches including λ red recombineering and inverse PCR to create a pKM101 “molecular toolkit” (154). This toolkit consists of non-polar deletions of each of the *tra* genes, as well as each *tra* gene expressed separately from the tightly-controlled P_{BAD} promoter. Among the most striking outcomes from these studies, I gained evidence that *traL*, which encodes a putative lytic transglycosylase, is completely dispensable for elaboration of a fully functional Tra_{pKM101} transfer channel as well as the conjugative pilus. Additionally, *traC*, which encodes a putative pilus tip protein, is also dispensable for elaboration of a functional transfer channel, but required for pilus production. I discuss these findings in the context of available information for other T4SSs and additional data from the Christie laboratory suggesting that TraC coordinates with another, previously uncharacterized protein called KikA to promote donor-recipient cell contacts even in the absence of pilus production.

Results

Complementation of *tra* Mutants in Filter Matings. I deleted 8 of 11 *tra* genes from the pKM101 plasmid by recombineering. I was not able to make deletions of *traL*, *traN*, and *traO*. I characterized the phenotypes of the 8 *tra* gene mutations, and through further studies by Roosheel Patel, we were able to evaluate the contributions of the remaining *tra* genes to assembly and function of the Tra_{pKM101} T4SS. Most of the deletions abolished plasmid transfer (Figure 4.2). Similar to previous reports from Winans and Walker, deletion of *traC* did not abolish plasmid transfer in solid-surface matings (153) (Figure 4.2). Complementation of each *tra* gene deletion with its respective native gene *in trans* from a P_{BAD} promoter restored pKM101 transfer. (Figure 4.2). Although most of the complementing *tra* genes restored transfer to levels similar to wild-type pKM101, complementation of IMC genes *traA*, *traD*, and *traE* only partially restored transfer (Figure 4.2). These results demonstrate that each of the *tra* gene deletions is able to be complemented with the respective native gene *in trans*.

Susceptibility of *tra* Mutants to PRD1 and IKE bacteriophages. Donor-specific bacteriophages utilize the T4SS, and more specifically the conjugative pilus, as a point of entry into the cell. Previous studies have sought to determine the genetic requirements for phage infection of host cells carrying pKM101 or other conjugative T4SSs. Mutations in the *tra* and *trb* genes of pKM101 and RP4, respectively, confer resistance to PRD1 phage (45,153). While PRD1 sensitivity was restored to RP4 *trb* mutants through complementation tests, no such experiments have been performed with pKM101 mutants. All eight of the Δtra mutations on the native pKM101 abolished PRD1 and IKE uptake. However, only the $\Delta traM$, $\Delta traF$, and $\Delta traG$ mutants exhibited phage sensitivity when the native gene was expressed *in trans* (Figure 4.3).

Figure 4.2 Genetic requirements for plasmid transfer through the pKM101 T4SS.

Bar diagram of *E. coli* matings monitoring the transfer of native pKM101 and the deletion mutants both with and without the complementing plasmid. Black bars represent non-complemented mutants, gray bars represent mutants complemented in filter matings, and white bars represent mutants complemented in broth matings. Experiments were performed in triplicate and the histograms represent the average results with standard deviations.

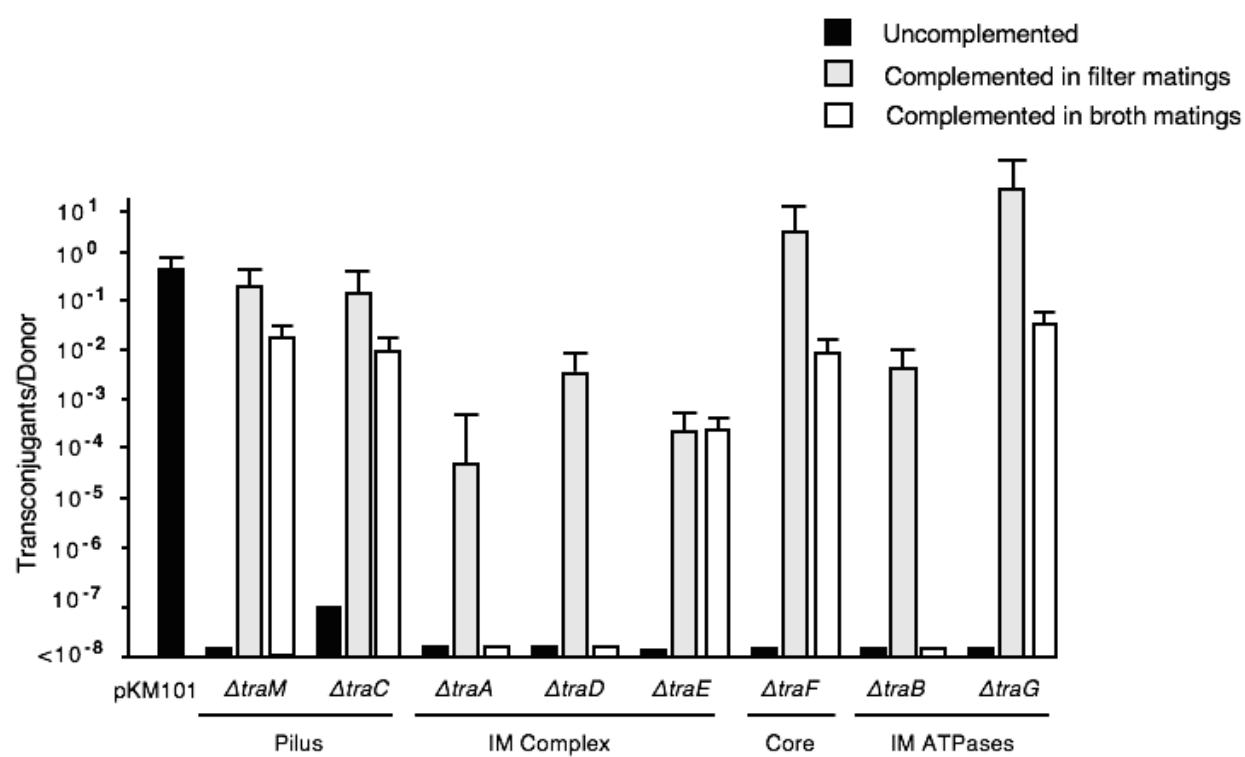
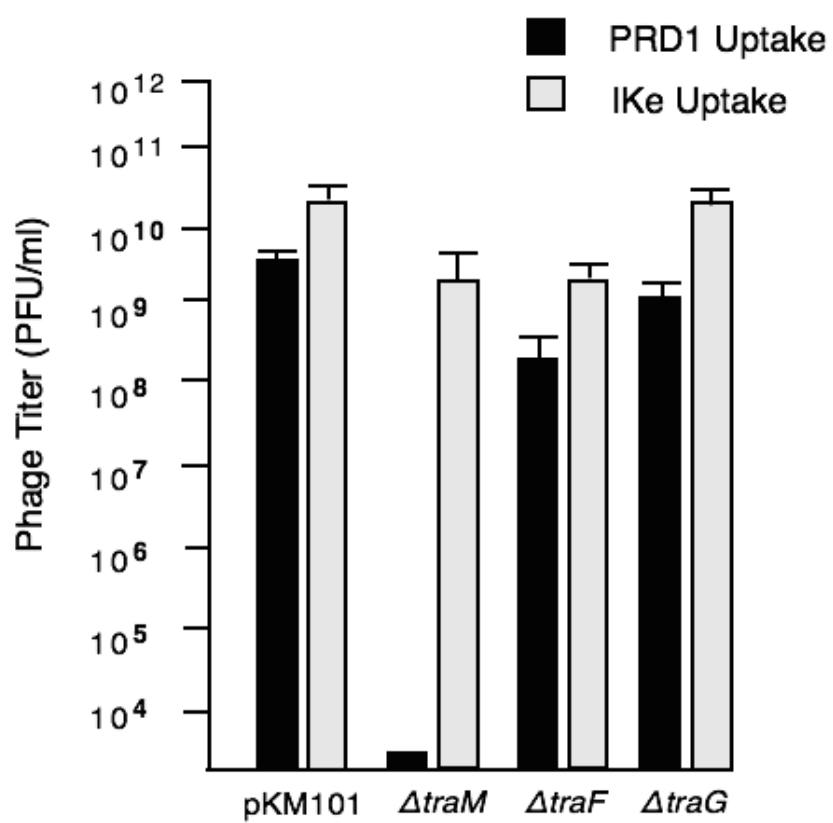


Figure 4.3 Restoration of PRD1 and IKE sensitivity. Bar diagram of *E. coli* infection assays monitoring uptake of PRD1 and IKE in complemented $\Delta traM$, $\Delta traF$, and $\Delta traG$ mutants. Sensitivity is measured as the number of plaque forming units/ml (PFU/ml). Black bars represent PRD1 infection while gray bars represent IKE infection. Experiments were performed in triplicate and the histograms represent the average results with standard deviations.



Lack of complementation of the other Δtra mutations is not easily explained, although it is possible that nonstoichiometric production of certain Tra proteins from the strong P_{BAD} promoter might interfere with phage binding or uptake.

Taken together, these results demonstrate that production of an intact Tra_{pKM101} T4SS is required for infection by the male-specific phages PRD1 and IKe.

Complementation of *tra* mutants in broth matings

E. coli cells efficiently transfer the F plasmid to recipients in liquid culture. This is due to the long, flexible pilus carried by F-plasmid-containing cells which is capable of attaching to recipient cells and retracting to form mating junctions (155,156). Plasmids such as pKM101, R388, and RP4 encode short, rigid pili, which are not thought to undergo dynamic rounds of extension and retraction (155). Therefore, cells containing these plasmids are not predicted to transfer DNA efficiently in broth.

Interestingly, however, I discovered that pKM101-containing donors are capable of transferring the plasmid in broth matings, albeit at levels 100-fold lower than on filters (Figure 4.2). The three complemented mutants, $\Delta traM$, $\Delta traF$, and $\Delta traG$, exhibiting phage sensitivity also served as efficient plasmid donors in broth matings. Additionally, complemented $\Delta traC$ and $\Delta traE$ mutants conjugatively transferred pKM101, although the $\Delta traE$ mutant was more attenuated than the others. The capacity of cells to transfer in liquid generally correlated with their phage sensitivity profiles, although some strains resistant to phage uptake served as proficient donors in broth.

Complementation of *tra* mutants in mini-pKM101

As mentioned previously, we were unable to create deletions of *traL*, *traN*, and *traO* on native pKM101. The ~10 kb region of pKM101 from the 3' end of *korB* through the 3' end of *traG* was cloned into pBAD33 to create pCGR100. I tested its ability to deliver plasmid pJG142, which contains the *oriT* sequence as well as genes encoding the TraI relaxase, TraK accessory factor, and TraJ substrate receptor, which collectively are responsible for *oriT* processing and delivery of the plasmid substrate to the T4SS channel. pCGR100 mediated transfer of pJG142 at levels 1,000-fold lower than native pKM101 (Figure 4.4). Complementation of a $\Delta traO$ mutant restored plasmid transfer to pCGR100 levels whereas the $\Delta traN$ mutant only had plasmid transfer partially restored (Figure 4.4). The $\Delta traO$ and $\Delta traN$ mutant strains remained resistant to phage even when expressing the corresponding *traO* or *traN* genes were expressed in trans (data not shown).

In previous studies, deletions of the cell wall hydrolases VirB1 and p19 associated with the VirB and F plasmid T4SSs, respectively, resulted in attenuated DNA transfer and loss of sensitivity to male-specific phages (67,157). Interestingly, however, deletion of *traL* from the pKM101 system had no detectable effect on plasmid transfer or phage susceptibility. Furthermore, complementation of a $\Delta traL$ mutant by expression of *traL* from the P_{BAD} promoter enhanced plasmid transfer by ~100-fold (Figure 4.4). I also observed a similar enhancement of plasmid transfer by donors carrying both the WT pKM101 and pCGR100 plasmids (Figure 4.5).

These results confirm that TraN and TraO are essential for building a functional translocation channel, whereas the TraL hydrolase is completely dispensable. However, cells that overproduce TraL might be capable of elaborating quantitatively more channels across the cell wall than $\Delta traL$ mutants or even cells expressing *traL* at WT levels.

Figure 4.4 Plasmid transfer through the mini-pKM101. Bar diagram of *E. coli* matings monitoring transfer of *oriT-IJK*_{pGB2} using either wild-type pCGR100 or deletion mutants with and without the complementing plasmid. Black bars represent non-complemented mutants, gray bars represent mutants complemented in filter matings, and white bars represent mutants complemented in broth matings. Experiments were performed in triplicate and the histograms represent the average results with standard deviations.

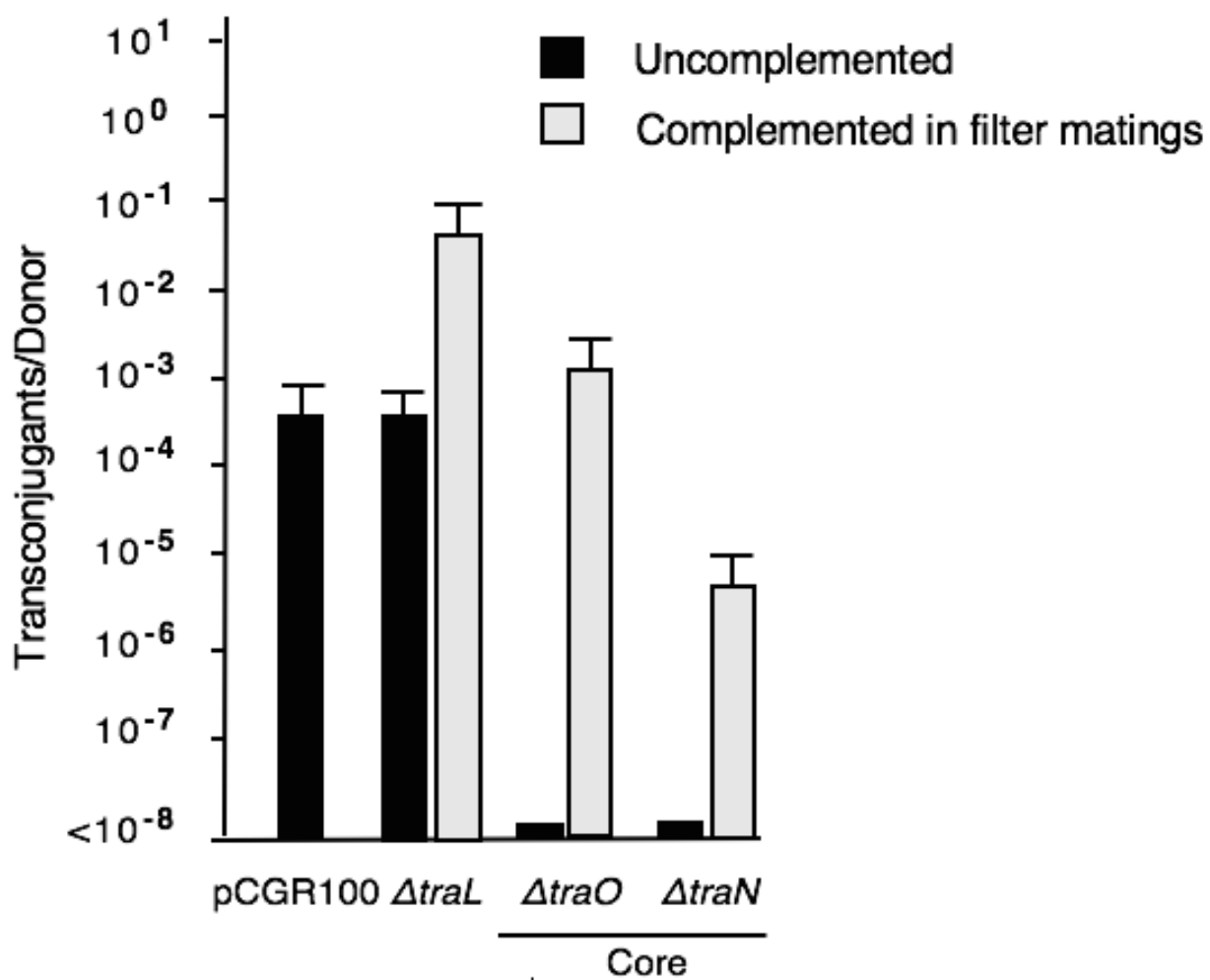
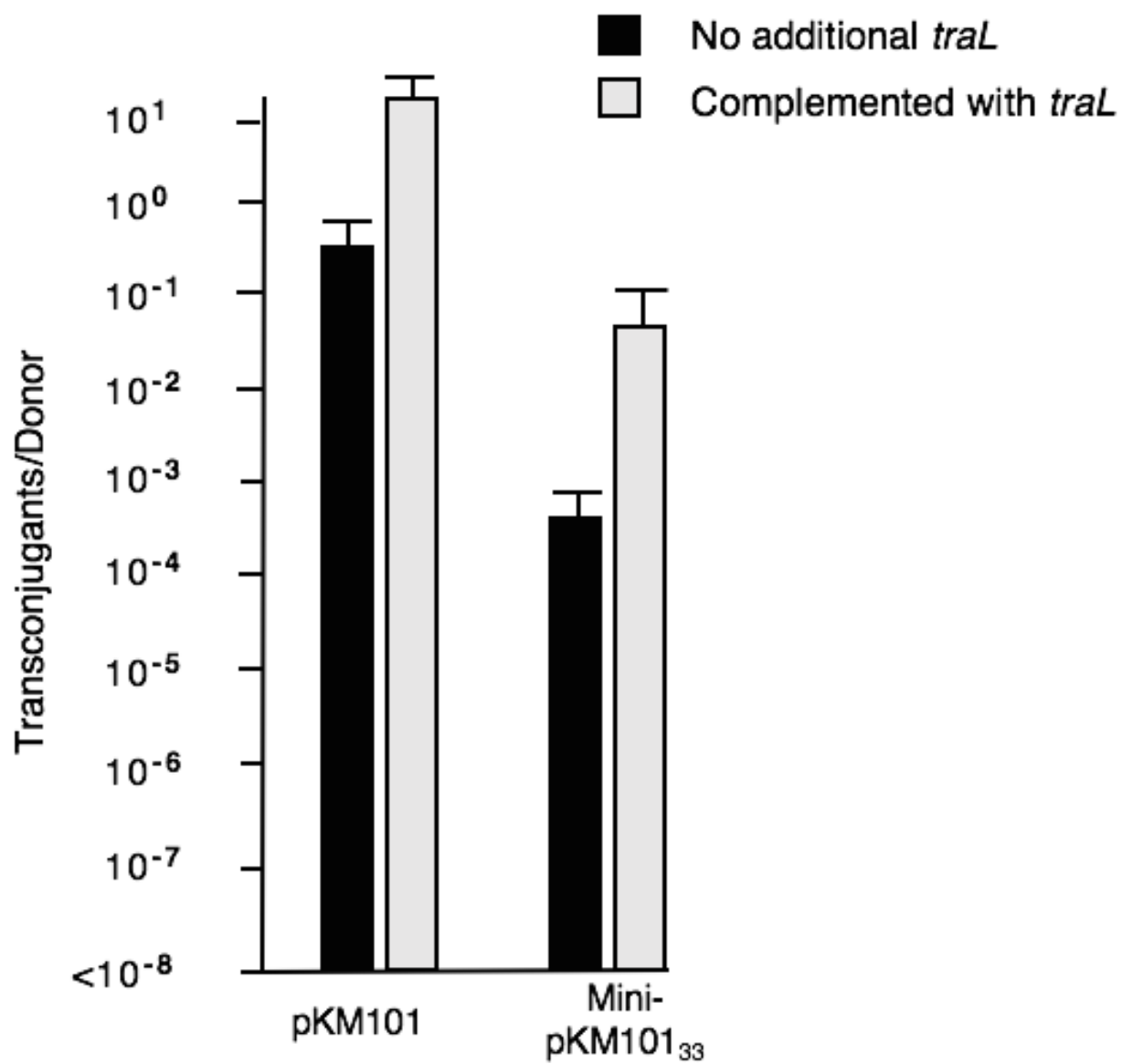


Figure 4.5 Enhancement of plasmid transfer through overexpression of *traL*

Bar diagram of *E. coli* matings monitoring the transfer of native pKM101 and pJG142 in the presence and absence of overproduced TraL. Black bars indicate the absence of *traL in trans* while gray bars indicate the presence of overexpressed *traL*. Experiments were performed in triplicate and the histograms represent the average results with standard deviations.



Discussion

Here, I developed a pKM101 “molecular toolkit” for the addressing current and future questions related to T4SS structure and function. I used complemented and uncomplemented pKM101 *tra* deletion mutants to identify the genetic requirements for construction of a functional machine. My studies represented the first systematic effort, other than that carried out by the Christie lab for the *A. tumefaciens* VirB/VirD4 T4SS, to define the contributions of individual T4SS genes through construction of markerless deletions. Below, I discuss my findings in comparison with previous analyses of other T4SSs.

Predictions about the genetic requirements for pKM101 were based on our previous studies in the VirB system. Similar to those studies and others in R388 and RP4, pKM101 *tra* gene deletions abolished all activity as monitored by mating assays and sensitivity to PRD1 and IKE phages. Similar to the results from Winans and Walker (153), I also showed that TraC is not essential for plasmid transfer. However, I also found that the cell wall hydrolase, TraL, is dispensable, and overexpression of *traL* in either a wild-type or $\Delta traL$ background enhanced transfer.

Contributions of TraC and KikA to pKM101 plasmid transfer

VirB5 has been described as the minor pilin subunit and has been observed at the *A. tumefaciens* pilus tip (158). Studies on pKM101-encoded TraC have demonstrated that it can be localized to the cell surface and form high molecular weight complexes in the presence of a functional T4SS (87). Because VirB5 in *A. tumefaciens* is located at the pilus tip, TraC is also predicted to be the pilus tip protein as point mutations can drastically alter cell susceptibility to filamentous phage IKE (142). Therefore, it is likely that TraC is involved in forming and

stabilizing recipient cell contact as part of the pilus. However, my results as well as those from Winans and Walker have demonstrated that TraC is not essential component of the pKM101 T4SS (153). Therefore, it is likely that other surface proteins are able to mediate recipient cell contact. Based on other studies from our lab, one possible candidate protein is KikA. The *kikA* (killing in *Klebisella A*) locus is located upstream of the *tra* operon and encodes a small surface protein. Although KikA is not critical for pKM101 mobilization on solid surfaces, previous studies have highlighted its importance in uptake of PRD1 phage (159). Recently, our lab has demonstrated that KikA is essential for processes including plasmid transfer in broth matings and mediating recipient cell contact as monitored by the *Pseudomonas aeruginosa* T6SS killing assay (discussed in the following chapter). Our lab has also demonstrated that creation of a double $\Delta traC/\Delta kikA$ mutant abolished residual plasmid transfer, indicating that KikA might partially substitute for TraC. Further characterization of the role of KikA in T4SS and its physical relationship with the channel is currently being investigated by our lab.

Contributions of TraL to pKM101 plasmid transfer and pilus biogenesis

Deletion of *virB1* in *A. tumefaciens* reduced T-DNA transfer to plants and abolished pilus biogenesis (67). Similar results were seen during analysis of the F-plasmid-encoded P19 cell wall hydrolase (157). However, my results revealed that the pKM101-encoded homolog, TraL, is nonessential. Additionally, overexpression of *traL* increased plasmid transfer. Therefore, TraL could be considered a rate limiting factor in plasmid transfer. By overproducing TraL, this could allow for production and insertion of more translocation channels into the membrane. Alternatively, TraL could be secreted into recipient cells and allow for more efficient translocation through degradation of the recipient cell wall. In order to address these questions,

future experiments should test the steady state levels of other Tra proteins in the presence and absence of overproduced TraL. Finally, export of TraL to the recipient cell periplasm can be tested using fluorescence microscopy to observe localization of fluorescently-labeled TraL and other recipient-encoded periplasmic proteins.

It is curious why the *traL* locus is present in the pKM101 *tra* operon if it is not essential. One plausible explanation relates to the fact that pKM101 is capable of transferring among a broad range of Gram-negative bacterial species. It is possible that TraL interacts with other T4SS components to localize cell wall degradation. In *E. coli*, the dispensability of TraL might be explained by redundant activities of other cell wall hydrolases or the assembly of the T4SS during the early growth phase when the cell wall is being actively remodeled. In other species, pKM101 might require its own lytic transglycosylase due to a lack of a compensating hydrolase or temporal differences in T4SS machine assembly in relation to the growth phase. Evolutionary pressures, therefore, might have maintained *traL* on pKM101 for retention of its broad-host-range properties.

Complementation of *tra* mutants for PRD1 and IKe infection

Complementation of *virB*, RP4 *trb*, and F-plasmid deletion mutants restored detectable pilus production, PRD1 and R17 sensitivity respectively (45,67,132). In my analysis of pKM101 *tra* deletion mutants, all of the deletion mutants with the exception of *traL* were resistant to both PRD1 and IKe. However, complementation only restored sensitivity to $\Delta traM$, $\Delta traF$, and $\Delta traG$ mutants.

For those Δtra mutants in which phage sensitivity was not restored by expression of the complementing gene *in trans*, there are a couple of possible explanations. They may not

elaborate pili or alternatively, they may elaborate wild-type pili, but sustain blocks in the phage uptake pathway subsequent to phage binding to the pilus receptor. While the PRD1 uptake pathway is not well understood, filamentous bacteriophages such as M13 and IKe utilize the TolQRA proteins to cross the IM (160,161). It is possible that overproduction of the Tra proteins blocks the ability of IKe to bind the cell surface or to interact with TolQRA. Future studies focused on elucidating the requirements for pKM101 pilus production as well as defining the pilus assembly pathway will require antibodies against the TraM pilus protein.

Transfer of pKM101 in broth matings

Conjugation in broth media is a well-documented phenomenon in studies of the F-plasmid. This is due to physical structure of the conjugative pilus, which is long and flexible, making it easy to feel around its physical environment and grab onto a recipient cell. Following attachment, these pili are able to retract and bring the recipient cell into close contact in spite of shear forces in the environment (156). Unlike the F-plasmid, pili encoded by pKM101, R388 and RP4 plasmids are short and brittle. Furthermore, there is no evidence of pili retracting or being involved in recipient cell contact and mating pair stabilization. My data suggests that production of conjugative pili is important for successful plasmid transfer in broth. However, further studies carried out by Dr. Christian Gonzalez-Rivera, a postdoctoral fellow in the Christie lab, suggest that two surface-exposed proteins, the pilus tip protein TraC and KikA, can promote donor-recipient contacts in broth even in the absence of detectable pilus production.

**Chapter 5: Defining the Role of a Novel Outer
Membrane Alpha Helical Domain in pKM101-encoded
TraF for Plasmid Transfer, Donor-Specific
Bacteriophage Sensitivity, and Recipient Cell Contact**

Introduction

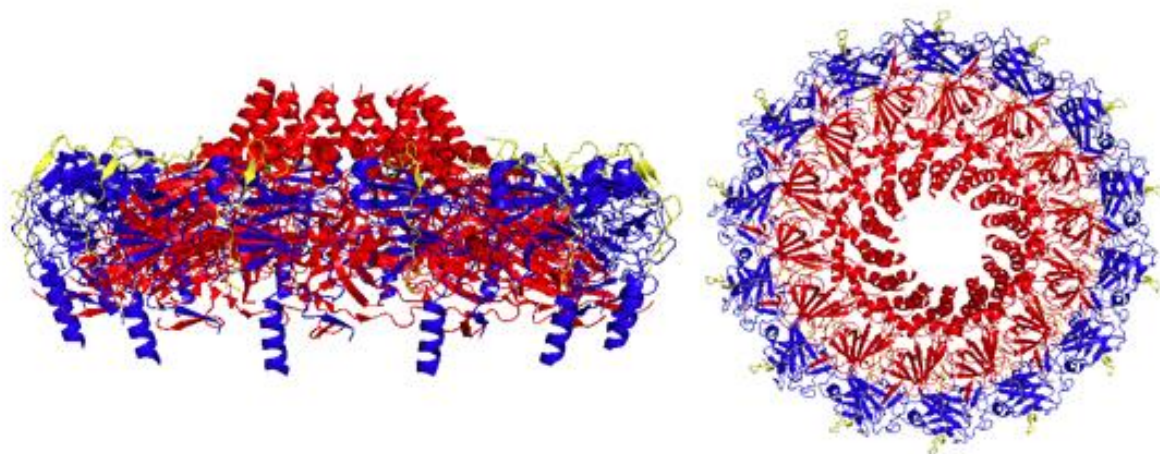
The T4SSs from Gram-negative bacteria are comprised of two large subassemblies: an inner membrane complex (IMC) and an outer membrane core complex (OMCC). The IMC is comprised the three inner membrane (IM) ATPases (VirD4, VirB4, and VirB11) and three IM subunits (VirB3, VirB6, and VirB8). Recent studies also suggest that VirB5 could also comprise a significant part of the IMC (84). The predicted role of the IMC is to recruit substrates to the T4SS and help transfer them across the IM. The OMCC is comprised of 14 copies of VirB7, VirB9, and VirB10 arranged into a large 1 MDa structure (82,90). The OMCC is predicted to be primarily involved in moving substrates across the OM and establishing contact with recipient cells (Figure 5.1) (162). Structural studies on the Trw_{R388} T4SS identified two distinct IMC and OMCC subassemblies connected together by a central stalk structure (84). All of these components were shown to be necessary to build a functional translocation channel in the VirB T4SS (67).

Unlike the other components of the T4SS, VirB10 is a unique protein in that it spans the length of the cell envelope. Because it makes contacts with subunits in both the IMC and the OMCC, it is predicted to act as a scaffolding protein linking the two subassemblies together (90,98). At the IM, it is predicted to make essential contacts with IM ATPases which are essential for initiating ATPase-mediated conformational changes in VirB10 (Figure 5.2) (95,98,107). These contacts are likely mediated through the VirB10 N-terminus as gradual truncations in this region reduced the affinity of VirD4 for VirB10 (127). The conformational change brought about by IM ATPase activity is predicted to transduce energy to the OMCC subunits, such as VirB7 and VirB9. VirB10 makes extensive contacts along its β -barrel with VirB9, which is anchored at the OM by the VirB7 lipoprotein (Figure 5.1) (90). Additionally,

Figure 5.1 The OMC and its potential role in plasmid transfer (A) Structure of the pKM101 OMC demonstrating the arrangements of TraN (yellow), TraO (blue), and TraF (red). The structure of the core complex O-layer was generated using Pymol (<http://pymol.org>) based on the 3ZBI file deposited into the NCBI protein database (B) Cryo-EM images of *E.coli* donors containing RP4 mixed with *E. coli* recipients. Black arrows indicate the positions of mating junctions.

Bottom images are from Samuels AL, Lanka E, Davies JE. *Conjugative junctions in RP4-mediated mating of Escherichia coli*. J Bacteriol. 2000 182:2709–15. The American Society for Microbiology allows for re-publication of its materials in a doctoral thesis.

A



B

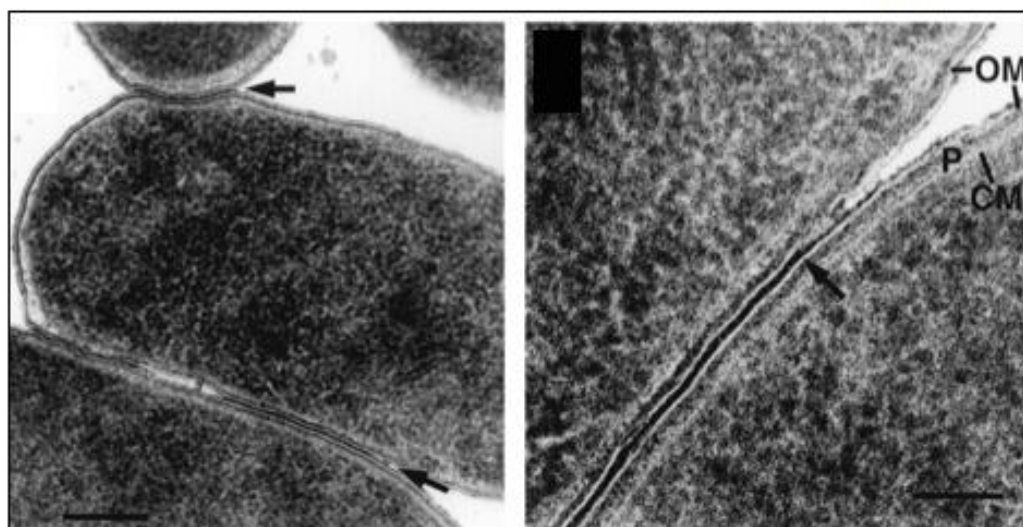
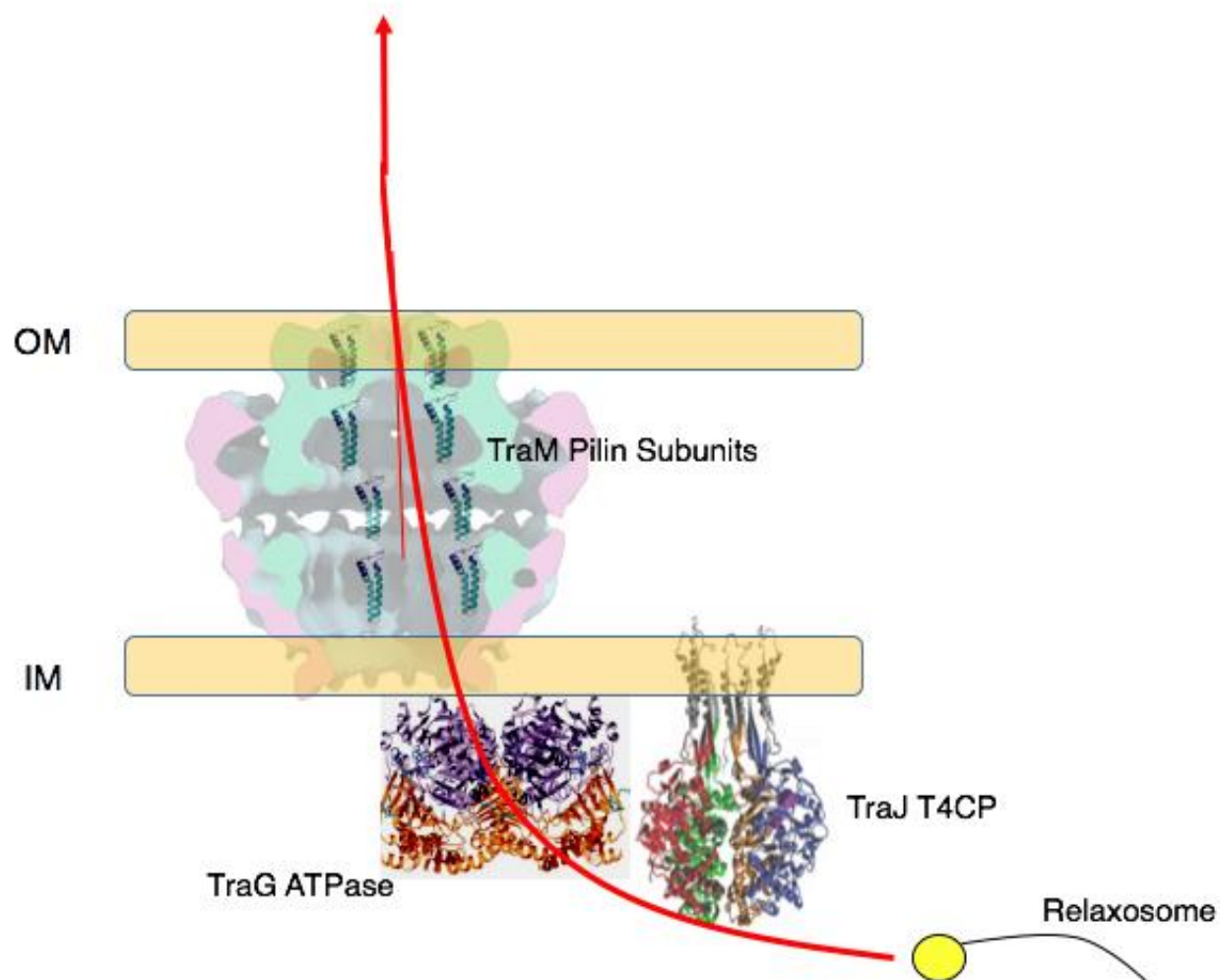


Figure 5.2 Plasmid transfer through the conjugative pilus. This model demonstrates the path of DNA through the conjugative T4SS. The positions of the TraJ and TraG ATPases and the conjugative pilus composed of TraM are indicated. The position of TraF within the cryo-EM structure of the is highlighted in green.

The structure of TrwB is Figure 2C from Gomis-Rüth FX et al. *The bacterial conjugation protein TrwB resembles ring helicases and F1-ATPase*. Nature 2001 409:637–41. This image was re-published with permission from Nature Publishing Group. License Number 4078401439237. The structure of the VirB11-like HP0525 was published as Figure 3C in Yeo HJ et al. *Crystal structure of the hexameric traffic ATPase of the Helicobacter pylori type IV secretion system* Mol Cell. 2000 6:1461–72. This image was re-published with permission from Elsevier. License Number 4078430588294. The pKM101 core complex structure is Figure 4 from Fronzes R, et al. *The structural biology of type IV secretion systems*. Nat Rev Microbiol. 2009 7:703–14. This image was re-published with permission from Nature Publishing Group. License # 4092681298982.



VirB10 likely makes critical contacts with VirB2 pilin subunits (Figure 5.2). While VirB2 is primarily localized to the IM before pilus biogenesis, VirB2 is essential for transfer of T-DNA across the OM (74). Because T-DNA does not make contact with VirB10, it likely makes contact with VirB2, possibly assembled as a short pilus in the OMCC lumen. This short pilus might comprise the translocation channel, allowing for passage of substrates to the cell surface (Figure 5.2).

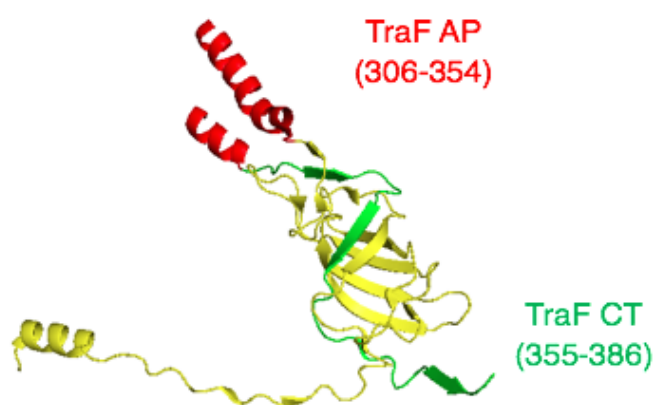
In Chapter 3 of this thesis, I analyzed the importance of the VirB10 antenna projection (AP) domain and C-terminal tail. Both of these regions were amenable to mutations without affecting plant tumor formation. However, these mutations either attenuated or abolished T-pilus production. One notable example was a substitution of the VirB10 AP and C-terminal tail for that of TraF. The C-terminal tail of VirB10 is 43 residues and is ~71% identical to that of TraF (Figure 5.3). Both of these tails contain a highly-conserved RDLDF sequence that was shown to be essential for T-DNA transfer and pilus biogenesis in VirB10 (127). Additionally, the crystal structure of TraF indicates that the C-terminal tail folds back into the lumen of the barrel (90). Accordingly, this domain might make contacts with substrates and/or pilin subunits as they pass through the channel (Figure 5.3).

In the previous chapter of this thesis, I highlighted the importance of the pKM101 Tra subunits for plasmid transfer and phage sensitivity. Complementation of a $\Delta traF$ mutant with wild-type *traF* restored both plasmid transfer and phage sensitivity to pKM101. In light of the structural information from the pKM101 TraN-TraO-TraF core complex and the functional data from the VirB10 AP, I hypothesized that the TraF AP is a surface exposed domain that is dispensable for the formation of an OM pore, but critical for pilus biogenesis and the formation of stable mating junctions through the formation of recipient cell contact. Here, I used chimeric

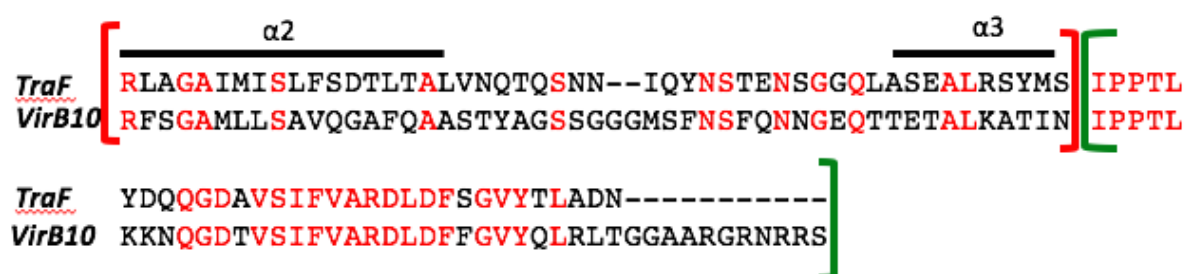
Figure 5.3 Similarities between the TraF and VirB10 AP and C-terminal domains.

(A) Crystal structure of TraF with the AP (residues 306-354) highlighted in red and the C-terminal tail (residues 355-386) highlighted in green. The structure of TraF was generated using Pymol (<http://pymol.org>) based on the 3ZBI file deposited into the NCBI protein database (B) Alignment of the TraF AP and C-terminal tails. The residues comprising the AP are surrounded by red brackets and the C-terminal tail residues are bracketed in green. Red letters indicate conserved residues between TraF and VirB10.

A



B



TraF/VirB10 proteins and TraF truncation mutants in order to identify regions within the AP and C-terminal tail that were critical for plasmid transfer and phage sensitivity. Additionally, I used chimeric T4SSs containing the IMC of pKM101 and the OMCC of either the VirB/VirD4_{Ti}, Trw_{R388}, or Ptl_{Bp} T4SSs to evaluate the importance of the OMCC, and in particular the AP, in establishing donor-recipient cell contacts.

Results

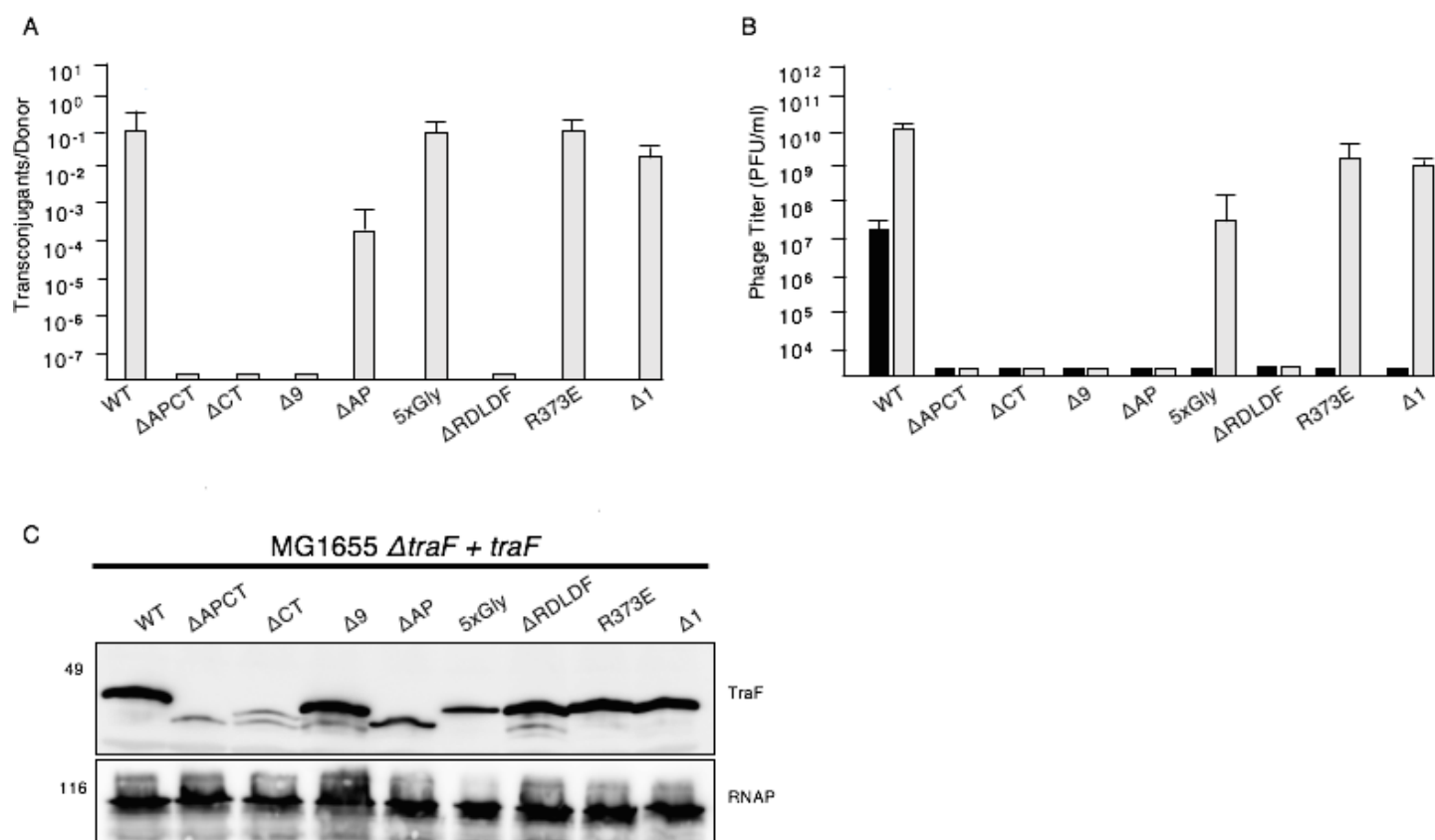
The TraF AP is critical for phage sensitivity, but dispensable for plasmid transfer

According to the pKM101 O-layer crystal structure, TraF lines the inner wall of the channel and forms an OM pore using its AP domain. Based on the functional conservation of the AP domains in VirB10 and TraF in addition to the dispensability of the VirB10 AP seen in Chapter 3, I predicted that the TraF AP domain is similarly dispensable for plasmid transfer, but required for pilus biogenesis. Here, I assayed strains producing various TraF AP and C-terminal mutants for plasmid transfer and phage sensitivity as an indicator of pilus production.

I began by making deletion mutations throughout the TraF AP. I first replaced the flexible loop region with a pentaglycine bridge (5xGly), which had no detectable effects on plasmid transfer (Figure 5.4). A larger deletion of the TraF AP (residues 302-355) resulted in only a modest decrease in intercellular pKM101 transfer (Figure 5.4). Additionally, neither of these mutations had any discernable effect on TraF protein accumulation (Figure 5.4). Taken together with the data presented in Chapter 3, we can conclude that the AP regions of both TraF and VirB10 are dispensable for DNA transfer, although their presence results in more efficient conjugation.

Replacement of the flexible loop with a pentaglycine bridge did not abolish IKE sensitivity, indicating that these mutants restore the presence of a functional conjugative pilus. However, the Δ AP mutant did not restore sensitivity to either PRD1 or IKE, suggesting that cells producing this TraF mutant lack pKM101-encoded pili. The TraF Δ AP strain behaved similarly to its VirB10 counterpart indicating that the AP helices are an essential factor for pilus biogenesis.

Figure 5.4 Functionality of TraF truncation mutants. (A) Bar diagram depicting the level of native pKM101 transfer from donors containing TraF truncation mutants. Frequencies are depicted as transconjugants per donor. Matings were repeated 3 times and the histogram represents the average with standard deviations. (B) Bar diagram representing the sensitivity of donors to PRD1 and IKE. Sensitivity is depicted as the number of plaque forming units per ml (PFU/ml). Black bars represent PRD1 infections while gray bars represent IKE infections. Plaque assays were repeated 3 times and the histogram represents the average value with the standard deviations. (C) Steady state levels of TraF truncation mutants containing an N-terminal 6xHis tag.



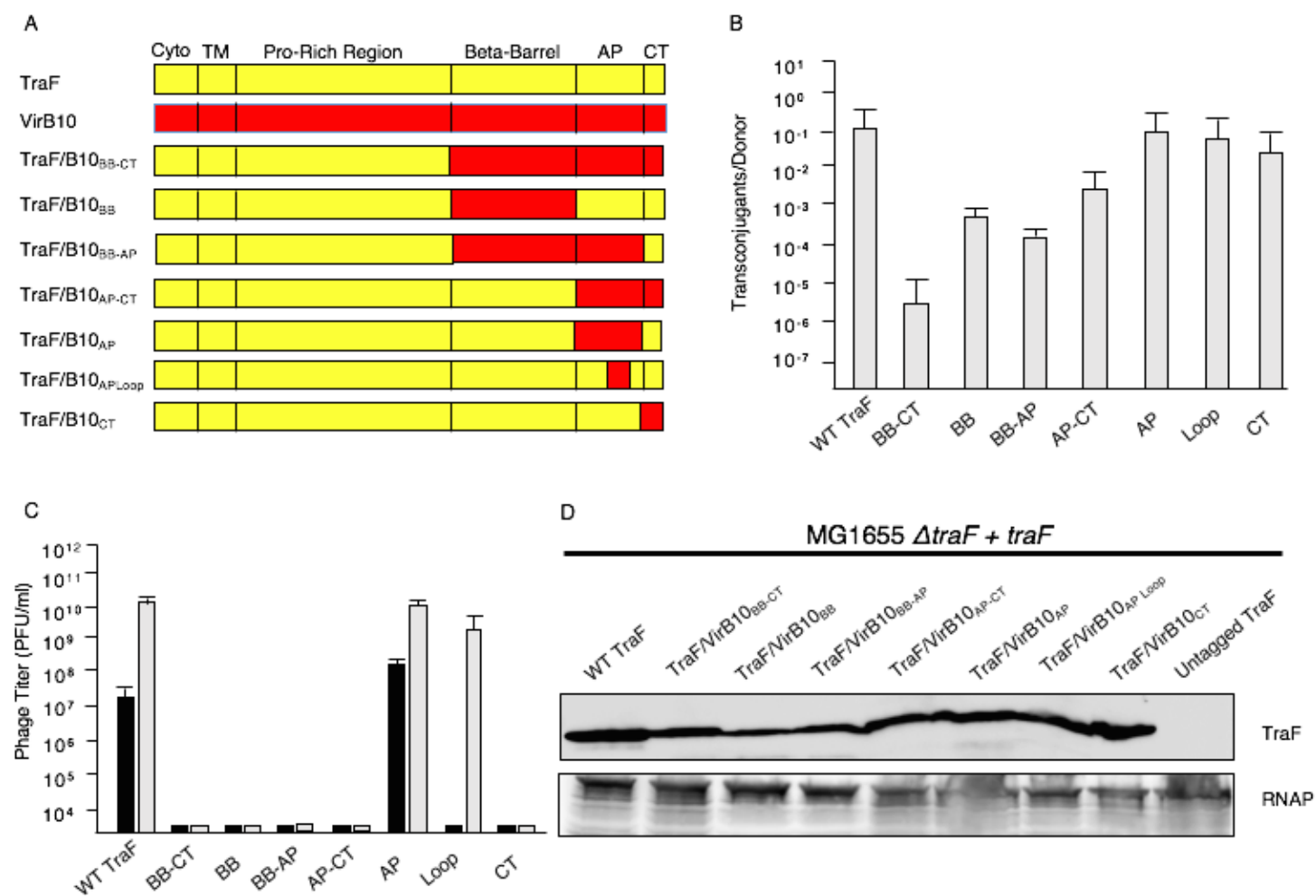
Because the AP domains of both TraF and VirB10 were permissive for mutations, another substitution was constructed by placing the VirB10 AP helices (residues 284-337) onto TraF (TraF/VirB10_{AP}). This chimera phenocopied wild-type TraF by restoring plasmid transfer and phage sensitivity to wild-type levels, (Figure 5.5). As with the previous AP swap, these results are striking due to the generally low level of identity (~31%) between the TraF and VirB10 AP domains. Further substitution of the VirB10 AP flexible loop onto TraF (TraF/VirB10_{AP_Loop}) still allowed for for plasmid transfer and IKe sensitivity (Figure 5.5). However, this mutant was not able to restore PRD1 sensitivity.

Taken together, these results demonstrate that the AP is dispensable for DNA transfer, but critical for pilus biogenesis in both TraF and VirB10. Despite its importance for pilus production, these domains are able to withstand mutations without significant phenotypic alterations.

The C-terminal domain of TraF is critical for both plasmid transfer and phage sensitivity

The region of highest identity between TraF and VirB10 is located in the C-terminal tail. These regions share ~71% identity with most of the homology occurring at the C-terminal end of the proteins (Figure 5.3). This region contains a highly conserved RDLDF motif found in all sequenced VirB10 family proteins. According to the TraF crystal structure, the C-terminal tail folds back into the channel lumen and is buried in the periplasmic β -barrel domain. Deletions of either the AP and C-terminal tail (Δ APCT) or just the C-terminal tail (Δ CT) resulted in the abolishment of both pKM101 transfer and phage sensitivity (Figure 5.4). However, these results

Figure 5.5 Functionality of the TraF/VirB10 chimeras. (A) Bar diagram depicting different swaps between TraF and VirB10. (B) Histogram depicting transfer frequencies of pKM101 from donors containing TraF/VirB10 chimeras during 2 hour filter matings. Frequencies are presented as transconjugants per donor. Matings were repeated 3 times and the histogram depicts the average values with standard deviations. (C) Bar diagram depicting the sensitivity of donors containing the TraF/VirB10 chimeras to PRD1 and IKE. Sensitivity is presented as the number of plaque forming units per ml (PFU/ml). Black bars represent PRD1 infections while gray bars represent IKE infections. Plaque assays were repeated 3 times and the histogram depicts the average values with standard deviations. (D) Steady state levels of TraF/VirB10 chimeras containing an N-terminal 6xHis tag.



are difficult to interpret as overall TraF levels in the donor cells was highly diminished. Deletion of the C-terminal 9 residues ($\Delta 9$) or the RDLDF sequence (Δ RDLDF) did not affect protein accumulation but abolished all detectable activity (Figure 5.4), suggesting that the C-terminal tail is critical for plasmid transfer and pilus biogenesis.

Because of the high level of identity of the C-terminal tails, I predicted that substitution of VirB10 C terminus (residues 335-377) for that of TraF (residues 354-386) would not affect plasmid transfer or phage sensitivity. Interestingly, the TraF chimera (TraF/VirB10_{CT}) as well as a chimera producing both the AP and C-terminal tail of VirB10 (TraF/VirB10_{AP-CT}) were not able to restore phage sensitivity, despite accumulating at abundant levels (Figure 5.5). These findings are consistent with the results seen with the VirB10/TraF_{AP-CT} chimera, further suggesting that the C terminus plays a critical role in biogenesis of the cognate pilus.

Taken together, these results demonstrate that the TraF and VirB10 C-terminal tails are critical for both DNA transfer and pilus biogenesis.

The N-terminal region of TraF does not tolerate substitutions of corresponding VirB10 domains.

The β -barrel regions of TraF (194-301) and VirB10 (173-284) share only ~35% identity. Because TraF tolerated mutations throughout the AP and C-terminal tail, I next wanted to test if TraF could withstand more extensive domain substitutions throughout its C-terminal half. A substitution of the VirB10 β -barrel, AP, and C-terminal tail onto TraF (TraF/VirB10_{BB-CT}) restored transfer to a $\Delta traF$ mutant, albeit at levels 10,000-fold lower than wild-type TraF (Figure 5.5). This mutant did not restore PRD1 or IKe sensitivity. These results demonstrate

that the β -barrel of VirB10 can functionally substitute for that of TraF, despite the low level of identity between the two domains.

Because the TraF C-terminal tail is critical for phage sensitivity, I predicted that addition of the TraF C-terminal tail back onto the TraF/VirB10_{BB-CT} could restore phage uptake. I constructed two new TraF mutants to test this hypothesis. One of these TraF mutants produced the β -barrel and AP of VirB10 (TraF/VirB10_{BB-AP}), where as the other produced only the VirB10 β -barrel (TraF/VirB10_{BB}). These mutants restored plasmid transfer to a $\Delta traF$ mutant at levels greater than the TraF/VirB10_{BB-CT} mutant (Figure 5.5). However, they were still unable to restore phage sensitivity (Figure 5.5). These results also implicate the TraF β -barrel as essential indicating a potential complex interplay between the β -barrel and C-terminal tail during pilus biogenesis.

The role of the N-terminal half of TraF remains undefined. Previous studies suggest that its N-terminal domain of VirB10 is required for interactions with the VirD4 T4CP (127). Other experiments with regards to regions such as the TM domain are not as clear. In the VirB_{At} T4SS, substitutions of the VirB10 TM domain with that of *E.coli* FtsN did not have an effect on T-DNA transfer (128). However, this was not the case in the Trw_{R388} system as the TM domain of TrwE appears to be critical for forming interactions with the TrwB T4CP (95,163). In order to elucidate the role of these domains in TraF, I created four new TraF chimeric proteins containing either the VirB10 N-terminal tail (TraF/VirB10_{NT}), TM domain (TraF/VirB10_{TM}), proline-rich region (TraF/VirB10_{PRR}) or TM through C-terminal tail (TraF/VirB10_{TM-CT}). These mutants were not able to restore plasmid transfer or phage sensitivity to a $\Delta traF$ mutant (Figure 5.6). The N-terminal half of TraF does not tolerate substitutions of VirB10 domains, suggesting that this region forms critical contacts with components of Tra_{pKM101}'s IMC subassembly.

Figure 5.6 Functionality of the TraF/VirB10 N-terminal chimeras. A) Bar diagrams depicting the N-terminal swaps of VirB10 onto TraF. (B) Histogram displaying the transfer frequencies of $\Delta traF$ mutants complemented with either the genes either for wild-type TraF or N-terminal chimeric TraF/VirB10 proteins. Mating frequencies are presented as transconjugants per donor and mating assays were repeated 3 times with the histogram depicting the average values with standard deviations. (C) Histogram depicting the sensitivity of $\Delta traF$ mutants to PRD1 and IKe when complemented with genes encoding either WT TraF or the TraF/VirB10 N-terminal chimeras. Sensitivity is presented as the number of plaque forming units per ml (PFU/ml). Black bars represent PRD1 infections while gray bars represent IKe infections. Plaque assays assays were repeated 3 times and the histogram depicts the average values with standard deviations. (D) Western blots measuring the steady state levels the TraF/VirB10 N-terminal chimeras.

Neither the AP nor the C-terminal tail are surface displayed

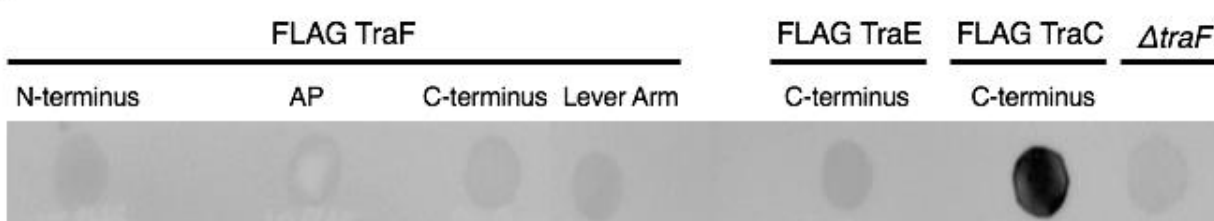
Previous reports have suggested that the TraF AP is surface displayed (90). However, these experiments lacked critical controls and conclusions were drawn based on the production of the TraN-TraO-TraF core complex rather than the entire T4SS. Additionally, my data suggests that the C-terminal tail is critical for pilus biogenesis. Based on my data with regards to the TraF/VirB10 chimeras, I predicted that the TraF AP and C-terminal tail are surface displayed. In order to test this hypothesis, I performed a dot blot experiment similar to those done with the OM lipoprotein RcsF (164). In these experiments, I placed FLAG tags in the AP loop (between residues 330 and 331) and at the end of the C-terminal tail. For a positive control, I put a FLAG tag at the C-terminal end of TraC, which has been demonstrated by our lab and others to be surface displayed (87). For negative controls, I inserted FLAG tags at the TraF N-terminal tail, in the lever arm at the periplasmic base of the β -barrel, and at the C-terminal domain of TraE predicted to be in the periplasm. Contrary to our hypothesis, the AP and the C-terminal FLAG tags were not detected on the cell surface (Figure 5.7). Additionally, C. Gonzalez-Rivera used BSA-conjugated maleimide to label cysteine residues placed at the C-terminal end of the AP (residue 360) and at the C-terminal tail (residue 386). Neither of these cysteine residues were labeled in whole cells. Together, these results suggest that the TraF AP and C-terminal tail are not surface accessible at least in the absence of target cell contact.

Heterologous OMCCs paired with the pKM101 IMC support plasmid transfer

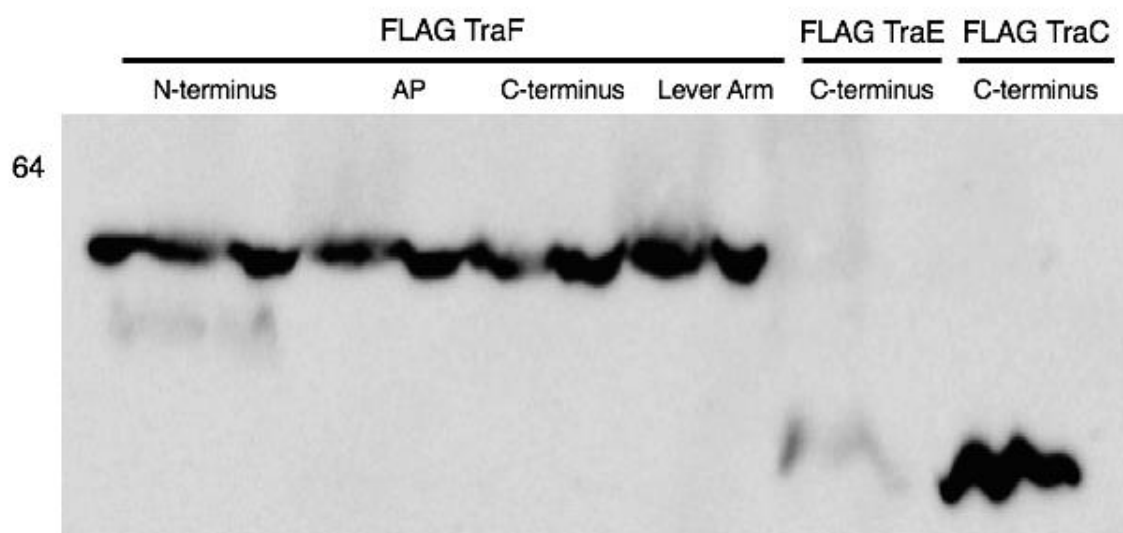
Although the extensive contacts between TraF and TraO were not critical for building a functional translocation channel, they may be important for building an efficient one. If this prediction is correct, replacing TraO with VirB9 might lead to more efficient transfer. Therefore,

Figure 5.7 Surface display of TraF (A) Colony immunoblots depicting the detection of FLAG tags placed throughout TraF and the C termini of TraE and TraC. (B) Western blots detecting the steady state levels of the different FLAG-tagged TraF proteins as well as C-terminal FLAG-tagged TraE and TraC.

A



B

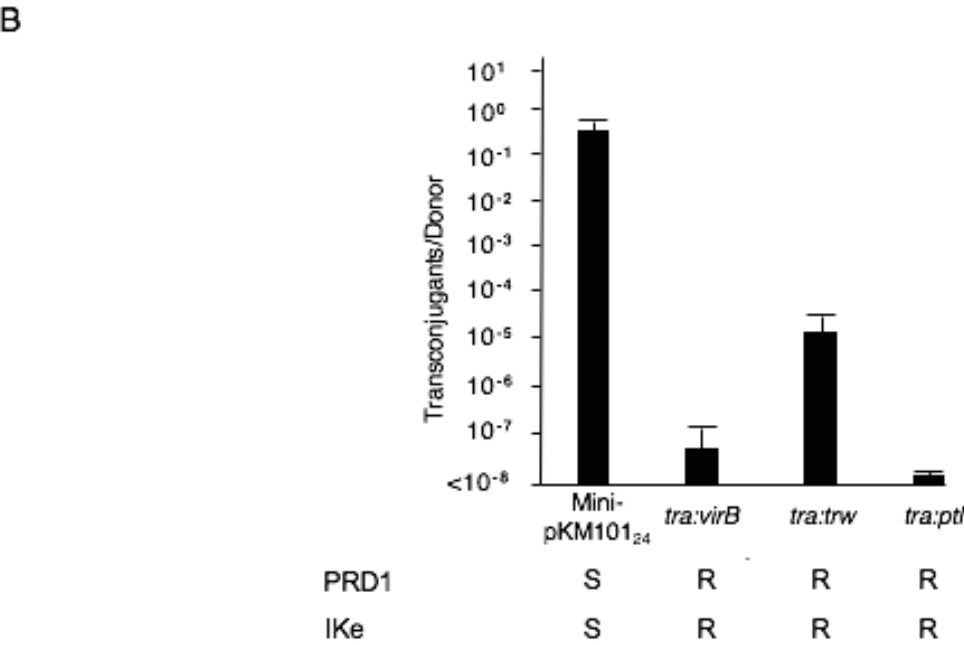
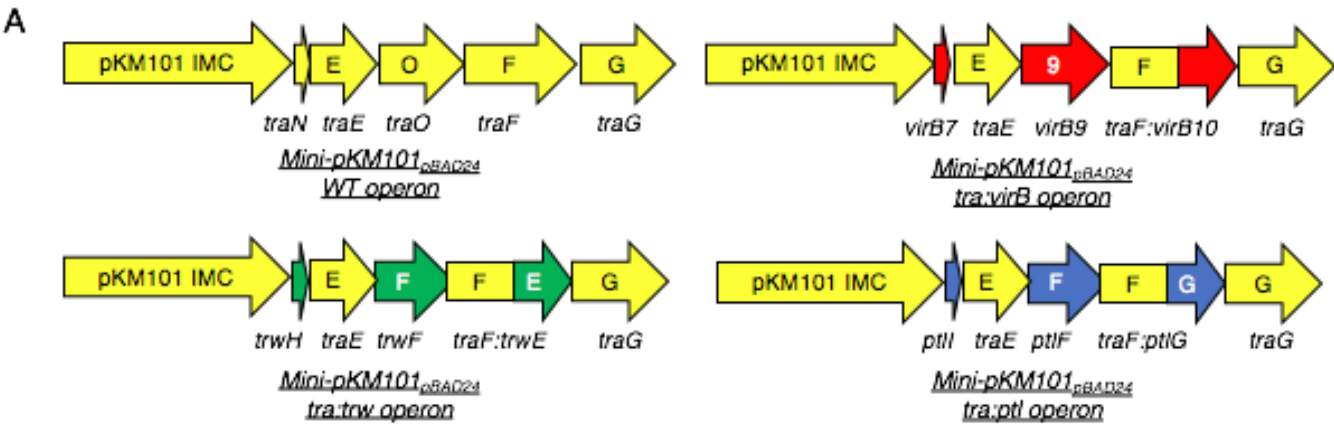


I constructed a chimeric T4SS containing the IMC of pKM101 and the OMCC from the VirB_{Ar} system. The pKM101 IMC contained TraA, TraB, TraC, TraD, TraE, and the N-terminal half of TraF (residues 1-193) while the VirB OMCC consisted of VirB7, VirB9, and the C-terminal half of VirB10 (residues 173-377). To ensure that the codon usage of *A. tumefaciens* didn't prevent optimal production of the VirB proteins, the *virB* genes were codon optimized for expression in *E. coli*. This chimeric Tra/VirB T4SS mediated transfer of the *oriT* plasmid pJG142, albeit at levels several orders of magnitude lower than observed for WT pKM101 (Figure 5.8). The Tra/VirB chimeric T4SS did not mediate PRD1 or IKe uptake, however, suggesting that these cells do not produce conjugative pili (Figure 5.8).

It is interesting that OMCCs from functionally distinct T4SSs can substitute for one another. We next wanted to test whether OMCCs from other T4SSs could substitute for that of pKM101. I first tested for functionality of a chimeric system composed of the OMCC from plasmid R388 and the IMC from pKM101. TraN and TraO were replaced with R388-encoded TrwH and TrwF, respectively. TraF was replaced with a TraF/TrwE chimera consisting of the N-terminal half of TraF (residues 1-193) and the C-terminal half of TrwE (residues 197-395). This chimeric T4SS mediated plasmid transfer at levels appreciably higher than observed for the Tra/VirB chimera (Figures 5.8). Similar to the Tra/VirB chimera, however, this machine did not mediate uptake of PRD1 and IKe, indicating a lack of pilus production.

I next tested whether a more phylogenetically and functionally distinct OMCC would functionally pair with the Tra IMC. For this, I made a chimeric Tra/Ptl T4SS. The Ptl T4SS is produced and utilized by *Bordetella pertussis* and is functionally unique in three ways. First, it does not contain a T4CP to recognize pertussis toxin subunits (5). Toxin subunits must go through the general secretory pathway prior to movement across the OM. Secondly, it does not

Figure 5.8 Functionality of chimeric T4SSs. (A) Genetic organization of the chimeric operons in mini-pKM101_{pBAD24}. (B) Bar diagram depicting the level of transfer of *oriT-IJK*_{pGB2} in donors containing either wild-type mini-pKM101_{pBAD24} or mini-pKM101_{pBAD24} encoding the chimeric T4SSs as well as the sensitivity to PRD1 and IKe. Mating frequencies are presented as transconjugants per donor and mating assays were repeated in triplicate the histogram represents the average of three experiments along with standard deviation. S:Sensitive, R:Resistant



contain a VirB5 or TraC homolog leading to an absence of detectable pili on the cell surface. Finally, it secretes pertussis toxin independently of recipient cell contact (165). TraN and TraO were replaced with PtlI and PtlF, respectively. TraF was substituted with a chimeric TraF/PtlG protein containing the N-terminal half of TraF (residues 1-172) and the C-terminal half of PtlG (residues 160-374). Similar to the *tra/virB* gene cluster, the *tra/ptl* gene cluster was codon optimized for expression in *E. coli*. The Tra/Ptl chimera mediated plasmid transfer at levels lower than the Tra/VirB, but above a threshold of detection. As with the other chimeras, the Tra/Ptl system did not mediate PRD1 or IKe uptake (Figure 5.8).

Together, these results support a proposal that the type IVa T4SSs are composed of functionally distinct IMC and OMCC subassemblies, and furthermore, that the OMCCs from different systems are highly conserved not only their overall architectures as shown by the structural studies (see Chapter 3), but also in their functions as structural scaffolds for the translocation channel. While all of the heterologous OMCCs were able to functionally pair with the pKM101 IMC, the more closely-related Trw OMCC paired in a more productive manner than its VirB and Ptl counterparts.

Neither the TraF AP nor the C-terminal tail are required for recipient cell contact

Pseudomonas aeruginosa contains a bactericidal type VI secretion system (T6SS), which is activated upon sensing membrane perturbation. When its membrane is perturbed through contacts by a neighboring cell, the *P. aeruginosa* T6SS is activated and in turn injects toxic effectors that kill the adjoining cell (13). The Mekalanos lab has previously demonstrated that *E. coli* containing a functional pKM101 T4SS are killed when incubated with *P. aeruginosa* containing a functional T6SS (140). This is likely due to mating junctions formed between *E.*

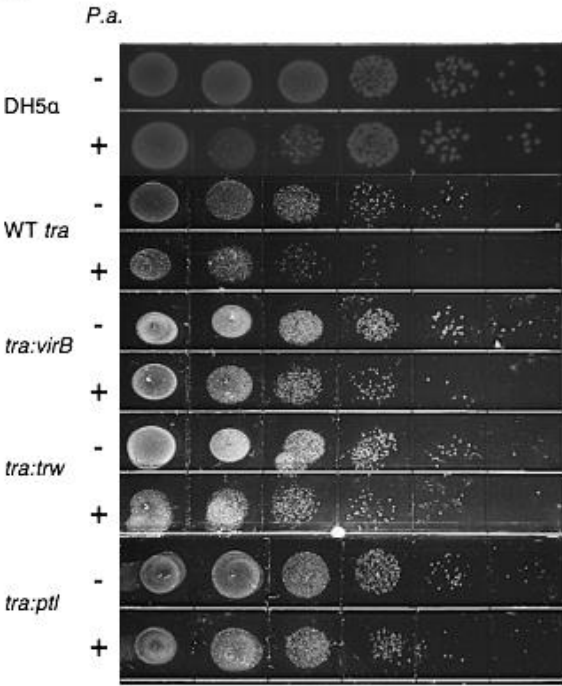
coli and *P. aeruginosa*. In recent years, the Christie lab has taken advantage of this in order to define the requirements for recipient cell contact. By measuring the sensitivity of *E. coli* containing pKM101 mutants to *P. aeruginosa*, we can further identify which steps in conjugation are blocked by various mutants.

I wanted to measure the sensitivity of *E. coli* containing the chimeric T4SSs to *P. aeruginosa* T6SS killing. Similar to previously described results, DH5 α without a T4SS was not susceptible to T6SS killing. The cell viability of DH5 α containing a wild-type pKM101 *tra* operon was reduced by ~ 10-fold (Figure 5.9). Cells containing the chimeric operons were also susceptible to T6SS killing, but at attenuated levels (Figure 5.9). These results demonstrate that the reduced levels of transfer are likely not due to the ability of these chimeric T4SSs to mediate recipient cell contact.

Utilizing the *P. aeruginosa* T6SS killing assay, I wanted to test my prediction about the importance of the TraF AP and C-terminal tail in establishing recipient cell contact. A series of alleles encoding the AP and C-terminal tail mutants were cloned in the native *traF* locus in mini-pKM101. Cells containing these plasmids were tested for their sensitivity to killing by *P. aeruginosa*. Wild-type *traF* cloned into its native locus restored sensitivity to ~10-fold (Figure 5.10). The TraF/TrwE_{AP-CT} mutant also gave similar levels of sensitivity as wild-type TraF. Surprisingly, the TraF _{Δ AP} also gave similar levels of sensitivity as wild-type TraF as well. These results indicate that the TraF AP is not necessary for establishing contact with recipient cells. TraF _{Δ RDLD} and TraF _{Δ CT9} also restored sensitivity, albeit at lower levels (Figure 5.10). The other AP-CT chimeras, TraF/VirB10 and TraF/PtlG, mediated sensitivity as well. Taken together, these results indicate that the AP and the C-terminal end of TraF are not essential for contacting recipient cells.

Figure 5.9 Measuring the ability of the chimeric T4SSs to make efficient recipient-cell contact. (A) Representative plate from the *P. aeruginosa* T6SS killing assay. (B) Quantification of the results in panel A. Results are presented in cell viability (CFU/ml). The *P. aeruginosa* T6SS killing assay was performed in triplicate and the histogram represents the average along with standard deviation. Statistical significance of the T6SS-mediated killing results was calculated using a Student's *t* test corresponding to plasmid-free *E. coli* cells (* $P < 0.05$, ** $P < 0.01$)

A



B

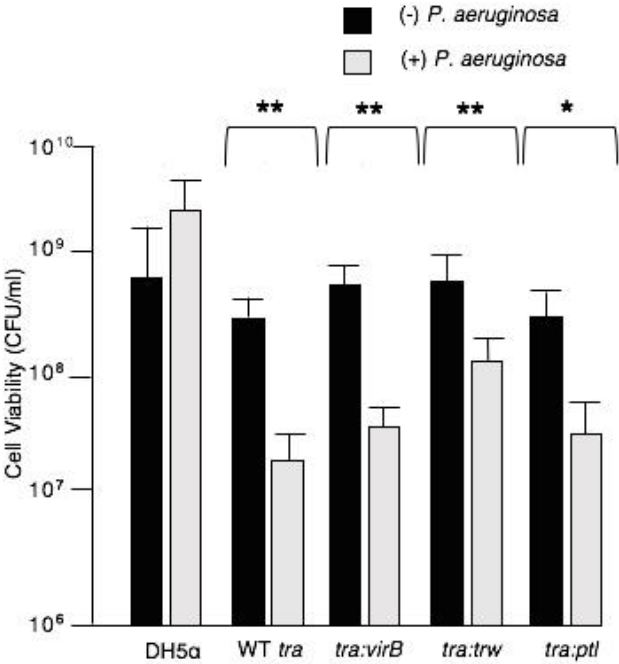
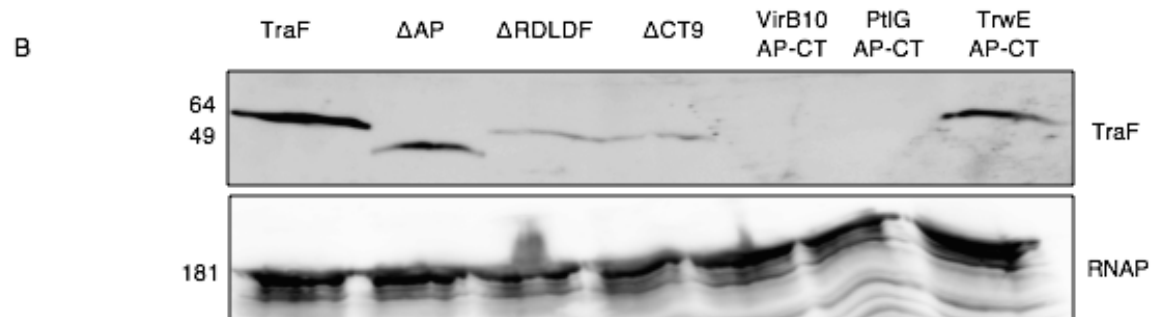
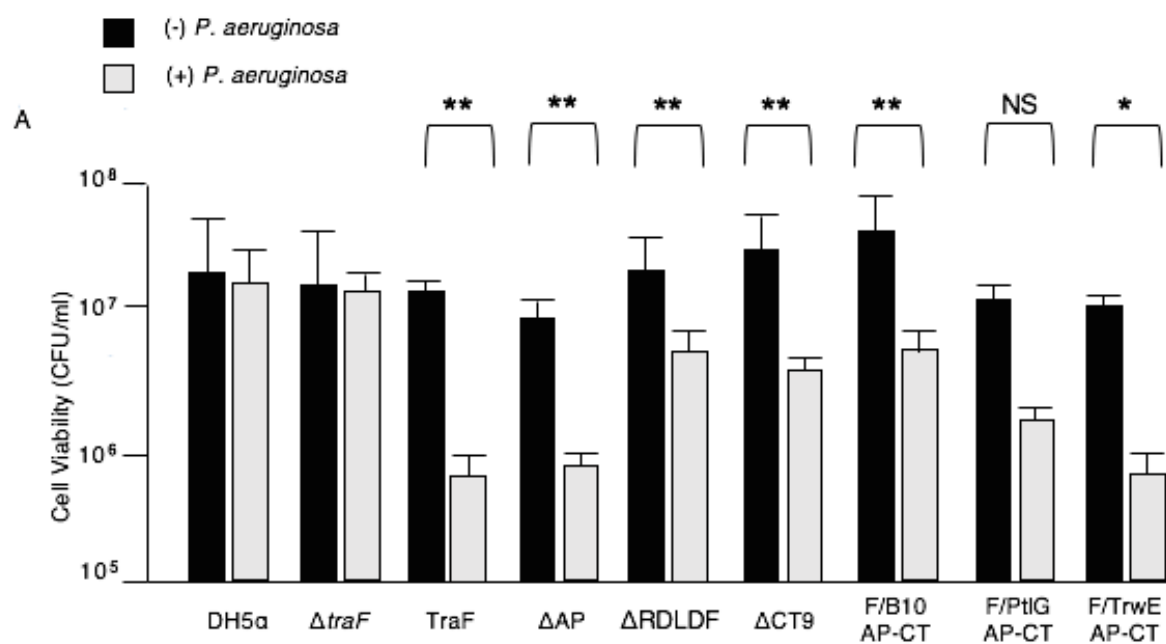


Figure 5.10 Determining the role of the TraF AP-CT in recipient cell contact (A)

Histogram depicting the sensitivity of either wild-type TraF or TraF AP-CT mutants when each of the alleles were cloned into the native *traF* locus on mini-pKM101. Results are presented in cell viability (CFU/ml). The *P. aeruginosa* T6SS killing assay was performed in triplicate and the histogram represents the average along with standard deviation. (B) Western blots of the WT TraF and AP-CT mutants when each *traF* allele is expressed from its native locus.

Statistical significance of the T6SS-mediated killing results was calculated using a Student's *t* test corresponding to plasmid-free *E. coli* cells (* $P < 0.05$, ** $P < 0.01$, NS: not significant)



Discussion

Bacteria containing a conjugative T4SS will utilize a conjugative pilus to attach to recipient cells prior to the formation of a stable mating junction. Once donor and recipient cells are in close contact, DNA will be transferred into the recipient cells. When I joined the Christie lab, one of my initial goals was to determine which regions of the OMCC were responsible for making direct contact with recipient cells. The crystal structure of the pKM101 OMCC O-layer highlighted a unique region of the VirB10 homolog, TraF, which seemed to project outwards towards the cell surface. I hypothesized that this region was critical for pilus biogenesis and recipient cell contact.

I began my investigation by making deletion mutations throughout the TraF and C-terminal tail in addition to TraF/VirB10 chimeras. Similar to the results seen with VirB10, the TraF AP helices are only required for building a cognate pilus. Additionally, I paired heterologous OMCCs from either VirB/VirD4_{Ti}, Trw_{R388}, or Ptl_{Bp} with the IMC of pKM101 and demonstrated that these chimeric T4SSs were capable of transferring DNA to recipient cells. These results highlight the plasticity of the Gram-negative bacterial T4SS and demonstrate that other factors besides OMCC-localized proteins play a significant role in recipient cell contact. Below, I will discuss my findings in more detail.

Contributions of the TraF AP to plasmid transfer and pilus biogenesis

The crystal structure of the pKM101 core complex features the TraF AP helices as a potential pore forming domain. However, my analysis of VirB10 suggested that the AP helices are not critical for substrate transfer. Based on these results, I predicted that deletion of the TraF AP helices (residues 302-353) would still allow for attenuated plasmid transfer. The TraF_{ΔAP}

mutant restored transfer to levels only 1,000-fold lower than wild-type TraF. Therefore, it is likely that the TraF AP is part of the OM pore, but is not essential for its formation.

Because the structure of the pKM101 core complex only highlights TraN, TraO, and TraF, it is likely that the OM pore contains other pKM101 components. As discussed in Chapter 3, pilus polymerization occurs either at an OM platform formed by the AP domain or at an IM platform within the channel. In both of these models, the pilus structure is protruding through the OMCC with assistance from the AP. Therefore, the conjugative pilus is likely the candidate pore-forming structure and the AP is solely involved in aiding the pilus outside of the OM efficiently.

Unlike plasmid transfer, the TraF AP is critical for pilus biogenesis. As mentioned above, TraM is likely in the core complex aiding substrates across the OM. However, the AP might make essential contacts with TraM subunits in the channel lumen and bring them to the surface. Additionally, our lab has observed TraC subunits secreted outside of the cell in the absence of the T4SS. In addition to formation of a pilus tip, TraC is also predicted to act as a pilus nucleation factor (discussed below). Therefore, the AP might also coordinate and localize extracellular TraC to the channel in order to trigger pilus biogenesis.

Contributions of the TraF C-terminal tail to plasmid transfer and pilus biogenesis

The crystal structure of TraF places the C-terminal tail (residues 354-386) inside the channel lumen buried within the β -barrel. The C-terminal tails of TraF and VirB10 share the highest region of identity between the two proteins (~71% identical) suggesting that this region has a conserved function. Deletion of the conserved RDLDF motif in VirB10 abolished T-DNA transfer and pilus biogenesis. My results demonstrated a similar phenomenon in TraF where

deletion of these residues abolished plasmid transfer and phage sensitivity. Therefore, this conserved sequence might be involved in pilus biogenesis through direct contact with pilin subunits and plasmid transfer through critical contacts with substrates such as the TraI relaxase.

Because of the high degree of homology between the TraF and VirB10 C-terminal tails, I predicted that the VirB10 C-terminal tail would functionally substitute for that of TraF. Although plasmid transfer was relatively unaffected, phage sensitivity was completely abolished. The C-terminal tail of VirB10 contains 11 extra residues. Therefore, it is likely that these mutants do produce pili, but the extra 11 residues from VirB10 interfere with phage infection. This prediction is based on other observations where a C-terminal FLAG tag on TraF does not abolish IKe sensitivity, indicating that the TraF C-terminal end can tolerate extensions and still support phage sensitivity.

While the C-terminal tail of TraF can handle the addition of epitope tags, it appears to be less tolerant to deletions. Deletion of the C-terminal residue, N386, abolished sensitivity to PRD1 and deletion of the C-terminal 9 residues abolished all phage sensitivity and plasmid transfer. Taken together, these results suggest that the length of the TraF C-terminal tail is critical for functionality. During plasmid transfer and pilus production, the C-terminal tail might be dynamic in that it might move inside and outside the OM as it shunts pilin subunits and substrates outside the cell. Therefore, the length of the TraF C-terminal tail would be critical for these steps. Unfortunately, I was unable to demonstrate surface display of TraF C-terminal tail. Other OM proteins or surface lipopolysaccharide might occlude this domain from various methods of detection. Future work in the Christie lab will focus on determining the spatial localization of the TraF C-terminal tail with respect to the OM.

The role of the TraF N-terminal half

Previous work from the Christie lab has highlighted the flexibility of the VirB10 N-terminal tail and TM domain. Insertions of Ala-Cys residues along the length of the VirB10 N-terminal tail and TM domain were phenotypically silent and replacement of the VirB10 TM domain with that of FtsN still allowed for T-DNA transfer (127,128). These results suggest that there are loose sequence requirements in the IMC. To examine whether N-terminal domains of VirB10 could be substituted for those in TraF, chimeric proteins were constructed. None of these chimeras were functional, however, suggesting that TraF's N-terminal domains might form specific contacts with subunits of the IMC. Future work in the Christie lab will focus on the use of unnatural amino acid-mediated photocrosslinking (discussed in Chapter 6) to determine the regions of contact between TraF and the TraJ T4CP.

Flexibility throughout Gram-negative bacterial T4SSs

While my experiments were the first to show sequence flexibility in the TraF and VirB10 family of proteins, other experiments have shown that a few other T4SS subunits can be functionally exchanged with homologs from other T4SS machines. Replacement of the periplasmic domain of *Brucella suis* VirB8 with that of the pSB102 VirB8 homolog, TraJ, partially restored the ability of *B. suis* to survive in macrophages (166). Additionally, previous work in the Christie lab has demonstrated that TraJ T4CPs containing the soluble domain of heterologous T4CPs are able to recognize and deliver heterologous substrates across the IM (29). Finally, with regards to pKM101, expression of either *traC*, *traL*, or *traD* was able to partially complement an *A. tumefaciens* $\Delta virB5$, $\Delta virB1$, or $\Delta virB6$ mutant respectively (87–89).

Together, these results highlight a common ancestry and most likely a common architecture for these T4SSs despite having diverse purposes.

Separation of the IMC from the OMC

Previous work from the Christie lab has suggested that the IMC is a functionally distinct subassembly from the OMC. When defining the pathway of T-DNA through the VirB_{At} T4SS, removal of VirB9, VirB10, or the VirB2 pilin subunit prevented movement of T-DNA across the OM, but did not affect contact with IM subunits VirB6 and VirB8 (74). Additionally, the R388 TrwM/VirB3-TrwE/VirB10 core structure revealed the presence of an IMC consisting of TrwM/VirB3, TrwK/VirB4, TrwJ/VirB5, TrwI/VirB6, and TrwG/VirB8 and an OMCC with TrwH/B7, TrwF/VirB9, and TrwE/VirB10 connected by a thin, central stalk (84).

These observations have lead to the “two-subassembly” model for building a T4SS where the IMC is responsible for recognition and delivery of substrates across the IM while the OMCC is responsible for translocation across the OM and recipient cell recognition. My data support this model. The sequence stringency at the IMC with regards to TraF appears to be stricter than in the OMCC indicating they contain different assembly requirements. Additionally, I was able to pair the pKM101 IMC with a heterologous OMCC, suggesting that these subassemblies are functionally different and are still able to interact in a productive manner. However, the OMCC does not appear to be responsible for contacting recipient cells as demonstrated by the Tra/Ptl T4SS. As *B. pertussis* secretes toxins into the extracellular milieu, the Ptl OMCC does not require the ability to contact recipient cells. Therefore, it is likely that other pKM101-encoded subunits other than the OMCC contribute to the formation of productive contacts with recipient cells.

Conclusions

Taken together, these results highlight the importance of the different domains within TraF with regards to plasmid transfer, phage sensitivity, and recipient-cell contact. In line with our initial prediction, the AP is not essential for forming the outer membrane pore, where as the C-terminal tail is critical for plasmid transfer and phage sensitivity. Despite being part of the OMCC, neither of these domains nor pilus is required for recipient-cell contact. Taking into account the data presented in this chapter, I am proposing the following unifying model for the role of the AP and C-terminal tail:

Model: In the absence of a recipient cell, the pKM101 T4SS exists as a “pilus machine” producing conjugative pili, which extend and slough into the extracellular environment. Once a target cell is contacted, the channel will switch from a pilus machine to a “substrate channel”. This switch is accompanied by the docking of the TraJ T4CP to the channel in addition to substrate processing and docking by the TraI relaxase. During pilus biogenesis, the AP and C-terminal tail are involved in producing an extracellular pilus by allowing the pilus to extend from the IM to the extracellular milieu. This region of TraF is involved in physical interactions with the growing pilus, which force it to the cell surface. As pilus structures are often sloughed off, the AP and C-terminal tail are likely candidate proteins for detaching the pilus from the cell surface.

Once the T4SS has switched to a substrate channel, TraJ will dock onto the IMC and will induce an ATPase-mediated conformational change in TraF upon substrate docking. TraF will then assist the pilus structure in pore formation. This conformational change is not critical for mating junction formation as a Δ AP mutation was still able to mediate efficient recipient cell contact as monitored by the T6SS killing assay. Substitution of the pKM101 OMCC for those of

VirB/VirD4_{Ti}, Trw_{R388}, or Ptl_{Bp} had little effect on recipient cell contact. This is surprising in light of the evidence to suggest that *B. pertussis* does not require recipient cell contact for Ptl-dependent toxin secretion. These data suggest that OMCC is not directly contacting recipient cells or the structural similarities between the Tra_{pKM101}, VirB/VirD4_{Ti} and Trw_{R388} with the Ptl_{Bp} allow for recipient contact, despite not being required for the formation of a mating junction.

Another protein predicted to be a central component during target cell contact is the surface protein KikA. Although not important for plasmid transfer on filters, our lab has recently established the importance of KikA in processes such as broth matings, the T6SS killing assay, and biofilm formation. C. Gonzalez-Rivera established that KikA produced in the absence of a T4SS is not sufficient to make contact with recipient *P. aeruginosa* cells. Therefore, I predict that the KikA is likely able to interact with all of these heterologous OMCCs in order to establish stable mating junctions. Current work in the Christie lab is focused on determining the role of KikA in building a functional T4SS.

Chapter 6: Summary and Future Directions

Summary

Gram-negative bacterial T4SSs contain separate IMCs and OMCCs responsible for recognizing and delivering substrates into the extracellular milieu or into target prokaryotic or eukaryotic cells. The goal of the work presented in this thesis was to develop the pKM101 molecular toolkit and define the role of the pKM101 OMCC in biologically relevant processes including plasmid transfer, pilus biogenesis, and recipient cell contact. When beginning my studies on the OMCC, I hypothesized that the AP and C-terminal tail were surface-localized domains that played a critical role in plasmid transfer through the formation of the OM pore, pilus biogenesis through direct contact with pilin subunits TraM and TraC, and recipient cell contact through target membrane perturbation.

In Chapter 3, I continued the analysis of the conserved GxxGxxG motif initiated by J. Kerr and demonstrated that each of the glycine residues is critical for T-DNA transfer as various mutations at each position attenuated tumor formation on plants. However, only G269 and G272 were critical for pilus biogenesis as G269R and G272R/W mutations abolished detectable levels of VirB2 on the cell surface. Although my mutational analyses did not uncover a mechanistic role of the GxxGxxG residues, my findings support the model that the distal end of the OMCC plays an important role especially for assembly of the T pilus.

Follow-up studies on the VirB10 AP cap began with creating a correct AP deletion. Previous deletions were based on the sequence alignment with the *H. pylori* ComB10 homolog and led to a partial AP deletion. This partial deletion of the VirB10 AP cap abolished detectable levels of pili as demonstrated by shearing assays. However, T-DNA transfer into plant cells was only partially attenuated. A full deletion based on the alignment with TraF phenocopied previous results demonstrating only a partial loss in T-DNA transfer and a full abolishment of

detectable VirB2 on the cell surface. Further mutagenesis involved insertion of large, 2x and 3x FLAG tags in the AP helices, none of which abolished T-DNA transfer or pilus biogenesis highlighting the importance for maintaining the AP domain, despite its ability to withstand large mutations. Finally, I tested for the functional conservation of the AP caps between VirB10 and TraF by substituting the AP of TraF on VirB10. This VirB10/TraF_{AP} chimera phenocopied WT VirB10, highlighting their functional similarity, despite a low level of sequence identity. Taken together with previous data from the Christie lab, the VirB10 AP cap is required to build a functional T-pilus, but dispensable for T-DNA transfer.

Chapter 4 focused on the development of our new pKM101 molecular toolkit now being used by the Christie lab to address important functional questions related to the T4SS structure. I, along with other members of our laboratory, created markerless deletions of each *tra* gene in the *traL-traG* (*virB1-virB11*) operon. We also constructed plasmids containing each of the *tra* genes cloned individually behind the tightly-regulated P_{BAD} promoter. In this study, I tested each of the cloned *tra* genes for the ability to complement its respective deletion for plasmid transfer and phage sensitivity. Similar lines of investigation have been performed in the VirB_{Ti}, Trw_{R388}, and Trb_{RP4}, and Tra_{pKM101}. Previous analyses of each of the conjugative plasmids have relied on the usage of transposon mutagenesis in each of the T4SS-encoding genes. Although it is simpler to utilize transposon mutagenesis on large, multicopy plasmids such as pKM101, these often impose polar effects on downstream genes. Therefore, these complementation experiments were critical for re-evaluation of the genetic requirements for plasmid transfer in addition to determining if we would be utilizing pKM101 as a model T4SS.

My initial deletion and complementation analysis showed that all of the *tra* genes except *traL* and *traC* are essential for substrate transfer. My results with the pKM101Δ*traC* mutant

were not surprising as Winans and Walker (153) previously showed that a *traC* transposon insertion mutation did not abolish pKM101 transfer. However, my results with the pKM101 Δ *traL* mutant differ from previous cell wall hydrolase deletion mutants. VirB1 and P19 do not contribute to the assembly of a functional VirB_{Ti} and Tra_F T4SS respectively, but removal of these proteins abolishes detectable levels of pili (67,157). Deletion of *traL* from pKM101 had no discernable effect on its ability to transfer plasmid pJG142 or mediate IKe uptake. Additionally, trans-expression of *traL* in a wild-type or a Δ *traL* background increased transfer by ~100-fold, raising the possibility that TraL is a rate-limiting factor for achieving wild-type levels of transfer.

In chapter 5, I utilized this new pKM101 molecular toolkit to continue my investigations into the role of the AP and C-terminal tail in plasmid transfer and pilus biogenesis. Truncations and internal deletions within these 86 residues identified the C-terminal tail as a critical factor in maintaining the functionality and stability of TraF. TraF mutants containing regions of the VirB10 AP and C-terminal tail restored plasmid transfer to a Δ *traF* mutant. Further substitutions along the length of the β -barrel identified a complex interplay in the periplasm critical for pilus production. In line with our initial hypothesis, the TraF AP is nonessential for plasmid transfer suggesting that other Tra OM subunits are responsible for forming the substrate pore.

In addition to the TraF AP cap region, Chapter 5 also highlighted the structural flexibility of the pKM101 T4SS through joining of the pKM101 IMC with the OMCCs of either VirB/VirD4_{At}, Trw_{R388}, and Ptl_{Bp}. I hypothesized that substitution of TraN and TraO for VirB7 and VirB9 respectively would increase the frequency of transfer through a channel containing the TraF/VirB10_{BB-CT} chimera. This chimera formed a functional translocation channel as monitored by pJG142 mobilization, though transfer frequencies were not elevated. Similar

results were seen with Tra/Trw and Tra/Ptl chimeric systems. None of these T4SSs were able to mediate sensitivity to PRD1 or IKE, suggesting that these cells lack conjugative pili. These data implicate stringent requirements at the OM for building a conjugative pilus.

With the use of T6SS killing assay, I was able to provide new insight into the role of the pKM101 OMC in mediating recipient cell contact. None of the TraF truncation mutants or AP/C-terminal tail chimeras reduced susceptibility to T6SS-mediated killing. These unexpected results demonstrate that these cells are able to mediate efficient contact with target cells, despite containing a non-functional TraF protein. I also tested my chimeric Tra/VirB, Tra/Trw and Tra/Ptl T4SSs in order to identify other OMCC components, which may play a role in recipient cell contact. All of these mutants made efficient contact, despite their reduced conjugation efficiency, highlighting the role of other pKM101-encoded surface components, such as KikA, in mediating the formation of mating junctions.

Remaining questions and future experiments

The data presented in this thesis has shed light on the role of the VirB and pKM101 OMCC with an emphasis on the OM cap region. However, many of the mechanisms that underlie these observations remain unclear. Below, I will address a subset of the questions that have been raised as a result of these data.

Do the TraF AP and C-terminal tail directly interact with pilin subunits TraM and TraC? In Chapters 3 and 5, I presented evidence to suggest that the AP and C-terminal tails of TraF and VirB10 are critical for pilus biogenesis. In order to gain a mechanistic insight into the role of the AP and C-terminal tail and the pilus biogenesis pathway, I along with other members of the Christie lab tested for interactions between TraF and TraC. C. Gonzalez-Rivera gained

evidence for a TraF-TraC interaction using BS³ crosslinking (Figure 6.1). However, these data do not present evidence for direct interactions.

I, along with other members of the Christie lab, have invested a large amount of time and effort into the development of unnatural amino acid-mediated photocrosslinking for detection of direct interactions between adjacent protein subunits. This technology has been utilized in the T2SS, T5SS, and the OM lipoprotein, RcsF, for detection of close interactions (164,167,168). For utilizing this technology, amber stop codons (TAG) are placed at a position in the allele of interest. This allele is co-transformed into the same strain as the plasmid pEVOL (151). The pEVOL plasmid contains the genes encoding a tRNA capable of recognizing the amber stop codon and an aminoacyl tRNA synthetase responsible for covalently linking the unnatural amino acid with the tRNA (Figure 6.2). The unnatural amino acid, p-benzoyl-L-phenylalanine (pBpa), is a phenylalanine derivative capable of crosslinking to any C-H bond within a 3Å distance (Figure 6.3).

During my initial attempts, I was able to demonstrate efficient incorporation of pBpa into 8 positions within the AP and C-terminal tail and one position in the periplasmic lever arm (Figures 6.4 and 6.5). Most pBpa-incorporated TraF proteins also displayed UV-dependent photocrosslinking as demonstrated by high-molecular weight bands in Figure 6.5. As only TraF was FLAG tagged at its C-terminal end, I combined cultures producing different pBpa incorporated TraF proteins followed by membrane isolation, solubilization, and anti-FLAG protein pulldowns (Figure 6.6). The combined sample was sent for protein identification using mass spectrometry. Unfortunately, I was not able to detect interactions with any pKM101-encoded Tra protein.

Figure 6.1 BS³ crosslinking of TraF and TraC. Alleles encoding C-terminally Strep-tagged TraC and N-terminally FLAG-tagged TraF were expressed in a mini-pKM101 pCGR108 backbone. Protein pulldowns were performed using α -Strep tag beads and elutions were run on SDS-PAGE gels followed by western blotting using α -Strep and α -FLAG antibodies to detect TraC and TraF respectively. These results were generated by Dr. Christian Gonzalez-Rivera. The structure of TraF was generated using Pymol (<http://pymol.org>) based on the 3ZBI file deposited into the NCBI protein database. The structure of TraC was generated using Pymol (<http://pymol.org>) based on the 1R8I file deposited into the NCBI protein database.

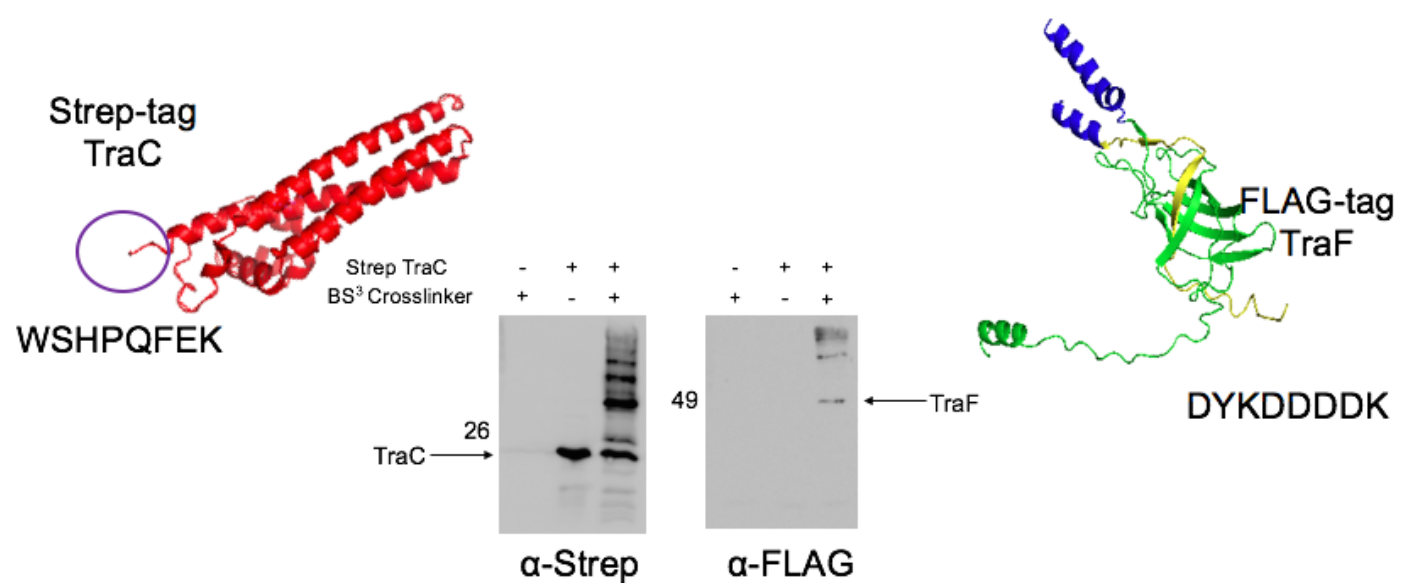


Figure 6.2 pBpa incorporation into TraF. (Left) Depiction of the pEVOL plasmid and pBAD24::*traF* plasmid. pEVOL contains genes encoding the tRNA responsible for recognizing amber stop codons and *aaRS* required for linking pBpa to the tRNA. pBAD24::*traF* contains a *traF* allele with an amber stop codon (indicated by a red circle). (Right) Once the tRNA is charged with the pBpa, it then recognizes the amber stop codon during translation and incorporates pBpa into the growing polypeptide chain.

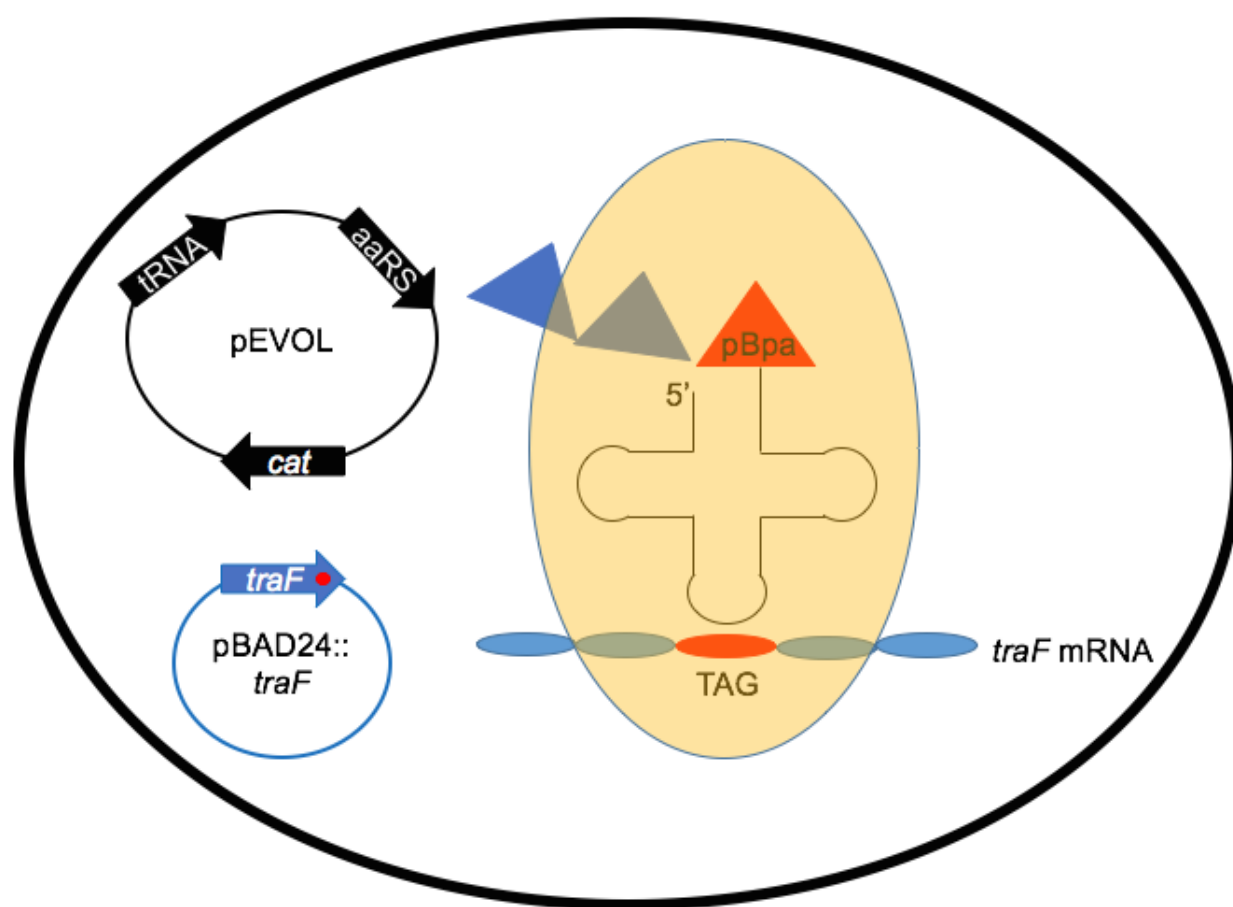


Figure 6.3 Mechanism of p-benzoyl-l-phenylalanine crosslinking. (Left) The structure of p-benzoyl-l-phenylalanine (pBpa). When exposed to UV light at 365nm, pBpa will crosslink to other proteins at a 3A distance. (Right) Once crosslinked, pBpa will form non-breakable covalent links which can be analyzed biochemically.

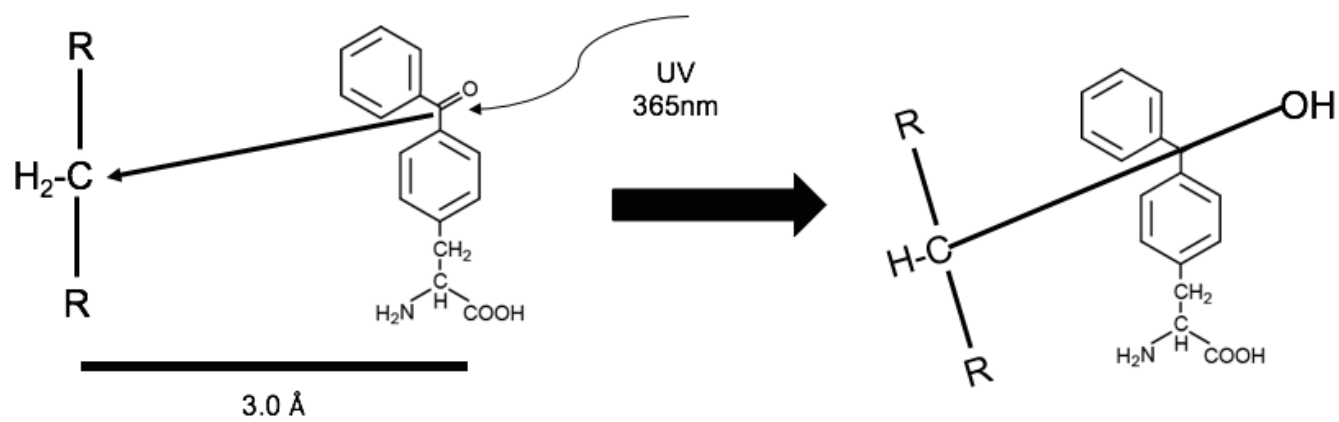


Figure 6.4 Locations of TraF pBpa incorporation. Crystal structure of the C-terminal half of TraF with pBpa positions highlighted. Positions include P185 (Lever arm), W304 and F316 (AP α 2 helix), N325 and Y334 (flexible loop), Q343 and Y352 (AP α 3 helix), F377 (conserved RDLDF motif), and N386 (C-terminal end). Each of these TraF mutants contains a C-terminal FLAG tag for protein enrichment and western blot detection. The structure of TraF was generated using Pymol (<http://pymol.org>) based on the 3ZBI file deposited into the NCBI protein database.

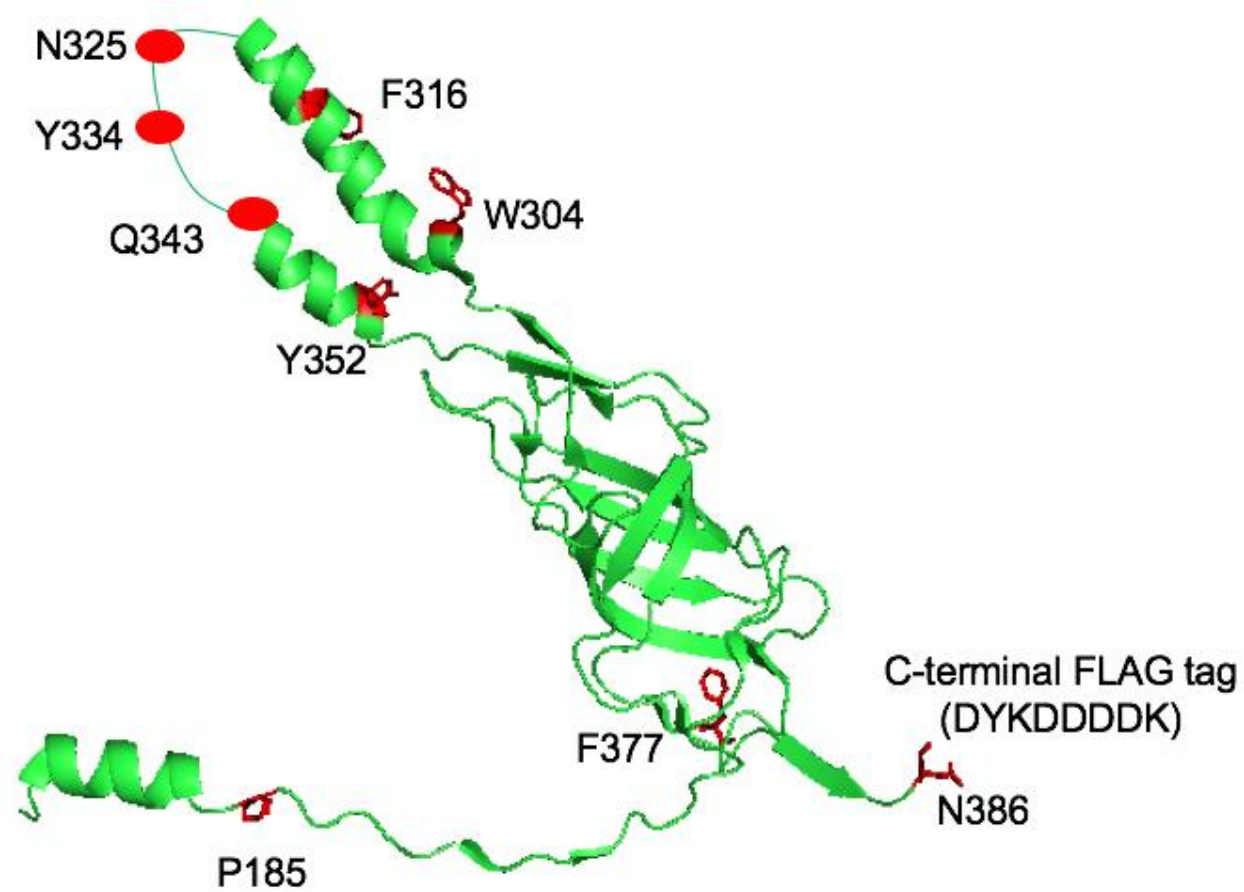


Figure 6.5 pBpa-mediated crosslinking of TraF. (Top) Steady state levels of TraF were observed when cells were grown in the presence versus absence of pBpa. TraF was detected with western blotting using α -FLAG antibodies. (Bottom) UV-mediated crosslinking of select TraF pBpa mutants. After pBpa incorporation and crosslinking, membranes were isolated and solubilized followed by purification with α -FLAG beads. Elutions from each sample were run on an SDS-PAGE gel followed by western blotting with α -FLAG antibodies.

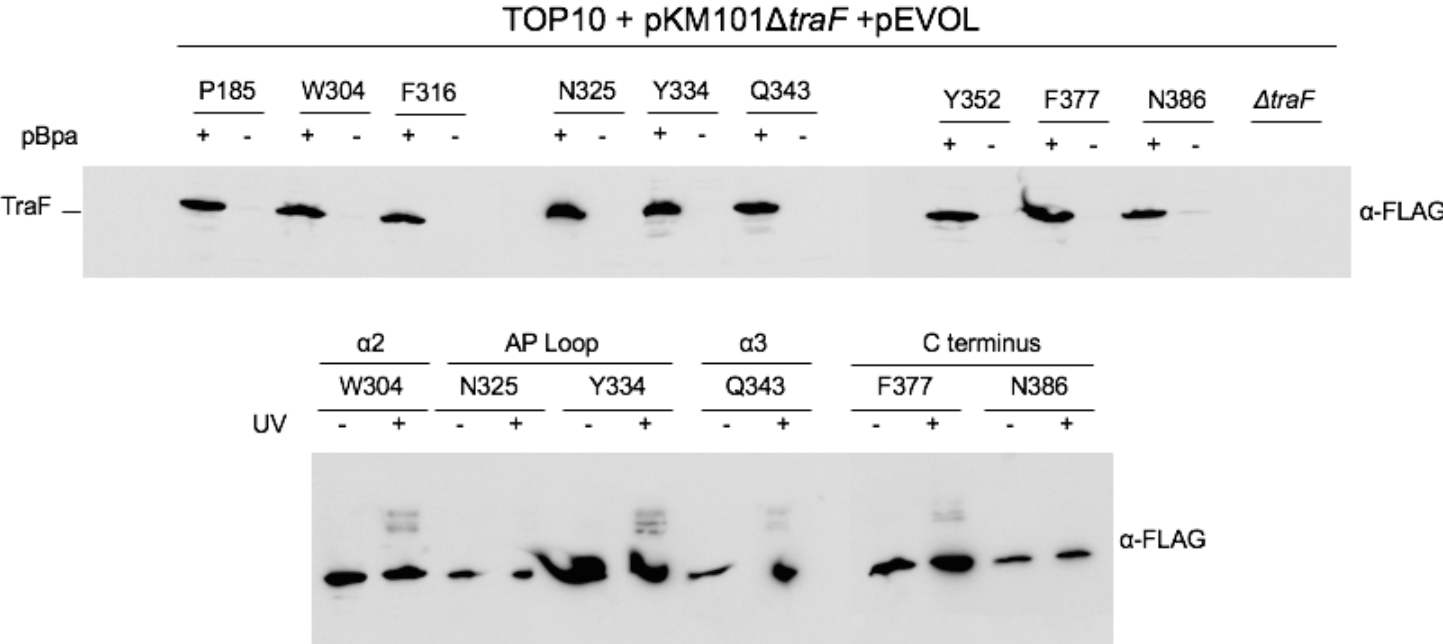
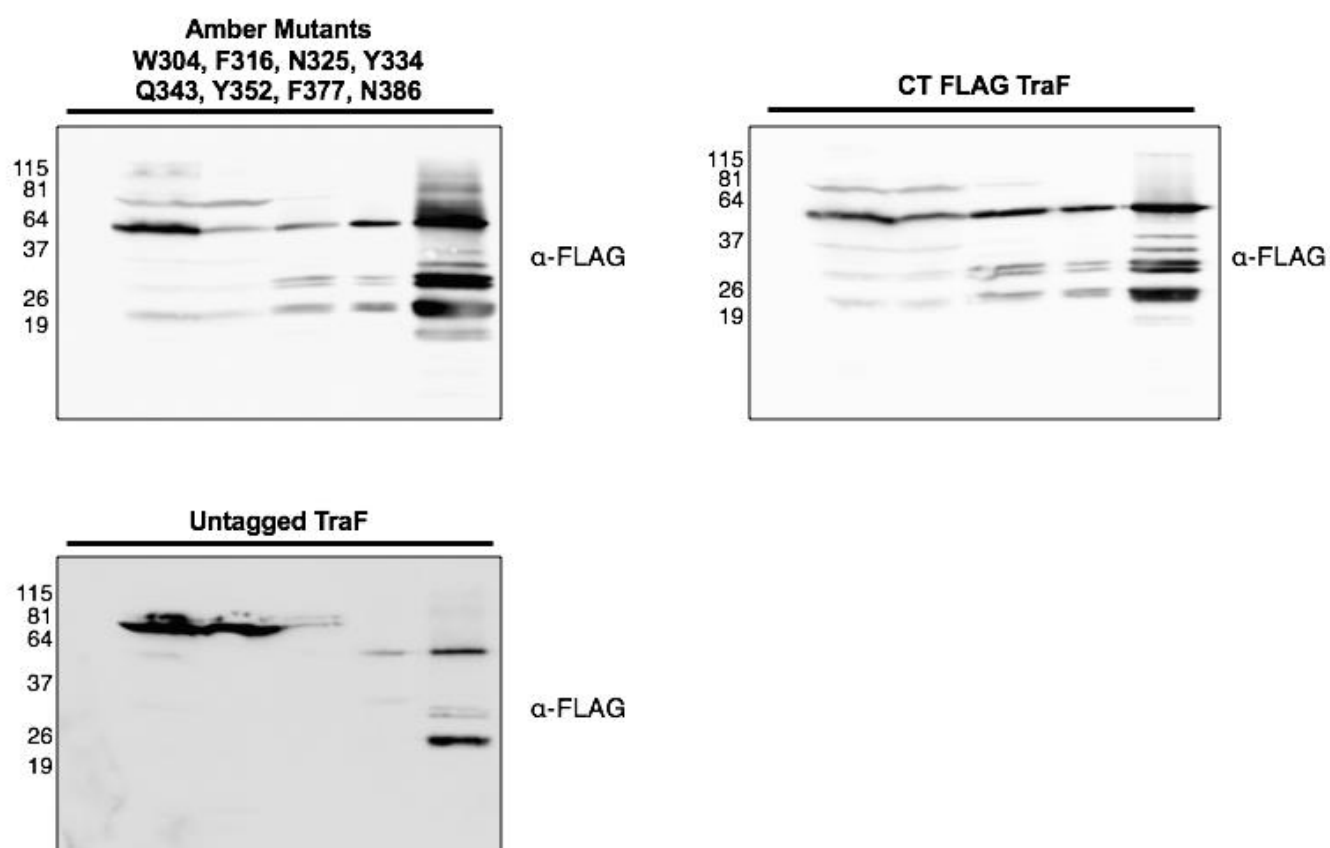


Figure 6.6 Sample preparation for mass spectrometry analysis. Three 1L cultures were grown and cells were incubated in the presence of 0.2% arabinose and 1mM pBpa followed by exposure to UV light. Following crosslinking TraF was enriched and sent for protein identification. The three samples analyzed were (1) All 8 AP/C-terminal pBpa, (2) C-terminally FLAG-tagged TraF, and (3) untagged TraF. From left to right, each gel contains the following lanes: (1) Whole cell lysate (2) Soluble fraction (3) Solubilized membrane fraction (4) Insoluble membrane fraction (5) Elution from α -FLAG magnetic beads. After washes, affinity beads were boiled for 5 minutes in Laemmli's buffer followed by separation of beads from the supernatant. TraF was detected by western blotting with α -FLAG antibodies. Elution samples were run on a separate SDS-PAGE gel, followed by extraction of the lane and mass spectrometry analysis.



Although not as versatile as pBpa-mediated photocrosslinking, Cys crosslinking provides an alternative route for detection of interactions between the TraF AP/C-terminal tail and pilin subunits. This method would rely on the insertion of Cys residues throughout the TraF AP/C-terminal tail, TraM, and TraC. Additionally, a crosslinking distance of 2Å or less is required for forming a detectable interaction. C. Gonzalez-Rivera and Maxim Bogisch, a former undergraduate student in the Christie lab, identified a close interaction between KikA and TraC using Cys residues placed in both proteins. These Cys mutants, along with Cys-substituted TraM, can be tested for interactions with Cys-substituted TraF.

What is the role of the conserved GxxGxxG sequence? Although a subset of mutations in the GxxGxxG sequence lead to reduced levels of T-DNA transfer and surface-displayed VirB2, there appeared to be a high degree of flexibility despite being conserved amongst all known VirB10 family of proteins. I hypothesized that these glycines allow for the structural flexibility required for substrates and pili to pass through. If this prediction is correct, there is likely close contacts being made between these glycine residues and substrates or pili. One approach to test this model involves the use of cysteine crosslinking. A G272C mutation still allowed for T-DNA transfer and detectable pilus biogenesis. Once a double *virB10/virB2* deletion is constructed on the Ti plasmid, the G272C *virB10* allele along with various other *virB2* Cys mutants can be co-expressed in the same cell and the mutant VirB10 and VirB2 proteins can be tested for close interactions through the formation of a disulfide bond. In addition to VirB2, Cys mutations can be constructed in substrates such as the VirD2 relaxase and VirE2. As these proteins are unfolded prior to translocation, Cys mutations at any location throughout the protein can be captured by Cys crosslinking provided that it creates close contact with the GxxGxxG sequence.

Due to the conservation of the GxxGxxG sequence in TraF, these experiments can also be performed using pKM101 through insertion of a Cys residue at G294 and throughout the length of TraI. Despite the recent utilization of pBpa-mediated photocrosslinking in the Christie lab, Cys crosslinking remains the ideal methodology for two reasons: (i) the crosslinking distance for Cys crosslinking is shorter (2Å) than the distance for pBpa crosslinking (3Å) and (ii) insertion of bulky aromatic residues at this location is less desirable than Cys residues (Figure 3.3).

How can phage sensitivity be restored to pKM101 deletion mutants? Previous studies on the VirB/VirD4_{At} and Trb_{RP4} T4SSs demonstrated a restoration of pilus biogenesis when deletion mutants were complemented with their respective gene *in trans*. This is not the case with our collection of pKM101*tra* deletion mutants as only $\Delta traM$, $\Delta traF$, and $\Delta traG$ mutants developed phage sensitivity when the native gene was expressed *in trans*. These results are peculiar as all of the complemented *tra* mutants had plasmid transfer restored, indicating the presence of a functional T4SS. I predicted that overproduction of these proteins interferes with the ability of IKE to interact with the TolQRA proteins in the IM, which are essential for infection (160). If Tra proteins are interfering with IKE's ability to interact with TolQRA, then overproduction of these proteins should allow for a restoration of phage sensitivity if the cells produce a conjugative pilus. These experiments would force us to reconsider our conclusions with regards to restoration of pilus biogenesis.

What is the composition of the OM pore? Based on the crystal structure of the pKM101 OMC, I predicted that the TraF AP helices are the primary factors involved in pore formation. Contrary to this prediction, deletions of the AP helices in both VirB10 and TraF only had a modest effect on DNA transfer. These experiments still have yet to identify the major

components of the OM pore. Possibilities include the other OMCC proteins, TraN/VirB7 and TraO/VirB9, or the pilin subunit, VirB2.

Gram-negative bacteria are normally resistant to the antibiotic vancomycin as it is not able to penetrate the OM. However, *A. tumefaciens* containing a viable T4SS has been demonstrated to uptake vancomycin due to the presence of an OM pore which allows the antibiotic to cross into the periplasm (125). Therefore, testing deletion mutants of *traO*, *traN*, and *traM* in a strain with wild-type TraF and TraF_{ΔAP} mutant should provide insight as to which proteins form the pore.

Are the IMC and OMC subassemblies functionally independent? The structure of the R388 TrwM/VirB3-TrwE/VirB10 structure highlights the unique structural composition of the IMC and OMCC assemblies. As mentioned earlier, work from E. Cascales demonstrated that OMCC subunits VirB9 and VirB10 are not essential for T-DNA interactions with IMC subunits (74). These data raise the interesting possibility of the IMC and OMCC functioning independently of one another. If these subassemblies are functionally separate, then secretion of substrates through the T4SS likely resembles the pathway of substrates through the T2SS in that they are first translocated to the periplasm followed by T4SS-dependent delivery past the OM (7). My experiments with the chimeric Tra/VirB, Tra/Trw, and Tra/Ptl T4SS support this model as each of these compositionally unique systems was able to efficiently contact target cells and deliver the pJG142 plasmid. I was not able to increase the frequency of transfer of the TraFVirB10_{BB-CT} and TraF/TrwE_{BB-CT} chimeras (10^{-6} and 10^{-2} transconjugants per donor respectively) through the assembly of the cognate OMCC as essential interactions with the IMC subunits were likely not present.

Although not discussed in this thesis, I also attempted to address this model through the use of chimeric T4CPs at the IMC. T. Berry demonstrated that chimeric TraJ proteins containing the native N-terminal TM domain and a heterologous soluble domain were able to mediate transfer of heterologous substrates through the pKM101 T4SS (29). It was demonstrated around this time that the VirB T4SS from the phytopathogen *Xanthomonas citri* is able to mediate the transfer of the toxic cell wall hydrolase Xac2609 to target *E. coli* cells (169). When *E. coli* cells containing pKM101 Δ traJ along with plasmids encoding TraJ/VirD4_{Xac}_SD, and Xac2609 were incubated with *E. coli* target cells, the donor cells were killed in a manner that was dependent on the presence of the T4SS, the chimeric T4CP, and the Xac2609 substrate (Figures 6.7 and 6.8). Production of the Xac2610 anti-toxin protein rescued these cells (Figure 6.8). These results suggest that Xac2609 is delivered into the periplasm in a manner that is dependent of the T4CP and T4SS, supporting a two-step translocation and two subassembly model for T4SSs.

In order to test for the functional independence of the IMC, our lab has expressed interest in creating an independent IMC through removal of VirB7, VirB9, and VirB10. To set up a strict screening process, the N terminus of TraI can be fused to beta lactamase and cells containing the IMC can be tested for growth in the presence of beta lactam antibiotics. A similar screening process can be set up with a PhoA-TraI fusion to test for periplasmic transfer.

Which pKM101-encoded proteins are responsible for recipient cell contact? My results with the T6SS killing assay highlight the dispensability of the TraF AP and C-terminal tail for contacting target cells. Therefore, there are other pKM101-encoded factors which perturb the target cell membrane. Recently, the Christie lab has focused on the role of the KikA surface protein. C. Gonzalez-Rivera demonstrated that addition of a plasmid encoding KikA

Figure 6.7 Schematic of TraJ/VirD4_{Xac} periplasmic translocation assay. Depiction of the chimeric T4CP containing the N-terminal TM domain of TraJ and the soluble domain of VirD4 from the bactericidal T4SS from *Xanthomonas citri*. Through recognition of the Xac2609 signal sequence (XacSig), this substrate should be delivered into the periplasm. This assay can be used to further test the genetic requirements for periplasmic translocation of T4SS substrates. The structure of TrwB is Figure 2C from Gomis-Rüth FX et al. *The bacterial conjugation protein TrwB resembles ring helicases and F1-ATPase*. Nature 2001 409:637–41. This image was re-published with permission from Nature Publishing Group. License Number 4078401439237.

TraJ Transmembrane Domain

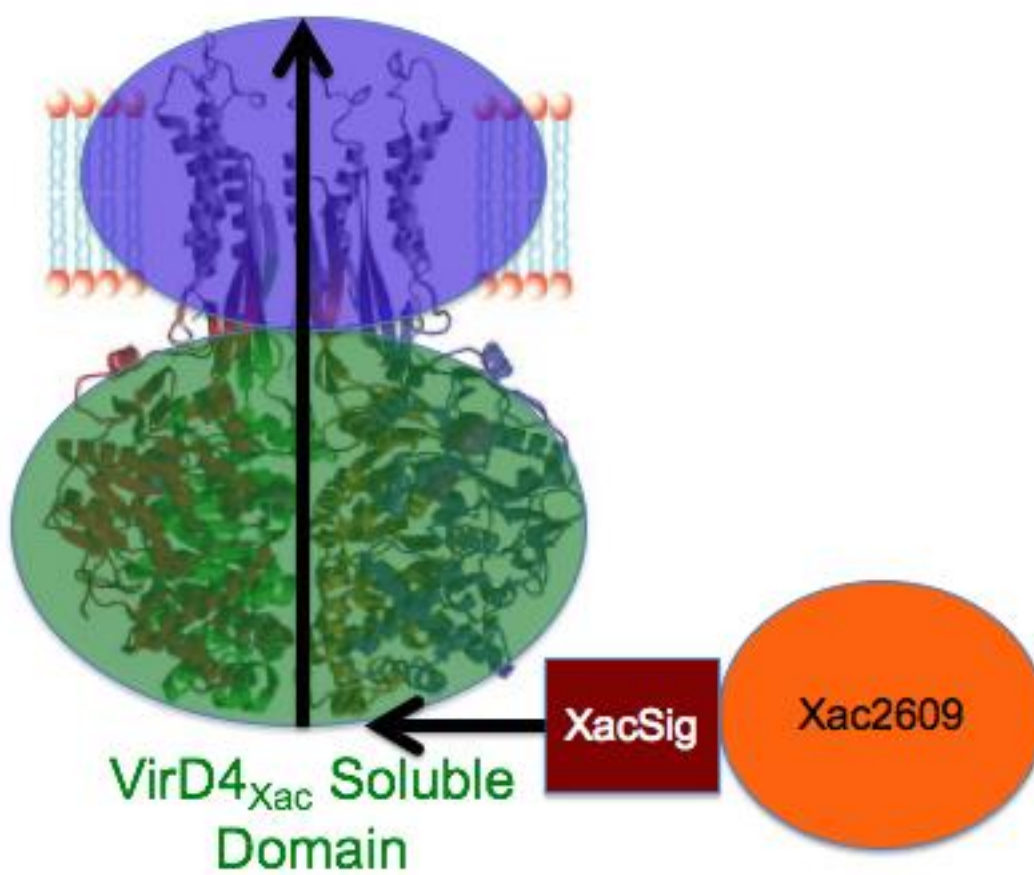
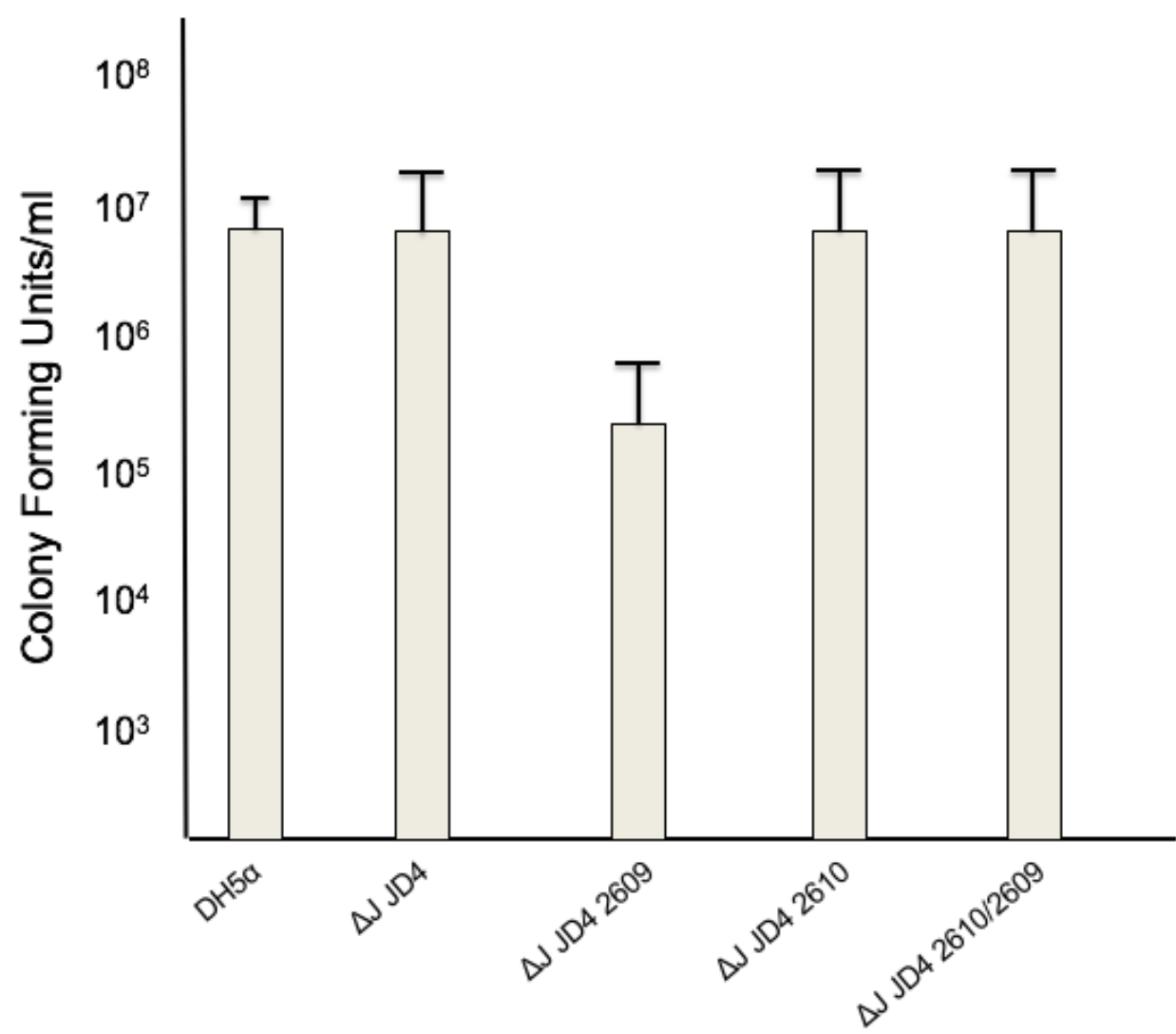


Figure 6.8 Xac2609 kills donor cells in a manner dependent on the presence of a functional T4SS.

Histogram depicting the results of donor killing assays. Cell viability was decreased in the presence of the TraJ/VirD4_{Xac} T4CP and the pKM101 T4SS as well as when Xac2610 is co-produced. Key: ΔJ: Native pKM101 containing a markerless deletion of *traJ*. JD4: The TraJ/VirD4_{Xac} chimeric T4CP.

While missing from the figure, expression of Xac2609 and JD4 individually did not lead to a decrease in cell viability.



restored the ability of cells containing mini-pKM101 plasmid pCGR108 to uptake PRD1, transfer pJG142 in broth and be killed by the *P. aeruginosa* H1 T6SS. KikA also interacts with the TraC pilus tip protein, suggesting that it could play a role in pilus extension. As KikA is localized to the cell surface, it is likely that KikA makes initial contact with target cells prior to translocation. In a manner similar to that observed in *Myxococcus xanthus*, one model suggests that KikA promotes membrane fusion with the recipient cell prior to DNA transfer (170). In order to test this hypothesis, donor and recipient cells would be labeled with different fluorescent lipids and membrane exchange could be examined using fluorescence microscopy in the presence and absence of donor-produced KikA.

Conclusion

During my time in the Christie lab, I significantly contributed to the development of the pKM101 model T4SS which our lab is currently using and continued previous lines of investigation into the role of the OMCC in both the VirB and pKM101 systems. My work has demonstrated that the OMCC is a functionally distinct subassembly from the IMC and this complex is primarily involved in pilus formation. This pilus, while not essential for recipient cell contact or plasmid transfer on filters, appears to be important for broth matings, highlighting its role in bringing recipient cells into close contact. Future directions in the Christie lab will focus on the contacts made along the length of TraF and how these contacts differ in pilus T4SSs versus substrate T4SSs.

References

1. Terradot L, Waksman G. Architecture of the *Helicobacter pylori* Cag-type IV secretion system. FEBS J. 2011 278:1213–22.
2. Segal G, Feldman M, Zusman T. The Icm/Dot type-IV secretion systems of *Legionella pneumophila* and *Coxiella burnetii*. FEMS Microbiol. Rev. 2005 29:65–81.
3. Kubori T, Nagai H. The Type IVB secretion system: an enigmatic chimera. Curr. Opin. Microbiol. 2016 29:22–9.
4. Shrivastava R, Miller JF. Virulence factor secretion and translocation by *Bordetella* species. Curr. Opin. Microbiol. 2009 12:88–93.
5. Alvarez-Martinez CE, Christie PJ. Biological diversity of prokaryotic type IV secretion systems. Microbiol. Mol. Biol. Rev. 2009 73:775–808.
6. Green ER, Mecsas J. Bacterial Secretion Systems: An Overview. Microbiol. Spectrum 4(1):VMBF-0012-2015.
7. Costa TRD, Felisberto-Rodrigues C, Meir A, Prevost MS, Redzej A, Trokter M, Waksman, G. Secretion systems in Gram-negative bacteria: structural and mechanistic insights. Nat. Rev. Microbiol. 2015 13:343–59.
8. Nivaskumar M, Francetic O. Type II secretion system: a magic beanstalk or a protein escalator. Biochim. Biophys. Acta. 2014 1843:1568–77.
9. Notti RQ, Stebbins CE. The structure and function of type III secretion systems. Microbiol. Spectrum 4(1):VMBF-0004- 2015.
10. Fan E, Chauhan N, Udatha DBRKG, Leo JC, Linke D. Type V secretion systems in bacteria. Microbiol. Spectr. 4(1): VMBF-0009-2015
11. Foegeding NJ, Caston RR, McClain MS, Ohi MD, Cover TL. An Overview of *Helicobacter pylori* VacA Toxin Biology. *Toxins* 2016, 8, 173.
12. González-Rivera C, Algood HMS, Radin JN, McClain MS, Cover TL. The intermediate region of *Helicobacter pylori* VacA is a determinant of toxin potency in a Jurkat T cell assay. Infect. Immun. 2012 80:2578–88.
13. Ho BT, Dong TG, Mekalanos JJ. A view to a kill: the bacterial type VI secretion system. Cell Host Microbe 2014 15:9–21.
14. Durand E, Nguyen VS, Zoued A, Logger L, Péhau-Arnaudet G, Aschtgen MS, Spinelli S, Desmyter A, Bardiaux B, Dujancourt A, Roussel A, Cambillau C, Cascales E, Fronzes R. Biogenesis and structure of a type VI secretion membrane core complex. Nature 2015 523:555–60.

15. Fernandez-Gonzalez E, Backert S. DNA transfer in the gastric pathogen *Helicobacter pylori*. J. Gastroenterol. 2014 49:594–604.
16. Binns AN, Beaupré CE, Dale EM. Inhibition of VirB-mediated transfer of diverse substrates from *Agrobacterium tumefaciens* by the IncQ plasmid RSF1010. J. Bacteriol. 1995 177:4890–9.
17. Vogel JP, Andrews HL, Wong SK, Isberg RR. Conjugative transfer by the virulence system of *Legionella pneumophila*. Science 1998 279:873–6.
18. Yang F, Merlo DJ, Gordon MP, Nester EW. Plasmid DNA of *Agrobacterium tumefaciens* detected in a presumed habituated tobacco cell line. Mol. Gen. Genet. 1980 179:223–6.
19. McPherson JC, Nester EW, Gordon MP. Proteins encoded by *Agrobacterium tumefaciens* Ti plasmid DNA (T-DNA) in crown gall tumors. Proc. Natl. Acad. Sci. U.S.A. 1980 77:2666–70.
20. Bohne J, Yim A, Binns AN. The Ti plasmid increases the efficiency of *Agrobacterium tumefaciens* as a recipient in virB-mediated conjugal transfer of an IncQ plasmid. Proc. Natl. Acad. Sci. U.S.A. 1998 95:7057–62.
21. Liu Z, Binns AN. Functional subsets of the virB type IV transport complex proteins involved in the capacity of *Agrobacterium tumefaciens* to serve as a recipient in virB-mediated conjugal transfer of plasmid RSF1010. J. Bacteriol. 2003 185:3259–69.
22. Zechner EL, Lang S, Schildbach JF. Assembly and mechanisms of bacterial type IV secretion machines. Philos. Trans. R. Soc. Lond. B Biol. Sci. 2012 367:1073–87.
23. Christie PJ, Whitaker N, González-Rivera C. Mechanism and structure of the bacterial type IV secretion systems. Biochim. Biophys. Acta. 2014 1843:1578–91.
24. Gonzalez-Rivera C, Bhatti M, Christie PJ. Mechanism and function of type IV secretion during infection of the human host. Microbiol. Spectrum 4(3):VMBF-0024-2015.
25. Backert S, Neddermann M, Maubach G, Naumann M. Pathogenesis of *Helicobacter pylori* infection. Helicobacter 2016 21:19–25.
26. Nagai H, Roy CR. The DotA protein from *Legionella pneumophila* is secreted by a novel process that requires the Dot/Icm transporter. EMBO J. 2001 20:5962–70.
27. Roy CR, Berger KH, Isberg RR. *Legionella pneumophila* DotA protein is required for early phagosome trafficking decisions that occur within minutes of bacterial uptake. Mol. Microbiol. 1998 28:663–74.
28. Alix E, Chesnel L, Bowzard BJ, Tucker AM, Delprato A, Cherfils J, Wood D, Kahn R, Roy C. The capping domain in RalF regulates effector functions. PLoS Pathog. 2012 8:e1003012.

29. Whitaker N, Berry TM, Rosenthal N, Gordon JE, Gonzalez-Rivera C, Sheehan KB, Truchan H, Newton I, Carlyon J, Christie P. Chimeric Coupling Proteins Mediate Transfer of Heterologous Type IV Effectors through the *Escherichia coli* pKM101-Encoded Conjugation Machine. *J. Bacteriol.* 2016 198:2701–18.
30. Lockwood S, Voth DE, Brayton KA, Beare PA, Brown WC, Heinzen RA, Broschat, S. Identification of *Anaplasma marginale* type IV secretion system effector proteins. *PLoS One* 2011 6:e27724.
31. Gillespie JJ, Phan IQH, Driscoll TP, Guillotte ML, Lehman SS, Rennoll-Bankert KE, Subramanian S, Beier-Sexton M, Myler P, Rahman S, Azad A. The Rickettsia type IV secretion system: unrealized complexity mired by gene family expansion. *Pathog. Dis.* 2016 74 (6).
32. Cheung AM, Farizo KM, Burns DL. Analysis of relative levels of production of pertussis toxin subunits and Ptl proteins in *Bordetella pertussis*. *Infect. Immun.* 2004 72:2057–66.
33. Craig-Mylius KA, Weiss AA. Mutants in the *ptlA-H* genes of *Bordetella pertussis* are deficient for pertussis toxin secretion. *FEMS Microbiol. Lett.* 1999 179:479–84.
34. Hausman SZ, Cherry JD, Heininger U, Wirsing von König CH, Burns DL. Analysis of proteins encoded by the *ptx* and *ptl* genes of *Bordetella bronchiseptica* and *Bordetella parapertussis*. *Infect. Immun.* 1996 64:4020–6.
35. Kotob SI, Hausman SZ, Burns DL. Localization of the promoter for the *ptl* genes of *Bordetella pertussis*, which encode proteins essential for secretion of pertussis toxin. *Infect. Immun.* 1995 63:3227–30.
36. Ricci S, Rappuoli R, Scarlato V. The pertussis toxin liberation genes of *Bordetella pertussis* are transcriptionally linked to the pertussis toxin operon. *Infect. Immun.* 1996 64:1458–60.
37. Hamilton HL, Dillard JP. Natural transformation of *Neisseria gonorrhoeae*: from DNA donation to homologous recombination. *Mol. Microbiol.* 2006 59:376–85.
38. Pachulec E, Siewering K, Bender T, Heller E-M, Salgado-Pabon W, Schmoller SK, Woodhams K, Dillard J, van der Does C. Functional analysis of the Gonococcal Genetic Island of *Neisseria gonorrhoeae*. *PLoS One* 2014 9:e109613.
39. Atmakuri K, Cascales E, Burton OT, Banta LM, Christie PJ. *Agrobacterium* ParA/MinD-like VirC1 spatially coordinates early conjugative DNA transfer reactions. *EMBO J.* 2007 26:2540–51.
40. Mierzejewska J, Jagura-Burdzy G. Prokaryotic ParA-ParB-parS system links bacterial chromosome segregation with the cell cycle. *Plasmid* 2012 67:1–14.
41. Toro N, Datta A, Yanofsky M, Nester E. Role of the *overdrive* sequence in T-DNA border cleavage in *Agrobacterium*. *Proc. Natl. Acad. Sci. U.S.A.* 1988 85:8558–62.

42. Toro N, Datta A, Carmi OA, Young C, Prusti RK, Nester EW. The *Agrobacterium tumefaciens* *virC1* gene product binds to *overdrive*, a T-DNA transfer enhancer. J. Bacteriol. 1989 171:6845–9.
43. Mysore KS, Bassuner B, Deng XB, Darbinian NS, Motchoulski A, Ream W, Gelvin S. Role of the *Agrobacterium tumefaciens* VirD2 protein in T-DNA transfer and integration. Mol. Plant-Microbe Interact. 1998 11:668–83.
44. Meyer R. Replication and conjugative mobilization of broad host-range IncQ plasmids. Plasmid 2009 62:57–70.
45. Haase J, Lurz R, Grahn AM, Bamford DH, Lanka E. Bacterial conjugation mediated by plasmid RP4: RSF1010 mobilization, donor-specific phage propagation, and pilus production require the same Tra2 core components of a proposed DNA transport complex. J. Bacteriol. 1995 177:4779–91.
46. Hamilton CM, Lee H, Li PL, Cook DM, Piper KR, von Bodman SB, Lanka E, Ream W, Farrand S. TraG from RP4 and TraG and VirD4 from Ti plasmids confer relaxosome specificity to the conjugal transfer system of pTiC58. J. Bacteriol. 2000 182:1541–8.
47. Lessl M, Balzer D, Weyrauch K, Lanka E. The mating pair formation system of plasmid RP4 defined by RSF1010 mobilization and donor-specific phage propagation. J. Bacteriol. 1993 175:6415–25.
48. Lessl M, Balzer D, Lurz R, Waters VL, Guiney DG, Lanka E. Dissection of IncP conjugative plasmid transfer: definition of the transfer region Tra2 by mobilization of the Tra1 region in trans. J. Bacteriol. 1992 174:2493–500.
49. Christie PJ, Gordon JE. The *Agrobacterium* Ti plasmids. Microbiol. Spectrum 2014 2(6):PLAS-0010-2013
50. Atmakuri K, Ding Z, Christie PJ. VirE2, a type IV secretion substrate, interacts with the VirD4 transfer protein at cell poles of *Agrobacterium tumefaciens*. Mol. Microbiol. 2003 49:1699–713.
51. Christie PJ, Ward JE, Winans SC, Nester EW. The *Agrobacterium tumefaciens* *virE2* gene product is a single-stranded-DNA-binding protein that associates with T-DNA. J. Bacteriol. 1988 170:2659–67.
52. Frenkiel-Krispin D, Wolf SG, Albeck S, Unger T, Peleg Y, Jacobovitch J, Michael Y, Daube S, Sharon M, Robinson C, Svergun D, Fass D, Tzfira T, Elbaum M. Plant transformation by *Agrobacterium tumefaciens*: modulation of single-stranded DNA-VirE2 complex assembly by VirE1. J. Biol. Chem. 2007 282:3458–64.
53. García-Rodríguez FM, Schrammeijer B, Hooykaas PJJ. The *Agrobacterium* VirE3 effector protein: a potential plant transcriptional activator. Nucleic Acids Res. 2006 34:6496–504.

54. Lacroix B, Vaidya M, Tzfira T, Citovsky V. The VirE3 protein of *Agrobacterium* mimics a host cell function required for plant genetic transformation. *EMBO J.* 2005 24:428–37.
55. Lacroix B, Citovsky V. Nopaline-type Ti plasmid of *Agrobacterium* encodes a VirF-like functional F-box protein. *Sci. Rep.* 2015 5:16610.
56. Schrammeijer B, Risseuw E, Pansegrau W, Regensburg-Tuink TJ, Crosby WL, Hooykaas PJ. Interaction of the virulence protein VirF of *Agrobacterium tumefaciens* with plant homologs of the yeast Skp1 protein. *Curr. Biol. CB.* 2001 11:258–62.
57. Schrammeijer B, Hemelaar J, Hooykaas PJ. The presence and characterization of a *virF* gene on *Agrobacterium vitis* Ti plasmids. *Mol. Plant-Microbe Interact.* 1998 11:429–33.
58. Alt-Mörbe J, Stryker JL, Fuqua C, Li PL, Farrand SK, Winans SC. The conjugal transfer system of *Agrobacterium tumefaciens* octopine-type Ti plasmids is closely related to the transfer system of an IncP plasmid and distantly related to Ti plasmid *vir* genes. *J. Bacteriol.* 1996 178:4248–57.
59. Das A, Xie YH. The *Agrobacterium* T-DNA transport pore proteins VirB8, VirB9, and VirB10 interact with one another. *J. Bacteriol.* 2000 182:758–63.
60. Kumar RB, Das A. Functional analysis of the *Agrobacterium tumefaciens* T-DNA transport pore protein VirB8. *J. Bacteriol.* 2001 183:3636–41.
61. Kumar RB, Xie YH, Das A. Subcellular localization of the *Agrobacterium tumefaciens* T-DNA transport pore proteins: VirB8 is essential for the assembly of the transport pore. *Mol. Microbiol.* 2000 36:608–17.
62. Yuan Q, Carle A, Gao C, Sivanesan D, Aly KA, Höppner C, Krall L, Domke N, Baron C. Identification of the VirB4-VirB8-VirB5-VirB2 pilus assembly sequence of type IV secretion systems. *J. Biol. Chem.* 2005 280:26349–59.
63. Sivanesan D, Hancock MA, Villamil Giraldo AM, Baron C. Quantitative analysis of VirB8-VirB9-VirB10 interactions provides a dynamic model of type IV secretion system core complex assembly. *Biochemistry* 2010 49:4483–93.
64. Sivanesan D, Baron C. The dimer interface of *Agrobacterium tumefaciens* VirB8 is important for type IV secretion system function, stability, and association of VirB2 with the core complex. *J. Bacteriol.* 2011 193:2097–106.
65. Paschos A, Patey G, Sivanesan D, Gao C, Bayliss R, Waksman G, O'callaghan D, Baron C. Dimerization and interactions of *Brucella suis* VirB8 with VirB4 and VirB10 are required for its biological activity. *Proc. Natl. Acad. Sci. U.S.A.* 2006 103:7252–7.
66. Höppner C, Carle A, Sivanesan D, Höppner S, Baron C. The putative lytic transglycosylase VirB1 from *Brucella suis* interacts with the type IV secretion system core components VirB8, VirB9 and VirB11. *Microbiology* 2005 151:3469–82.

67. Berger BR, Christie PJ. Genetic complementation analysis of the *Agrobacterium tumefaciens* *virB* operon: *virB2* through *virB11* are essential virulence genes. *J. Bacteriol.* 1994 176:3646–60.
68. Audette GF, Manchak J, Beatty P, Klimke WA, Frost LS. Entry exclusion in F-like plasmids requires intact TraG in the donor that recognizes its cognate TraS in the recipient. *Microbiology* 2007 153:442–51.
69. Lin Y-H, Gao R, Binns AN, Lynn DG. Capturing the VirA/VirG TCS of *Agrobacterium tumefaciens*. *Adv. Exp. Med. Biol.* 2008 631:161–77.
70. Lin Y-H, Pierce BD, Fang F, Wise A, Binns AN, Lynn DG. Role of the VirA histidine autokinase of *Agrobacterium tumefaciens* in the initial steps of pathogenesis. *Front. Plant Sci.* 2014 5:195.
71. Winans SC, Mantis NJ, Chen CY, Chang CH, Han DC. Host recognition by the VirA, VirG two-component regulatory proteins of *Agrobacterium tumefaciens*. *Res. Microbiol.* 1994 145:461–73.
72. White CE, Winans SC. Cell-cell communication in the plant pathogen *Agrobacterium tumefaciens*. *Philos. Trans. R. Soc. Lond. B Biol Sci.* 2007 362:1135–48.
73. Fronzes R, Christie PJ, Waksman G. The structural biology of type IV secretion systems. *Nat. Rev. Microbiol.* 2009 7:703–14.
74. Cascales E, Christie PJ. Definition of a bacterial type IV secretion pathway for a DNA substrate. *Science* 2004 304:1170–3.
75. Ames BN, Mccann J, Yamasaki E. Methods for detecting carcinogens and mutagens with the *Salmonella*/mammalian-microsome mutagenicity test. *Mutat. Res.* 1975 31:347–64.
76. McNally KP, Freitag NE, Walker GC. LexA-independent expression of a mutant *mucAB* operon. *J. Bacteriol.* 1990 172:6223–31.
77. Goldsmith M, Sarov-Blat L, Livneh Z. Plasmid-encoded MucB protein is a DNA polymerase (pol RI) specialized for lesion bypass in the presence of MucA', RecA, and SSB. *Proc. Natl. Acad. Sci. U.S.A.* 2000 97:11227–31.
78. Shiba T, Iwasaki H, Nakata A, Shinagawa H. Proteolytic processing of MucA protein in SOS mutagenesis: both processed and unprocessed MucA may be active in the mutagenesis. *Mol. Gen. Genet.* 1990 224:169–76.
79. Elledge SJ, Walker GC. The *muc* genes of pKM101 are induced by DNA damage. *J. Bacteriol.* 1983 155:1306–15.
80. Perry KL, Walker GC. Identification of plasmid (pKM101)-coded proteins involved in mutagenesis and UV resistance. *Nature* 1982 300:278–81.

81. Walker GC. Mutagenesis-enhancement by plasmids in mutagenesis tester strains. *Basic Life Sci.* 1985 34:111–20.
82. Fronzes R, Schäfer E, Wang L, Saibil HR, Orlova EV, Waksman G. Structure of a type IV secretion system core complex. *Science* 2009 323:266–8.
83. Chandran V, Fronzes R, Duquerroy S, Cronin N, Navaza J, Waksman G. Structure of the outer membrane complex of a type IV secretion system. *Nature* 2009 462:1011–5.
84. Low HH, Gubellini F, Rivera-Calzada A, Braun N, Connery S, Dujeancourt A, Lu F, Redzej A, Fronzes R, Orlova E, Waksman G. Structure of a type IV secretion system. *Nature* 2014 508:550–3.
85. Rivera-Calzada A, Fronzes R, Savva CG, Chandran V, Lian PW, Laeremans T, Pardon E, Steyaert J, Remaut H, Waksman G, Orlova E. Structure of a bacterial type IV secretion core complex at subnanometre resolution. *EMBO J.* 2013 32:1195–204.
86. Draper O, César CE, Machón C, de la Cruz F, Llosa M. Site-specific recombinase and integrase activities of a conjugative relaxase in recipient cells. *Proc. Natl. Acad. Sci. U.S.A.* 2005 102:16385–90.
87. Schmidt-Eisenlohr H, Domke N, Baron C. TraC of IncN plasmid pKM101 associates with membranes and extracellular high-molecular-weight structures in *Escherichia coli*. *J. Bacteriol.* 1999 181:5563–71.
88. Hapfelmeier S, Domke N, Zambryski PC, Baron C. VirB6 is required for stabilization of VirB5 and VirB3 and formation of VirB7 homodimers in *Agrobacterium tumefaciens*. *J. Bacteriol.* 2000 182:4505–11.
89. Höppner C, Liu Z, Domke N, Binns AN, Baron C. VirB1 orthologs from *Brucella suis* and pKM101 complement defects of the lytic transglycosylase required for efficient type IV secretion from *Agrobacterium tumefaciens*. *J. Bacteriol.* 2004 186:1415–22.
90. Chandran V, Fronzes R, Duquerroy S, Cronin N, Navaza J, Waksman G. Structure of the outer membrane complex of a type IV secretion system. *Nature* 2009 462:1011–5.
91. Gomis-Rüth FX, Moncalián G, Pérez-Luque R, González A, Cabezón E, de la Cruz F, Coll M. The bacterial conjugation protein TrwB resembles ring helicases and F1-ATPase. *Nature* 2001 409:637–41.
92. Vogelmann J, Ammelburg M, Finger C, Guezguez J, Linke D, Flötenmeyer M, Stierhof Y, Wohleben W, Muth G. Conjugal plasmid transfer in *Streptomyces* resembles bacterial chromosome segregation by FtsK/SpoIIIE. *EMBO J.* 2011 30:2246–54.
93. Thoma L, Muth G. The conjugative DNA-transfer apparatus of *Streptomyces*. *Int. J. Med. Microbiol.* 2015 305:224–9.

94. Thoma L, Muth G. Conjugative DNA-transfer in *Streptomyces*, a mycelial organism. *Plasmid* 2016 87–88:1–9.
95. Llosa M, Zunzunegui S, de la Cruz F. Conjugative coupling proteins interact with cognate and heterologous VirB10-like proteins while exhibiting specificity for cognate relaxosomes. *Proc. Natl. Acad. Sci. U.S.A.* 2003 100:10465–70.
96. Abajy MY, Kopeć J, Schiwon K, Burzynski M, Döring M, Bohn C, Grohmann E. A type IV-secretion-like system is required for conjugative DNA transport of broad-host-range plasmid pIP501 in Gram-positive bacteria. *J. Bacteriol.* 2007 189:2487–96.
97. Whitaker N, Chen Y, Jakubowski SJ, Sarkar MK, Li F, Christie PJ. The all-alpha domains of coupling proteins from the *Agrobacterium tumefaciens* VirB/VirD4 and *Enterococcus faecalis* pCF10-encoded type IV secretion systems confer specificity to binding of cognate DNA substrates. *J. Bacteriol.* 2015 197:2335–49.
98. Atmakuri K, Cascales E, Christie PJ. Energetic components VirD4, VirB11 and VirB4 mediate early DNA transfer reactions required for bacterial type IV secretion. *Mol. Microbiol.* 2004 54:1199–211.
99. Berger BR, Christie PJ. The *Agrobacterium tumefaciens* *virB4* gene product is an essential virulence protein requiring an intact nucleoside triphosphate-binding domain. *J. Bacteriol.* 1993 175:1723–34.
100. Arechaga I, Peña A, Zunzunegui S, del Carmen Fernández-Alonso M, Rivas G, de la Cruz F. ATPase activity and oligomeric state of TrwK, the VirB4 homologue of the plasmid R388 type IV secretion system. *J. Bacteriol.* 2008 190:5472–9.
101. Peña A, Matilla I, Martín-Benito J, Valpuesta JM, Carrascosa JL, de la Cruz F, Cabezón E, Arechaga I. The hexameric structure of a conjugative VirB4 protein ATPase provides new insights for a functional and phylogenetic relationship with DNA translocases. *J. Biol. Chem.* 2012 287:39925–32.
102. Walldén K, Williams R, Yan J, Lian PW, Wang L, Thalassinou K, Orlova E, Waksman G. Structure of the VirB4 ATPase, alone and bound to the core complex of a type IV secretion system. *Proc. Natl. Acad. Sci. U.S.A.* 2012 109:11348–53.
103. Li F, Alvarez-Martinez C, Chen Y, Choi K-J, Yeo H-J, Christie PJ. *Enterococcus faecalis* PrgJ, a VirB4-like ATPase, mediates pCF10 conjugative transfer through substrate binding. *J. Bacteriol.* 2012 194:4041–51.
104. Kerr JE, Christie PJ. Evidence for VirB4-mediated dislocation of membrane-integrated VirB2 pilin during biogenesis of the *Agrobacterium* VirB/VirD4 type IV secretion system. *J. Bacteriol.* 2010 192:4923–34.
105. Yeo HJ, Savvides SN, Herr AB, Lanka E, Waksman G. Crystal structure of the hexameric traffic ATPase of the *Helicobacter pylori* type IV secretion system. *Mol. Cell* 2000 6:1461–72.

106. Akeda Y, Galán JE. Chaperone release and unfolding of substrates in type III secretion. *Nature* 2005 437(7060):911–5.
107. Cascales E, Christie PJ. *Agrobacterium* VirB10, an ATP energy sensor required for type IV secretion. *Proc. Natl. Acad. Sci. U.S.A.* 2004 101:17228–33.
108. Ripoll-Rozada J, Zunzunegui S, de la Cruz F, Arechaga I, Cabezón E. Functional interactions of VirB11 traffic ATPases with VirB4 and VirD4 molecular motors in type IV secretion systems. *J. Bacteriol.* 2013 195:4195–201.
109. Mossey P, Hudacek A, Das A. *Agrobacterium tumefaciens* type IV secretion protein VirB3 is an inner membrane protein and requires VirB4, VirB7, and VirB8 for stabilization. *J. Bacteriol.* 2010 192:2830–8.
110. Jakubowski SJ, Krishnamoorthy V, Christie PJ. *Agrobacterium tumefaciens* VirB6 protein participates in formation of VirB7 and VirB9 complexes required for type IV secretion. *J. Bacteriol.* 2003 185:2867–78.
111. Terradot L, Bayliss R, Oomen C, Leonard GA, Baron C, Waksman G. Structures of two core subunits of the bacterial type IV secretion system, VirB8 from *Brucella suis* and ComB10 from *Helicobacter pylori*. *Proc. Natl. Acad. Sci. U.S.A.* 2005 102:4596–601.
112. Goessweiner-Mohr N, Grumet L, Arends K, Pavkov-Keller T, Gruber CC, Gruber K, Birner-Gruenberger R, Kropec-Huebner A, Huebner J, Grohmann E, Keller W. The 2.5 Å structure of the *Enterococcus* conjugation protein TraM resembles VirB8 type IV secretion proteins. *J. Biol. Chem.* 2013 288:2018–28.
113. Gillespie JJ, Phan IQH, Scheib H, Subramanian S, Edwards TE, Lehman SS, Piitulainen H, Rahman M, Rennoll-Bankert K, Staker B, Taira S, Stacy R, Myler P, Azad A, Pulliainen A. Structural insight into how bacteria prevent interference between multiple divergent type IV secretion systems. *mBio.* 2015 6:01867-01815.
114. Casu B, Smart J, Hancock MA, Smith M, Sygusch J, Baron C. Structural Analysis and Inhibition of TraE from the pKM101 Type IV Secretion System. *J. Biol. Chem.* 2016 291:23817–29.
115. Judd PK, Kumar RB, Das A. The type IV secretion apparatus protein VirB6 of *Agrobacterium tumefaciens* localizes to a cell pole. *Mol. Microbiol.* 2005 55:115–24.
116. Kumar RB, Das A. Polar location and functional domains of the *Agrobacterium tumefaciens* DNA transfer protein VirD4. *Mol. Microbiol.* 2002 43:1523–32.
117. Fernandez D, Dang TA, Spudich GM, Zhou XR, Berger BR, Christie PJ. The *Agrobacterium tumefaciens* virB7 gene product, a proposed component of the T-complex transport apparatus, is a membrane-associated lipoprotein exposed at the periplasmic surface. *J. Bacteriol.* 1996 178:3156–67.

118. Fernandez D, Spudich GM, Zhou XR, Christie PJ. The *Agrobacterium tumefaciens* VirB7 lipoprotein is required for stabilization of VirB proteins during assembly of the T-complex transport apparatus. *J. Bacteriol.* 1996 178:3168–76.
119. Beaupré CE, Bohne J, Dale EM, Binns AN. Interactions between VirB9 and VirB10 membrane proteins involved in movement of DNA from *Agrobacterium tumefaciens* into plant cells. *J. Bacteriol.* 1997 179:78–89.
120. Spudich GM, Fernandez D, Zhou XR, Christie PJ. Intermolecular disulfide bonds stabilize VirB7 homodimers and VirB7/VirB9 heterodimers during biogenesis of the *Agrobacterium tumefaciens* T-complex transport apparatus. *Proc. Natl. Acad. Sci. U.S.A.* 1996 93:7512–7.
121. Anderson LB, Hertzelt AV, Das A. *Agrobacterium tumefaciens* VirB7 and VirB9 form a disulfide-linked protein complex. *Proc. Natl. Acad. Sci. U.S.A.* 1996 93:8889–94.
122. Bayliss R, Harris R, Coutte L, Monier A, Fronzes R, Christie PJ, Driscoll P, Waksman G. NMR structure of a complex between the VirB9/VirB7 interaction domains of the pKM101 type IV secretion system. *Proc. Natl. Acad. Sci. U.S.A.* 2007 104:1673–8.
123. de Paz HD, Sangari FJ, Bolland S, García-Lobo JM, Dehio C, de la Cruz F, Llosa M. Functional interactions between type IV secretion systems involved in DNA transfer and virulence. *Microbiology* 2005 151:3505–16.
124. Rohde M, Püls J, Buhrdorf R, Fischer W, Haas R. A novel sheathed surface organelle of the *Helicobacter pylori* cag type IV secretion system. *Mol. Microbiol.* 2003 49:219–34.
125. Banta LM, Kerr JE, Cascales E, Giuliano ME, Bailey ME, McKay C, Chandran V, Waksman G, Christie PJ. An *Agrobacterium* VirB10 mutation conferring a type IV secretion system gating defect. *J. Bacteriol.* 2011 193:2566–74.
126. Jakubowski SJ, Cascales E, Krishnamoorthy V, Christie PJ. *Agrobacterium tumefaciens* VirB9, an outer-membrane-associated component of a type IV secretion system, regulates substrate selection and T-pilus biogenesis. *J. Bacteriol.* 2005 187:3486–95.
127. Jakubowski SJ, Kerr JE, Garza I, Krishnamoorthy V, Bayliss R, Waksman G, Christie PJ. *Agrobacterium* VirB10 domain requirements for type IV secretion and T-pilus biogenesis. *Mol. Microbiol.* 2009 71:779–94.
128. Garza I, Christie PJ. A putative transmembrane leucine zipper of *Agrobacterium* VirB10 is essential for T-pilus biogenesis but not type IV secretion. *J. Bacteriol.* 2013 195:3022–34.
129. Babic A, Lindner AB, Vulic M, Stewart EJ, Radman M. Direct visualization of horizontal gene transfer. *Science* 2008 319:1533–6.
130. Harrington LC, Rogerson AC. The F pilus of *Escherichia coli* appears to support stable DNA transfer in the absence of wall-to-wall contact between cells. *J. Bacteriol.* 1990 172:7263–4.

131. Lawley TD, Gordon GS, Wright A, Taylor DE. Bacterial conjugative transfer: visualization of successful mating pairs and plasmid establishment in live *Escherichia coli*. *Mol. Microbiol.* 2002 44:947–56.
132. Arutyunov D, Frost LS. F conjugation: back to the beginning. *Plasmid* 2013 70:18–32.
133. Lai E-M, Eisenbrandt R, Kalkum M, Lanka E, Kado CI. Biogenesis of T pili in *Agrobacterium tumefaciens* requires precise VirB2 propilin cleavage and cyclization. *J. Bacteriol.* 2002 184:327–30.
134. Eisenbrandt R, Kalkum M, Lai EM, Lurz R, Kado CI, Lanka E. Conjugative pili of IncP plasmids, and the Ti plasmid T-pilus are composed of cyclic subunits. *J. Biol. Chem.* 1999 274:22548–55.
135. Majdalani N, Ippen-Ihler K. Membrane insertion of the F-pilin subunit is Sec independent but requires leader peptidase B and the proton motive force. *J. Bacteriol.* 1996 178:3742–7.
136. Harris RL, Sholl KA, Conrad MN, Dresser ME, Silverman PM. Interaction between the F plasmid TraA (F-pilin) and TraQ proteins. *Mol. Microbiol.* 1999 34:780–91.
137. Maneewannakul K, Maneewannakul S, Ippen-Ihler K. Characterization of *traX*, the F plasmid locus required for acetylation of F-pilin subunits. *J. Bacteriol.* 1995 177:2957–64.
138. Moore D, Hamilton CM, Maneewannakul K, Mintz Y, Frost LS, Ippen-Ihler K. The *Escherichia coli* K-12 F plasmid gene *traX* is required for acetylation of F pilin. *J. Bacteriol.* 1993 175:1375–83.
139. Costa TRD, Ilangovan A, Ukleja M, Redzej A, Santini JM, Smith TK, Egelman EH, Waksman G. Structure of the bacterial sex F-pilus reveals an assembly of a stoichiometric protein-phospholipid complex. *Cell* 2016 166:1436–1444.
140. Ho BT, Basler M, Mekalanos JJ. Type 6 secretion system-mediated immunity to type 4 secretion system-mediated gene transfer. *Science* 2013 342:250–3.
141. Olsen RH, Siak JS, Gray RH. Characteristics of PRD1, a plasmid-dependent broad host range DNA bacteriophage. *J. Virol.* 1974 14:689–99.
142. Yeo HJ, Yuan Q, Beck MR, Baron C, Waksman G. Structural and functional characterization of the VirB5 protein from the type IV secretion system encoded by the conjugative plasmid pKM101. *Proc. Natl. Acad. Sci. U.S.A.* 2003 100:15947–52.
143. Blattner FR, Plunkett G, Bloch CA, Perna NT, Burland V, Riley M, Collado-Vides J, Glasner JD, Rode CK, Mayhew GF, Gregor J, Davis NW, Kirkpatrick HA, Goeden MA, Rose DJ, Mau B, Shao Y. The complete genome sequence of *Escherichia coli* K-12. *Science* 1997 277:1453–62.

144. Singer M, Baker TA, Schnitzler G, Deischel SM, Goel M, Dove W, Jaacks KJ, Grossman AD, Erickson JW, Gross CA. A collection of strains containing genetically linked alternating antibiotic resistance elements for genetic mapping of *Escherichia coli*. *Microbiol. Rev.* 1989 53:1–24.
145. Peters JE, Thate TE, Craig NL. Definition of the *Escherichia coli* MC4100 genome by use of a DNA array. *J. Bacteriol.* 2003 185:2017–21.
146. Garfinkel DJ, Simpson RB, Ream LW, White FF, Gordon MP, Nester EW. Genetic analysis of crown gall: fine structure map of the T-DNA by site-directed mutagenesis. *Cell* 1981 27:143–53.
147. Guzman LM, Belin D, Carson MJ, Beckwith J. Tight regulation, modulation, and high-level expression by vectors containing the arabinose PBAD promoter. *J. Bacteriol.* 1995 177:4121–30.
148. Prentki P, Krisch HM. In vitro insertional mutagenesis with a selectable DNA fragment. *Gene* 1984 29:303–13.
149. Churchward G, Belin D, Nagamine Y. A pSC101-derived plasmid which shows no sequence homology to other commonly used cloning vectors. *Gene* 1984 31:165–71.
150. de Paz HD, Larrea D, Zunzunegui S, Dehio C, de la Cruz F, Llosa M. Functional dissection of the conjugative coupling protein TrwB. *J. Bacteriol.* 2010 192:2655–69.
151. Chin JW, Martin AB, King DS, Wang L, Schultz PG. Addition of a photocrosslinking amino acid to the genetic code of *Escherichia coli*. *Proc. Natl. Acad. Sci. U.S.A.* 2002 99:11020–4.
152. Pohlman RF, Genetti HD, Winans SC. Common ancestry between IncN conjugal transfer genes and macromolecular export systems of plant and animal pathogens. *Mol. Microbiol.* 1994 14:655–68.
153. Winans SC, Walker GC. Conjugal transfer system of the IncN plasmid pKM101. *J. Bacteriol.* 1985 161:402–10.
154. Thomason L, Court DL, Bubunenko M, Costantino N, Wilson H, Datta S, Oppenheim A. Recombineering: Genetic Engineering in Bacteria Using Homologous Recombination. *Current Protocols in Molecular Biology.* 2014 106:V:1.16:1.16.1–1.16.39.
155. Bradley DE. Morphological and serological relationships of conjugative pili. *Plasmid* 1980 4:155–69.
156. Clarke M, Maddera L, Harris RL, Silverman PM. F-pili dynamics by live-cell imaging. *Proc. Natl. Acad. Sci. U.S.A.* 2008 105:17978–81.

157. Bayer M, Iberer R, Bischof K, Rassi E, Stabentheiner E, Zellnig G, Koraimann G. Functional and mutational analysis of p19, a DNA transfer protein with muramidase activity. *J. Bacteriol.* 2001 183:3176–83.
158. Aly KA, Baron C. The VirB5 protein localizes to the T-pilus tips in *Agrobacterium tumefaciens*. *Microbiology* 2007 153:3766–75.
159. Holcík M, Iyer VN. A novel plasmid gene involved in bacteriophage PRD1 infection and conjugative host-range. *Plasmid* 1996 35:204–10.
160. Bradley DE, Whelan J. *Escherichia coli* *tolQ* mutants are resistant to filamentous bacteriophages that adsorb to the tips, not the shafts, of conjugative pili. *J. Gen. Microbiol.* 1989 135:1857–63.
161. Rakonjac J, Bennett NJ, Spagnuolo J, Gagic D, Russel M. Filamentous bacteriophage: biology, phage display and nanotechnology applications. *Curr. Issues Mol. Biol.* 2011 13:51–76.
162. Samuels AL, Lanka E, Davies JE. Conjugative junctions in RP4-mediated mating of *Escherichia coli*. *J. Bacteriol.* 2000 182:2709–15.
163. Segura RL, Aguila-Arcos S, Ugarte-Urbe B, Vecino AJ, de la Cruz F, Goñi FM, Alkorta I. The transmembrane domain of the T4SS coupling protein TrwB and its role in protein-protein interactions. *Biochim. Biophys. Acta.* 2013 1828:2015–25.
164. Konovalova A, Perlman DH, Cowles CE, Silhavy TJ. Transmembrane domain of surface-exposed outer membrane lipoprotein RcsF is threaded through the lumen of β -barrel proteins. *Proc. Natl. Acad. Sci. U.S.A.* 2014 111:E4350–4358.
165. Christie PJ. Type IV secretion: intercellular transfer of macromolecules by systems ancestrally related to conjugation machines. *Mol. Microbiol.* 2001 40:294–305.
166. Patey G, Qi Z, Bourg G, Baron C, O’Callaghan D. Swapping of periplasmic domains between *Brucella suis* VirB8 and a pSB102 VirB8 homologue allows heterologous complementation. *Infect. Immun.* 2006 74:4945–9.
167. Pineau C, Guschinskaya N, Robert X, Gouet P, Ballut L, Shevchik VE. Substrate recognition by the bacterial type II secretion system: more than a simple interaction. *Mol. Microbiol.* 2014 94:126–40.
168. Ieva R, Tian P, Peterson JH, Bernstein HD. Sequential and spatially restricted interactions of assembly factors with an autotransporter beta domain. *Proc. Natl. Acad. Sci. U.S.A.* 2011 108:E383–391.
169. Souza DP, Oka GU, Alvarez-Martinez CE, Bisson-Filho AW, Dunger G, Hobeika L, Cavalcante NS, Alegria MC, Barbosa LR, Salinas RK, Guzzo CR, Farah CS. Bacterial killing via a type IV secretion system. *Nat. Commun.* 2015 6:6453.

170. Wall D. Molecular recognition in myxobacterial outer membrane exchange: functional, social and evolutionary implications. *Mol. Microbiol.* 2014 91:209–20.

Vita

Jay Elliot Gordon was born on December 20th, 1986 in Galveston, Texas. He is the son of Gerilyn Farb Gordon and John Gordon, brother of Jeffrey Gordon, and husband of Ilyse Kornblau. After completing high school at the Robert M. Beren Academy in 2005, he began his studies at The University of Kansas in Lawrence, Kansas. He graduated in 2009 with a Bachelors of Science in Microbiology. During this time, he worked for Dr. Fusao Takusagawa in the Department of Molecular Biosciences. He entered the The University of Texas MD Anderson Cancer Center UTHHealth Graduate School of Biomedical Sciences in the Summer of 2010.

Permanent Address:

5239 Jason St.

Houston, TX 77096